Supercollider physics

E. Eichten

Fermi National Accelerator Laboratory, P.O. Box 500, Batavia, Illinois 60510

I. Hinchliffe

Lawrence Berkeley Laboratory, Berkeley, California 94720

K. Lane

The Ohio State University, Columbus, Ohio 43210

C. Quigg

Fermi National Accelerator Laboratory, P.O. Box 500, Batavia, Illinois 60510

Eichten *et al.* summarize the motivation for exploring the 1-TeV ($=10^{12}$ eV) energy scale in elementary particle interactions and explore the capabilities of proton-(anti)proton colliders with beam energies between 1 and 50 TeV. The authors calculate the production rates and characteristics for a number of conventional processes, and discuss their intrinsic physics interest as well as their role as backgrounds to more exotic phenomena. The authors review the theoretical motivation and expected signatures for several new phenomena which may occur on the 1-TeV scale. Their results provide a reference point for the choice of machine parameters and for experiment design.

CONTENTS

I. INTRODUCTION

The physics of elementary particles has undergone a remarkable development during the past decade. A host of new experimental results made accessible by a new generation of particle accelerators and the accompanying rapid convergence of theoretical ideas have brought to the subject a new coherence. Our current outlook has been shaped by the identification of quarks and leptons as fundamental constituents of matter and by the gauge theory synthesis of the fundamental interactions.[1] These developments represent an important simplification of

[1]For expositions of the current paradigm, see the textbooks by Okun (1981), Perkins (1982), Aitchison and Hey (1982), Leader and Predazzi (1982), Quigg (1983), and Halzen and Martin (1984) and the summer school proceedings edited by Gaillard and Stora (1983).

basic concepts and the evolution of a theoretical strategy with broad applicability.

One of the strengths of our current theoretical framework is that it defines the frontier of our ignorance—the energy scale of about 1 TeV on which new phenomena must occur, and where experimental guidance toward a more complete understanding must be found. It is to explore this realm that plans are being developed (Wojcicki *et al.*, 1983) for the construction of a multi-TeV high-luminosity hadron-hadron collider. The physics capabilities of such a device and the demands placed upon accelerator parameters by the physics are the subject of this paper.

Three things are done in the remainder of this introductory section. First, we give a brief description of the present understanding of the strong, weak, and electromagnetic interactions. Second, we examine the incompleteness and shortcomings of this picture and explain why, in general terms, exploration of the 1-TeV scale is interesting and necessary. Finally, we describe the goals and contents of this paper.

A. Where we stand

The picture of the fundamental constituents of matter and the interactions among them that has emerged in recent years is one of great beauty and simplicity. All matter appears to be composed of *quarks* and *leptons,* which are pointlike, structureless, spin-$\frac{1}{2}$ particles. If we leave aside gravitation, which is a negligible perturbation at the energy scales usually considered, the interactions among these particles are of three types: weak, electromagnetic, and strong. All three of these interactions are described by gauge theories, and are mediated by spin-1 gauge bosons. The quarks experience all three interactions; the leptons participate only in the weak and electromagnetic interactions.

The systematics of the charged-current (β-decay) weak interactions suggest grouping the six known leptons into three families:

$$\begin{bmatrix} \nu_e \\ e \end{bmatrix}, \quad \begin{bmatrix} \nu_\mu \\ \mu \end{bmatrix}, \quad \begin{bmatrix} \nu_\tau \\ \tau \end{bmatrix}. \tag{1.1}$$

Similarly, the five known quarks appear in the doublets

$$\begin{bmatrix} u \\ d' \end{bmatrix}, \quad \begin{bmatrix} c \\ s' \end{bmatrix}, \quad \begin{bmatrix} [t] \\ b' \end{bmatrix}, \tag{1.2}$$

where the primes denote generalized Cabibbo (1963)—Kobayashi and Maskawa (1973) mixing among the charge $-\frac{1}{3}$ flavors. Symmetry considerations and the features of b-quark decay suggest the existence of a third quark of charge $+\frac{2}{3}$, designated t. Current experiments set a lower limit on its mass of (Yamada, 1983)

$$M_t \gtrsim 22.5 \text{ GeV}/c^2 . \tag{1.3}$$

Recently, the UA-1 Collaboration (Rubbia, 1984) has announced preliminary evidence for the top quark, with $30 \lesssim M_t \lesssim 60$ GeV/c^2. Each quark flavor comes in three distinguishable varieties, called colors. Color is what distinguishes the quarks from the leptons. Since the leptons are inert with respect to the strong interactions, it is natural to interpret color as a strong interaction charge.

The theory of strong interactions, quantum chromodynamics (QCD) (Bardeen, Fritzsch, and Gell-Mann, 1973; Gross and Wilczek, 1973b; Weinberg, 1973) is based upon the exact local color gauge symmetry $SU(3)_c$. Strong interactions are mediated by an SU(3) octet of colored gauge bosons called gluons. The gauge symmetry is exact, and the gluons are massless particles. However, it is widely believed, if not yet rigorously proved, that in QCD quarks and gluons are permanently confined within color singlet hadrons. A crucial property of non-Abelian gauge theories in general and of QCD in particular is asymptotic freedom (Gross and Wilczek, 1973a; Politzer, 1973); the tendency of the coupling strength to diminish at short distances. This behavior suggests a resolution to the parton model paradox that quarks behave as free particles within hadrons, but can never be liberated.

A unified description of the weak and electromagnetic interactions is provided by the Glashow (1961)—Weinberg (1967)—Salam (1968) theory based on the gauge group $SU(2)_L \otimes U(1)_Y$. In this theory, unlike QCD, the local gauge invariance is spontaneously broken, or hidden, by the Higgs (1964) mechanism. This causes the intermediate bosons W^+, W^-, and Z^0 of the weak interactions to acquire large masses, while leaving the photon massless. A consequence of this form of spontaneous symmetry breaking is the existence of a scalar Higgs boson of unspecified mass. The $SU(2)_L \otimes U(1)_Y$ model has a number of notable successes: the prediction and detailed description of the weak neutral current interactions first observed by Hasert *et al.* (1973a,1973b,1974) and Benvenuti *et al.* (1974), the prediction of charm (Cazzoli *et al.*, 1975; Goldhaber *et al.*, 1976; Peruzzi *et al.*, 1976), and the predictions of the masses of the charged (Arnison *et al.*, 1983a; Banner *et al.*, 1983) and neutral (Arnison *et al.*, 1983c; Bagnaia *et al.*, 1983b) intermediate bosons.

The so-called "standard model" of QCD plus the $SU(2)_L \otimes U(1)_Y$ electroweak theory incorporates all the principal systematics of elementary-particle phenomenology, and achieves a wide-ranging synthesis of elementary phenomena. It is of great importance to continue to test the standard model, and to explore the predictions of unified theories of the strong, weak, and electromagnetic interactions (Georgi and Glashow, 1974; Pati and Salam, 1973a,1973b,1974), which seem a natural next step. The degree of current experimental support for the electroweak theory, for QCD, and for the idea of grand unification is rather different. For the electroweak theory the task is now to refine precise quantitative tests of very detailed predictions and to explore the Higgs sector. In the case of QCD, most comparisons of theory and experiment are still at the qualitative level, either because a precise theoretical analysis has not been carried out, or because of the difficulties of the required measurement. We find ourselves in the curious position of having a plausible

theory which we have not been able to exploit in full. So far as unified theories are concerned, we are only beginning to explore their consequences experimentally. Although the simplest model provides an elegant example of how unification might occur, no "standard" unified theory has yet been selected by experiment.

Over the next decade, the vigorous experimental program at accelerators now operating or under construction will subject QCD and the electroweak theory to ever more stringent testing, and nonaccelerator experiments, such as searches for nucleon instability, will explore some of the dramatic consequences of unified theories. Surprises may well be encountered, but it is likely that our efforts to understand why the standard model works and to construct more complete descriptions of nature will remain unfulfilled. In order to explain what sort of experimental guidance will be required, we next consider why the standard model cannot be the final answer, and where new phenomena are to be expected.

B. The importance of the 1-TeV scale

It is essential to recognize that the current paradigm leaves unanswered some central questions. Even if we go beyond what has been persuasively indicated by experiment, and suppose that the idea of a unified theory of the strong, weak, and electromagnetic interactions is correct, there are several areas in which accomplishments fall short of complete understanding. There are also a number of specific problems to be faced.

- The most serious structural problem is associated with the scalar, or Higgs, sector of the electroweak theory. This sector is responsible for the most obvious feature of electroweak symmetry, namely, that it is broken. Yet the dynamical nature of this sector is the least understood aspect of the theory. In the standard model, the interactions of the Higgs boson are not prescribed by the gauge symmetry in the manner of those of the intermediate bosons. Whereas the masses of the W and Z are specified by the theory, the mass of the Higgs boson is constrained only to lie within the range 7 GeV/c^2 (Linde, 1976; Weinberg, 1976a) to 1 TeV/c^2 (Veltman, 1977; Lee, Quigg, and Thacker, 1977). While the lower bound is strictly valid only in the simplest version of the standard model with one elementary Higgs doublet, the upper bound is fairly model independent. If the Higgs boson mass exceeds this bound, weak interactions must become strong on the TeV scale. This is perhaps the most compelling argument that new physics of some sort must show up at or before the energy scale of ~ 1 TeV is reached. In a unified theory, the problem of the ambiguity of the Higgs sector is heightened by the requirement that there be a dozen orders of magnitude between the masses of $W^{\pm}$ and Z^0 and those of the leptoquark bosons that would mediate proton decay.
- No particular insight has been gained into the pattern of quark and lepton masses or into the mixing between different quark flavors. This fact may be quantified by noting that the number of apparently arbitrary parameters needed to specify the theory is 20 or more. This is at odds with our viewpoint, fostered by a history of repeated simplifications, that the world should be comprehensible in terms of a few simple laws. Much of the progress represented by the gauge theory synthesis is associated with the reduction of ambiguity made possible by a guiding principle. Since so much of the dynamical origin of the masses and mixing angles of quarks and leptons has to do with their coupling to the electroweak scalar sector, here again we have good reason to hope that a thorough study of 1-TeV physics will yield important answers.
- The violation of CP invariance in the weak interaction does not arise gracefully. The currently most popular interpretation attributes this phenomenon to the possibility of complex couplings of quarks to the Higgs boson, but, at least in the simplest model, this scenario has a serious problem: large CP violations in the strong interactions. Once again, our experimental ignorance of the scalar sector is hindering our theoretical understanding.
- The requirement that the electroweak theory be anomaly free suggests grouping quark and lepton doublets into fermion "generations." Although this idea is supported by the explanation of charge quantization in unified theories, we do not know why generations repeat or how many there are. Indeed, with the large number of quarks and leptons that we now have, it is natural to ask whether these fermionic constituents are truly elementary. If it should turn out that they are in fact composite structures, then the successes of the standard model imply that their characteristic size is less than $\sim 10^{-17}$ cm, corresponding to an energy scale ≥ 1 TeV.
- Finally, we may ask what the origin of the gauge symmetries themselves is, why the weak interactions are left-handed, and whether there are new fundamental interactions to be discovered.

Given this list, it is not surprising that there are many directions of theoretical speculation departing from the current paradigm. Many of these have important implications which cannot yet be tested. Although theoretical speculation and synthesis is valuable and necessary, we cannot advance without new observations. The experimental clues needed to answer questions like those posed above can come from several sources, including

experiments at high-energy accelerators;
experiments at low-energy accelerators and nuclear reactors;
nonaccelerator experiments;
deductions from astrophysical measurements.

However, according to our present knowledge of elementary particle physics, our physical intuition, and our past experience, most clues and information will come from experiments at the highest-energy accelerators.

Since many of the questions we wish to pose are beyond the reach of existing accelerators and those under construction, further progress in the field will depend on our ability to study phenomena at higher energies, or

equivalently, on shorter scales of time and distance. What energy scale must we reach, and what sort of new instruments do we require?

Field theories with elementary scalars are notoriously unstable (Wilson, 1971) against large radiative corrections to masses. As a consequence, although the Higgs phenomena might possibly occur at less than 1 TeV, building a comprehensive theory in which this occurs proves to be a very difficult problem, unless some new physics intervenes.

One possible solution to the Higgs mass problem involves introducing a complete new set of elementary particles whose spins differ by one-half unit from the known quarks, leptons, and gauge bosons. These postulated new particles are consequences of a new "supersymmetry" which relates particles of integral and half-integral spin. The conjectured supersymmetry would stabilize the mass of the Higgs boson at a value below 1 TeV/c^2, and the supersymmetric particles are likely themselves to have masses less than about 1 TeV/c^2. Up to the present, there is no experimental evidence for these superpartners.

A second possible solution to the Higgs problem is based on the idea that the Higgs boson is not an elementary particle at all, but is in reality a composite object made out of elementary constituents analogous to the quarks and leptons. Although they would resemble the usual quarks and leptons, these new constituents would be subject to a new type of strong interactions (often called "technicolor") that would confine them within about 10^{-17} cm. Such new forces could yield new phenomena as rich and diverse as the conventional strong interactions, but on an energy scale a thousand times greater—around 1 TeV. The new phenomena would include a rich spectrum of technicolor-singlet bound states, akin to the spectrum of known hadrons. Again, there is no evidence yet for these new particles.

We thus see that both general arguments such as unitarity constraints and specific conjectures for resolutions of the Higgs problem imply 1 TeV as an energy scale on which new phenomena crucial to our understanding of the fundamental interactions must occur. The dynamical origin of electroweak symmetry breaking is of course only one of the important issues that define the frontier of elementary particle physics. However, because of its immediacy and its fundamental significance it must guide our planning for future facilities.

Either an electron-positron collider with beams of 1—3 TeV or a proton-(anti)proton collider with beams of 5—20 TeV would allow an exploration of the TeV region for hard collisions. The higher beam energy required for protons simply reflects the fact that the proton's energy is shared among its quark and gluon constituents. The partitioning of energy among the constituents has been thoroughly studied in experiments on deeply inelastic scattering, so the rate of collisions among constituents of various energies may be calculated with some confidence.

The physics capabilities of the electron-positron and proton-(anti)proton options are both attractive and somewhat complementary. The hadron machine reaches to higher energy and provides a wider variety of constituent collisions, which allows for a greater diversity of phenomena. The simple initial state of the electron-positron machine represents a considerable measurement advantage. However, the results of the CERN proton-antiproton collider (Banner *et al.*, 1982; Arnison *et al.*, 1983b) indicate that hard collisions at very high energies are relatively easy to identify. Because the current state of technology favors the hadron collider, it is the instrument of choice for the first exploration of the TeV regime. Some studies of the accelerator physics and technology required for a multi-TeV collider have already been carried out (Tigner, 1983; Diebold, 1983; Marx, 1984).

C. The purpose and goals of this paper

We have reviewed the principal rationale for a multi-TeV hadron collider: it is a device to illuminate the physics of electroweak symmetry breaking. At the same time, it is necessary to anticipate that the supercollider will reveal more than this. Surprises and unexpected insights have always been encountered in each new energy regime, and we confidently expect the same result at TeV energies. No one knows what form these discoveries will take, but is essential that the supercollider provide the means to make them. Fortunately, both the conventional possibilities of the standard model and the new phenomena implied by existing speculations can serve the important function of calibrating the capacity for discovery of a planned facility. They also help to fix the crucial parameters for a new machine: the energy per beam and the luminosity, or rate at which collisions occur. In any case, the expected phenomena are important as backgrounds for the unexpected, and for each other.

Our principal goal in this paper is to set out the most obvious possibilities in enough detail that we may begin to assess the demands of the physics upon beam energy and luminosity, and to consider the relative merits of the pp and $\bar{p}p$ options. In addition, we intend to provide a reference point for the design of detectors and experiments. Earlier work relevant to these issues has been reported in the Proceedings of the 1982 Snowmass Workshop (Donaldson, Gustafson, and Paige, 1982) and of the 1983 Berkeley Detector Workshop (Loken and Nemethy, 1983). We also wish to identify areas in which further work is required.

Hard-scattering phenomena make the most stringent demands upon machine performance. Accordingly, we shall not discuss the low transverse momentum phenomena known as "log$s$ physics." Some of these considerations are treated in the lectures by Cahn (1982) and Jacob (1983). For the same reason, we do not address the physics interest of the conjectured new state of matter known as quark-gluon plasma (McLerran, 1983). We also omit any discussion of fixed target physics with multi-TeV beams, for which the opportunities and concerns are rather different. This topic has been considered in the Snowmass (Pondrom, 1982), Diablerets (Amaldi, 1980),

and Woodlands (McIntyre *et al.*, 1984) workshops.

A detailed description of the material presented in this paper appears in the Table of Contents. A brief summary is in order here. Section II is devoted to a review of the renormalization-group—improved-parton model and the nucleon structure functions required to make predictions of production rates. The hard-scattering hadron jet phenomena predicted by QCD that provide a window on constituent interactions are taken up in Sec. III. In Sec. IV we discuss the standard electroweak theory, in particular as it pertains to searches for heavy Higgs bosons. Sections III and IV, then, are concerned with processes which are intrinsically interesting as definitive tests of the standard model, and which produce the principal backgrounds to the new physics the supercollider is intended to explore.

The four sections that follow concentrate on several of the more frequently discussed possibilities for new physics. The simplest extensions of the standard $SU(2)_L \otimes U(1)_Y$ theory, new quark and lepton flavors and additional intermediate bosons are treated in Sec. V. We then turn to more speculative possibilities: technicolor (Sec. VI), supersymmetry (Sec. VII), and quark-lepton compositeness (Sec. VIII). In each of these cases we review the motivations for the conjecture and discuss the expected experimental signatures. We also examine the potential backgrounds and assess the physics reach of the collider as a function of energy and luminosity for pp and $\bar{p}p$ collisions. The reason for covering these proposals in some detail is not that any one of them necessarily is correct. Rather, they provide a very wide range of experimental challenges which we must expect the supercollider to meet if it is to explore thoroughly and effectively the physics of the 1-TeV scale. Some tentative conclusions from our study are given in Sec. IX.

II. PRELIMINARIES

A high-energy proton beam may usefully be regarded as an unseparated, broadband beam of quarks, antiquarks, and gluons. For the hard-scattering phenomena that are the principal interest of this paper, it is the rate of encounters among energetic constituents that determines interaction rates. We adopt the spirit of the parton model in which the cross section for the hadronic reaction

$$a+b\to c+\text{ anything} \tag{2.1}$$

is given schematically by

$$d\sigma(a+b\to c+X)=\sum_{\substack{\text{partons}\\ i,j}} f_i^{(a)} f_j^{(b)} d\hat{\sigma}(i+j\to c+X') , \tag{2.2}$$

where $f_i^{(a)}$ is the probability of finding constituent i in hadron a, and $\hat{\sigma}(i+j\to c+X')$ is the cross section for the elementary process leading to the desired final state. This picture of hard collisions is not only highly suggestive, it also in many circumstances provides a reliable estimate of reaction rates, as we shall document below.

Two ingredients are therefore required in order to compute cross sections and experimental distributions: the elementary cross sections and the parton distributions. It is straightforward to calculate the elementary cross sections, at least at low orders in perturbation theory, from the underlying theory. At a given scale, the parton distributions can be measured in deeply inelastic lepton-hadron scattering. The evolution of these distributions to larger momentum scales is then prescribed by standard methods of perturbative quantum chromodynamics.

Three things are done in this section. First, we give a brief summary of the basic ideas of the QCD-improved parton model. We then turn to the task of constructing parton distributions which are appropriate to the very large momentum scales of interest for a multi-TeV hadron collider. In the final part of this section, we present the luminosities for parton-parton collisions and discuss their implications in general terms. These will be used in the rest of this paper to estimate the rates for particular physics processes.

A. Parton model ideas

The essence of the parton model is to regard a high-energy proton (or other hadron) as a collection of quasi-free partons which share its momentum. Thus we envisage a proton of momentum P as being made of partons carrying longitudinal momenta $x_i P$, where the momentum fractions x_i satisfy

$$0\le x_i\le 1 \tag{2.3}$$

and

$$\sum_{\substack{\text{partons}\\ i}} x_i = 1 . \tag{2.4}$$

The idealization that the partons carry negligible transverse momentum will be adequate for our purposes.

The prototype hadron-hadron reaction is depicted in Fig. 1. The general ideas of the parton model are

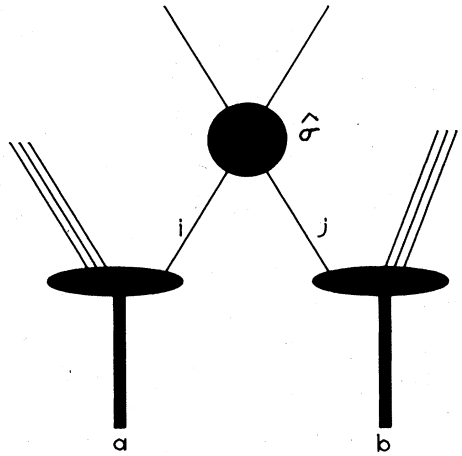

FIG. 1. Parton-model representation of a hadron-hadron reaction.

thoroughly explained in Feynman (1972). Many interesting applications of the parton model philosophy to hadronic interactions were introduced by Berman, Bjorken, and Kogut (1971). The cross section for reaction (2.1) is given by

$$d\sigma(a+b\to c+X)=\sum_{ij} f_i^{(a)}(x_a) f_j^{(b)}(x_b)\, d\hat{\sigma}(i+j\to c+X') , \tag{2.5}$$

where $f_i^{(a)}(x)$ is the number distribution of partons of species i. The summation runs over all contributing parton configurations. If we denote the invariant mass of the i-j system as

$$\sqrt{\hat{s}}=\sqrt{s\tau} \tag{2.6}$$

and its longitudinal momentum in the hadron-hadron c.m. by

$$p=x\sqrt{s}/2 , \tag{2.7}$$

then the kinematic variables $x_{a,b}$ of the elementary process are related to those of the hadronic process by

$$x_{a,b}=\tfrac{1}{2}[(x^2+4\tau)^{1/2}\pm x] . \tag{2.8}$$

These parton momentum fractions satisfy the obvious requirements

$$x_a x_b=\tau , \tag{2.9}$$

$$x_a-x_b=x . \tag{2.10}$$

We shall present detailed cross-section formulas in the text, in connection with the discussion of specific phenomena. However, one situation—two-body parton scattering—occurs so frequently that it is appropriate to develop the kinematics here. We consider the generic process

$$a+b\to c+d+\text{ anything} , \tag{2.11}$$

where the masses of the final-state particles are M_c and M_d. Then if particle c is produced at c.m. angle θ with transverse momentum

$$p_\perp=x_\perp\sqrt{s}/2 , \tag{2.12}$$

the invariant cross section for reaction (2.11) is

$$E\frac{d\sigma}{d^3p}=\frac{1}{\pi}\sum_{ij}\int_{x_{\min}}^{1}\frac{dx_a}{x_a-x_\perp\left[\dfrac{\chi+\cos\theta}{2\sin\theta}\right]}\times x_a x_b f_i^{(a)}(x_a) f_j^{(b)}(x_b)\frac{d\hat{\sigma}}{d\hat{t}}(\hat{s},\hat{t},\hat{u}) . \tag{2.13}$$

The kinematic invariants of the elementary reaction

$$i+j\to c+d \tag{2.14}$$

are given by

$$\hat{s}=x_a x_b s ,$$

$$\hat{t}=M_c^2-x_a x_\perp s\left[\frac{\chi-\cos\theta}{2\sin\theta}\right] , \tag{2.15}$$

$$\hat{u}=M_c^2-x_b x_\perp s\left[\frac{\chi+\cos\theta}{2\sin\theta}\right] .$$

Here

$$x_b=\frac{2\Delta+x_a x_\perp s\left[\dfrac{\chi-\cos\theta}{\sin\theta}\right]}{2x_a s-x_\perp s\left[\dfrac{\chi+\cos\theta}{\sin\theta}\right]} , \tag{2.16}$$

$$x_{\min}=\frac{2\Delta+x_\perp s\left[\dfrac{\chi+\cos\theta}{\sin\theta}\right]}{2s-x_\perp s\left[\dfrac{\chi-\cos\theta}{\sin\theta}\right]} , \tag{2.17}$$

$$\chi\equiv\left[1+\frac{4M_c^2\sin^2\theta}{x_\perp^2 s}\right]^{1/2} , \tag{2.18}$$

and

$$\Delta\equiv M_d^2-M_c^2 . \tag{2.19}$$

The elementary parton model as sketched here is, at best, an approximation to reality. For our purposes, the most important modification to the elementary picture is due to the strong interaction (QCD) corrections to the parton distributions. In leading logarithmic approximation (Gribov and Lipatov, 1972a,1972b) these corrections are process independent and can be incorporated by the replacement

$$f_i^{(a)}(x_a)\to f_i^{(a)}(x_a,Q^2) . \tag{2.20}$$

There is some ambiguity surrounding the choice of scale Q^2 in a particular process. It should be of the order of the subenergy,

$$Q^2\approx\hat{s} , \tag{2.21}$$

but the choice affects event rates, and the particular value of Q^2 used for each process will be stated in the relevant section below.

We shall consistently adopt the Born approximation to the elementary cross section and neglect higher-order strong interaction corrections. Experience in specific cases (Altarelli, Ellis, and Martinelli, 1978; Ellis *et al.*, 1980) shows that the resulting estimates of cross sections should be reliable within a factor of about 2. We also ignore "higher-twist" or hadronic wave function effects. These will produce corrections to the calculated rates which are proportional to $(M^2/Q^2)^d$, $d>1$, where M is a scale characteristic of hadronic binding. The effects should therefore be negligible for the processes we discuss.

B. Q^2-dependent parton distributions

In order to predict production cross sections in a hadron collider, we require parton distributions as functions of the Bjorken scaling variable x and Q^2. For the study of a process with characteristic mass M, the parton distributions must be known for

$$Q^2 \approx M^2 \tag{2.22}$$

and

$$x > M^2/s \ . \tag{2.23}$$

The typical momentum fraction contributing to such a process will be

$$x \approx M/\sqrt{s} \ . \tag{2.24}$$

Since we shall be concerned with characteristic masses in the range

$$10 \text{ GeV}/c^2 \lesssim M \lesssim 10 \text{ TeV}/c^2 \tag{2.25}$$

and c.m. energies between 10 and 100 TeV, the range of interest for the kinematic variables is

$$100 \text{ GeV}^2 \lesssim Q^2 \lesssim 10^8 \text{ GeV}^2 \tag{2.26}$$

and

$$x \gtrsim 10^{-4} \ . \tag{2.27}$$

Although the distributions have not been measured at such enormous values of Q^2, it is in principle quite straightforward to obtain them. Existing data from deeply inelastic scattering can be used to fix the parton distributions at some reference value of $Q^2 = Q_0^2$ over most of the x range. Evolution to $Q^2 > Q_0^2$ is then predicted (Georgi and Politzer, 1974; Gross and Wilczek, 1974) by QCD in the form of the Altarelli-Parisi (1977) equations. The resulting distributions can be checked against cross sections measured at the CERN $S\bar{p}pS$ Collider and later at the Fermilab Tevatron.

Rather than utilizing any of the parametrizations of parton distributions that appear in the literature, we have developed our own set in order to ensure reasonable behavior over the full range of variables given by (2.26) and (2.27). It is convenient to parametrize the distributions in a valence plus sea plus gluon form. The proton contains

$$\begin{aligned}
&\text{up quarks: } u_v(x,Q^2)+u_s(x,Q^2) \ , \\
&\text{down quarks: } d_v(x,Q^2)+d_s(x,Q^2) \ , \\
&\text{up antiquarks: } u_s(x,Q^2) \ , \\
&\text{down antiquarks: } d_s(x,Q^2) \ , \\
&\text{strange, charm, bottom, and top} \\
&\quad \text{quarks and antiquarks: } q_s(x,Q^2) \ , \\
&\text{gluons: } G(x,Q^2) \ .
\end{aligned} \tag{2.28}$$

The flavor quantum numbers of the proton are carried by the valence quarks. Those distributions must therefore satisfy the number sum rules

$$\begin{aligned}
&\int_0^1 dx \, u_v(x,Q^2) = 2 \ , \\
&\int_0^1 dx \, d_v(x,Q^2) = 1 \ .
\end{aligned} \tag{2.29}$$

The parton distributions are also constrained by the momentum sum rule

$$\int_0^1 dx \, x[u_v + d_v + G + 2(u_s + d_s + s_s + c_s + b_s + t_s)] = 1 \ . \tag{2.30}$$

To improve numerical convergence in the neighborhood of $x = 0$, it is convenient to recast the familiar Altarelli-Parisi equations as integro-differential equations for x times the parton distributions. The valence, or "nonsinglet," distributions satisfy

$$\begin{aligned}
\frac{dp(x,Q^2)}{d\ln Q^2} = \frac{2\alpha_s(Q^2)}{3\pi} \int_x^1 dz \frac{(1+z^2)p(y,Q^2) - 2p(x,Q^2)}{1-z} \\
+ \frac{\alpha_s(Q^2)}{\pi} \left[1 + \frac{4\ln(1-x)}{3} \right] p(x,Q^2) \ ,
\end{aligned} \tag{2.31}$$

where

$$p(x,Q^2) = xu_v(x,Q^2) \text{ or } xd_v(x,Q^2) \tag{2.32}$$

and

$$y = x/z \ .$$

The evolution of the gluon momentum distribution

$$g(x,Q^2) = xG(x,Q^2) \tag{2.33}$$

is given by

$$\begin{aligned}
\frac{dg(x,Q^2)}{d\ln Q^2} = \frac{\alpha_s(Q^2)}{\pi} \int_x^1 dz \left[\frac{3[zg(y,Q^2) - g(x,Q^2)]}{1-z} + \frac{3(1-z)(1+z^2)g(y,Q^2)}{z} \right. \\
\left. + \frac{2}{3} \frac{1+(1-z)^2}{z} \sum_{\substack{\text{flavors} \\ q}} y[q_v(y,Q^2) + 2q_s(y,Q^2)] \right] \\
+ \frac{\alpha_s(Q^2)}{\pi} \left[\frac{11}{4} - \frac{N_f}{6} + 3\ln(1-x) \right] g(x,Q^2) \ ,
\end{aligned} \tag{2.34}$$

where N_f is the number of flavors participating in the evolution at Q^2.

The evolution of the momentum distributions of the light sea quarks

$$l(x,Q^2)=xu_s(x,Q^2) \text{ or } xd_s(x,Q^2) \text{ or } xs_s(x,Q^2) \tag{2.35}$$

is described by

$$\frac{dl(x,Q^2)}{d\ln Q^2}=\frac{2\alpha_s(Q^2)}{3\pi}\int_x^1 dz\left[\frac{(1+z^2)l(y,Q^2)-2l(x,Q^2)}{1-z}+\tfrac{3}{8}[z^2+(1-z)^2]g(y,Q^2)\right]$$
$$+\frac{\alpha_s(Q^2)}{\pi}[1+\tfrac{4}{3}\ln(1-x)]l(x,Q^2)\,. \tag{2.36}$$

For the evolution of the momentum distributions of heavy sea quarks

$$h(x,Q^2)=xc_s(x,Q^2) \text{ or } xb_s(x,Q^2) \text{ or } xt_s(x,Q^2)\,, \tag{2.37}$$

we adopt the prescription of Glück, Hoffman, and Reya (1982),

$$\frac{dh(x,Q^2)}{d\ln Q^2}=\frac{2\alpha_s(Q^2)}{3\pi}\int_x^1 dz\left[\frac{(1+z^2)h(y,Q^2)-2h(x,Q^2)}{1-z}\right.$$
$$+\frac{3}{4\beta}\left[\frac{1}{2}-z(1-z)+\frac{M_q^2}{Q^2}\frac{(3-4z)z}{1-z}-\frac{16M_q^4z^2}{Q^4}\right]g(y,Q^2)$$
$$\left.-\frac{3M_q^2}{2Q^2}\left[z(1-3z)+\frac{4M_q^2z^2}{Q^2}\right]\ln\left[\frac{1+\beta}{1-\beta}\right]g(y,Q^2)\right]\theta(\beta^2)$$
$$+\frac{\alpha_s(Q^2)}{\pi}[1+\ln(1-x)]h(x,Q^2)\,, \tag{2.38}$$

where M_q is the heavy quark mass,

$$\theta(x)=\begin{cases}0, & x<0\\ 1, & x>0\,,\end{cases} \tag{2.39}$$

and

$$\beta=[1-4M_q^2/Q^2(1-z)]^{1/2}\,. \tag{2.40}$$

The running coupling constant of the strong interactions $\alpha_s(Q^2)$ may be expressed in terms of the QCD scale parameter Λ as

$$1/\alpha_s(Q^2)\equiv\frac{33-2N_f}{12\pi}\ln(Q^2/\Lambda^2)\,. \tag{2.41}$$

A prescription is required for the variation of N_f and $\alpha_s(Q^2)$ as a threshold is crossed. Since the value of Λ we shall adopt has been determined for $N_f=4$, it will be consistent to write

$$1/\alpha_s(Q^2)=\frac{25}{12\pi}\ln(Q^2/\Lambda^2)$$
$$-\frac{1}{6\pi}\sum_{i=b,t,\ldots}\theta(Q^2-16M_i^2)\ln(Q^2/16M_i^2)\,. \tag{2.42}$$

This form ensures a smooth crossing of thresholds and is equivalent to other prescriptions in common use, modulo higher-order QCD corrections which we ignore. As Q^2 approaches infinity, the contributions of all quarks become equal.

The procedure we follow is to begin with input distributions inferred from experiment at $Q_0^2=5$ GeV^2 and to integrate the evolution equations (2.31), (2.34), (2.36), and (2.38) numerically. The advantage of this over the moment method which is often employed is that for each value of x we require input information only for larger values of x, and not over the full range from 0 to 1. This is important in practice, because structure functions are poorly known at small values of x. In evolving the distributions to larger values of Q^2 we ignore all higher-twist effects. Our neglect of higher-twist effects is justified by the fact that the starting distributions were derived from data with $\langle Q^2\rangle\approx 5-50$ GeV^2. We omit higher-order QCD corrections (for which see Buras, 1980). These higher-order corrections, which are suppressed by one power of α_s, contain terms proportional to $\ln(1-x)$ and $\ln(x)$. These terms destroy the validity of QCD perturbation theory at large and small x. In the large-x region techniques are available to resume the terms of the form $\alpha_s^N\ln^{N-1}(1-x)$ for all N; effectively $\alpha_s(Q^2)$ is replaced by $\alpha_s[Q^2(1-x)]$ (Amati *et al.*, 1980; Peterman, 1980). Since the structure functions are very small in this region, this change does not affect our results significantly. The situation at small x has been considered by Gribov, Levin, and Ryskin (1983) and recently by Collins (1984). Higher-order corrections appear to be small at $x\geq 10^{-4}$ over the Q^2 range we consider. Any remaining uncertainty of course does not affect our estimates of the discovery limits for various processes, which depend only on $x>0.1$.

We must next discuss the input distributions. At the present time, the data of the CERN-Dortmund-Heidelberg-Saclay (CDHS) neutrino experiment at CERN (Abramowicz *et al.*, 1982,1983) have the greatest statistical power. We shall therefore take the CDHS structure functions as a reasonable starting point. Some of the experimental uncertainties will be addressed below.

Neutrino data are particularly useful, because measurement of the structure function $x\mathscr{F}_3$ from an isoscalar target determines the valence distributions as

$$x\mathscr{F}_3(x,Q^2)=\frac{\pi}{G_F^2 ME}\frac{1}{1-(1-y)^2}\left[\frac{d\sigma(\nu N\to\mu^- X)}{dx\,dy}-\frac{d\sigma(\bar{\nu}N\to\mu^+ X)}{dx\,dy}\right]$$
$$=x[u_v(x,Q^2)+d_v(x,Q^2)]\ , \tag{2.43}$$

where G_F is the Fermi constant, M is the nucleon mass, E is the neutrino beam energy, and the Bjorken scaling variables are defined by

$$x\equiv Q^2/2M\nu \tag{2.44}$$

and

$$y=\nu/E\ , \tag{2.45}$$

where $\nu=E-E_\mu$ is the inelasticity parameter. The CDHS measurements give

$$x\mathscr{F}_3(x,Q_0^2)=1.66x^{0.374}(1-x)^{3.31}(1+5.86x)\ , \tag{2.46}$$

for $x>0.03$ and $Q_0^2=5$ GeV^2. The normalization has been fixed by continuing to $x=0$ and enforcing the baryon number sum rule. A lowest-order QCD fit used to evolve the parametrization (downward) to $Q^2=Q_0^2$ yielded the leading-order scale parameter

$$\Lambda=275\pm 80\ \text{MeV}\ . \tag{2.47}$$

The up- and down-quark valence distributions can be separated using charge-current cross sections for hydrogen and deuterium targets. Data from the CDHS and the Big European Bubble Chamber (BEBC) (Bosetti *et al.*, 1982) experiments are shown in Fig. 2, which suggests the parametrization (Eisele, 1982)

$$d_v(x)/u_v(x)=0.57(1-x)\ . \tag{2.48}$$

The data are insufficient to exhibit any Q^2 dependence, and are consistent with the SLAC-MIT electron scattering measurements (Bodek *et al.*, 1979). The simplest guess that $d_v(x)/u_v(x)=\frac{1}{2}$ is not in agreement with the data.

Once the valence distributions are known, the sea distributions may be determined from measurements of the structure function $\mathscr{F}_2$ on isoscalar targets. Data on the flavor dependence of the sea are rather sparse. In principle, the ratio $u_s(x)/d_s(x)$ can be extracted from neutrino data; it is consistent with unity (Eisele, 1982). The strange sea can be measured directly in antineutrino-induced dimuon production. The shape of $s_s(x)$ is shown in Fig. 3 to be consistent with the shape of $u_s(x)+d_s(x)$ determined from $\mathscr{F}_2$. The CDHS parametrizations we use are derived using

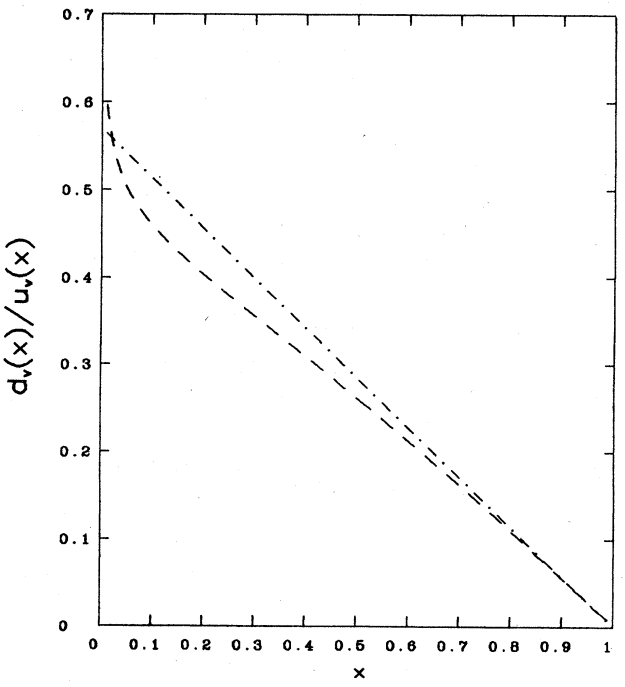

FIG. 2. Ratio (dotted-dashed line) of valence distributions of up and down quarks (after Eisele, 1982). The dashed line is the result of the parton distributions given by (2.55).

$$2s_s(x)/[u_s(x)+d_s(x)]=0.43 \tag{2.49}$$

at $Q^2=5$ GeV^2.

Bounds on the rate of same-sign dimuon production in neutrino-nucleon collisions (Abramowicz *et al.*, 1982, 1983; Eisele, 1982) limit the charmed sea:

$$\int_0^1 dx\, xc_s(x)\le\tfrac{1}{2}\int_0^1 dx\, xs_s(x)\ . \tag{2.50}$$

We shall assume that at $Q^2=5$ GeV^2 the sea distributions of charmed and heavier quarks can be neglected.

Once the quark distributions have been determined, the integral $\int_0^1 dx\, xG(x)$ of the gluon momentum distribution can be determined from the momentum sum rule. The shape of $G(x)$ cannot be measured directly in electroweak interactions, but a constraint on the shape can be inferred as follows. With increasing Q^2, QCD evolution causes gluons with momentum fraction x_1 to generate antiquarks with momentum fraction $x_0<x_1$. A failure to find antiquarks at values of x larger than some value x_0 thus constrains $G(x,Q_0^2)$. There is of course a strong correlation between $G(x,Q^2)$ and the QCD scale parameter Λ. The larger Λ is, the more rapidly $G(x,Q^2)$ will steepen, and the broader the input distribution $G(x,Q_0^2)$ can be. Ideally one would determine Λ from the evolution of the nonsinglet structure function and then extract $G(x,Q^2)$ from singlet structure functions. The existing data do not permit this to be done unambiguously.

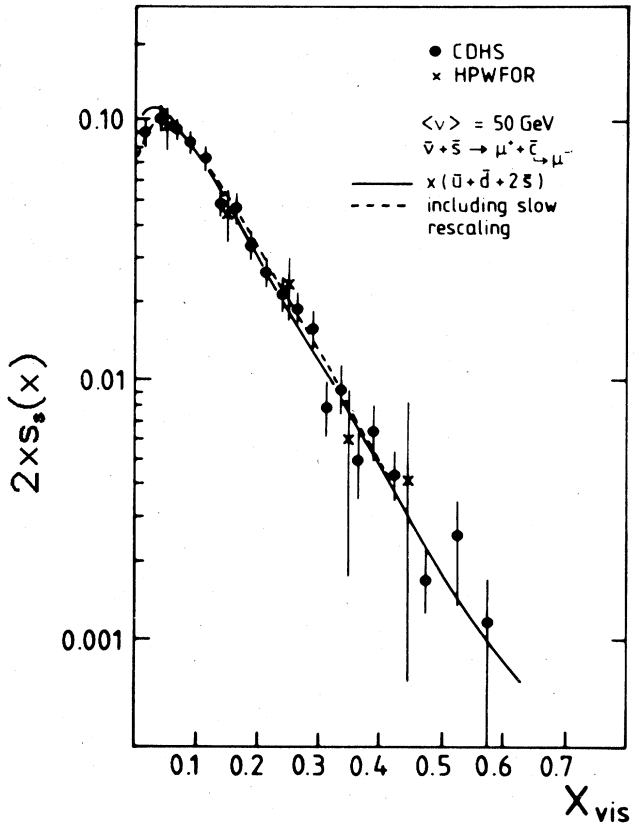

FIG. 3. Comparison of the shape of the strange quark distribution determined in opposite-sign dimuon events (data points) with the antiquark distribution (solid line) deduced from $\mathscr{F}_2$ (after Eisele, 1982).

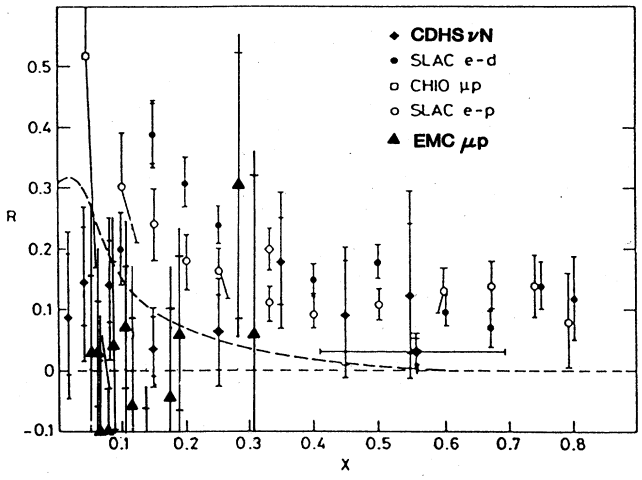

FIG. 4. The ratio $R=\sigma_L/\sigma_T$ as a function of x for the CDHS neutrino data (Abramowicz *et al.*, 1983), compared with measurements in *ep* and *ed* scattering (Bodek *et al.*, 1979) and μN scattering (Gordon *et al.*, 1979; Aubert *et al.*, 1983a). The curve is the QCD prediction for the kinematic range of the CDHS experiment.

It is therefore necessary to use the singlet structure functions $\mathscr{F}_2(x,Q^2)$ together with the antiquark distributions $q_s(x,Q^2)$ to make a simultaneous fit to Λ and $G(x,Q^2)$. The difficult-to-measure ratio $R=\sigma_L/\sigma_T$ enters the analysis. The available data, summarized in Fig. 4, do not determine R precisely. Two fits have been presented to the CDHS data.

Under the assumption that $R=0.1$, Abramowicz *et al.* (1983) determine the combination

$$q_v(x,Q_0^2)\equiv x[u_s(x,Q_0^2)+d_s(x,Q_0^2)+2s_s(x,Q_0^2)] =0.52(1-x)^{8.54}, \tag{2.51}$$

$$\mathscr{F}_2(x,Q_0^2)=x\{u_v(x,Q_0^2)+d_v(x,Q_0^2) +2[u_s(x,Q_0^2)+d_s(x,Q_0^2)+s_s(x,Q_0^2)]\} =(1.1+4.07x)(1-x)^{3.19}, \tag{2.52}$$

and

$$xG(x,Q_0^2)=(2.62+9.17x)(1-x)^{5.90}, \tag{2.53}$$

with

$$\Lambda=180\pm20\ \text{MeV} \tag{2.54}$$

and $Q_0^2=5$ GeV^2. In Fig. 5 we show the quantities $q_v(x,Q_0^2)$, $xG(x,Q_0^2)$, and $x[u_v(x,Q_0^2)+d_v(x,Q_0^2)]$ determined from (2.49) and (2.51)–(2.53). We shall use the following parametrization which reproduces these distributions:

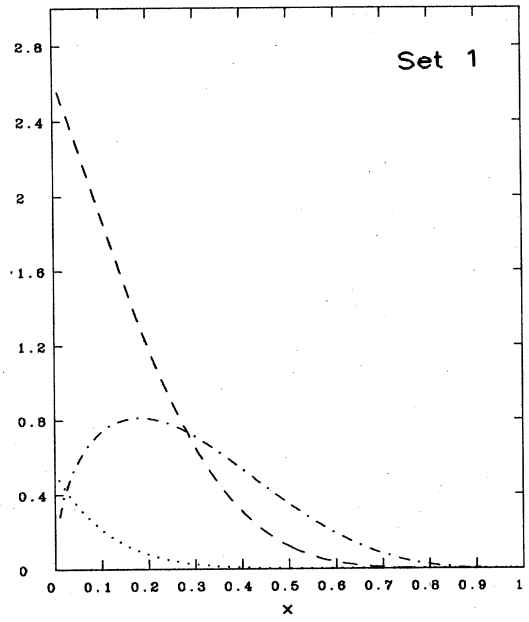

FIG. 5. Parton distributions of Set 1 at $Q^2=5$ GeV^2: valence quark distribution $x[u_v(x)+d_v(x)]$ (dotted-dashed line), $xG(x)$ (dashed line), and $q_v(x)$ (dotted line).

$$
\begin{aligned}
&xu_v(x,Q_0^2)=1.78x^{0.5}(1-x^{1.51})^{3.5}\,,\\
&xd_v(x,Q_0^2)=0.67x^{0.4}(1-x^{1.51})^{4.5}\,,\\
&xu_s(x,Q_0^2)=xd_s(x,Q_0^2)=0.182(1-x)^{8.54}\,,\\
&xs_s(x,Q_0^2)=0.081(1-x)^{8.54}\,,\\
&xG(x,Q_0^2)=(2.62+9.17x)(1-x)^{5.90}\,,\\
&\Lambda=200\text{ MeV}\,.
\end{aligned}
\tag{2.55}
$$

The d_v/u_v ratio implied by this set is consistent with the measurements collected in Fig. 2. We shall refer to this parametrization as Set 1.

Under the assumption that $R=\sigma_L/\sigma_T$ has the behavior prescribed by QCD, Abramowicz *et al.* (1983) find

$$q_v(x,Q_0^2)=0.53(1-x)^{7.12}\,, \tag{2.56}$$

$$\mathcal{F}_2(x,Q_0^2)=(1.18+3.859x)(1-x)^{3.12}\,, \tag{2.57}$$

and

$$xG(x,Q_0^2)=(1.75+15.575x)(1-x)^{6.03}\,, \tag{2.58}$$

with

$$\Lambda=290\pm30\text{ MeV} \tag{2.59}$$

and $Q_0^2=5$ GeV^2. The resulting valence quark and gluon distributions and the combination $q_v(x,Q_0^2)$ are shown in Fig. 6. Notice that the larger value of Λ is correlated with a harder gluon distribution at Q_0^2, i.e., one with more gluons at large values of x. These are reproduced by the following parametrization (Set 2):

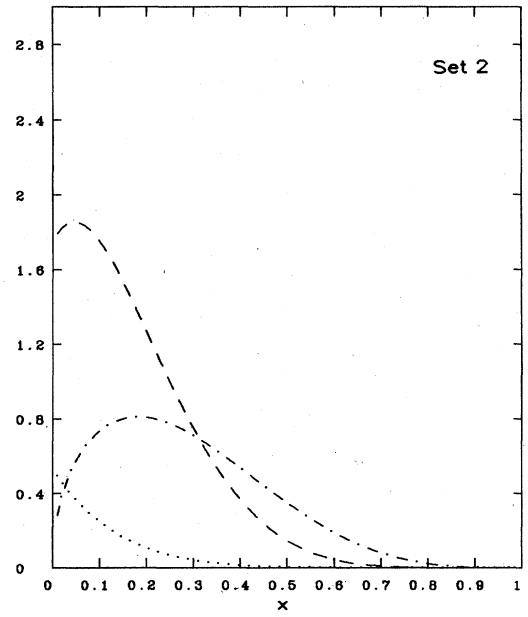

FIG. 6. Parton distributions of Set 2 at $Q^2=5$ GeV^2: valence quark distribution $x[u_v(x)+d_v(x)]$ (dotted-dashed line), $xG(x)$ (dashed line), and $q_v(x)$ (dotted line).

$$
\begin{aligned}
&xu_s(x,Q_0^2)=xd_s(x,Q_0^2)=0.185(1-x)^{7.12}\,,\\
&xs_s(x,Q_0^2)=0.0795(1-x)^{7.12}\,,\\
&xG(x,Q_0^2)=(1.75+15.575x)(1-x)^{6.03}\,,\\
&\Lambda=290\text{ MeV}\,,
\end{aligned}
\tag{2.60}
$$

with the valence distributions $xu_v(x,Q_0^2)$ and $xd_v(x,Q_0^2)$ given in (2.55).

It is appropriate to compare our two input distributions with other determinations of parton distribution functions. In Figs. 7 and 8 we compare our parametrizations with the determinations of the valence, sea, and gluon distributions presented by the CHARM neutrino experiment at CERN (Bergsma *et al.*, 1983) at $Q^2=10$ and 50 GeV^2. The agreement of the valence and gluon distributions is satisfactory, but the disagreement seen in the sea distribution is striking. We remark that whereas our distributions satisfy the momentum sum rule to better than 1%, momentum conservation was not explicitly enforced in the CHARM Collaboration fits.

There are two other indications that the CDHS analysis might somewhat underestimate the sea quark distributions. The ratio of deeply inelastic lepton scattering on neutron and proton targets has been measured by the SLAC-MIT Collaboration (Bodek *et al.*, 1979) and by the European Muon Collaboration (Aubert *et al.*, 1983b). Their data are compared in Fig. 9 with the prediction of our Set 2 at $Q^2=10$ GeV^2. The prediction does not depend appreciably upon Q^2 and is similar for Set 1. The

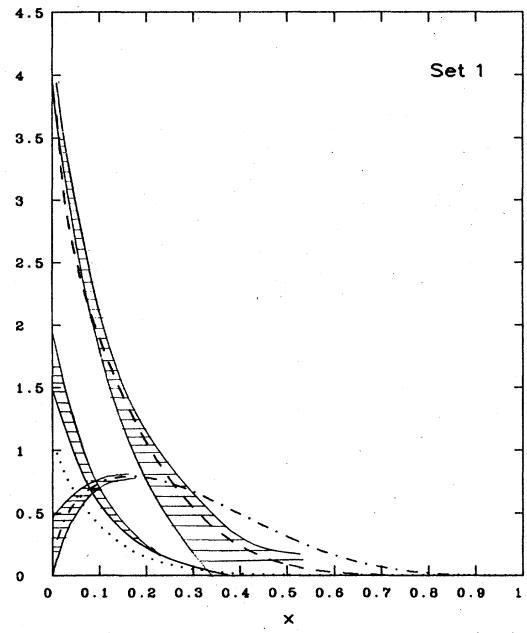

FIG. 7. Comparison of the gluon distribution $xG(x,Q^2)$ (dashed line), the valence quark distribution $x[u_v(x,Q^2)+d_v(x,Q^2)]$ (dotted-dashed line), and the sea quark distribution $2x[u_s(x,Q^2)+d_s(x,Q^2)+s_s(x,Q^2)+c_s(x,Q^2)]$ (dotted line) of Set 1 with the determination (shaded bands) of Bergsma *et al.* (1983) at $Q^2=10$ GeV^2.

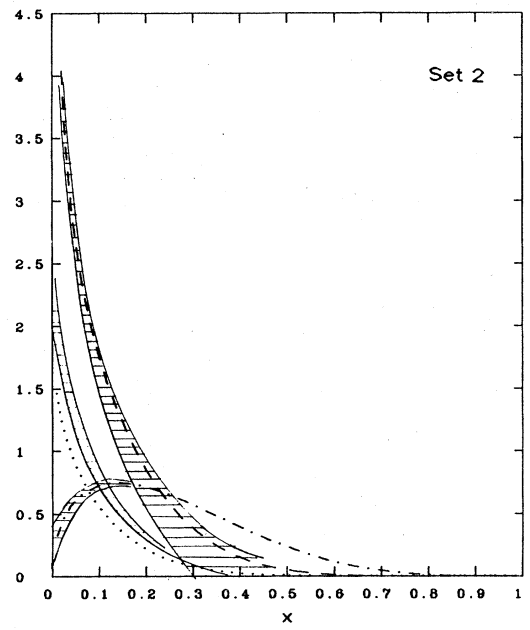

FIG. 8. Same comparison as Fig. 7, for Set 2 at $Q^2=50$ GeV^2.

fact that the curve approaches unity at small x less rapidly than the data do suggests the need for an enhanced sea contribution. A second, independent suggestion that a stronger sea may be required comes from the data of the Caltech-Columbia-Fermilab-Rochester-Rockefeller neutrino experiment (MacFarlane *et al.*, 1983), in which $\mathcal{F}_2(x,Q^2)$ is more strongly peaked at small x than in the CDHS measurements.

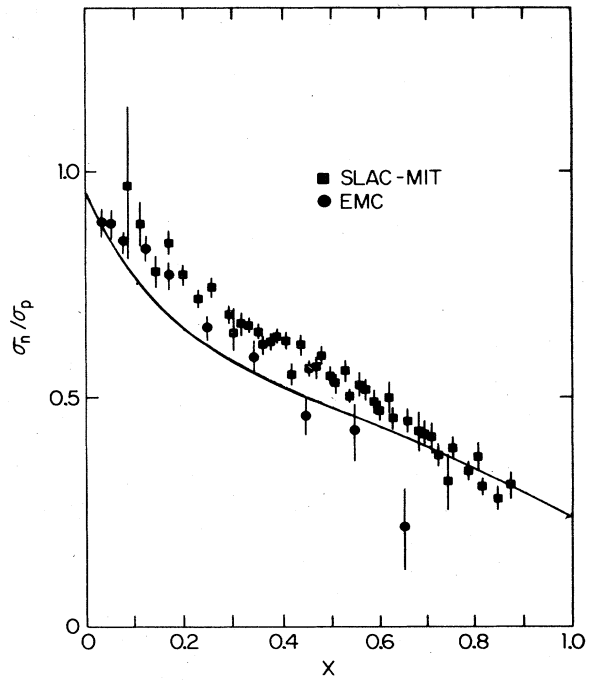

FIG. 9. x dependence of the ratio $\sigma(l^{\pm}n)/\sigma(l^{\pm}p)$ of the cross sections for deeply inelastic scattering on nucleons. The solid curve is given by the parton distributions of Set 2 at $Q^2=10$ GeV^2. The data are from Bodek *et al.* (1979) and Aubert *et al.* (1983b).

The calculated Q^2 dependence of $xG(x,Q^2)$ and $xu_s(x,Q^2)$ are shown for Set 1 in Figs. 10 and 11. The expected growth of the distributions at small x is apparent. The corresponding results for Set 2 are shown in Figs. 12 and 13. The flavor composition of the sea can be deduced from Figs. 14–17, which show the evolution of $xs_s(x,Q^2)$, $xc_s(x,Q^2)$, $xb_s(x,Q^2)$, and $xt_s(x,Q^2)$ for Set 2.

We include only the perturbative evolution of the heavy quark sea from the process $g\to Q\bar{Q}$, and neglect the nonperturbative, or intrinsic, component proposed by Brodsky *et al.* (1980,1981). Experiments (Aubert *et al.*, 1983d,1983e; Ritchie *et al.*, 1983) have not given any positive indication for an important intrinsic charm component. In deriving the heavy quark distributions we have used

$$M_b=5.5\ \text{GeV}/c^2\ ,\qquad M_t=30\ \text{GeV}/c^2\ . \tag{2.61}$$

It can be seen that flavor SU(3) symmetry of the sea is rapidly established at small x, but that mass effects suppress the heavier flavors even at $Q^2=10^8$ GeV$^2=100$ TeV^2, where $u_s{:}s_s{:}c_s{:}b_s{:}t_s::1{:}0.89{:}0.36{:}0.33{:}0.21$ at $x=0.01$. Parametrizations of the Q^2-dependent structure functions are given in the Appendix.

Let us now examine further some of the uncertainties and ambiguities of the structure functions. The distribution functions are not well measured at small values of x. As a consequence, we may be concerned that there are important uncertainties in that region. To be more specific, present data do not extend below $x=0.01$ and are rather sparse in the interval $0.01<x<0.1$. Fits to structure functions therefore have to be based on plausible but poorly controlled extrapolations to $x=0$. Sum rules provide broad constraints. For example, the requirement that the momentum integral of the gluon distribution be finite means that $xG(x,Q^2)$ must be less singular than

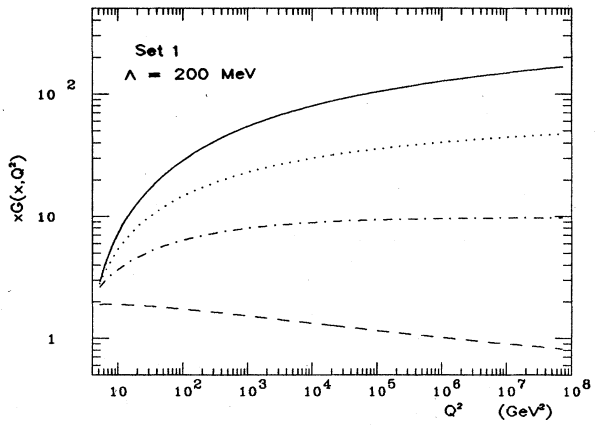

FIG. 10. Q^2 evolution of the gluon distribution $xG(x,Q^2)$ of Set 1: $x=10^{-4}$ (solid line), 10^{-3} (dotted line), 10^{-2} (dotted-dashed line), 0.1 (dashed line).

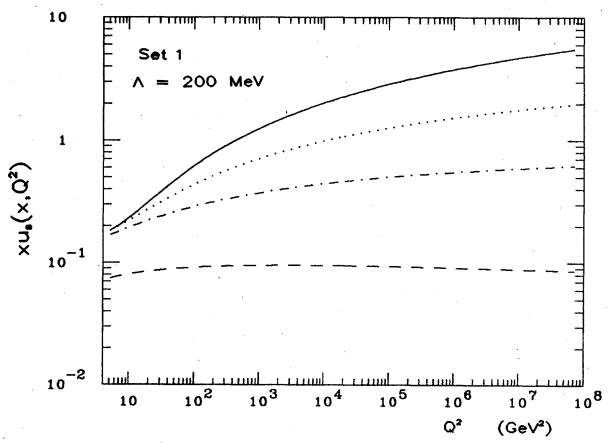

FIG. 11. Q^2 evolution of the up antiquark distribution $xu_s(x,Q^2)$ of Set 1. The down antiquark distribution $xd_s(x,Q^2)$ is equal. Same values of x as Fig. 10.

$1/x$ at $x=0$.

To explore the uncertainties in the small-x region we consider two modifications to the gluon distribution of Set 1, as follows:

$$xG(x,Q_0^2)=(2.62+9.17x)(1-x)^{5.90}\ ,\quad x>0.01\ , \tag{2.62}$$

and

$$xG(x,Q_0^2)=\begin{cases}0.444x^{-1/2}-1.886 & \text{(a)}\\ 25.56x^{1/2} & \text{(b)}\end{cases}\ \text{for } x<0.01\ . \tag{2.63}$$

These modifications match continuously at $x=0.01$ and are constrained to change the gluon momentum integral by no more than 10%; we demand that

$$\int_0^1 dx\, xG(x,Q_0^2)=0.55\pm0.05\ . \tag{2.64}$$

The results of these changes are presented in Figs. 18–20, which show the Q^2 variation of $xG(x,Q^2)$ at $x=10^{-2}$, 10^{-3}, and 10^{-4} for Set 1, modification (a), and modification (b), respectively. The drastic differences built into the distributions at low Q^2 diminish rapidly as Q^2 rises. At $Q^2=Q_0^2=5$ GeV^2, the values of $xG(x,Q^2)$ given by modifications (a) and (b) differ by a factor of 160 at $x=10^{-4}$. After evolution to $Q^2=10^3$ GeV^2, quite a modest value on the supercollider scale, this difference is diminished to a factor of 2. We regard this example as extremely reassuring, for it implies that the gluon distribution at small x and large Q^2 may be much better determined than is commonly believed.

Another source of uncertainty is variation of the QCD scale parameter Λ. To study this effect we have evolved the starting distributions of Set 1 with $\Lambda=100$ MeV. The results are shown in Fig. 21 for $xG(x,Q^2)$ and in Fig. 22 for $xu_s(x,Q^2)$. Comparing these with the plots of Figs. 10 and 11, we find that over the range $Q^2=10^4-10^8$ GeV^2 the effect of this charge is to alter the distributions by no more than 20%.

The input structure functions we use have been derived principally from neutrino scattering from heavy nuclei under the assumption that these are related additively to proton and neutron structure functions. Recent data (Au-

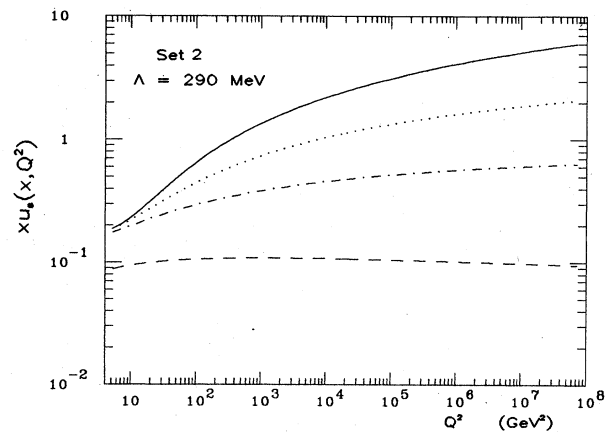

FIG. 13. Q^2 evolution of the up antiquark distribution $xu_s(x,Q^2)$ of Set 2. Same x values as Fig. 10.

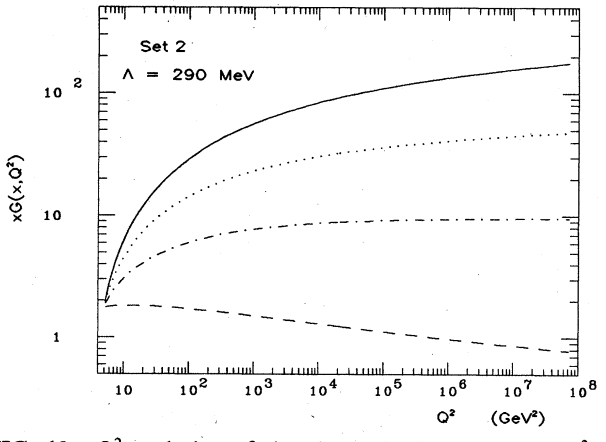

FIG. 12. Q^2 evolution of the gluon distribution $xG(x,Q^2)$ of Set 2. Same x values as Fig. 10.

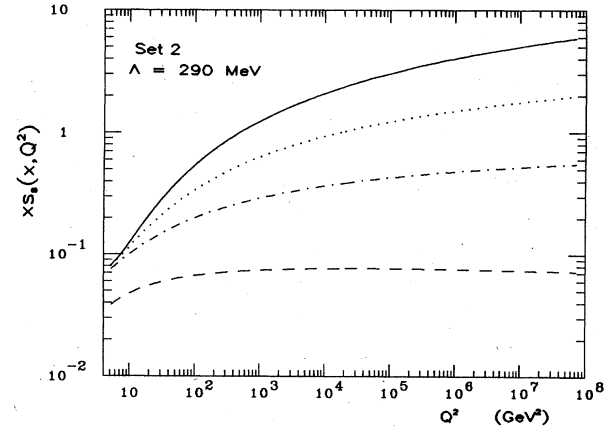

FIG. 14. Q^2 evolution of the strange quark distribution $xs_s(x,Q^2)$ of Set 2. Same x values as Fig. 10.

bert *et al.*, 1983c; Bodek *et al.*, 1983a,1983b; Cooper *et al.*, 1984; Asratyan *et al.*, 1983; Arnold *et al.*, 1984) indicate that this is not the case. Representative measurements are shown in Fig. 23. It is generally agreed that the ratio F_2^{Fe}/F_2^D of the structure function per nucleon (extracted neglecting nuclear effects) is 10—15% below unity at $x \approx 0.6$. This behavior cannot be explained by Fermi motion (Bodek and Ritchie, 1981) within the nucleus. At small values of x the experimental situation is confused. The European Muon Collaboration data (Aubert *et al.*, 1983c) show a significant enhancement of the iron structure function at $x \lesssim 0.1$, but this is not confirmed by the SLAC data of Arnold *et al.* (1983) at somewhat smaller values of Q^2. These observations suggest that the valence distributions we have used may be about 10% too small in the neighborhood of $x=0.6$ and that the sea distributions could be as much as 15% too large at $x=0.1$. Given the earlier hints that the sea distributions may be slightly too small, we do not regard this as a serious problem. Better data at larger values of Q^2 would again be helpful, as would a theoretical understanding of the nuclear phenomenon.[2] The effect of the nuclear environment on $G(x,Q_0^2)$ and Λ is not known.

We conclude this discussion with a brief comment on other parametrizations of parton distributions (Glück, Hoffmann, and Reya, 1982; Baier, Engels, and Petersson, 1979; Owens and Reya, 1978; Duke and Owens, 1984). The standard practice has been to evolve input distributions at Q_0^2 over a range in Q^2 and to fit the resulting distributions to analytic forms in x and Q^2. Most of these fits have been available for several years and entail values of the scale parameter Λ of order 400 MeV, somewhat larger than the current best fits. For comparison with the input distributions we have used, which are shown in Figs. 5 and 6, we plot in Figs. 24—27 the parton distributions at $Q^2=5$ GeV^2 of Baier, Engels, and Petersson (1979), and of Glück, Hoffmann, and Reya (1982), both with $\Lambda=400$ MeV, and both the "hard-gluon" ($\Lambda=400$ MeV) and "soft-gluon" ($\Lambda=200$ MeV) distributions of Duke and Owens (1984). The distributions which involve the large value of $\Lambda=400$ MeV have harder gluon distributions than do our parametrizations, as expected. We do not display the Owens-Reya (1978) distributions, because the low value of $Q_0^2=1.8$ GeV^2 used there invites distortions due to higher-twist effects, and because they are superseded by the work of Duke and Owens (1984). The distributions of Baier *et al.* (1979) and of Duke and Owens (1984) have SU(3)-symmetric sea distributions and do not include heavy flavors. In addition, Baier and collaborators (1979) have fixed $u_v(x,Q^2)=2d_v(x,Q^2)$ at all values of x and Q^2.

The Q^2 evolution of these fits is shown in Figs. 28—31, where we display the gluon momentum distribution $xG(x,Q^2)$. Figure 28 shows that the parametrization of

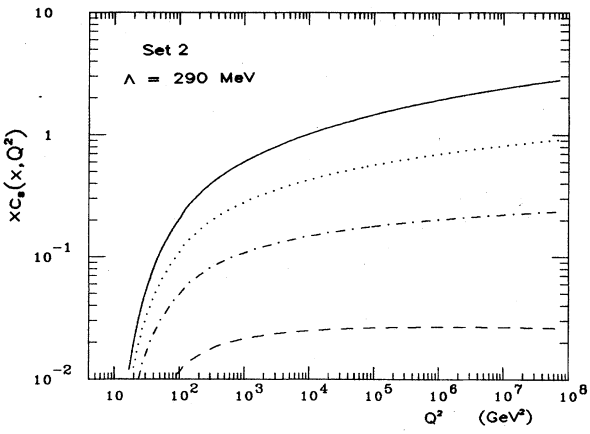

FIG. 15. Q^2 evolution of the charmed quark distribution $xc_s(x,Q^2)$ of Set 2. Same x values as Fig. 10.

Baier *et al.* (1979) is unreliable for $Q^2 \gtrsim 10^3$ GeV^2, where $xG(x=0.1,Q^2)$ begins to increase with Q^2. The parametrization of Glück *et al.* (1982) is correctly claimed (see Fig. 29) to be sensible for $x>0.01$ and $Q^2<4\times10^4$ GeV^2. Notice, however, the odd behavior at small values of x that results from blind extrapolation of their fit. Moreover, this parametrization deviates by as much as 20% from the exact result obtained by evolution even within the claimed domain of validity. Figure 30 shows that the "hard-gluon" parametrization of Duke and Owens (1984) cannot be trusted for $Q^2 \gtrsim 10^5$ GeV^2. Their soft-gluon parametrization behaves reasonably all the way to $Q^2=10^8$ GeV^2, as shown in Fig. 31. Comparison with Figs. 10 and 12 shows that our distributions contain fewer gluons at small x and large Q^2 than did these earlier parametrizations.

C. Parton-parton luminosities

In the succeeding sections of this paper we shall use the parton distributions derived in Sec. II.B to compute differential and total cross sections for many reactions of po-

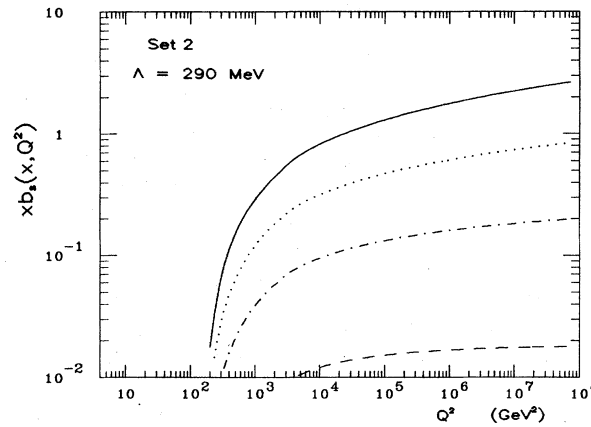

FIG. 16. Q^2 evolution of the bottom quark distribution $xb_s(x,Q^2)$ of Set 2. Same x values as Fig. 10.

[2]For a review and a list of theoretical references, see Llewellyn Smith (1983).

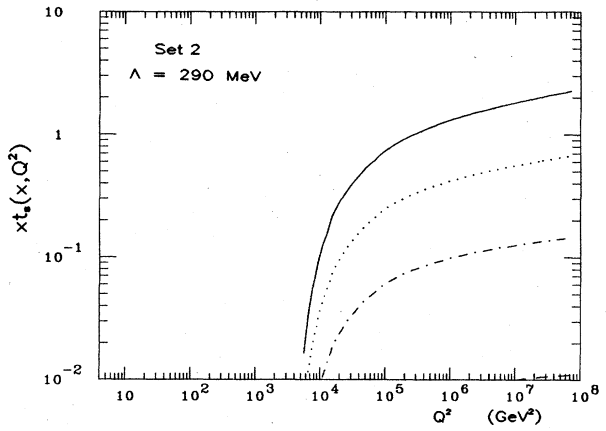

FIG. 17. Q^2 evolution of the top quark distribution $xt_s(x,Q^2)$ of Set 2. Same x values as Fig. 10.

tential interest at the supercollider. Such detailed calculations are of unquestioned value for detector studies and for in-depth consideration of the physics possibilities. However, much can be learned about the general issues of beam type, energy, and luminosity by comparing the luminosities of parton-parton collisions as a function of $w=\sqrt{\hat{s}}$, the c.m. energy of the colliding partons. One convenient quantity is the differential luminosity

$$\tau\frac{d\mathscr{L}}{d\tau}\equiv\frac{\tau}{1+\delta_{ij}}\int_\tau^1 dx[f_i^{(a)}(x)f_j^{(b)}(\tau/x) +f_j^{(a)}(x)f_i^{(b)}(\tau/x)]/x\ , \tag{2.65}$$

where $f_i^{(a)}(x)$ is the number distribution of partons of species i carrying momentum fraction x of hadron a. For hadrons colliding with c.m. energy $\sqrt{s}$, the scaling variable τ is given by

$$\tau=w^2/s=\hat{s}/s\ . \tag{2.66}$$

The differential luminosity represents the number of parton-parton collisions with scaled c.m. energies in the interval $(\tau,\tau+d\tau)$ per hadron-hadron collision. Thus the differential cross section for the hadronic reaction

$$a+b\to\alpha+\text{anything} \tag{2.67}$$

is given by

$$\frac{d\sigma}{d\tau}(ab\to\alpha X)=\sum_{ij}\frac{d\mathscr{L}_{ij}}{d\tau}\hat{\sigma}(ij\to\alpha)\ , \tag{2.68}$$

where $\hat{\sigma}(ij\to\alpha)$ is the cross section for the operative elementary process. Explicit forms of $\hat{\sigma}$ will be cited elsewhere in this paper.

The interesting hard-scattering processes that define much of the physics motivation of a multi-TeV collider have a common asymptotic form prescribed by dimensional analysis

$$\sigma(\hat{s})=c/\hat{s}\ . \tag{2.69}$$

For a strong-interaction process, such as jet pair production, c is typically of order $(\alpha_s/\pi)^2$. For a typical electroweak process such as lepton pair production, c is ap-

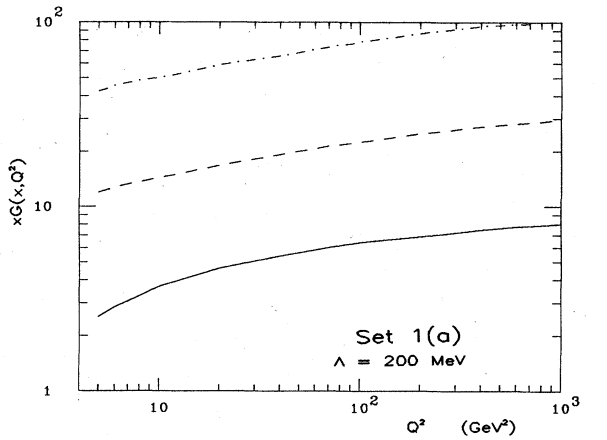

FIG. 19. Q^2 evolution of the gluon distribution function $xG(x,Q^2)$ of Set 1(a) for $x=10^{-2}$ (solid line), 10^{-3} (dashed line), 10^{-4} (dotted-dashed line).

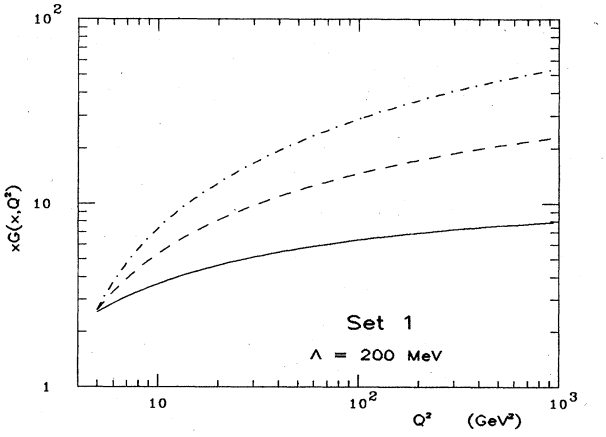

FIG. 18. Q^2 evolution of the gluon distribution function $xG(x,Q^2)$ of Set 1 for $x=10^{-2}$ (solid line), 10^{-3} (dashed line), 10^{-4} (dotted-dashed line).

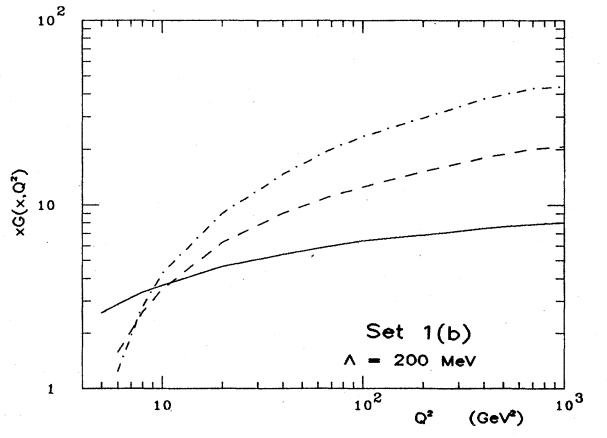

FIG. 20. Q^2 evolution of the gluon distribution function $xG(x,Q^2)$ of Set 1(b) for $x=10^{-2}$ (solid line), 10^{-3} (dashed line), 10^{-4} (dotted-dashed line).

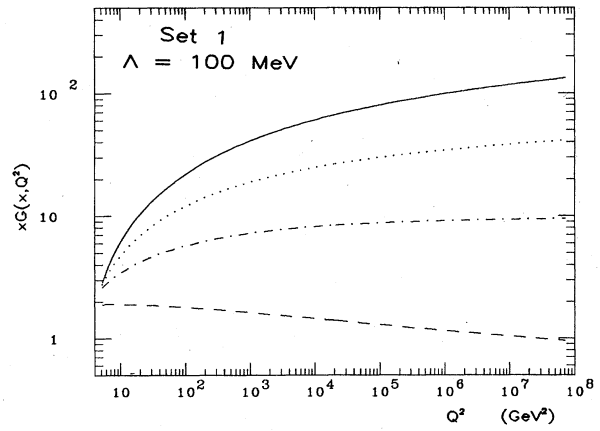

FIG. 21. Q^2 evolution of the gluon distribution function $xG(x,Q^2)$ of Set 1 with $\Lambda=100$ MeV. Same x values as Fig. 10.

proximately $(\alpha/\pi)^2$. Resonance production cross sections are proportional to τ. Consequently, the quantity $(\tau/\hat{s})d\mathcal{L}/d\tau$, which has dimensions of a cross section, provides a useful measure of the reach of a collider of given energy and hadron-hadron luminosity. In Figs. 32—50 we plot $(\tau/\hat{s})d\mathcal{L}/d\tau$ as a function of $\hat{s}$, the square of the parton-parton c.m. energy, for a number of parton combinations in proton-proton collisions at total c.m. energies of 2, 10, 20, 40, 70, and 100 TeV. These luminosities are based upon Set 2 of parton distributions characterized by $\Lambda=290$ MeV, as specified in Eq. (2.60); we have taken $Q^2=\hat{s}$. Some additional luminosities are displayed in Figs. 51—56 for proton-antiproton collisions, where those differ appreciably from their counterparts in proton-proton collisions.

The difference between pp and $\bar{p}p$ collisions is particularly pronounced for the $u\bar{u}$ luminosity, because the antiproton carries valence antiquarks, whereas the proton does not. The ratio of $\tau d\mathcal{L}/d\tau$ for $u\bar{u}$ interactions in $\bar{p}p$ and pp collisions is plotted as a function of the parton-parton c.m. energy w in Fig. 57 for several collider energies. Roughly speaking, the advantage of $\bar{p}p$ over pp collisions in this channel becomes appreciable for $\sqrt{\tau}=w/\sqrt{s}\gtrsim 0.1$. Whether this advantage at large values of $\sqrt{\tau}$ can be exploited depends upon the event rate determined by cross section and luminosity.

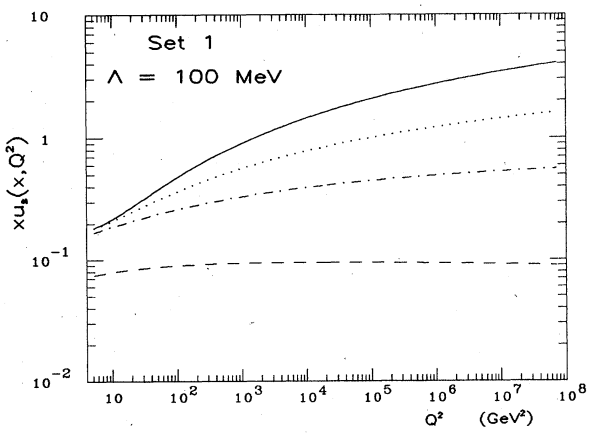

FIG. 22. Q^2 evolution of the up antiquark distribution $xu_s(x,Q^2)$ of Set 1 with $\Lambda=100$ MeV. Same x values as Fig. 10.

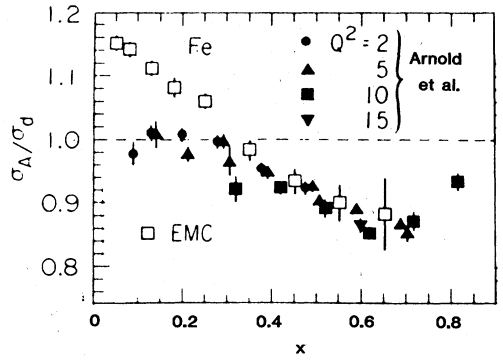

FIG. 23. The ratio of the nucleon structure functions F_2^A measured on iron and deuterium as a function of x. Data are from the European Muon Collaboration (Aubert *et al.*, 1983c) and SLAC Experiment E-139 (Arnold *et al.*, 1983).

Especially useful for judging the effects of changes in luminosity or beam energy are contour plots showing at each energy $\sqrt{s}$ the parton-parton energy $\sqrt{\hat{s}}$ corresponding to a particular value of $(\tau/\hat{s})d\mathcal{L}/d\tau$. Some important cases are displayed in Figs. 58—63 for the parton distributions of Set 2, and in Figs. 64—69 for the parton distributions of Set 1.

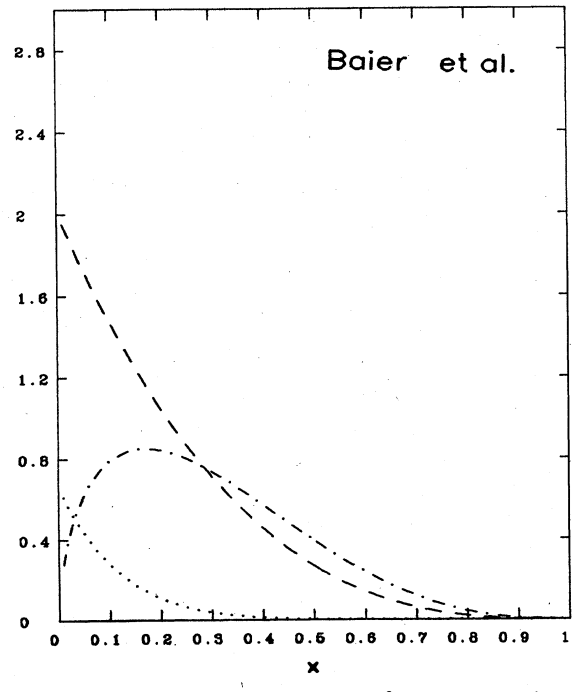

FIG. 24. The parton distributions of Baier, Engels, and Petersson (1979), at $Q^2=5$ GeV^2: valence quark distribution $x[u_v(x)+d_v(x)]$ (dotted-dashed line), $xG(x)$ (dashed line), and $q_v(x)$ (dotted line).

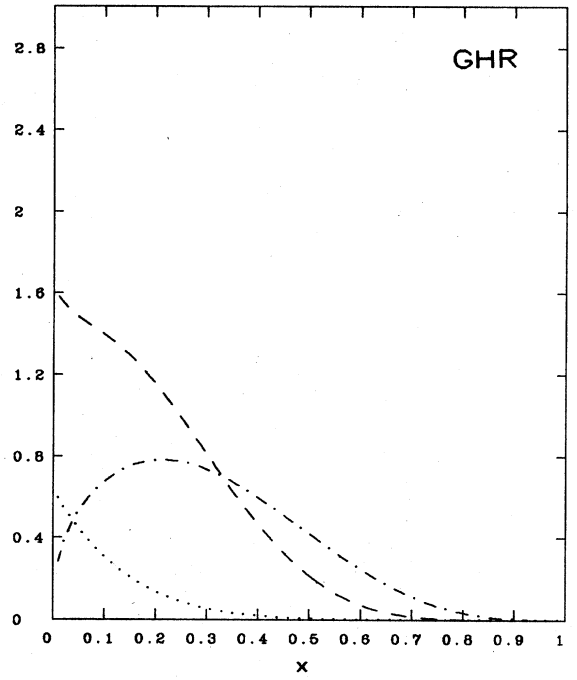

FIG. 25. Parton distributions of Glück, Hoffmann, and Reya (1982), at $Q^2=5$ GeV^2: valence quark distribution $x[u_v(x)+d_v(x)]$ (dotted-dashed line), $xG(x)$ (dashed line), and q_v (dotted line).

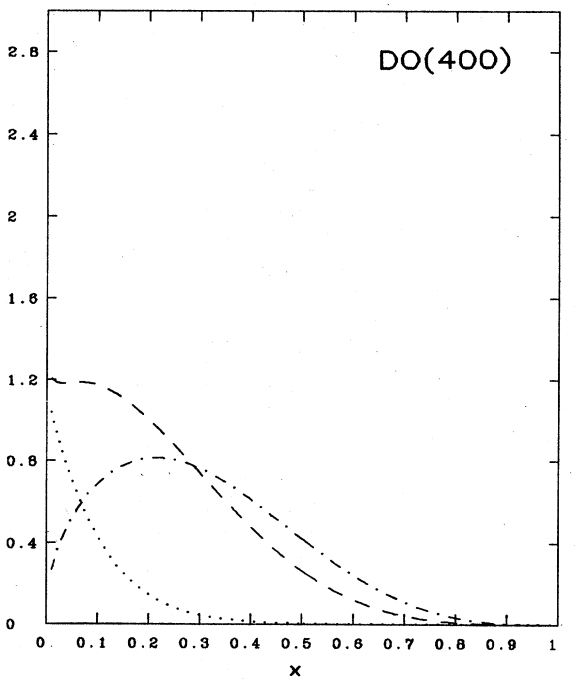

FIG. 26. "Hard-gluon" ($\Lambda=400$ MeV) parton distributions of Duke and Owens (1984) at $Q^2=5$ GeV^2: valence quark distribution $x[u_v(x)+d_v(x)]$ (dotted-dashed line), $xG(x)$ (dashed line), and $q_v(x)$ (dotted line).

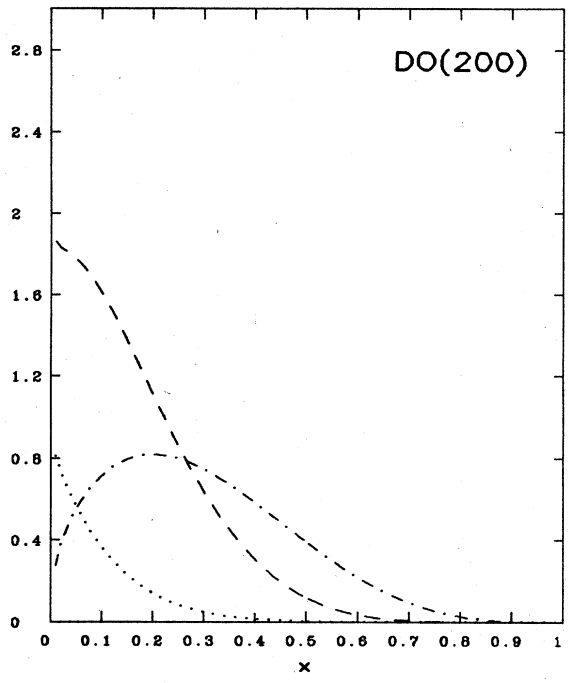

FIG. 27. "Soft-gluon" ($\Lambda=200$ MeV) parton distributions of Duke and Owens (1984) at $Q^2=5$ GeV^2: valence quark distribution $x[u_v(x)+d_v(x)]$ (dotted-dashed line), $xG(x)$ (dashed line), and $q_v(x)$ (dotted line).

The contour plots contain a great deal of information, and will reward a detailed study. Here we call attention to only one particularly general and important feature. Contour lines rise less rapidly than $\sqrt{\hat{s}}=\text{const}\times\sqrt{s}$, principally because of the $1/\hat{s}$ behavior of the hard-scattering cross sections. This means in general that to take full advantage of the potential increase in discovery reach afforded by higher collider energies, it is necessary to increase luminosity as well as beam energy. This effect is universal, but is more pronounced for valence-valence interactions than for gluon-gluon interactions.

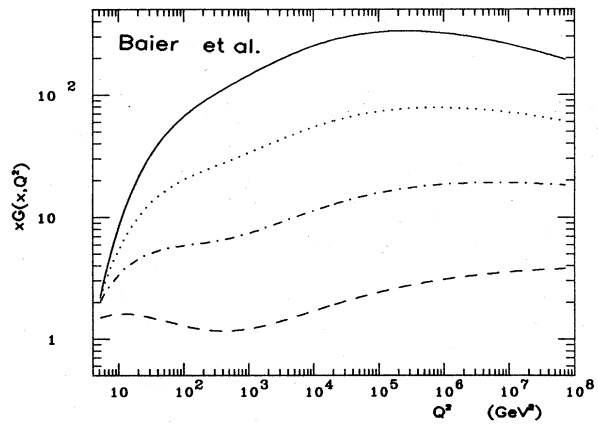

FIG. 28. Q^2 evolution of the gluon distribution $xG(x,Q^2)$ of Baier, Engels, and Petersson (1979). Same x values as Fig. 10.

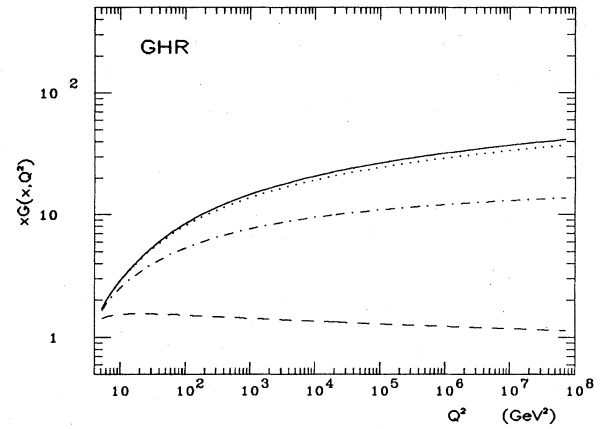

FIG. 29. Q^2 evolution of the gluon distribution $xG(x,Q^2)$ of Glück, Hoffmann, and Reya (1982). Same x values as Fig. 10.

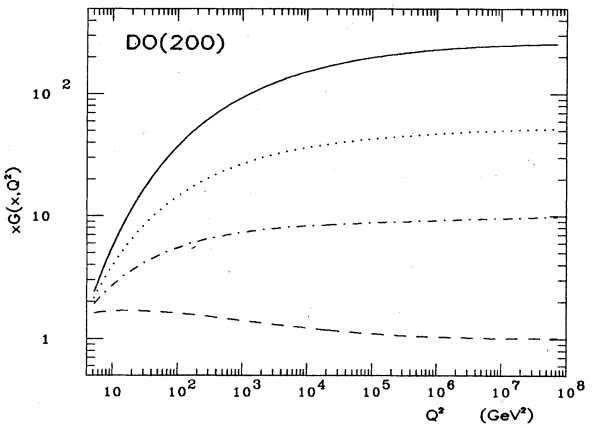

FIG. 31. Q^2 evolution of the "soft-gluon" ($\Lambda=200$ MeV) distribution $xG(x,Q^2)$ of Duke and Owens (1984). Same x values as Fig. 10.

III. PHYSICS OF HADRONIC JETS

A. Generalities

This section deals with the production of jets of hadrons that emerge with high momentum transverse to the direction of the incident beams. Experiments at the CERN $S\bar{p}pS$ Collider (Arnison *et al.*, 1983d,1983e; Bagnaia *et al.*, 1983a) and at the CERN Intersecting Storage Rings (Albrow, 1983) have shown that for an important class of events the jets are well collimated, isolated, and straightforward to analyze.

The simple parton-model picture of jet production in QCD was represented in Fig. 1. Constituents (quarks, antiquarks, or gluons) of the incident hadrons appear with momenta distributed according to the parton distribution functions $f_i^{(a)}(x_a,Q^2)$ introduced in Sec. II. These constituents then scatter at wide angles into outgoing partons which then materialize into the hadrons which are observed experimentally.

The details of this hadronization are beyond the scope of perturbative QCD. However, perturbative methods do suffice (Sterman and Weinberg, 1977; Shizuya and Tye, 1978; Einhorn and Weeks, 1978) to show that distinct jets should exist, and should become increasingly collimated with increasing jet energies. The angle $\delta(E)$, which defines the outermost angular distance from the jet axis at which any appreciable hadronic energy is to be found, is expected to decrease roughly as $E^{-1/4}$. There is also a suggestion that at very high energies, gluon jets should be somewhat broader than quark jets, with

$$\delta(\text{gluon}) \approx [\delta(\text{quark})]^{4/9} . \tag{3.1}$$

In principle, the hadronization could be calculated in complete detail by nonperturbative methods. This is akin to a complete solution of the confinement problem, for which practical techniques are not yet available. As a consequence, a variety of models (Ali *et al.*, 1979a,

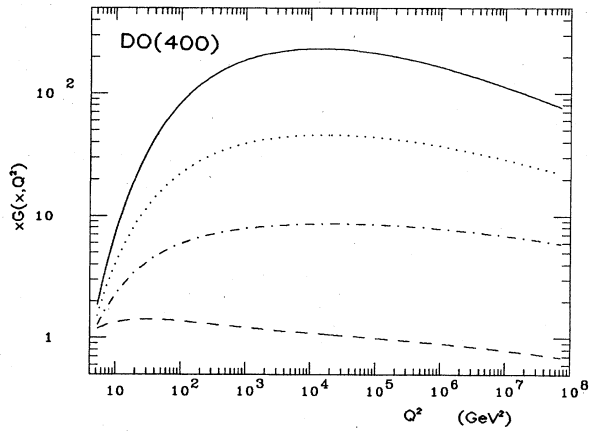

FIG. 30. Q^2 evolution of the "hard-gluon" ($\Lambda=400$ MeV) distribution $xG(x,Q^2)$ of Duke and Owens (1984). Same x values as Fig. 10.

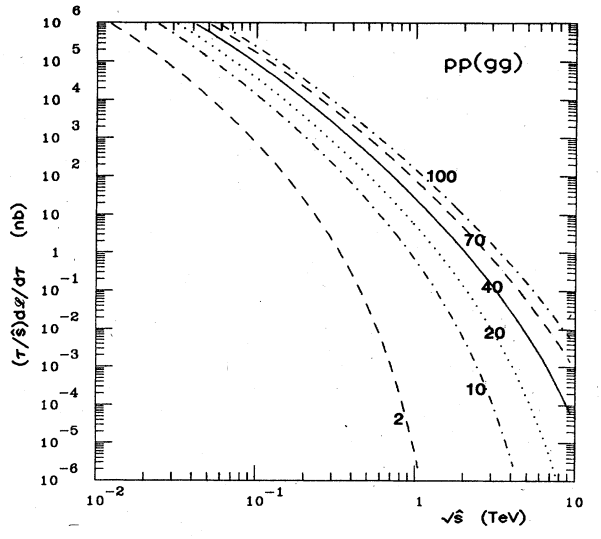

FIG. 32. The quantity $(\tau/\hat{s})d\mathcal{L}/d\tau$ for gluon-gluon interactions in proton-proton collisions. Collider energies $\sqrt{s}$ are given in TeV.

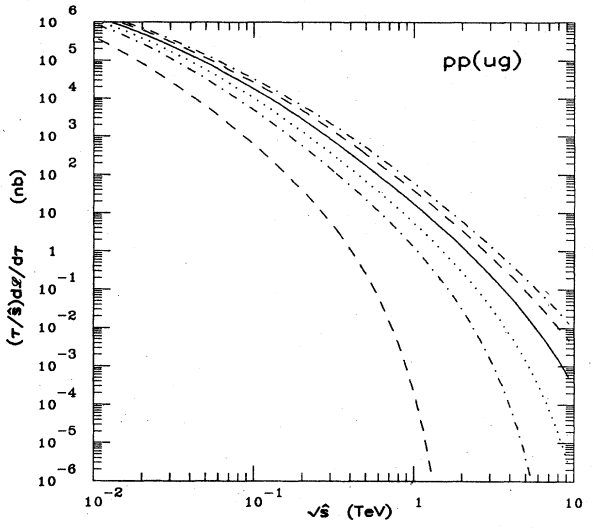

FIG. 33. Quantity $(\tau/\hat{s})d\mathscr{L}/d\tau$ for ug interactions in proton-proton collisions.

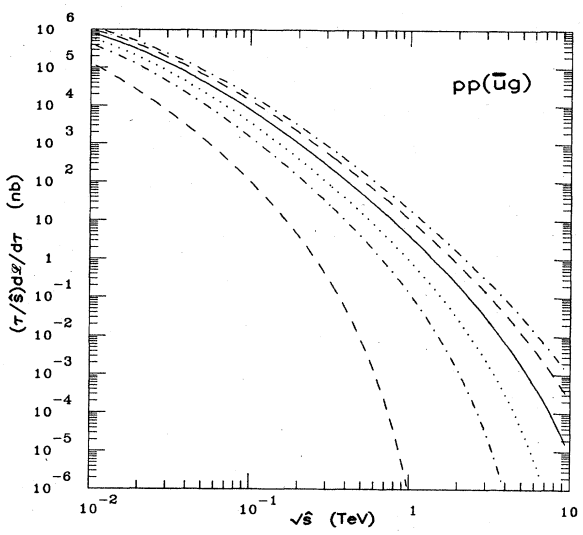

FIG. 35. Quantity $(\tau/\hat{s})d\mathscr{L}/d\tau$ for $\bar{u}g$ interactions in proton-proton collisions.

1979b,1980; Hoyer *et al.*, 1979; Paige and Protopopescu, 1980; Andersson *et al.*, 1983; Odorico, 1980a,1980b,1983; Mazzanti and Odorico, 1980; Field and Wolfram, 1983; Gottschalk, 1984; Field, 1983) have been constructed to simulate the evolution of partons into hadrons. Although they differ in detail, all have the common feature that jets become easier to isolate at high energies. This is in agreement with the observation that the jets observed in pp collisions at $\sqrt{s}=63$ GeV (Albrow, 1983) or in e^+e^- collisions at $\sqrt{s}=7.4$ GeV (Hanson *et al.*, 1975) are less distinct than those measured in $\bar{p}p$ collisions at $\sqrt{s}=540$ GeV (Arnison *et al.*, 1983d; Bagnaia *et al.*, 1983a) or in e^+e^- collisions at $\sqrt{s}=30$ GeV (Mess and Wiik, 1983). The perturbative QCD prediction quoted above encourages the hope that the situation will become still simpler at higher energies.

Jet studies in hadron-hadron collisions have traditionally been viewed as less incisive than those carried out in electron-positron annihilations or in lepton-nucleon scattering because of the added complexity of events. The *SppS* experience indicates that, as hoped, the hard-scattering events take on a much simpler aspect at high energies, and there is no impediment to detailed analyses. We may therefore expect to take advantage of the higher energies attainable in hadron-hadron collisions and of the greater diversity of elementary interactions made possible by our unseparated broadband parton beams.

What will be the goals of jet studies at supercollider energies? Jets unquestionably will constitute one of the major sources of conventional background to new discoveries, so it is crucial that they be well understood, if only for engineering purposes. For example, a thorough

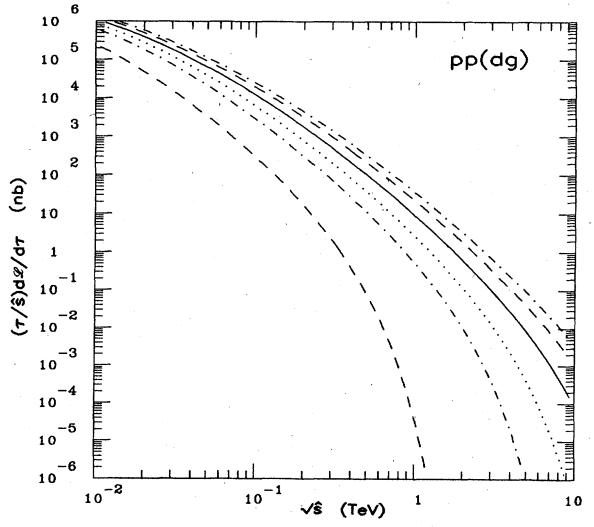

FIG. 34. Quantity $(\tau/\hat{s})d\mathscr{L}/d\tau$ for dg interactions in proton-proton collisions.

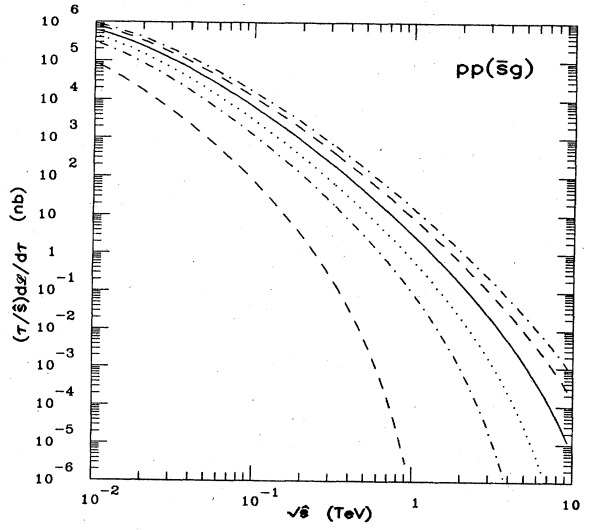

FIG. 36. Quantity $(\tau/\hat{s})d\mathscr{L}/d\tau$ for $\bar{s}g$ interactions in proton-proton collisions.

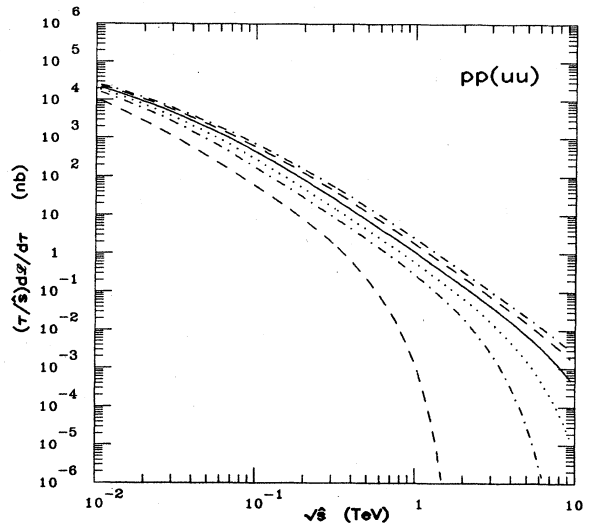

FIG. 37. Quantity $(\tau/\hat{s})d\mathscr{L}/d\tau$ for uu interactions in proton-proton collisions.

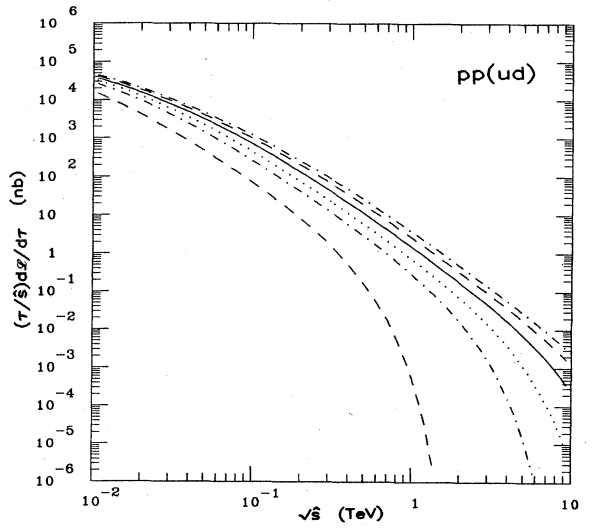

FIG. 38. Quantity $(\tau/\hat{s})d\mathscr{L}/d\tau$ for ud interactions in proton-proton collisions.

study of conventional sources of jets will be an important prelude to multijet spectroscopy, which may be an extremely valuable search technique. It may even be possible, in time, to use jets as a parton luminosity monitor, as Bhabha scattering is used in e^+e^- collisions. The study of hadronization and the investigation of differences between quark jets and gluon jets benefits in an obvious way from high jet energies and from the possibility of tagging (or enriching a sample of) quark or gluon jets. Finally, tests of short-distance behavior such as searches for evidence of compositeness, rely on an understanding of the behavior anticipated in QCD.

B. Two-jet final states

The reactions that may occur at lowest order (α_s^2) in QCD all are two-body to two-body processes leading to final states consisting of two jets with equal and opposite transverse momenta. The cross section is conveniently written in terms of the rapidities y_1 and y_2 of the two jets and their common transverse momentum $p_\perp$. (Here and throughout this paper, we neglect the intrinsic transverse momentum carried by the partons.) It is

$$\frac{d\sigma}{dy_1 dy_2 dp_\perp}=\frac{2\pi\tau}{\hat{s}}p_\perp\sum_{ij}[f_i^{(a)}(x_a,M^2)f_j^{(b)}(x_b,M^2)\hat{\sigma}_{ij}(\hat{s},\hat{t},\hat{u})+f_j^{(a)}(x_a,M^2)f_i^{(b)}(x_b,M^2)\hat{\sigma}_{ij}(\hat{s},\hat{u},\hat{t})]/(1+\delta_{ij})\ , \tag{3.2}$$

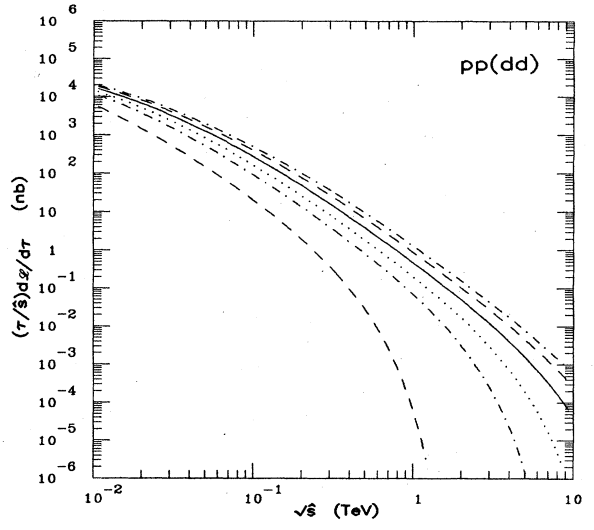

FIG. 39. Quantity $(\tau/\hat{s})d\mathscr{L}/d\tau$ for dd interactions in proton-proton collisions.

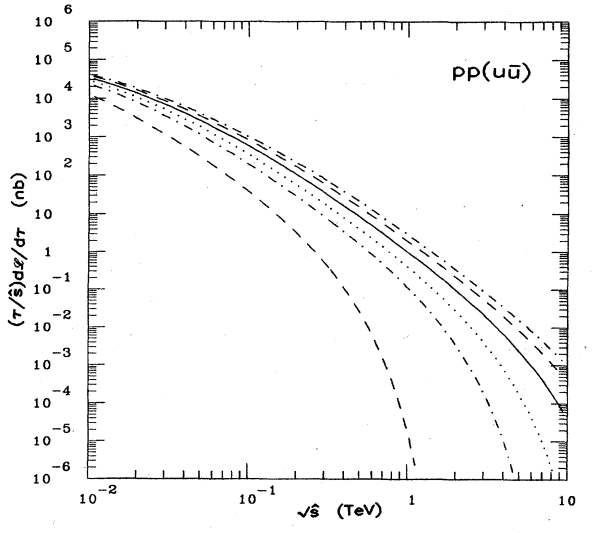

FIG. 40. Quantity $(\tau/\hat{s})d\mathscr{L}/d\tau$ for $u\bar{u}$ interactions in proton-proton collisions.

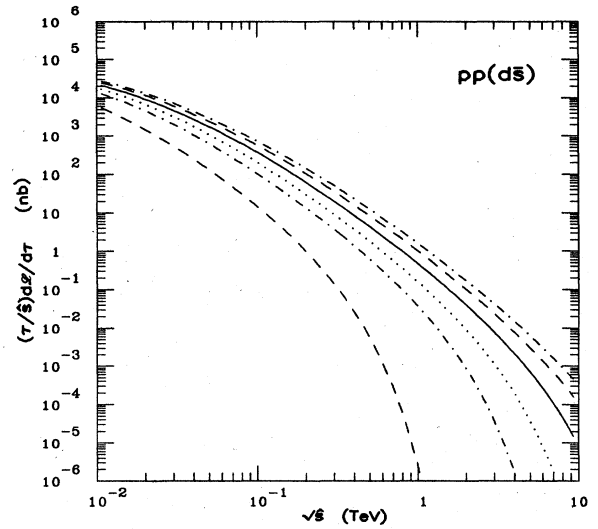

FIG. 41. Quantity $(\tau/\hat{s})d\mathcal{L}/d\tau$ for $d\bar{s}$ interactions in proton-proton collisions.

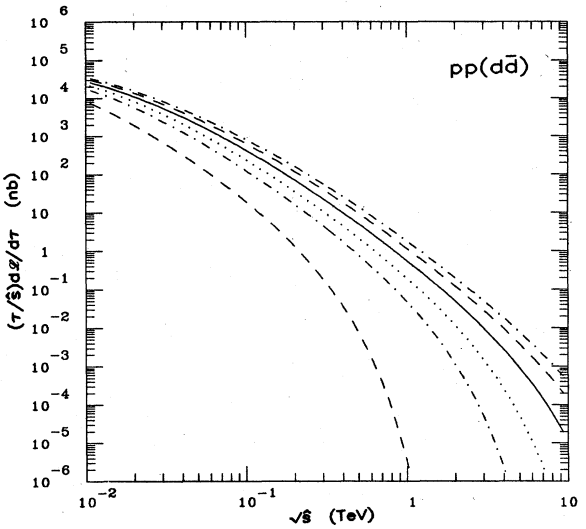

FIG. 43. Quantity $(\tau/\hat{s})d\mathcal{L}/d\tau$ for $d\bar{d}$ interactions in proton-proton collisions.

where $\hat{s}=s\tau$ is the square of the parton-parton subenergy. Defining

$$y^*=\tfrac{1}{2}(y_1-y_2) \tag{3.3}$$

and

$$y_{\text{boost}}=\tfrac{1}{2}(y_1+y_2)\,, \tag{3.4}$$

we may write

$$\tau=\frac{4p_\perp^2}{s}\cosh^2 y^* \tag{3.5}$$

and

$$x_a=\sqrt{\tau}e^{y_{\text{boost}}}\,,$$
$$x_b=\sqrt{\tau}e^{-y_{\text{boost}}}\,. \tag{3.6}$$

Finally, the invariants may be expressed in terms of

$$\cos\theta=(1-4p_\perp^2/\hat{s})^{1/2}\,, \tag{3.7}$$

the cosine of the scattering angle in the parton-parton c.m., as

$$\hat{t}=-\frac{\hat{s}}{2}(1-\cos\theta)\,,$$
$$\hat{u}=-\frac{\hat{s}}{2}(1+\cos\theta)\,. \tag{3.8}$$

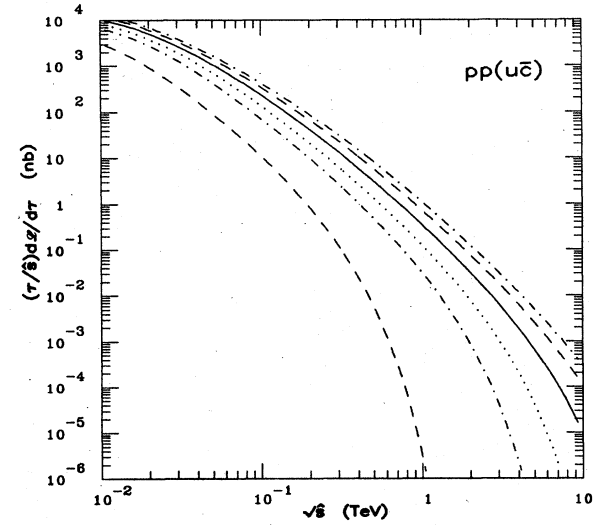

FIG. 42. Quantity $(\tau/\hat{s})d\mathcal{L}/d\tau$ for $u\bar{c}$ interactions in proton-proton collisions.

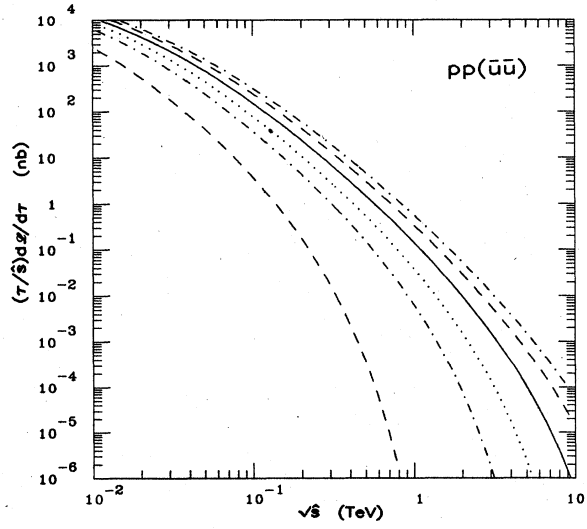

FIG. 44. Quantity $(\tau/\hat{s})d\mathcal{L}/d\tau$ for $\bar{u}\bar{u}$ interactions in proton-proton collisions.

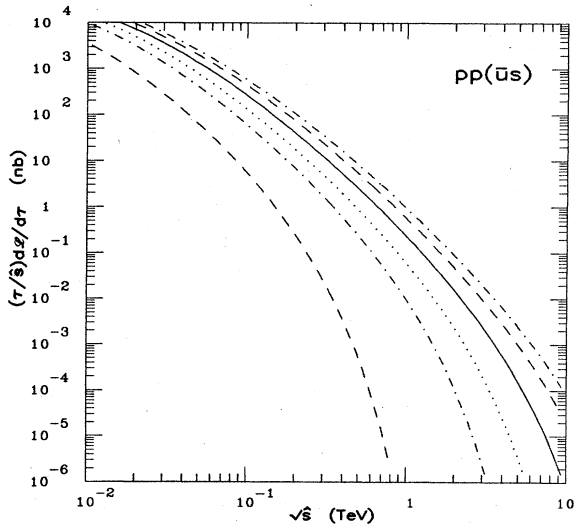

FIG. 45. Quantity $(\tau/\hat{s})d\mathscr{L}/d\tau$ for $\bar{u}s$ interactions in proton-proton collisions.

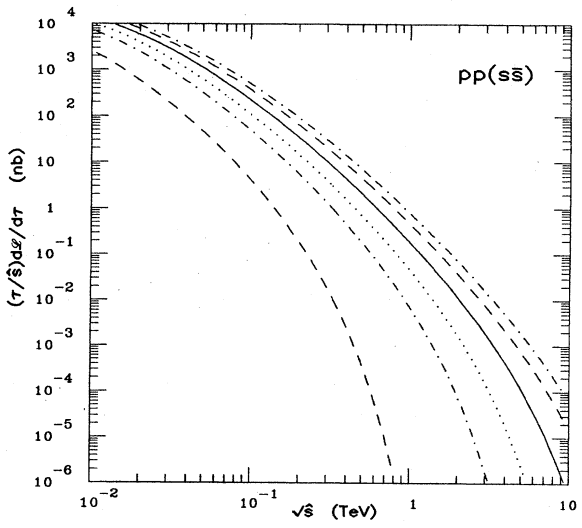

FIG. 47. Quantity $(\tau/\hat{s})d\mathscr{L}/d\tau$ for $s\bar{s}$ interactions in proton-proton collisions.

The sum in (3.2) runs over all parton species i and j.

The elementary cross sections have been calculated by many authors, and have been summarized by Owens, Reya, and Glück (1978). There are seven processes of interest; we treat them in turn.

The scattering of quarks or antiquarks of different flavors proceeds by t-channel gluon exchange, as shown in Fig. 70. The cross section is

$$\hat{\sigma}(q_i q_j' \to q_i q_j') = \frac{4\alpha_s^2}{9\hat{s}} \frac{\hat{s}^2+\hat{u}^2}{\hat{t}^2} . \tag{3.9}$$

Quark-antiquark annihilation occurs through gluon exchange in the direct channel, as shown in Fig. 71. The cross section is

$$\hat{\sigma}(q_i\bar{q}_i \to q_j\bar{q}_j) = \frac{4\alpha_s^2}{9\hat{s}} \frac{\hat{t}^2+\hat{u}^2}{\hat{s}^2}, \quad i \neq j . \tag{3.10}$$

The scattering of quarks and antiquarks of the same flavor has both an annihilation component and an exchange component, shown in Fig. 72. The elementary cross section is

$$\hat{\sigma}(q_i\bar{q}_i \to q_i\bar{q}_i) = \frac{4\alpha_s^2}{9\hat{s}} \left[\frac{\hat{t}^2+\hat{u}^2}{\hat{s}^2} + \frac{\hat{s}^2+\hat{u}^2}{\hat{t}^2} - \frac{2\hat{u}^2}{3\hat{s}\hat{t}} \right] . \tag{3.11}$$

Two-gluon annihilation of a quark-antiquark pair occurs through the s-, t-, and u-channel diagrams pic-

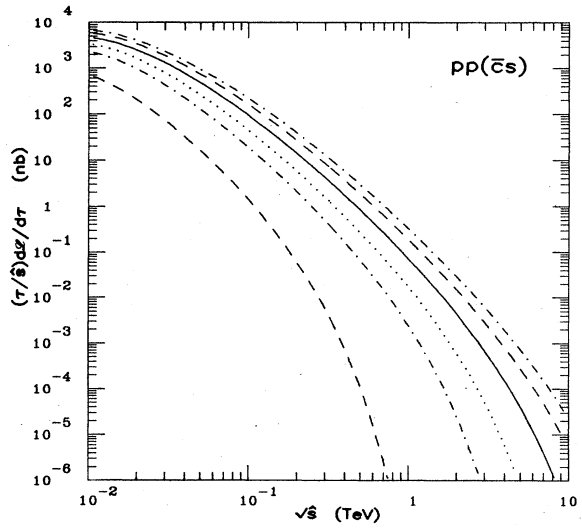

FIG. 46. Quantity $(\tau/\hat{s})d\mathscr{L}/d\tau$ for $\bar{c}s$ interactions in proton-proton collisions.

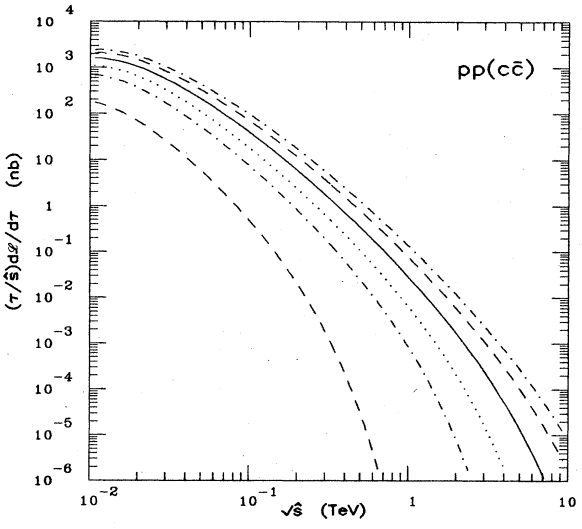

FIG. 48. Quantity $(\tau/\hat{s})d\mathscr{L}/d\tau$ for $c\bar{c}$ interactions in proton-proton collisions.

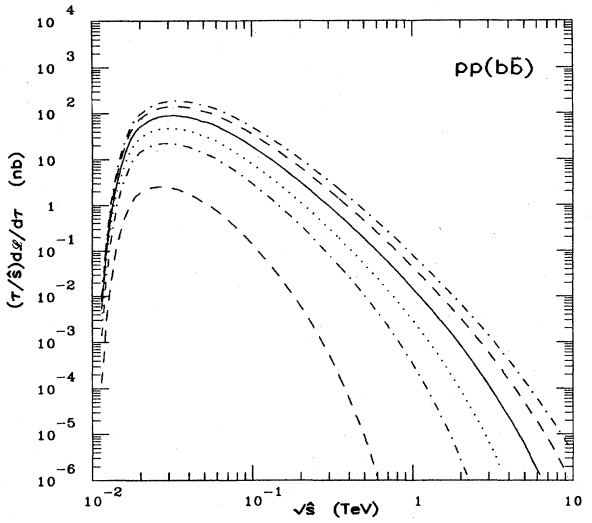

FIG. 49. Quantity $(\tau/\hat{s})d\mathscr{L}/d\tau$ for $b\bar{b}$ interactions in proton-proton collisions.

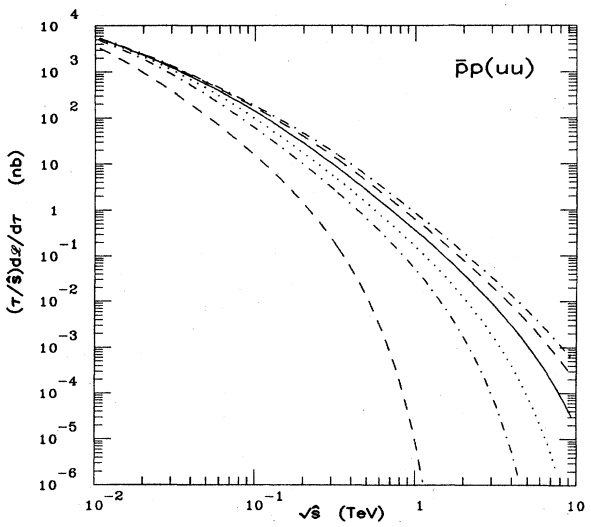

FIG. 51. Quantity $(\tau/\hat{s})d\mathscr{L}/d\tau$ for uu or $\bar{u}\bar{u}$ interactions in proton-antiproton collisions.

tured in Fig. 73. The elementary cross section for this process is

$$\hat{\sigma}(q_i\bar{q}_i\to gg)=\frac{8\alpha_s^2(\hat{t}^2+\hat{u}^2)}{3\hat{s}}\left[\frac{4}{9\hat{t}\,\hat{u}}-\frac{1}{\hat{s}^2}\right]. \quad (3.12)$$

The cross section for the inverse process, for which the diagrams are shown in Fig. 74, differs only in the color average $[(\frac{1}{8})^2$ rather than $(\frac{1}{3})^2]$. It is

$$\hat{\sigma}(gg\to q_i\bar{q}_i)=\frac{3\alpha_s^2(\hat{t}^2+\hat{u}^2)}{8\hat{s}}\left[\frac{4}{9\hat{t}\,\hat{u}}-\frac{1}{\hat{s}^2}\right]. \quad (3.13)$$

The scattering of a gluon from a quark or antiquark is driven by the s-, t-, and u-channel exchanges shown in Fig. 75. The cross section may be expressed as

$$\hat{\sigma}(gq\to gq)=\frac{\alpha_s^2(\hat{s}^2+\hat{u}^2)}{\hat{s}}\left[\frac{1}{\hat{t}^2}-\frac{4}{9\hat{s}\,\hat{u}}\right]. \quad (3.14)$$

Gluon-gluon scattering proceeds by a contact term in addition to gluon exchanges in s-, t-, and u-channels (see Fig. 76). The elementary cross section is

$$\hat{\sigma}(gg\to gg)=\frac{9\alpha_s^2}{2\hat{s}}\left[3-\frac{\hat{t}\,\hat{u}}{\hat{s}^2}-\frac{\hat{s}\,\hat{u}}{\hat{t}^2}-\frac{\hat{s}\,\hat{t}}{\hat{u}^2}\right]. \quad (3.15)$$

Before Eq. (3.2) can be evaluated, we must fix the scale M^2 appearing in the structure functions and the scale Q^2 at which $\alpha_s(Q^2)$, the running coupling constant of the strong interactions, is determined. If QCD perturbation theory is to apply, these scales should be characteristic of

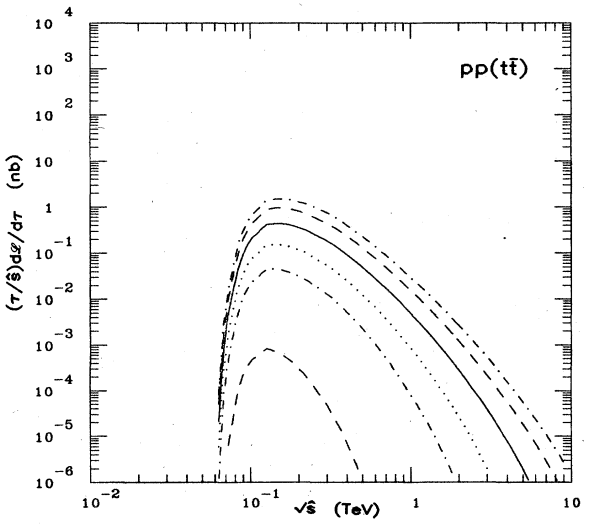

FIG. 50. Quantity $(\tau/\hat{s})d\mathscr{L}/d\tau$ for $t\bar{t}$ interactions in proton-proton collisions. The t-quark mass is taken to be 30 GeV/c^2.

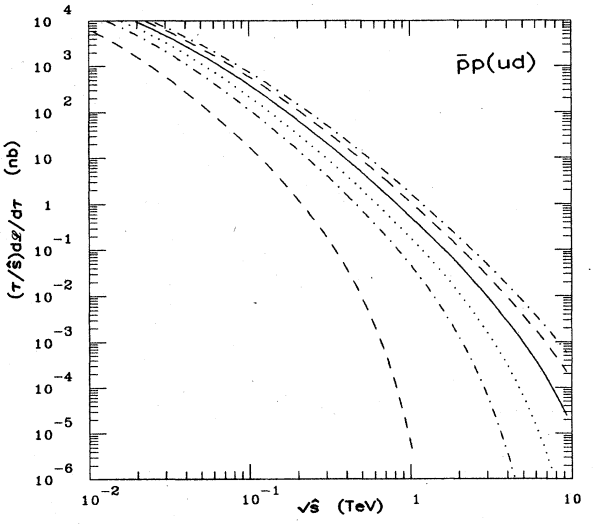

FIG. 52. Quantity $(\tau/\hat{s})d\mathscr{L}/d\tau$ for ud or $\bar{u}\bar{d}$ interactions in proton-antiproton collisions.

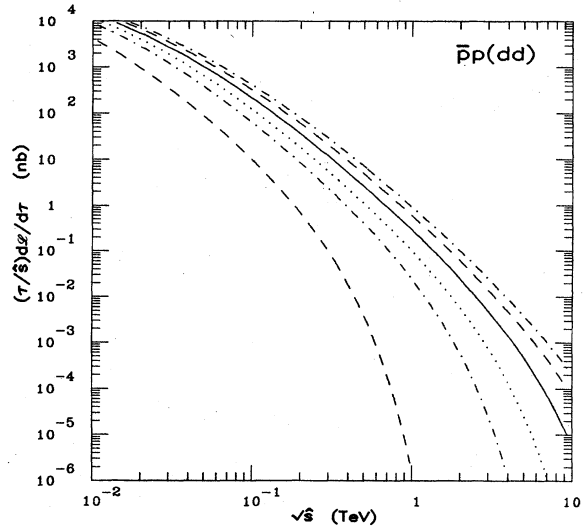

FIG. 53. Quantity $(\tau/\hat{s})d\mathcal{L}/d\tau$ for dd or $\bar{d}\bar{d}$ interactions in proton-antiproton collisions.

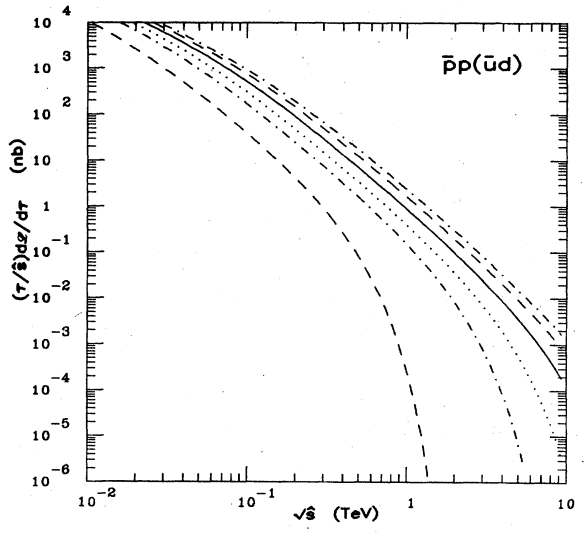

FIG. 55. Quantity $(\tau/\hat{s})d\mathcal{L}/d\tau$ for $u\bar{d}$ or $\bar{u}d$ interactions in proton-antiproton collisions.

the hard-scattering process. Several alternatives [among them $\hat{s}$, $\hat{t}$, $\hat{u}$, $p_\perp^2$, or $2\hat{s}\hat{t}\hat{u}/(\hat{s}^2+\hat{t}^2+\hat{u}^2)$] suggest themselves. Different choices, including different values for M^2 and Q^2, lead to cross sections which may differ by 20% in the kinematical regime of interest to us.

At lowest order in perturbation theory the choice is ambiguous, because, as is well known (Hinchliffe, 1982; Lepage, 1983), any shift in M^2 or Q^2 induces terms in σ_{ij} of order α_s^3 and these are being neglected. The $O(\alpha_s^3)$ corrections to σ_{ij} are known only for the reaction $q_iq_j \to q_iq_j$ (Ellis *et al.*, 1980; Słominski, 1981), where they are large and positive. These corrections are reduced by the choice of small values of M^2 and Q^2. Having chosen a scheme in which the α_s^3 corrections are relatively small, one is left to hope that successive terms in the perturbation expansion will be small, so that the Born term at $O(\alpha_s^2)$ will give a good approximation to the exact all-orders result. We make this choice

$$M^2=Q^2=p_\perp^2/4 \tag{3.16}$$

for all high-$p_\perp$ processes; as a consequence of this reasonable but arbitrary choice, the cross sections we quote will be uncertain by 20%, even if the parton distributions are known exactly. With these caveats, we now present our results.

We first show the one-jet differential cross section $d\sigma/dp_\perp dy\,|_{y=0}$ for pp collisions, at c.m. energies of 10, 40, and 100 TeV in Figs. 77–79. The figures show separately the contributions of gluon-gluon final states ($gg \to gg$ and $\bar{q}q \to gg$, dotted-dashed lines), gluon-quark final states ($g\overset{(-)}{q} \to g\overset{(-)}{q}$, dotted lines), and quark-quark fi-

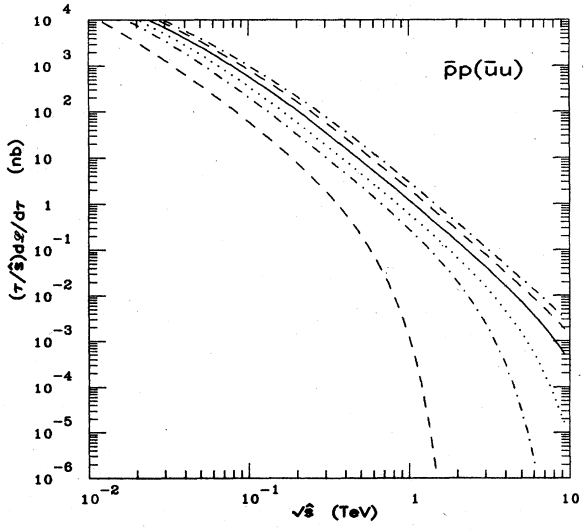

FIG. 54. Quantity $(\tau/\hat{s})d\mathcal{L}/d\tau$ for $u\bar{u}$ interactions in proton-antiproton collisions.

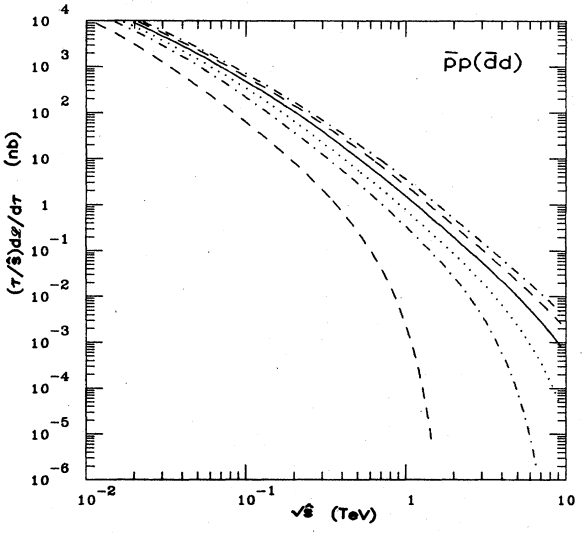

FIG. 56. Quantity $(\tau/\hat{s})d\mathcal{L}/d\tau$ for $d\bar{d}$ interactions in proton-antiproton collisions.

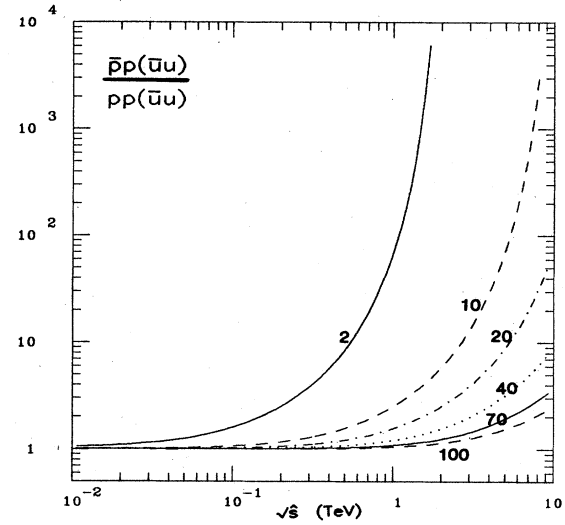

FIG. 57. Ratio of $(\tau/\hat{s})d\mathcal{L}/d\tau$ for $u\bar{u}$ interactions in $\bar{p}p$ and pp collisions, according to the parton distributions of Set 2. Collider energies $\sqrt{s}$ are given in TeV.

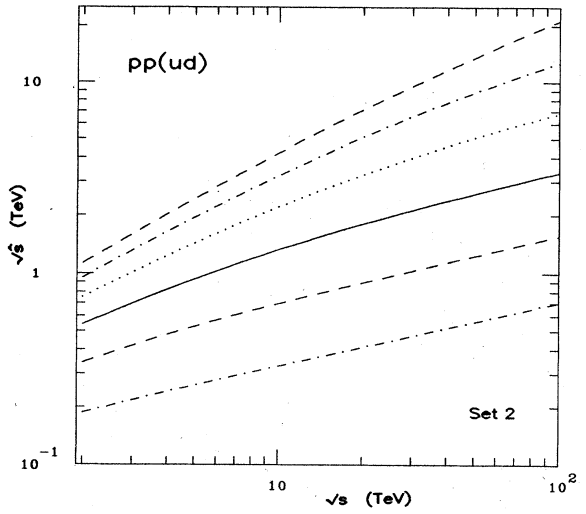

FIG. 59. Contours of $(\tau/\hat{s})d\mathcal{L}/d\tau$ for ud interactions in pp collisions according to the parton distributions of Set 2. Lines correspond to 10^4, 10^3, 10^2, 10, 1, and 0.1 pb.

nal states $(\bar{q})(\bar{q}) \to (\bar{q})(\bar{q})$ and $gg \to \bar{q}q$, dashed lines). In our calculations we have included six quark flavors, without any threshold suppression. Over the kinematic range of interest, this approximation leads to negligible errors in the rate estimates. At small transverse momentum the two-gluon final state dominates. This is a consequence of the large cross section (3.15) for the reaction $gg \to gg$ and the large gluon distribution at small values of x (cf. Fig. 5). As $p_\perp$ increases, the gluon-quark final state grows in importance, and at the very largest values of $p_\perp$ the two-quark final state dominates. At 90°, the two-quark regime is essentially unreachable. For an integrated luminosity of $\int \mathcal{L}\,dt = 10^{40}$ cm^{-2} at 40 TeV, we expect no more than one event per year per GeV/c of $p_\perp$ per unit of rapidity in this region.

Figure 80 shows the effect of a change in the distribution functions (to Set 1, with $\Lambda = 200$ MeV) at $\sqrt{s} = 40$ TeV. The resultant change is quite small: a 10% decrease at $p_\perp = 1$ TeV/c. While we cannot be certain that this represents the widest variation to be expected from changes in the parton distributions, it does give us confidence that reasonable changes in the distributions will not lead to wild variations in the conclusions.

Proton-proton and proton-antiproton jet cross sections at 90° are essentially equal at $\sqrt{s} = 10$ TeV, and of course at higher energies. The proton-antiproton cross section is plotted in Fig. 81, to be compared with Fig. 77. For completeness we show in Figs. 82 and 83 the jet cross sections in $\bar{p}p$ collisions at 540 GeV and 2 TeV. At these low values of $p_\perp$ the results are slightly more sensitive to the

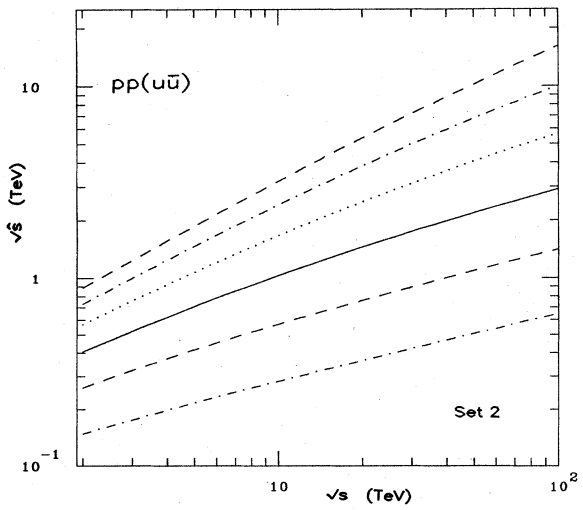

FIG. 58. Contours of $(\tau/\hat{s})d\mathcal{L}/d\tau$ for $u\bar{u}$ interactions in pp collisions according to the parton distributions of Set 2. Lines correspond to 10^4, 10^3, 10^2, 10, 1, and 0.1 pb.

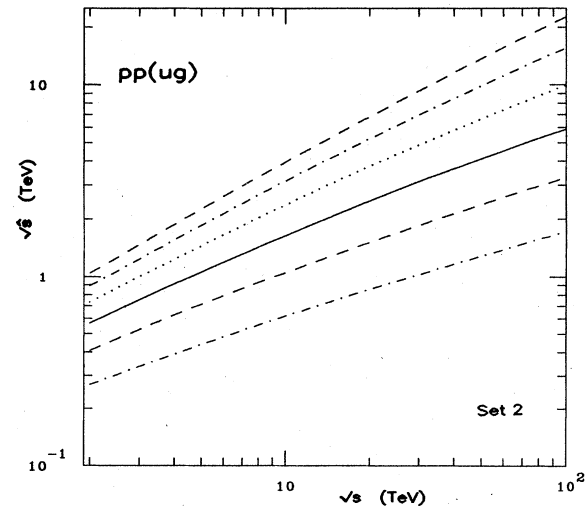

FIG. 60. Contours of $(\tau/\hat{s})d\mathcal{L}/d\tau$ for ug interactions in pp collisions according to the parton distributions of Set 2. Lines correspond to 10^4, 10^3, 10^2, 10, 1, and 0.1 pb.

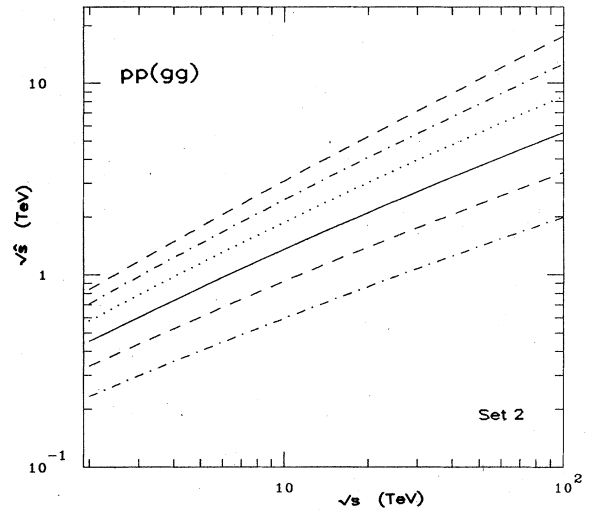

FIG. 61. Contours of $(\tau/\hat{s})d\mathcal{L}/d\tau$ for gg interactions in $p^{\pm}p$ collisions according to the parton distributions of Set 2. Lines correspond to 10^4, 10^3, 10^2, 10, 1, and 0.1 pb.

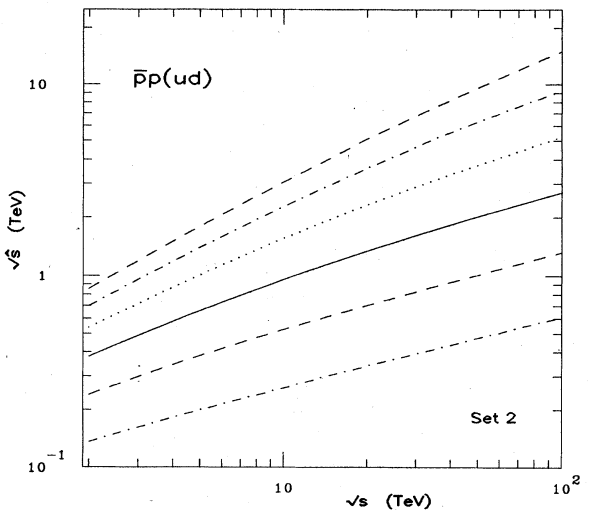

FIG. 63. Contours of $(\tau/\hat{s})d\mathcal{L}/d\tau$ for ud or $\bar{u}\bar{d}$ interactions in $\bar{p}p$ collisions according to the parton distributions of Set 2. Lines correspond to 10^4, 10^3, 10^2, 10, 1, and 0.1 pb.

different sets of distribution functions. The differences can be seen by comparing Figs. 82(a) (Set 2) and 82(c) (Set 1). There we have plotted recent data from the UA-1 experiment (Arnison *et al.*, 1983d) and the UA-2 experiment (Bagnaia *et al.*, 1983a,1984). The errors plotted there are statistical only. For the UA-1 data, there is in addition a $\pm 7.5\%$ uncertainty in the $p_\perp$ scale, which has the effect of an overall normalization uncertainty of a factor of $(1.5)^{\pm 1}$. The overall additional systematic uncertainty in the UA-2 data is $\pm 40\%$. The precise agreement between the data and our calculation is thus better than one has a right to expect. If the scale Q^2 is increased—say, to $p_\perp^2$—then the cross section falls slightly. This can be seen in Fig. 82(b). This effect is less important at higher energies.

The presence of t-channel and u-channel poles in the elementary cross sections $\hat{\sigma}_{ij}$ means that at fixed values of $\hat{s}$, the cross sections are peaked in the forward and backward directions in the parton-parton c.m., which is to say at large values of y^*. For a fixed value of $p_\perp$ the mean values of x_a and x_b increase at large values of y^*. The consequent fall in the parton distributions tends to reduce the peaking in the elementary cross sections. Figures 84—89 show the quantity $d\sigma/dp_\perp dy_{\text{boost}} dy^*$ for fixed values of y_{boost} and $p_\perp$. As y_{boost} increases for fixed values of y^* and $p_\perp$, x_a increases and x_b decreases [cf. Eqs. (3.5) and (3.6)]. Because of the rapid decrease of the parton distributions at large x (faster for gluons than for valence quarks), this causes the cross sections to fall, and moreover changes the relative contributions of different

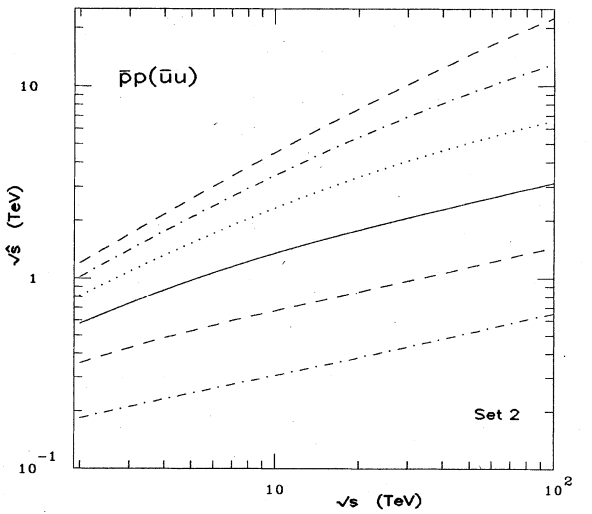

FIG. 62. Contours of $(\tau/\hat{s})d\mathcal{L}/d\tau$ for $u\bar{u}$ interactions in $\bar{p}p$ collisions according to the parton distributions of Set 2. Lines correspond to 10^4, 10^3, 10^2, 10, 1, and 0.1 pb.

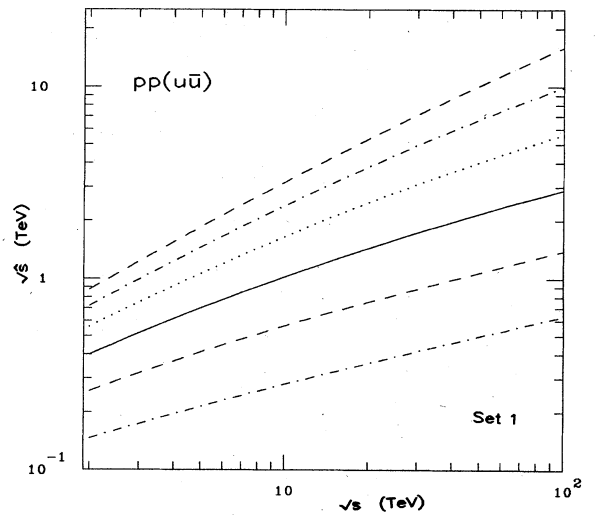

FIG. 64. Contours of $(\tau/\hat{s})d\mathcal{L}/d\tau$ for $u\bar{u}$ interactions in pp collisions according to the parton distributions of Set 1. Lines correspond to 10^4, 10^3, 10^2, 10, 1, and 0.1 pb.

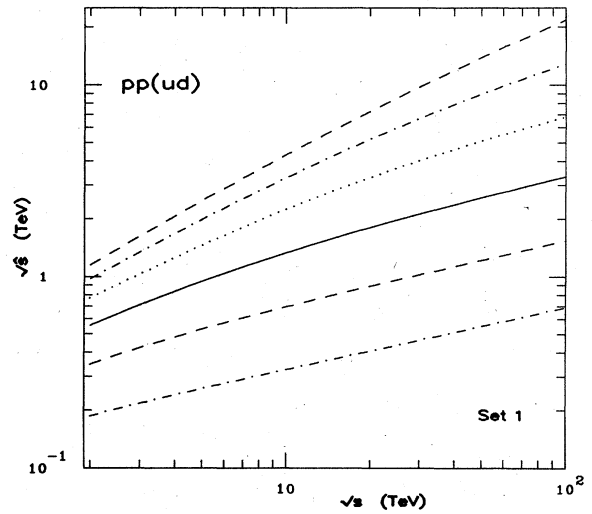

FIG. 65. Contours of $(\tau/\hat{s})d\mathcal{L}/d\tau$ for ud interactions in pp collisions according to the parton distributions of Set 1. Lines correspond to 10^4, 10^3, 10^2, 10, 1, and 0.1 pb.

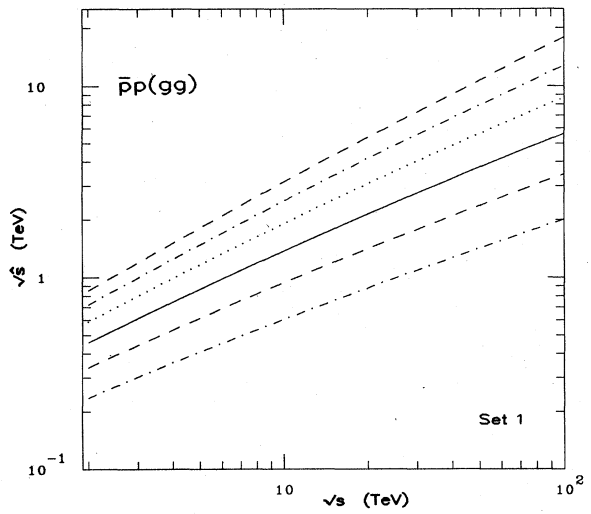

FIG. 67. Contours of $(\tau/\hat{s})d\mathcal{L}/d\tau$ for gg interactions in $p^{\pm}p$ collisions according to the parton distributions of Set 1. Lines correspond to 10^4, 10^3, 10^2, 10, 1, and 0.1 pb.

final states.

This effect is exhibited in Figs. 84–86 for $p_\perp = 1$ TeV/c. At $y_{\text{boost}}=0$, the gluon-gluon final state dominates in the neighborhood of $y^*=0$, but at $y_{\text{boost}}=2$ the gluon-quark final state dominates over the entire rapidity range. As both y_{boost} and $p_\perp$ increase further, the two-quark final state becomes dominant, as illustrated in Fig. 87 for $y_{\text{boost}}=0$ and $p_\perp = 5$ TeV/c.

Figures 88 and 89 enable a comparison of jet production in pp and $\bar{p}p$ collisions. As for the integrated cross sections, the differences are not gross.

The ability to select different final states by varying rapidity and transverse momentum could be of great importance. As we remarked in the introduction to this section, a complete description of hadronization in QCD has not yet been achieved. For the moment we have perturbative suggestions, but do not know the consequences of nonperturbative effects. In addition to the results on jet size mentioned in Sec. III.A, perturbative QCD indicates that gluon jets should yield a higher hadron multiplicity than quark jets (Mueller 1983a,1983b; Furmanski *et al.*, 1979).

The experimental sample at present consists of predominantly quark jets from e^+e^- annihilations and a mixed sample from the CERN collider. The exact nature of the mix is in principle dependent on the structure functions. As can be seen from Figs. 82(a) and 82(c), at any given value of $p_\perp$, the mix is quite similar at 540 GeV for the two sets of structure functions we consider. A preliminary comparison between e^+e^- jets and CERN collider jets (Arnison *et al.*, 1983e) reveals no overt differences. In

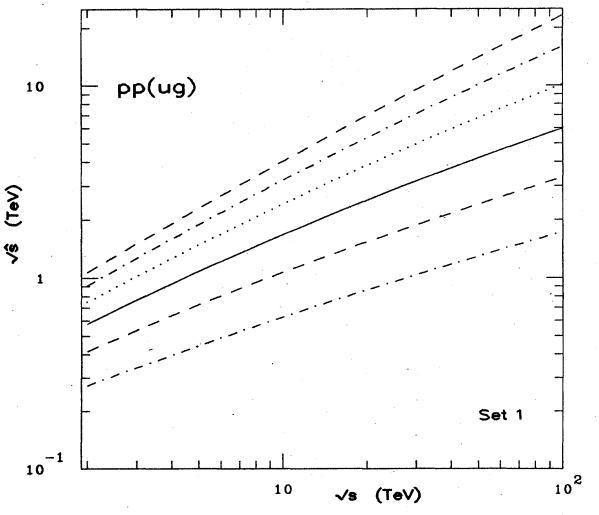

FIG. 66. Contours of $(\tau/\hat{s})d\mathcal{L}/d\tau$ for ug interactions in pp collisions according to the parton distributions of Set 1. Lines correspond to 10^4, 10^3, 10^2, 10, 1, and 0.1 pb.

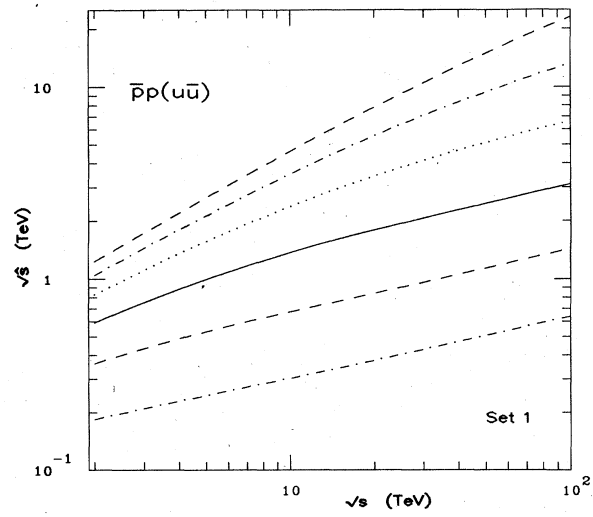

FIG. 68. Contours of $(\tau/\hat{s})d\mathcal{L}/d\tau$ for $u\bar{u}$ interactions in $\bar{p}p$ collisions according to the parton distributions of Set 1. Lines correspond to 10^4, 10^3, 10^2, 10, 1, and 0.1 pb.

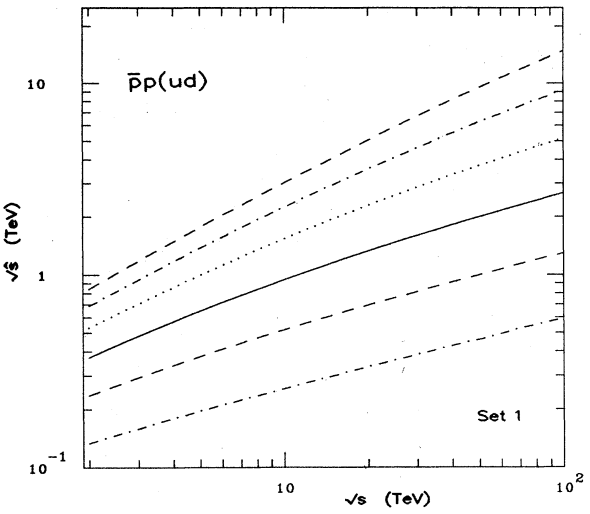

FIG. 69. Contours of $(\tau/\hat{s})d\mathscr{L}/d\tau$ for ud interactions in $\bar{p}p$ collisions according to the parton distributions of Set 1. Lines correspond to 10^4, 10^3, 10^2, 10, 1, and 0.1 pb.

order to make an incisive comparison, it is essential to remove from the putative large-$p_\perp$ jets particles associated with beam fragments in $\bar{p}p$ collisions. Any procedure for assigning particles to beam jets and to high-$p_\perp$ jets necessarily introduces ambiguities into the resulting fragmentation function at small values of $z \equiv E_{\text{hadron}}/E_{\text{jet}}$, and will particularly affect the determination of multiplicity. Complementary data from a common source (e.g., gluon jets from $e^+e^- \to$toponium$\to ggg$ or a clean sample of quark jets in $p^\pm p$ scattering) would greatly advance the study of hadronization.

Another interesting observable is the distribution of two-jet invariant masses $\mathscr{M}$. If we constrain the rapidities of both jets to lie in the interval

$$-Y \le y_1, y_2 \le Y \,, \tag{3.17}$$

then the invariant mass spectrum is given by

$$\frac{d\sigma}{d\mathscr{M}} = \frac{\pi \mathscr{M}\tau}{2} \int_{-Y}^{Y} dy_1 \int_{y_{\min}}^{y_{\max}} dy_2 \sum_{ij} \frac{1}{(1+\delta_{ij})\hat{s}\cosh^2 y^*} [f_i^{(a)}(x_a, M^2) f_j^{(b)}(x_b, M^2) \hat{\sigma}_{ij}(\hat{s},\hat{t},\hat{u}) + f_j^{(a)}(x_a, M^2) f_i^{(b)}(x_b, M^2) \hat{\sigma}_{ij}(\hat{s},\hat{u},\hat{t})] \,, \tag{3.18}$$

where

$$y_{\min} \equiv \max(-Y, \ln\tau - y_1) \,,$$
$$y_{\max} \equiv \min(Y, -\ln\tau - y_1) \,. \tag{3.19}$$

The restriction to central rapidities is necessary to avoid the "collinear" singularities arising from t-channel and u-channel poles in $\hat{\sigma}_{ij}$, as well as to circumvent the experimental difficulty of particles associated with jets escaping down the beam pipe.

Figures 90–92 show the mass spectra $d\sigma/d\mathscr{M}$ with $Y = 1.5$ for pp collisions at 10, 40, and 100 TeV using the parton distributions of Set 2. Again we have plotted the contributions of the gluon-gluon, gluon-quark, and quark-quark final states. The results are changed by less than 10% over the range shown if the parton distributions of Set 1 are used, and there is little difference at these energies between pp and $\bar{p}p$ collisions. In Figs. 93 and 94 we show the two-jet mass spectra for $\bar{p}p$ collisions

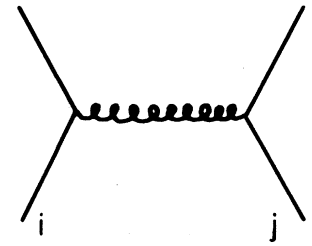

FIG. 70. Lowest-order Feynman graph for the reaction $q_iq_j \to q_iq_j$ (or $q_i\bar{q}_j \to q_i\bar{q}_j$, $i \neq j$) in QCD.

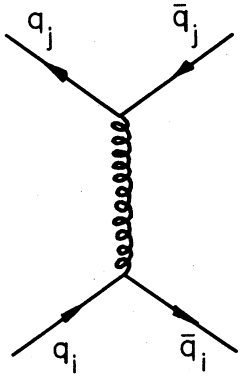

FIG. 71. Lowest-order Feynman graph for the reaction $q_i\bar{q}_i \to q_j\bar{q}_j$, $i \neq j$, in QCD.

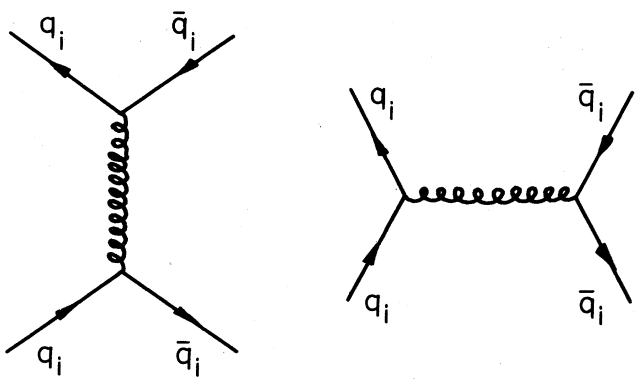

FIG. 72. Lowest-order Feynman diagrams for the reaction $q_i\bar{q}_i \to q_i\bar{q}_i$ in QCD.

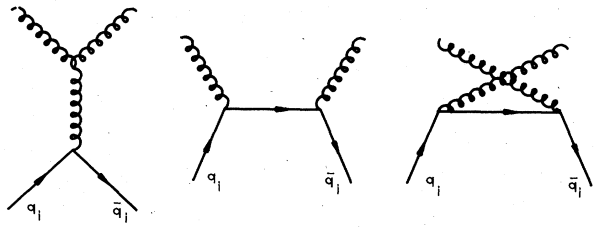

FIG. 73. Feynman diagrams for the reaction $q_i\bar{q}_i \to gg$, in lowest-order QCD.

at 540 GeV and 2 TeV, with a tighter rapidity cut given by $Y=0.85$. Also shown in Fig. 93 are the data of the UA-2 experiment (Bagnaia *et al.*, 1983a). As in the case of the transverse momentum cross sections of Figs. 82(a) and 82(c), the dependence on structure functions is rather mild. Considering the $\pm 40\%$ normalization uncertainty carried by the data, the agreement is quite satisfactory. These jet-jet mass spectra represent a background for any new particles, such as new gauge bosons or Higgs bosons, that decay into jet pairs. We shall refer to them in assessing the observability of new phenomena.

C. Multijet phenomena

At order α_s^3 in QCD occur two-body to three-body subprocesses such as $gg \to ggg$ which can give rise to three jets with large transverse momentum. Because of the kinematical richness of this topology (five independent variables for the $2 \to 3$ reaction plus one for motion relative to the lab frame), a full simulation is for many purposes indispensible. However, more restricted calculations have great value for orientation, and we will restrict our attention to questions that may be addressed without Monte Carlo programs.

In order to describe the elementary reaction, it is convenient to label the momenta of the participating partons as indicated in Fig. 95 and to use the coordinates introduced by Sivers and Gottschalk (1980). We work in the c.m. frame of the three-jet system, defined by the condition

$$\mathbf{p}_1+\mathbf{p}_2+\mathbf{p}_3=0 \ . \tag{3.20}$$

In this frame the energies of the individual jets may be written as

$$E_k=\hat{x}_k\mathcal{M}/2, \quad k=1,2,3 \ , \tag{3.21}$$

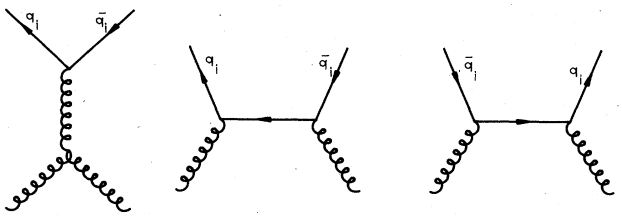

FIG. 74. Feynman diagrams for the reaction $gg \to q_i\bar{q}_i$, in lowest-order QCD.

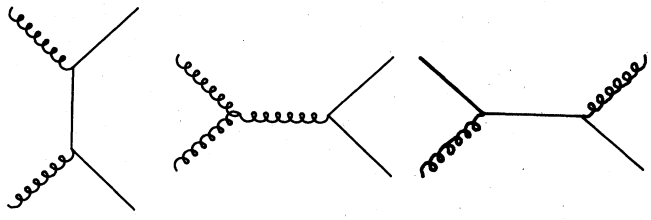

FIG. 75. Lowest-order Feynman diagrams for the reaction $gq \to gq$ (or $g\bar{q} \to g\bar{q}$) in QCD.

where $\mathcal{M}=\sqrt{\hat{s}}$ and $0 \le \hat{x}_k \le 1$, so that

$$\hat{x}_1+\hat{x}_2+\hat{x}_3=2 \ . \tag{3.22}$$

The normal to the plane defined by $\mathbf{p}_1,\mathbf{p}_2,\mathbf{p}_3$, makes an angle θ with the beam direction. The azimuthal orientation of the normal is specified by the angle φ. The four-momenta of the incoming and outgoing partons may be expressed as

$$\begin{aligned}
p_i &= \frac{\mathcal{M}}{2}(1;\sin\theta\cos\varphi,\sin\theta\sin\varphi,\cos\theta) \ , \\
p_j &= \frac{\mathcal{M}}{2}(1;-\sin\theta\cos\varphi,-\sin\theta\sin\varphi,-\cos\theta) \ , \\
p_1 &= \frac{\hat{x}_1\mathcal{M}}{2}(1;1,0,0) \ , \\
p_2 &= \frac{\hat{x}_2\mathcal{M}}{2}(1;\cos\theta_{12},\sin\theta_{12},0) \ , \\
p_3 &= \frac{\hat{x}_3\mathcal{M}}{2}(1;\cos\theta_{13},-\sin\theta_{13},0) \ ,
\end{aligned} \tag{3.23}$$

where θ_{kl}, the angle between $\mathbf{p}_k$ and $\mathbf{p}_l$, is given by

$$\cos\theta_{kl}=1-2(\hat{x}_k+\hat{x}_l-1)/\hat{x}_k\hat{x}_l \ . \tag{3.24}$$

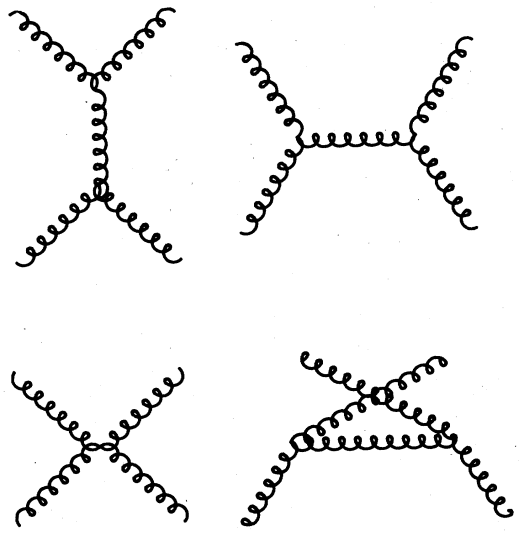

FIG. 76. Lowest-order Feynman diagrams for gluon-gluon elastic scattering in QCD.

An additional variable is needed to completely describe the system. An apt choice is the rapidity

$$y_{\text{boost}} \equiv (y_1+y_2+y_3)/3 \tag{3.25}$$

of the three-jet system in the c.m. frame of the colliding hadrons.

After these preliminaries, we may write the three-jet cross section as

$$\frac{d\sigma}{d\hat{x}_1 d\hat{x}_2 dy_{\text{boost}} d\mathcal{M}\, d\Omega} = \frac{\alpha_s^3(Q^2)\tau}{8\pi\mathcal{M}} \sum_{ij} \frac{1}{1+\delta_{ij}} [f_i^{(a)}(x_a,M^2) f_j^{(b)}(x_b,M^2) A_{ij} + f_j^{(a)}(x_a,M^2) f_i^{(b)}(x_b,M^2) A_{ji}] , \tag{3.26}$$

where $\tau=\mathcal{M}^2/s$ and as usual

$$x_a=\sqrt{\tau}e^{y_{\text{boost}}}, \quad x_b=\sqrt{\tau}e^{-y_{\text{boost}}} , \tag{3.27}$$

The quantity A_{ij} is the absolute square of the invariant amplitude for the process depicted in Fig. 95. The matrix elements for the processes of interest have been given in compact form by Berends *et al.* (1981).[3]

There are four basic processes to be considered.

For the elementary reaction

$$q_m(p_i)+q_n(p_j)\to q_m(p_1)+q_n(p_2)+g(p_3), \quad m\neq n \tag{3.28}$$

the result is

$$A = F(p_i,p_j,p_1,p_2,p_3) , \tag{3.29}$$

where

$$F(k_i,k_j,k_1,k_2,k_3)=\frac{\hat{s}^2+s'^2+\hat{u}^2+u'^2}{8\hat{t}t'k_{i3}k_{j3}k_{13}k_{23}}\{C_1[(\hat{u}+u')(\hat{s}s'+\hat{t}t'-\hat{u}u')+\hat{u}(\hat{s}\hat{t}+s't')+u'(\hat{s}t'+s'\hat{t})]$$
$$-C_2[(\hat{s}+s')(\hat{s}s'-\hat{t}t'-\hat{u}u')+2\hat{t}t'(\hat{u}+u')+2\hat{u}u'(\hat{t}+t')]\} , \tag{3.30}$$

with

$$\begin{aligned} &C_1=16/27, \quad C_2=2/27 , \\ &k_{mn}=k_m\cdot k_n , \\ &\hat{s}=(k_i+k_j)^2, \quad s'=(k_1+k_2)^2 , \\ &\hat{t}=(k_i-k_1)^2, \quad t'=(k_j-k_2)^2 , \\ &\hat{u}=(k_i-k_2)^2, \quad u'=(k_j-k_1)^2 . \end{aligned} \tag{3.31}$$

For the scattering of identical quarks,

$$q_m(p_i)+q_m(p_j)\to q_m(p_1)+q_m(p_2)+g(p_3) , \tag{3.32}$$

the exchange terms make for additional complexity. In this case the result is

$$A = F'(p_i,p_j,p_1,p_2,p_3) , \tag{3.33}$$

where

$$F'(k_i,k_j,k_1,k_2,k_3)=F(k_i,k_j,k_1,k_2,k_3)+F(k_i,k_j,k_2,k_1,k_3)$$
$$+\frac{(\hat{s}^2+s'^2)(\hat{s}s'-\hat{t}t'-\hat{u}u')}{8\hat{t}t'\hat{u}u'k_{i3}k_{j3}k_{13}k_{23}}\{C_3[(\hat{s}+s')(\hat{s}s'-\hat{t}t'-\hat{u}u')+2\hat{t}t'(\hat{u}+u')+2\hat{u}u'(\hat{t}+t')]$$
$$+C_4[(\hat{s}+s')(\hat{s}s'-\hat{t}t'-\hat{u}u')-2\hat{t}t'(\hat{u}+u')-2\hat{u}u'(\hat{t}+t')$$
$$-2\hat{s}(\hat{t}\hat{u}+t'u')-2s'(\hat{t}u'+t'\hat{u})]\} , \tag{3.34}$$

[3]The more complicated formulas given by Sivers and Gottschalk (1980) appear to contain typographical errors.

with

$$C_3=10/81\ ,\quad C_4=8/81\ . \tag{3.35}$$

For the three-quantum annihilation reaction

$$\bar{q}_m(p_i)q_m(p_j)\to g(p_1)+g(p_2)+g(p_3)\ , \tag{3.36}$$

the square of the amplitude is

$$A=H(p_i,p_j,p_1,p_2,p_3)\ , \tag{3.37}$$

where

$$H(k_i,k_j,k_1,k_2,k_3)=\frac{2}{81}\sum_{l=1}^{3}\frac{k_{il}k_{jl}(k_{il}^2+k_{jl}^2)}{k_{i1}k_{i2}k_{i3}k_{j1}k_{j2}k_{j3}}\left[\frac{\hat{s}}{2}+9\left[\frac{\hat{s}}{2}-\frac{(ij;12)}{k_{12}}-\frac{(ij;13)}{k_{13}}-\frac{(ij;23)}{k_{23}}\right]\right.$$
$$\left.+\frac{81}{\hat{s}}\left[\frac{(ij;33)(ij;12)}{k_{13}k_{23}}+\frac{(ij;11)(ij;23)}{k_{12}k_{13}}+\frac{(ij;22)(ij;13)}{k_{12}k_{23}}\right]\right]\ , \tag{3.38}$$

where

$$(ij;mn)\equiv k_{im}k_{jn}+k_{in}k_{jm}\ . \tag{3.39}$$

Finally, for gluon-gluon scattering

$$g(p_i)+g(p_j)\to g(p_1)+g(p_2)+g(p_3) \tag{3.40}$$

the result can be written as

$$A=G(p_i,p_j,p_1,p_2,p_3)\ , \tag{3.41}$$

where

$$G(k_i,k_j,k_1,k_2,k_3)=\frac{27}{160}\frac{\sum_{m<n}k_{mn}^4}{\prod_{m<n}k_{mn}}\sum_{\text{perms}}(ij\,123)\ , \tag{3.42}$$

with

$$(ij\,123)\equiv k_{ij}k_{j1}k_{12}k_{23}k_{3i}\ . \tag{3.43}$$

Here the indices m and n run over $i,j,1,2,3$, and for the restriction $m<n$ we interpret $i<j<1$.

TABLE I. Squared matrix elements A_{ij} of Eq. (3.26) for $2\to3$ processes in QCD. The labels m and n refer to quark flavors; repeated indices are not summed. The results are averaged over initial-state spins and color, and summed over final-state spins and colors. The functions F, F', G, and H are defined in Eqs. (3.30), (3.34), (3.42), and (3.38), respectively.

Process $ij\to123$	A_{ij}
$q_mq_n\to q_mq_ng$	$F(p_i,p_j,p_i,p_2,p_3)$
$q_mq_m\to q_mq_mg$	$F'(p_i,p_j,p_1,p_2,p_3)$
$q_m\bar{q}_n\to q_m\bar{q}_ng$	$F(p_i,p_2,-p_1,-p_j,p_3)$
$q_m\bar{q}_m\to q_m\bar{q}_mg$	$F'(p_i,-p_2,p_1,-p_j,p_3)$
$q_m\bar{q}_m\to\bar{q}_nq_ng$	$F(p_i,-p_1,-p_j,p_2,p_3)$
$q_mg\to q_mq_n\bar{q}_n$	$(-\frac{3}{8})F(p_i,-p_3,p_1,p_2,-p_j)$
$q_mg\to q_mq_m\bar{q}_m$	$(-\frac{3}{8})F'(p_i,-p_3,p_1,p_2,-p_j)$
$gg\to ggg$	$G(p_i,p_j,p_1,p_2,p_3)$
$q_m\bar{q}_m\to ggg$	$H(p_i,p_j,p_1,p_2,p_3)$
$q_mg\to q_mgg$	$(-\frac{3}{8})H(p_i,-p_1,-p_j,p_2,p_3)$
$gg\to q_m\bar{q}_mg$	$(\frac{9}{64})H(-p_2,-p_1,-p_j,-p_i,p_3)$

The squared matrix elements for all the other $2\to3$ reactions may be obtained from these results by crossing symmetry. They are listed in Table I. Notice that symmetry factors have not been included when there are identical particles in the final state.

For the numerical results presented below we assume that the detector does not distinguish between quark or antiquark jets and gluon jets. As a result, we sum over the contributions for all permutations of the final-state momentum assignments to distinguishable particles. We have chosen the scales appearing in (3.26) as

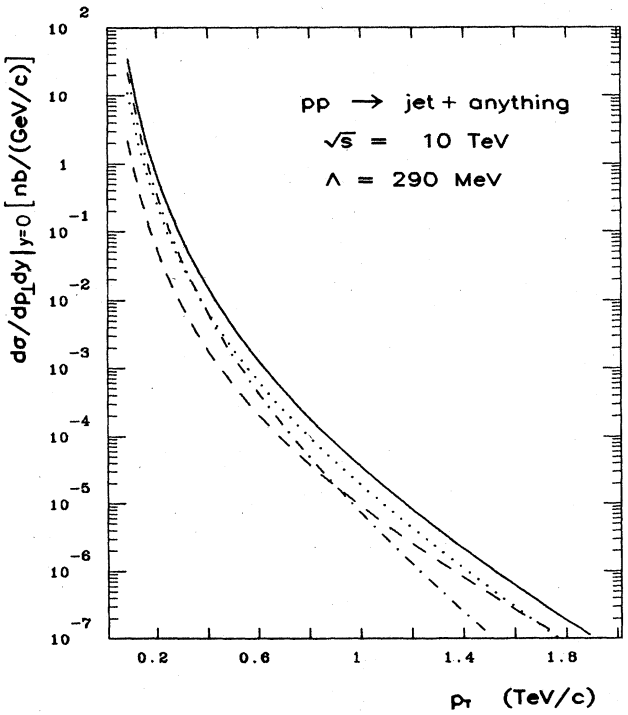

FIG. 77. Differential cross section (solid line) for jet production at $y=0$ (90° c.m.) in pp collisions at 10 TeV, according to the parton distributions of Set 2. The gg (dotted-dashed line), gq (dotted line), and qq (dashed line) components are shown separately.

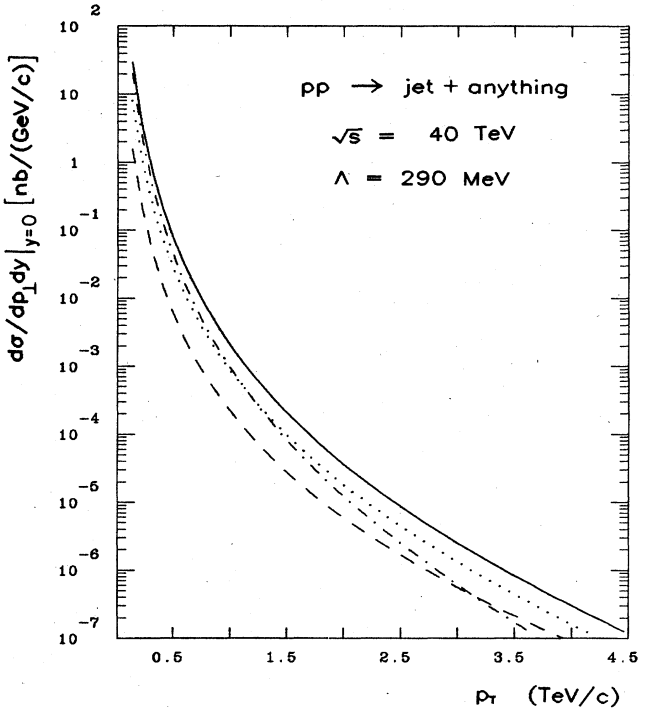

FIG. 78. Differential cross section for jet production at $y=0$ (90° c.m.) in pp collisions at 40 TeV, according to the parton distributions of Set 2.

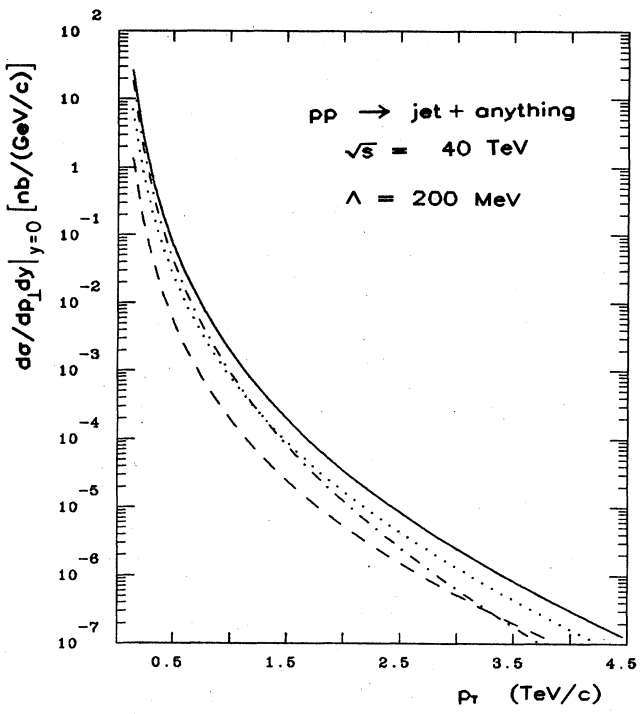

FIG. 80. Differential cross section for jet production at $y=0$ (90° c.m.) in pp collisions at 40 TeV, according to the parton distributions of Set 1.

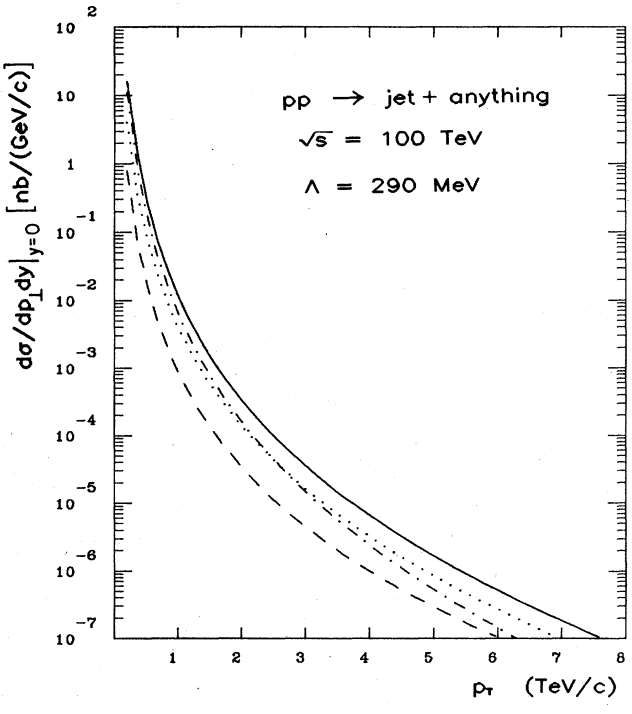

FIG. 79. Differential cross section for jet production at $y=0$ (90° c.m.) in pp collisions at 100 TeV, according to the parton distributions of Set 2.

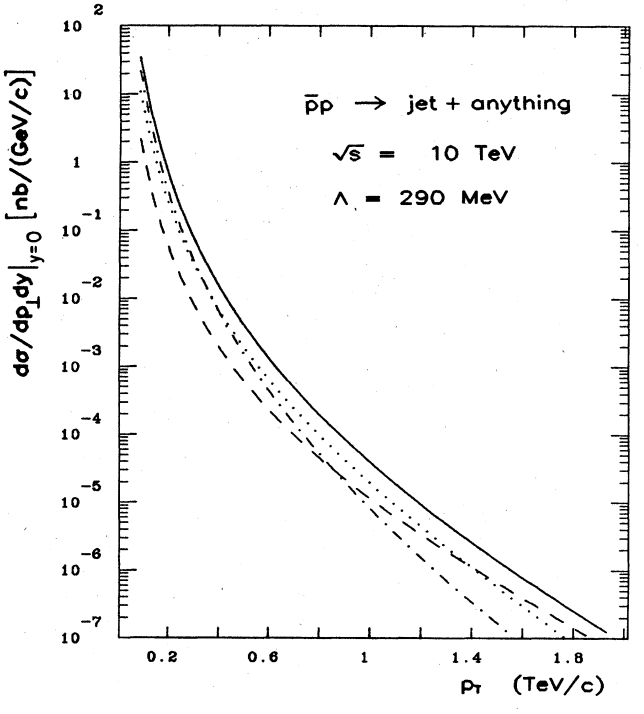

FIG. 81. Differential cross section for jet production at $y=0$ (90° c.m.) in $\bar{p}p$ collisions at 10 TeV, according to the parton distributions of Set 2.

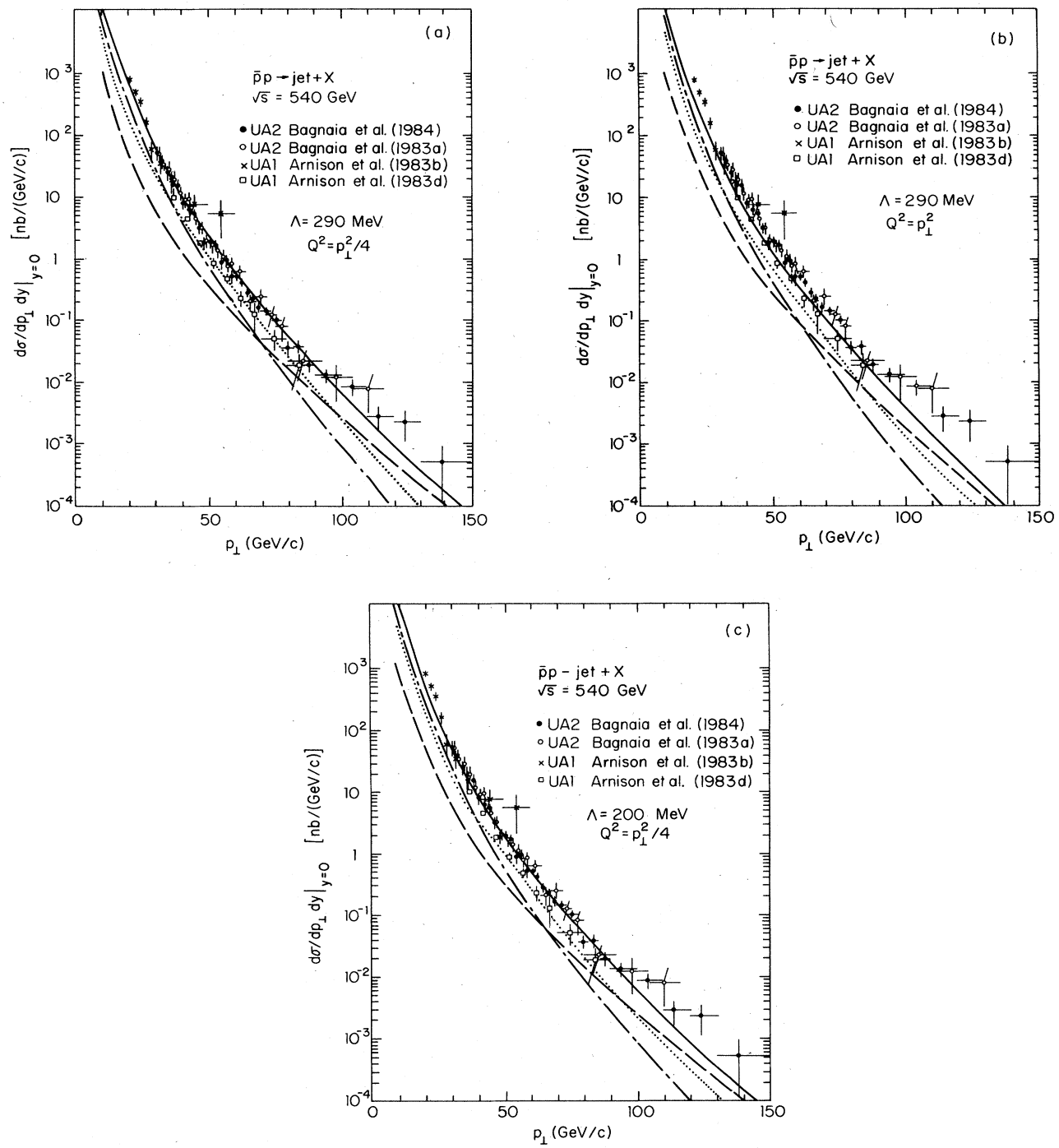

FIG. 82. Differential cross section for jet production at $y=0$ (90° c.m.) in $\bar{p}p$ collisions at 540 GeV, (a) according to the parton distributions of Set 2; (b) with the scale $Q^2=M^2=p_\perp^2$; (c) according to the parton distributions of Set 1. The data are from Arnison *et al.* (1983d) and Bagnaia *et al.* (1983a,1984).

$$Q^2=M^2=\mathcal{M}^2/4\ ; \tag{3.44}$$

as noted in Sec. III.B, they are undetermined to this order in α_s.

The three-jet cross section becomes singular as $\hat{x}_k$, the fractional energy of any jet in the c.m. frame of the three-jet system, approaches zero or one. In the former case the zero-energy jet cannot be distinguished. In the latter case the remaining two jets become parallel and coalesce. Either configuration will be identified as a two-jet event.

The most characteristic three-jet events are those in which three jets of equal energies are emitted at 90° in the colliding beam c.m. frame. In terms of the kinematic

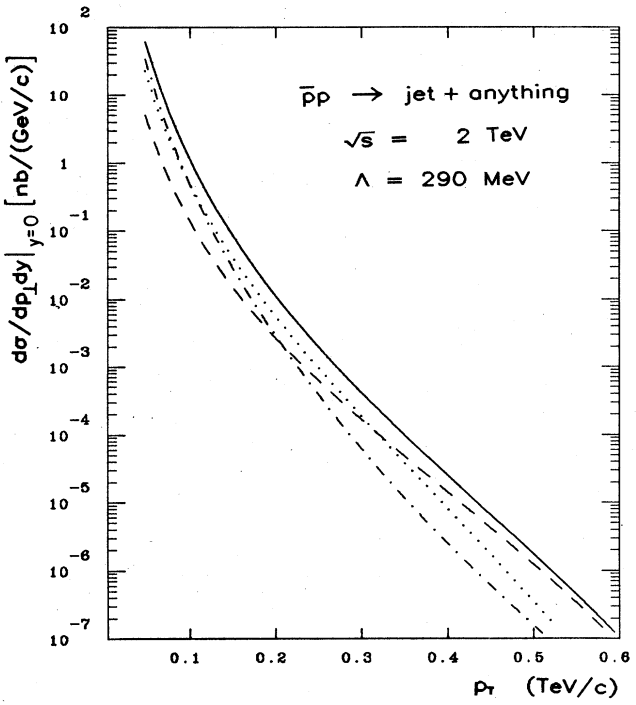

FIG. 83. Differential cross section for jet production at $y=0$ (90° c.m.) in $\bar{p}p$ collisions at 2 TeV, according to the parton distributions of Set 2.

variables introduced above, this corresponds to the parameter values $\hat{x}_1=\hat{x}_2=\hat{x}_3=\frac{2}{3}$, $y_{\text{boost}}=0$, and $\theta=0$. We show in Figs. 96–99 the differential cross section $d\sigma/d\hat{x}_1 d\hat{x}_2 dy_{\text{boost}} d\mathcal{M}\, d(\cos\theta)$ for this symmetric configuration at four collider energies. (In this situation the cross section does not depend upon the azimuthal angle φ, so the φ integration has been performed.) In events of this kind, the total transverse energy is

$$E_T=\mathcal{M}\ . \tag{3.45}$$

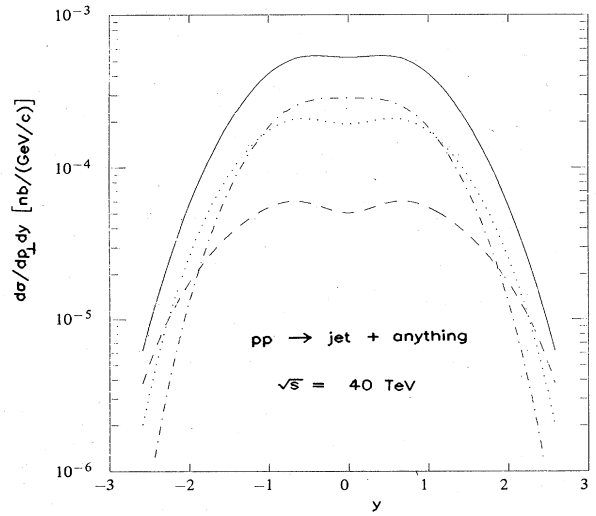

FIG. 84. Differential cross section for jet production in 40-TeV pp collisions, for $y_{\text{boost}}=0$ and $p_\perp=1$ TeV/c, according to the parton distributions of Set 2.

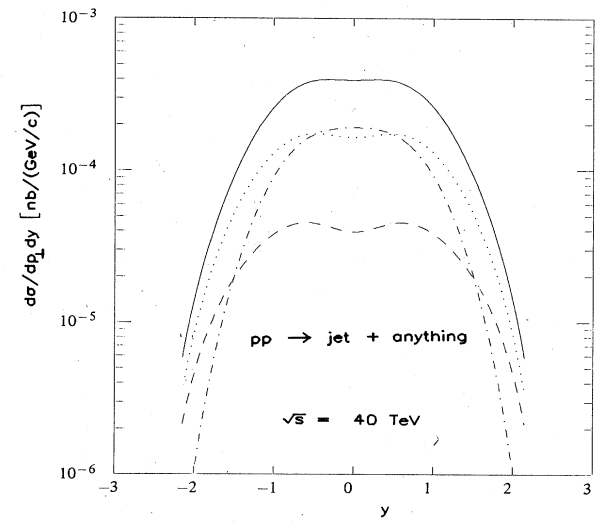

FIG. 85. Differential cross section for jet production in 40-TeV pp collisions, for $y_{\text{boost}}=1$ and $p_\perp=1$ TeV/c, according to the parton distributions of Set 2.

One measure of the relative importance of two-jet and three-jet events may therefore be obtained by comparing the symmetric three-jet cross section with $d\sigma/dp_\perp dy\,|_{y=0}$ for the two-jet case, evaluated at $p_\perp=\mathcal{M}/2$. This amounts to comparing two-jet and three-jet events with the same transverse energy. To make the comparison, it is necessary to integrate the three-jet cross section over appropriate intervals in $\hat{x}_1$, $\hat{x}_2$, and $\cos\theta$. One typically finds that at the same value of E_T, the two-jet cross section is larger by 1–2 orders of magnitude than the three-jet cross section. Of course, this particular three-jet configuration is in some sense the smallest, since the $\hat{x}_i$ are well away from the singular regions.

The contributions from the distinct final states (ggg,

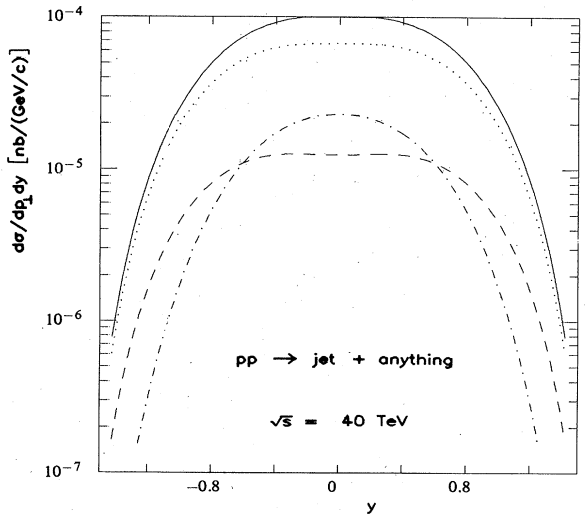

FIG. 86. Differential cross section for jet production in 40-TeV pp collisions, for $y_{\text{boost}}=2$ and $p_\perp=1$ TeV/c, according to the parton distributions of Set 2.

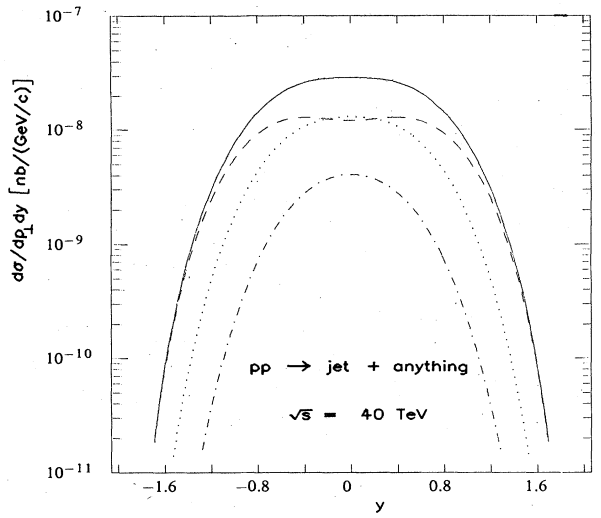

FIG. 87. Differential cross section for jet production in 40-TeV pp collisions, for $y_{\text{boost}}=0$ and $p_\perp=5$ TeV/c, according to the parton distributions of Set 2.

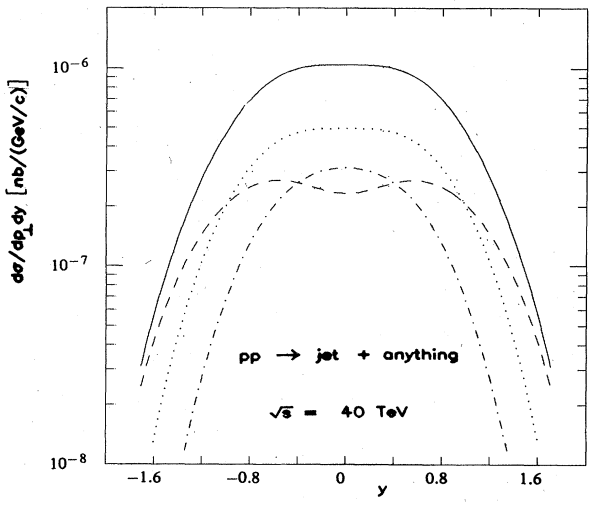

FIG. 89. Differential cross section for jet production in 40-TeV pp collisions, for $y_{\text{boost}}=0$ and $p_\perp=3$ TeV/c, according to the parton distributions of Set 2.

$gg\bar{q}^{(-)}, g\bar{q}^{(-)}\bar{q}^{(-)}$, and $\bar{q}^{(-)}\bar{q}^{(-)}\bar{q}^{(-)}$) are shown separately in the figures. At values of $\mathcal{M}$ small in comparison with $\sqrt{s}$, corresponding to parton momentum fractions

$$x_a=x_b=\mathcal{M}/\sqrt{s}\ll 1\ , \tag{3.46}$$

the process $gg\to ggg$ dominates. Just as in the two-jet events, the final state consists almost exclusively of gluon jets. As $\mathcal{M}$ increases, the process $gq\to ggq$ becomes important and eventually dominant. The three-quark final state is always negligible. Because of the preeminence of gg and gq collisions, differences between pp and $\bar{p}p$ collisions at the same energy occur only at the 10% level.

Some insight into the variation of the cross section with $\hat{x}_1$ and $\hat{x}_2$ may be gained from Fig. 100, which shows the differential cross section $d\sigma/d\hat{x}_1 d\hat{x}_2 dy_{\text{boost}} d\mathcal{M} \times d(\cos\theta)$ at $\hat{x}_1=0.3$ and $\hat{x}=0.8$ (so that $\hat{x}_3=0.9$), still with $y_{\text{boost}}=0$ and $\cos\theta=1$, for pp collisions at 40 TeV. This is close to the limiting situation in which the third jet ceases to be identifiable. The cross section is larger by about a factor of 3 than for the symmetric configuration, and the three-jet to two-jet ratio is correspondingly larger, but the relative importance of the different final states is essentially unchanged.

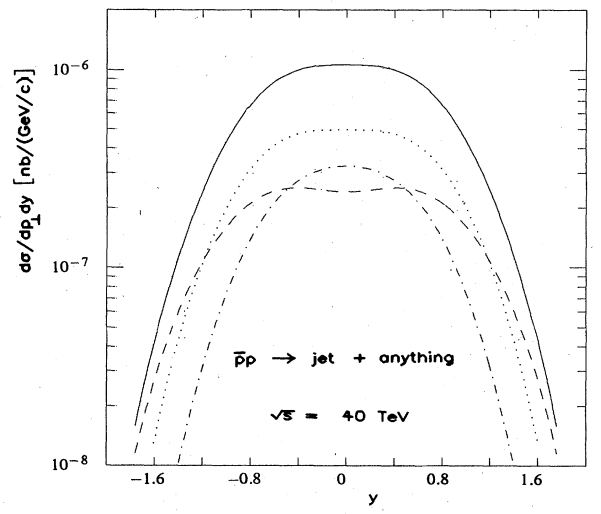

FIG. 88. Differential cross section for jet production in 40-TeV $\bar{p}p$ collisions, for $y_{\text{boost}}=0$ and $p_\perp=3$ TeV/c, according to the parton distributions of Set 2.

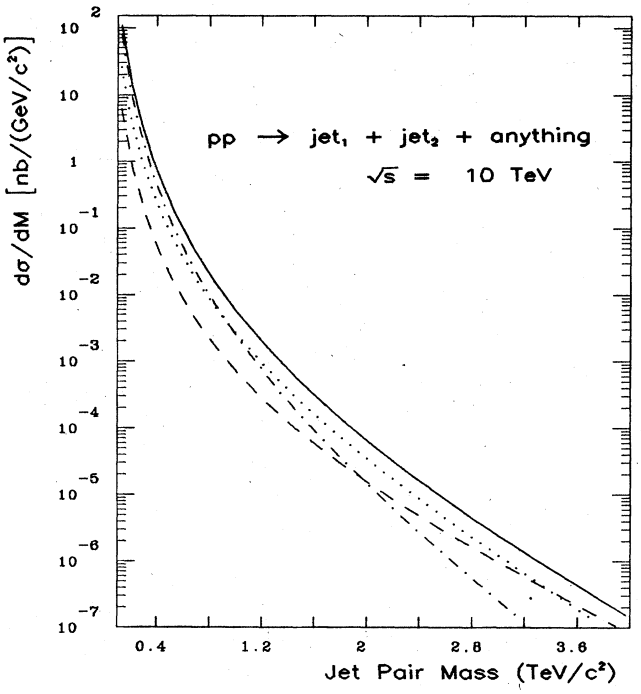

FIG. 90. Invariant mass spectrum for two-jet events produced in proton-proton collisions at $\sqrt{s}=10$ TeV, according to the parton distributions of Set 2. Both jets must satisfy $|y_i|<1.5$.

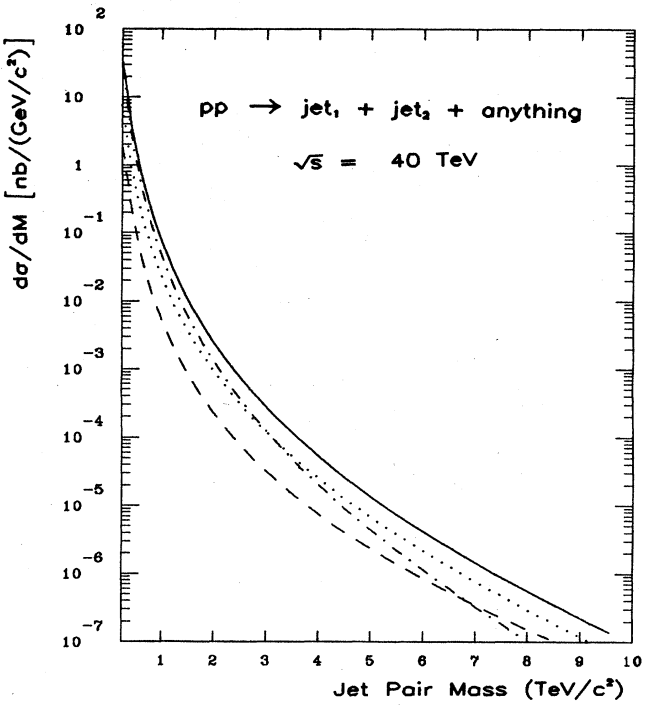

FIG. 91. Invariant mass spectrum for two-jet events produced in proton-proton collisions at $\sqrt{s}=40$ TeV, according to the parton distributions of Set 2. Both jets must satisfy $|y_i|<1.5$.

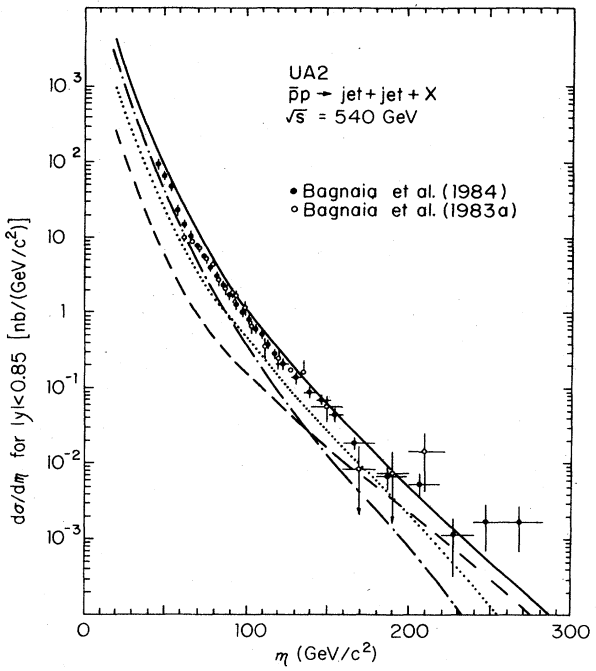

FIG. 93. Invariant mass spectrum for two-jet events produced in proton-antiproton collisions at $\sqrt{s}=540$ GeV, according to the parton distributions of Set 1. Both jets must satisfy $|y_i|<0.85$. The data are from Bagnaia *et al.* (1983a,1984); errors are statistical only.

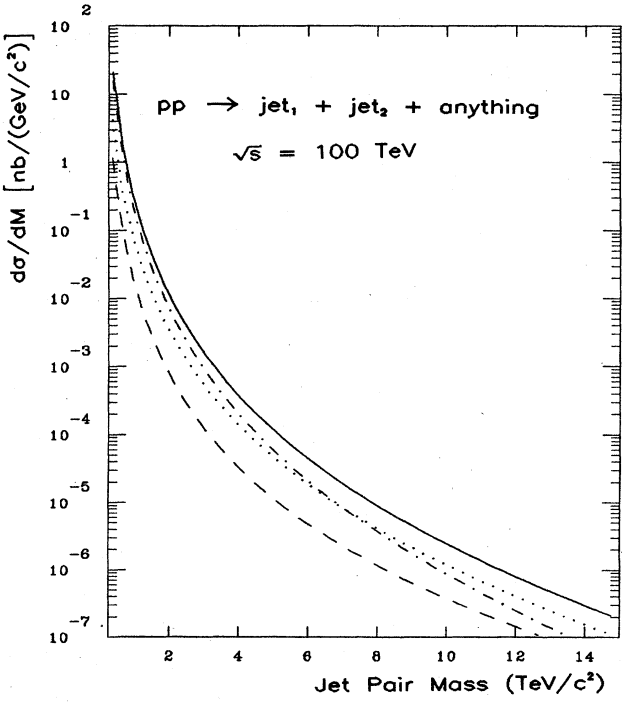

FIG. 92. Invariant mass spectrum for two-jet events produced in proton-proton collisions at $\sqrt{s}=100$ TeV, according to the parton distributions of Set 2. Both jets must satisfy $|y_i|<1.5$.

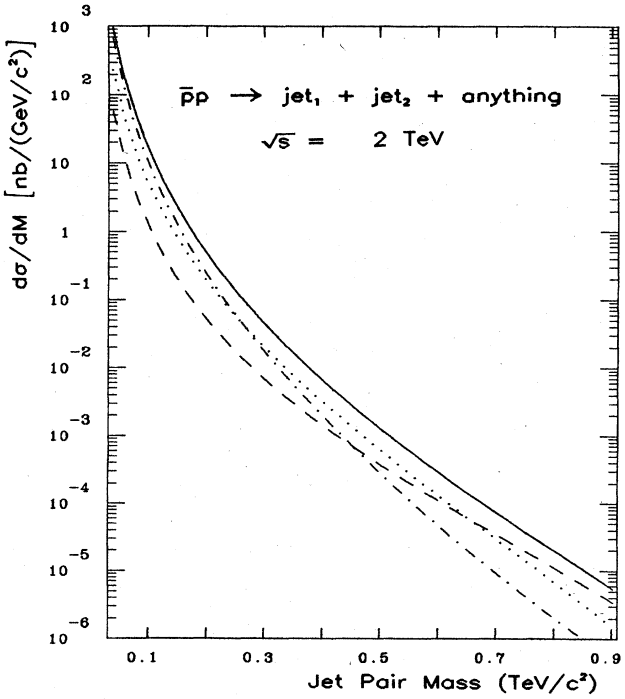

FIG. 94. Invariant mass spectrum for two-jet events produced in proton-antiproton collisions at $\sqrt{s}=2$ TeV, according to the parton distributions of Set 2. Both jets must satisfy $|y_i|<0.85$.

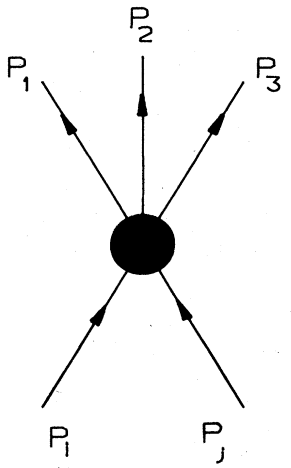

FIG. 95. A generic 2→3 process in QCD.

As the plane of the three jets approaches the beam direction with other kinematic variables held constant, the cross section increases, as shown in Fig. 101. This results from the approach to the collinear singularities in A_{ij} at $\hat{t}=0$, etc.

To determine more meaningfully the dependence of the cross section upon the orientation of the event plane we must impose some experimental cuts to ensure that all the jets are distinct. As an example we show in Fig. 102 the three-jet cross section at $y_{\text{boost}}=0$ and $\mathcal{M}=1$ TeV/c^2, subject to the requirements that each jet has an energy of

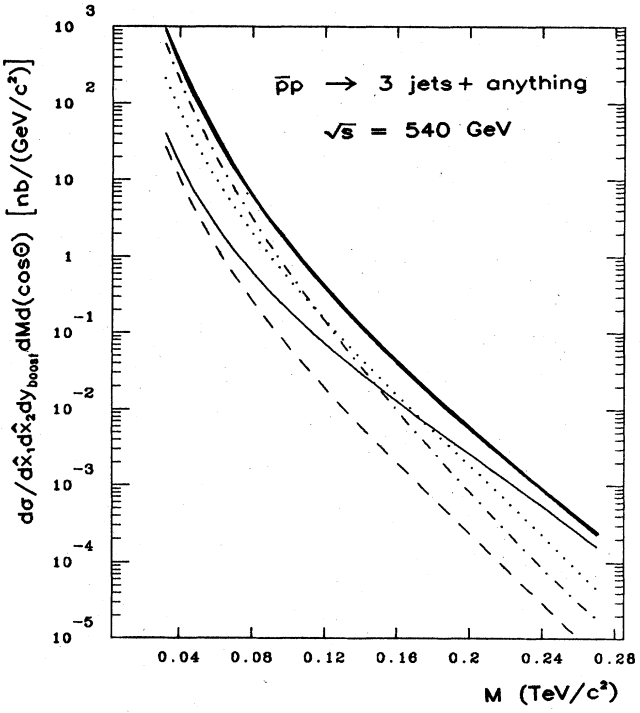

FIG. 96. Differential cross section (thick line) for symmetric 3-jet production in $\bar{p}p$ collisions at 540 GeV, according to the parton distributions of Set 2. The *ggg* (dotted-dashed line), *ggq* (dotted line), *qqg* (thin line), and *qqq* (dashed line) components are shown separately.

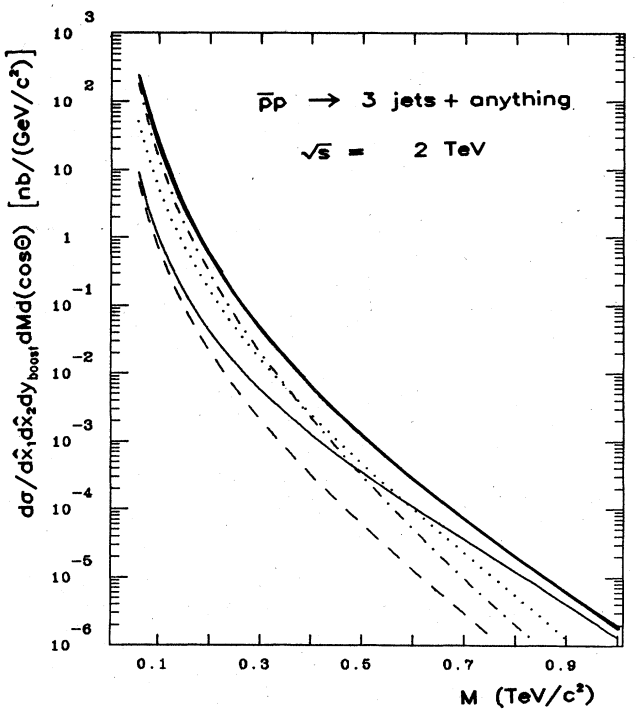

FIG. 97. Differential cross section for symmetric three-jet production in $\bar{p}p$ collisions at 2 TeV, according to the parton distributions of Set 2.

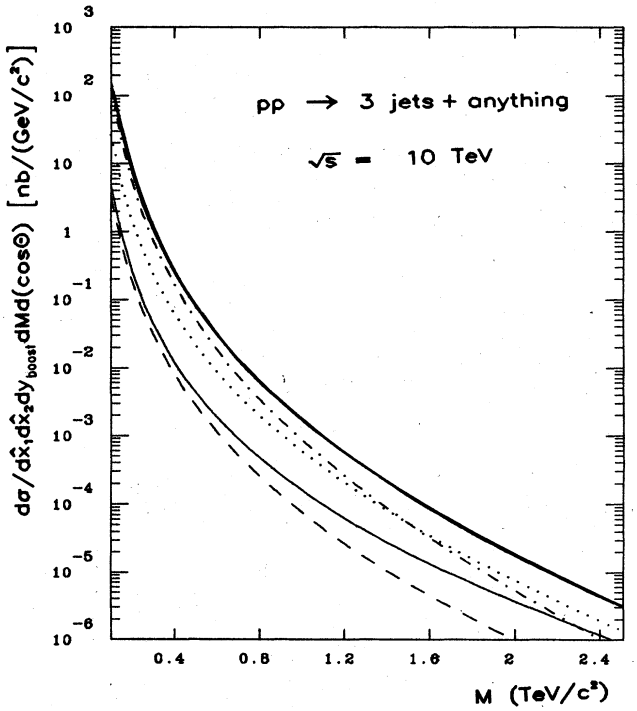

FIG. 98. Differential cross section for symmetric three-jet production in *pp* collisions at 10 TeV, according to the parton distributions of Set 2.

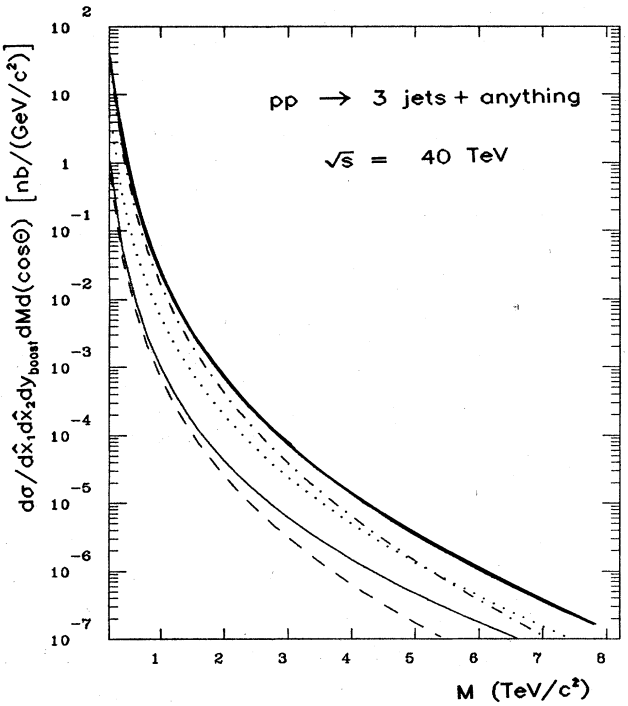

FIG. 99. Differential cross section for symmetric three-jet production in pp collisions at 40 TeV, according to the parton distributions of Set 2.

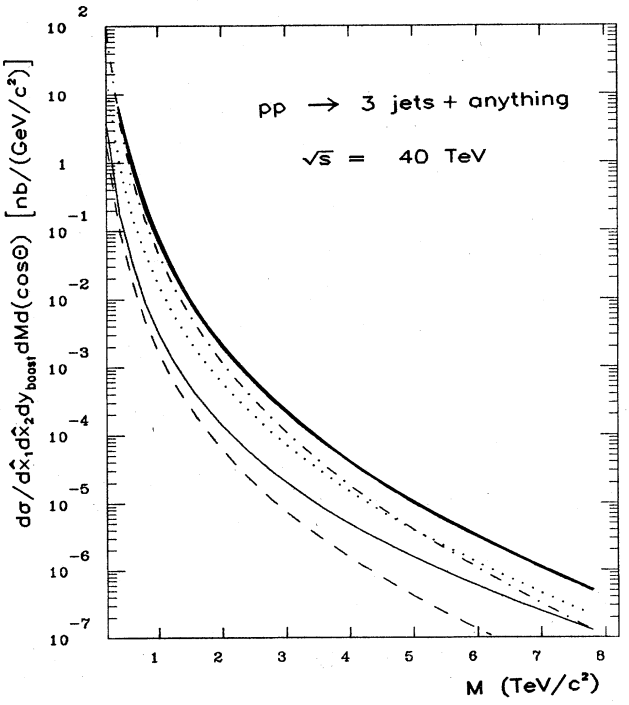

FIG. 100. Differential cross section for production of three jets at 90° in the c.m. in pp collisions at 40 TeV, according to the parton distributions of Set 2. The energy fractions of the three jets are $\hat{x}_1=0.3$, $\hat{x}_2=0.8$, and $\hat{x}_3=0.9$.

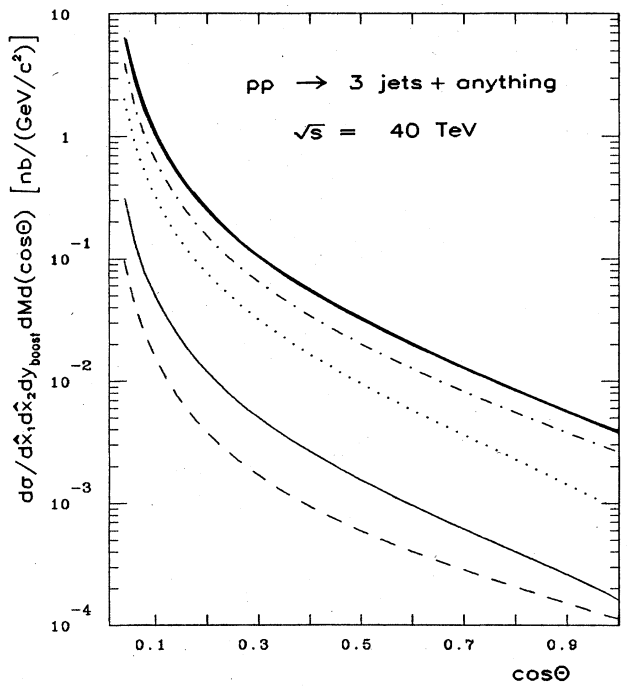

FIG. 101. Dependence upon the orientation of the three-jet plane of the differential cross section for symmetric three-jet production in pp collisions at 40 TeV, according to the parton distributions of Set 2. The invariant mass of the three-jet system is $\mathcal{M}=1$ TeV/c^2.

no less than 50 GeV, and that the angle θ_{mn} between any pair of jets or any jet and the beam direction exceeds 18°, so that $\cos\theta_{mn}<0.95$. These cuts ensure that no jet will be confused with the normal, low-$p_\perp$ beam jets, and also cut off the rise of the cross section as $\cos\theta\to 0$. The resulting cross section is concentrated around $\cos\theta=0.35$.

We can compare two-jet and three-jet contributions to $d\sigma/dE_T dy$ as follows. First, consider the interval $0.9\leq\cos\theta\leq 1$ in Fig. 102. The integrated cross section in this bin is approximately 7×10^{-3} nb/GeV, at $E_T\approx 1$

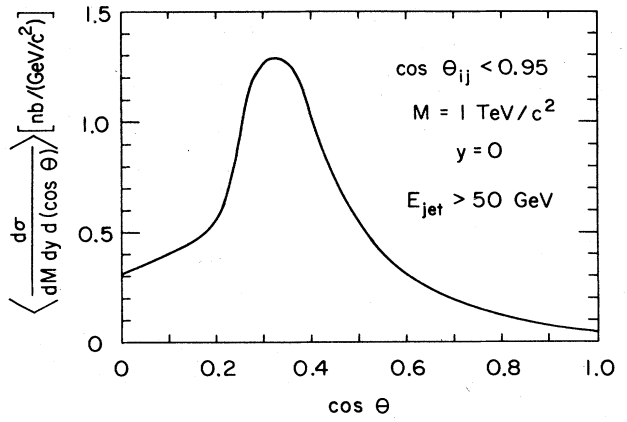

FIG. 102. Three-jet cross section in 40-TeV pp collisions integrated over azimuth and the energy fractions $\hat{x}_1$ and $\hat{x}_2$, subject to the restrictions described in the text. The three-jet invariant mass is $\mathcal{M}=1$ TeV/c^2.

TeV. From Fig. 78 we find the corresponding two-jet cross section (at $p_\perp = 0.5$ TeV/c) to be about 7×10^{-2} nb/GeV, which is larger by an order of magnitude. Let us next consider the cross section in the neighborhood of the peak in Fig. 102. The integrated cross section in the bin $0.3 \leq \cos\theta \leq 0.4$ is approximately 0.1 nb/GeV, with transverse energy given roughly by $\langle E_T \rangle \approx (1 \text{ TeV}) \times \langle \cos\theta \rangle = 350$ GeV. The corresponding two-jet cross section, again from Fig. 78, is approximately 10 nb/GeV, which is larger by 2 orders of magnitude. In fact, we have certainly underestimated $\langle E_T \rangle$ and thus somewhat overestimated the two-jet/three-jet ratio in this second case.

We draw two conclusions from this very casual analysis:

At least at small-to-moderate values of E_T, two-jet events should account for most of the cross section.

The three-jet cross section is large enough that a detailed study of this topology should be possible.

It is apparent that these questions are amenable to detailed investigation with the aid of realistic Monte Carlo simulations. Given the elementary two→three cross sections and reasonable parametrizations of the fragmentation functions, this exercise can be carried out with some degree of confidence.

For multijet events containing more than three jets, the theoretical situation is considerably more primitive. A specific question of interest concerns the QCD four-jet background to the detection of W^+W^- pairs in their nonleptonic decays. The cross sections for the elementary two→four processes have not been calculated, and their complexity is such that they may not be evaluated in the foreseeable future. It is worthwhile to seek estimates of the four-jet cross sections, even if these are only reliable in restricted regions of phase space.

Another background source of four-jet events is double parton scattering, as shown in Fig. 103. If all the parton momentum fractions are small, the two interactions may be treated as uncorrelated. The resulting four-jet cross section with transverse energy E_T may then be approximated by

$$\sigma_4(E_T) \simeq \int_\varepsilon^{E_T-\varepsilon} dE_{T1} \int_\varepsilon^{E_T-\varepsilon} dE_{T2} \frac{\sigma_2(E_{T1})\sigma_2(E_{T2})\delta(E_{T1}+E_{T2}-E_T)}{\sigma_{\text{total}}} , \tag{3.47}$$

where $\sigma_2(E_{T1})$ is the two-jet cross section and ε denotes the minimum E_T required for a discernable two-jet event. For a recent study of double parton scattering at $S\bar{p}pS$ and Tevatron energies, see Paver and Treleani (1983).

In view of the promise that multijet spectroscopy holds, improving our understanding of the QCD background is an urgent priority for further study.

D. Summary

We conclude this section with a brief summary of the ranges of jet energy which are accessible for various beam energies and luminosities. We find essentially no differences between pp and $\bar{p}p$ collisions, so only pp results will be given except at $\sqrt{s} = 2$ TeV where $\bar{p}p$ rates are quoted. Figure 104 shows the E_T range which can be explored at the level of at least one event per GeV of E_T per unit rapidity at 90° in the c.m. (compare Figs. 77–79 and 83). The results are presented in terms of the transverse energy per event E_T, which corresponds to twice the transverse momentum $p_\perp$ of a jet. In Fig. 105 we plot the values of E_T that distinguish the regimes in which the two-gluon, quark-gluon, and quark-quark final states are dominant. Comparing with Fig. 104, we find that while the accessible ranges of E_T are impressive, it seems extremely difficult to obtain a clean sample of quark jets. Useful for estimating trigger rates is the total cross section for two jets integrated over $E_T(=2p_\perp) > E_{T_0}$ for both jets in a rapidity interval of -2.5 to $+2.5$. This is shown for pp collisions in Fig. 106.

IV. ELECTROWEAK PHENOMENA

In this section we discuss the supercollider processes associated with the standard model of the weak and electromagnetic interactions (Glashow, 1961; Weinberg, 1967; Salam, 1968). By "standard model" we understand the $SU(2)_L \otimes U(1)_Y$ theory applied to three quark and lepton doublets, and with the gauge symmetry broken by a single complex Higgs doublet. The particles associated with the electroweak interactions are therefore the (left-handed) charged intermediate bosons $W^\pm$, the neutral intermedi-

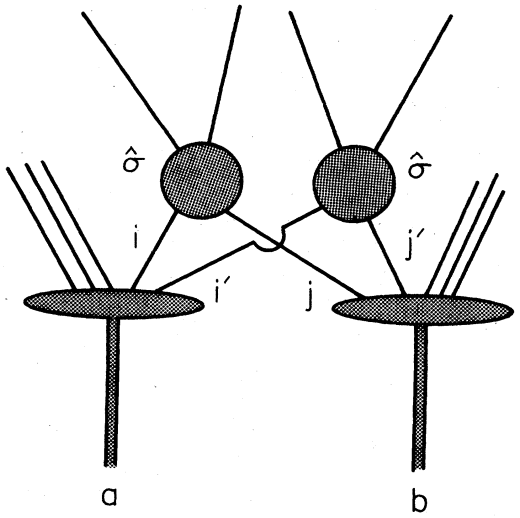

FIG. 103. Four-jet topology arising from two independent parton interactions.

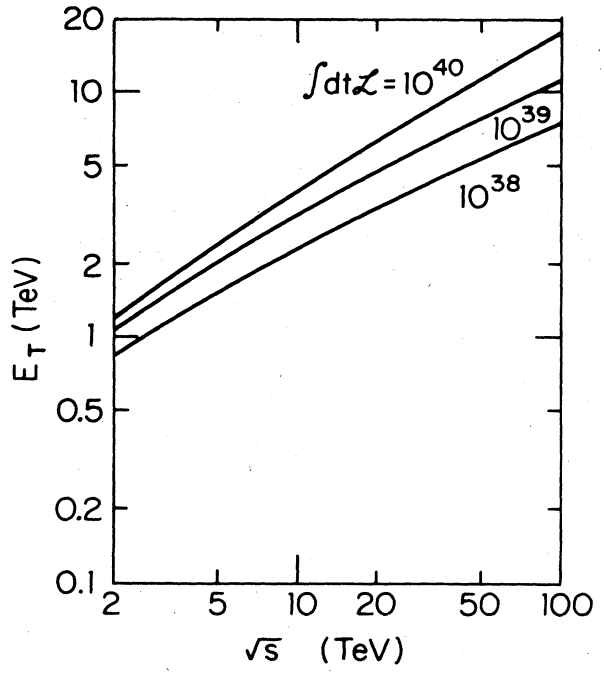

FIG. 104. Discovery reach of hadron colliders for the observation of two-jet events, according to the parton distributions of Set 2, for integrated luminosities of 10^{38}, 10^{39}, and 10^{40} cm^{-2}.

ate boson Z^0, and an elementary Higgs scalar H^0.

The principal standard model issues to be addressed with a multi-TeV hadron collider are these.

●The rate of $W^{\pm}$ and Z^0 production. This is chiefly of interest for investigations of the production mechanism

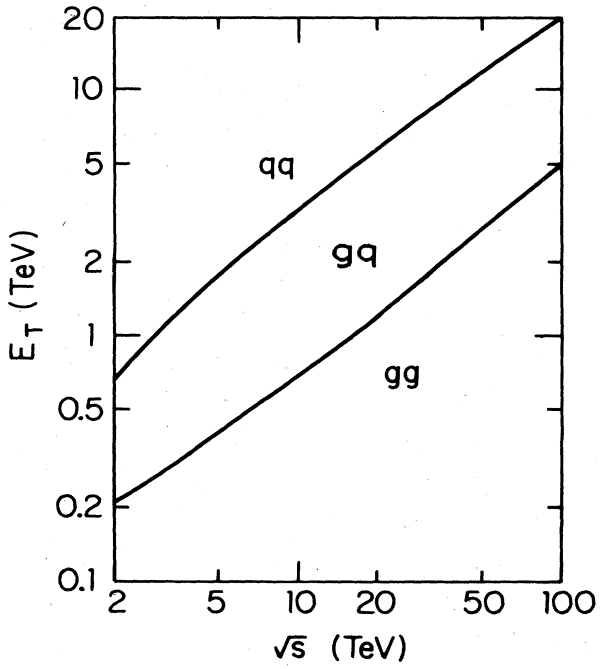

FIG. 105. Parton composition of the two-jet final states produced in pp collisions at 90° in the c.m. The curves separate the regions in which gg, gq, and qq final states are dominant.

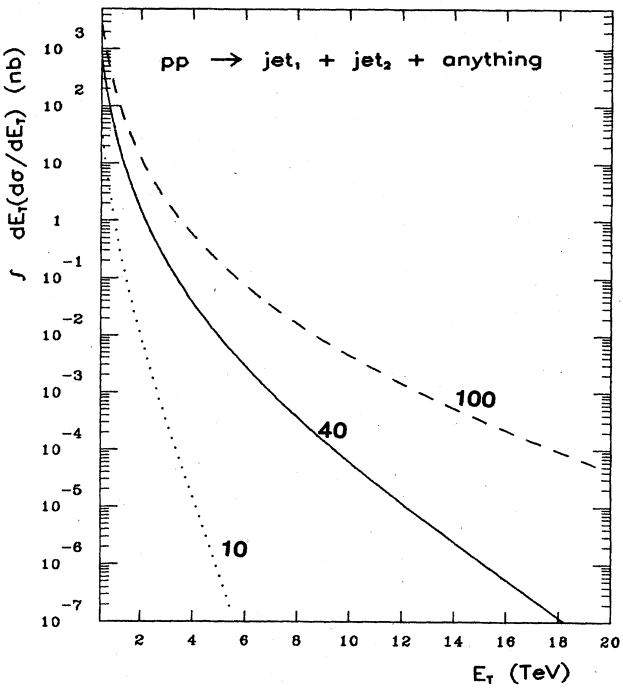

FIG. 106. The total cross section for two jets integrated over y_1 and y_2 and E_T $(=2\ p_T)$ subject to the constraints $|y_1|$, $|y_2| < 2.5$, and $E_T > E_{T_0}$ as a function of E_{T_0} for various $\sqrt{s}$, according to the parton distributions of Set 2.

itself and for the study of rare decays of the intermediate bosons. We expect that by the time a supercollider comes into operation more basic measurements, such as precision determinations of the masses and widths of the intermediate bosons, will have been accomplished.

●The cross sections for pair production of gauge bosons. These are sensitive to the structure of the trilinear couplings among gauge bosons, and must be understood as potential backgrounds to the observation of heavy Higgs bosons, composite scalars, and other novel phenomena. They would also be influenced significantly by unconventional strong interactions among the gauge bosons (Veltman, 1983).

●The Higgs boson itself. In the standard electroweak model, this is the lone boson remaining to be found. As we have emphasized in the Introduction, elucidating the structure of the Higgs sector is one of the fundamental goals of experimentation in the TeV regime.

We now shall treat in turn the conventional phenomena associated with the standard model. For each of them we shall briefly review the physics interest and discuss the anticipated rates. In the case of the Higgs boson, we shall pay particular attention to the prospects for observing and making sense of the expected experimental signatures.

A. Dilepton production

In the context of the 1-TeV scale, the reaction

$$p^{\pm}p \to l^+l^- + \text{anything} \tag{4.1}$$

is chiefly of interest as a source of background to searches for heavy quarks and other objects and as a window on perturbative QCD calculations. The elementary process we consider is the lowest-order Drell-Yan (1970,1971) mechanism,

$$q\bar{q}\to\gamma^*\to l^+l^- \tag{4.2}$$

illustrated in Fig. 107. The differential cross section for the production of a lepton pair with invariant mass M in the reaction $a+b\to l^+l^-+\text{anything}$ is given by

$$\frac{d\sigma}{dM\,dx}=\left[\frac{8\pi\alpha^2}{3M^3}\right]F(\tau,x,M^2)\ , \tag{4.3}$$

where the function

$$F(\tau,x,M^2)=\frac{x_a x_b}{(x^2+4\tau)^{1/2}}g(x_a,x_b,M^2) \tag{4.4}$$

depends upon the scaled variables

$$\tau=M^2/s \tag{4.5}$$

and

$$x=2p_{||}^{(\text{c.m.})}/\sqrt{s} \tag{4.6}$$

in the combinations

$$x_{a,b}=\tfrac{1}{2}[(x^2+4\tau)^{1/2}\pm x]\ . \tag{2.8}$$

Information about the quark-antiquark luminosity is contained in the function

$$g(x_a,x_b,M^2)=\tfrac{1}{3}\sum_{\substack{\text{flavors}\\ i}} e_i^2[f_i^{(a)}(x_a,M^2)f_{\bar{i}}^{(b)}(x_b,M^2) +f_{\bar{i}}^{(a)}(x_a,M^2)f_i^{(b)}(x_b,M^2)]\ , \tag{4.7}$$

where e_i is the charge of quark flavor i in units of the proton charge and $f_i^{(a)}(x_a,Q^2)$ is the number distribution of i quarks in hadron a. The factor $\frac{1}{3}$ is a consequence of color: the quark and antiquark that annihilate into a virtual photon must have the same color as well as flavor.

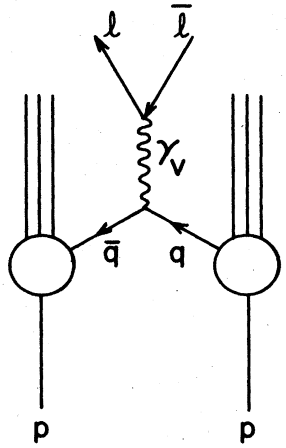

FIG. 107. Drell-Yan mechanism for massive lepton-pair production in pp collisions.

In high-energy collisions it is frequently convenient to work in terms of the c.m. rapidity variable

$$y=\frac{1}{2}\ln\left[\frac{E^{(\text{c.m.})}+p_{||}^{(\text{c.m.})}}{E^{(\text{c.m.})}-p_{||}^{(\text{c.m.})}}\right]\ , \tag{4.8}$$

which is related to x, x_a, and x_b through

$$x=2\sqrt{\tau}\sinh y\ , \tag{4.9}$$

$$x_{a,b}=\sqrt{\tau}e^{\pm y}\ . \tag{4.10}$$

The differential cross section is given by

$$\frac{d\sigma}{dM\,dy}=(x^2+4\tau)^{1/2}\frac{d\sigma}{dM\,dx} =\left[\frac{8\pi\alpha^2}{3M^3}\right]\tau g(\sqrt{\tau}e^{y},\sqrt{\tau}e^{-y},M^2)\ . \tag{4.11}$$

The integrated cross section for dilepton production is

$$\frac{d\sigma}{dM}=\left[\frac{8\pi\alpha^2}{3M^3}\right]\tau\int_\tau^1\frac{dx\,g(x,\tau/x,M^2)}{x} =\left[\frac{8\pi\alpha^2}{9M^3}\right]\sum_i e_i^2\left[\frac{\tau\,d\mathscr{L}_{i\bar{i}}}{d\tau}\right]\ . \tag{4.12}$$

Apart from the gentle M dependence of the differential luminosity which arises from scaling violations in the parton distributions, the quantity $M^3d\sigma/dM$ is a function of the dimensionless variable τ alone. Although there are important strong-interaction corrections to the parton model for this process, the scaling behavior has been established experimentally to good approximation.[4]

At the masses which have been accessible in experiments to date, the virtual photon mechanism of Fig. 107 is an adequate approximation. At higher masses it is necessary to include the contributions of a real or virtual neutral intermediate boson in the elementary process

$$q\bar{q}\to Z^0\to l^+l^-\ . \tag{4.13}$$

This may readily be done by making the replacement

$$e_i^2\to e_i^2-\frac{M^2(M^2-M_z^2)(L_e+R_e)(L_q+R_q)}{8x_W(1-x_W)[(M^2-M_Z^2)^2+M_Z^2\Gamma_Z^2]}e_i +\frac{M^4(L_e^2+R_e^2)(L_q^2+R_q^2)}{64x_W^2(1-x_W)^2[(M^2-M_Z^2)^2+M_Z^2\Gamma_Z^2]} \tag{4.14}$$

in the definition of $g(x_a,x_b,Q^2)$ in Eq. (4.7), and in (4.12). Here the chiral couplings of the neutral weak current are

$$L_e=2x_W-1\ , \qquad R_e=2x_W\ , \tag{4.15}$$

[4]See, for example, the data compiled in Fig. 7-15 of Quigg (1983).

for the electron (or sequential charged lepton) and

$$L_q=\tau_3-2e_q x_W\ ,$$
$$R_q=-2e_q x_W\ , \tag{4.16}$$

for the quarks, where τ_3 is the weak isospin projection of the quark and $x_W=\sin^2\theta_W$ is the weak mixing angle. In the standard model, the width of the Z^0 is

$$\Gamma_Z=\frac{G_F M_Z^3\sqrt{2}}{3\pi}\left[1-2x_W+\frac{8x_W^2}{3}\right]D\ , \tag{4.17}$$

where D is the number of kinematically accessible quark and lepton doublets and

$$M_Z^2=M_W^2/(1-x_W)=\frac{\pi\alpha}{G_F\sqrt{2}x_W(1-x_W)}$$
$$=(37.3\ \text{GeV}/c^2)^2/x_W(1-x_W)\ . \tag{4.18}$$

With $x_W=0.22$ and $D=3$, we expect

$$M_Z\approx 90\ \text{GeV}/c^2 \tag{4.19}$$

and

$$\Gamma_Z=2.6\ \text{GeV}\ . \tag{4.20}$$

The partial width into charged lepton pairs is

$$\Gamma(Z^0\to l^+l^-)=\frac{G_F M_Z^3}{12\pi\sqrt{2}}(1-4x_W+8x_W^2)$$
$$=(1-4x_W+8x_W^2)\Gamma(Z^0\to\nu\bar{\nu})\ . \tag{4.21}$$

With $x_W=0.22$ and $D=3$, the branching ratio into a pair of electrons, muons, or taus is approximately 3%.

We display in Fig. 108 the quantity $d\sigma/dM\,dy\,|_{y=0}$ for pp collisions at c.m. energies of 2, 10, 20, 40, 70, and 100 TeV. The cross sections shown are based on the parton distributions of Set 2. In general we shall present results only for Set 2, unless the two sets yield significantly different cross sections. For an integrated luminosity of 10^{40} cm^{-2}, we anticipate a yield of one event per GeV/c^2 per unit rapidity for

$$M\approx\begin{cases}300\ \text{GeV}/c^2 & \text{at } \sqrt{s}=2\ \text{TeV}\\ 500\ \text{GeV}/c^2 & \text{at } \sqrt{s}=10\ \text{TeV}\\ 600\ \text{GeV}/c^2 & \text{at } \sqrt{s}=20\ \text{TeV}\\ 700\ \text{GeV}/c^2 & \text{at } \sqrt{s}=40\ \text{TeV}\\ 800\ \text{GeV}/c^2 & \text{at } \sqrt{s}=70\ \text{TeV}\\ 850\ \text{GeV}/c^2 & \text{at } \sqrt{s}=100\ \text{TeV}\ .\end{cases} \tag{4.22}$$

The energy dependence of the cross section, and thus of the maximum attainable pair mass, can readily be inferred from the contour plot Fig. 63 of the rate of $\bar{u}u$ interactions in pp collisions, using the connection of Eq. (4.12). The Drell-Yan cross section for $\bar{p}p$ collisions is reported in Fig. 109. The yields are slightly, but not significantly, higher than those expected in proton-proton collisions.

The Drell-Yan mechanism operates for the pair pro-

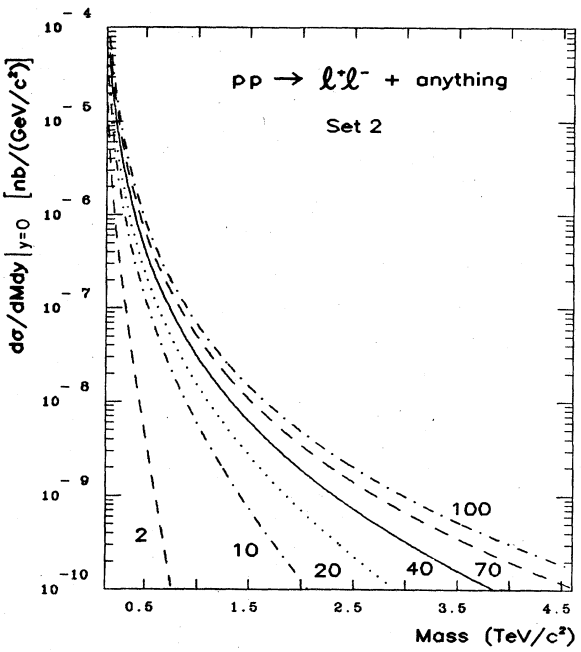

FIG. 108. Cross section $d\sigma/dM\,dy\,|_{y=0}$ for the production of lepton pairs in proton-proton collisions. The contributions of γ^* and Z intermediate states are included. The energies shown are 2, 10, 20, 40, 70, and 100 TeV. Set 2 of parton distributions was used.

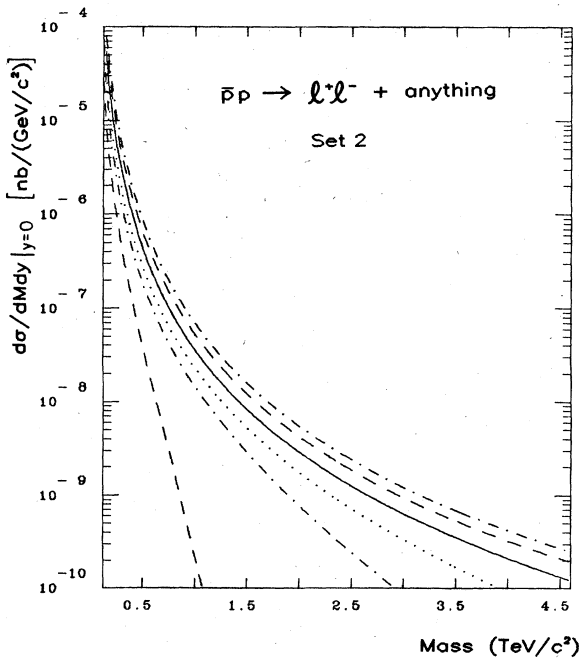

FIG. 109. Cross section $d\sigma/dM\,dy\,|_{y=0}$ for the production of lepton pairs in proton-antiproton collisions. The contributions of γ^* and Z intermediate states are included. The energies shown are 2, 10, 20, 40, 70, and 100 TeV. Set 2 of parton distributions was used.

duction of any pointlike charged lepton. If the lepton mass m_L is not negligible compared to the pair mass M, there is a kinematical suppression of the cross section in the form of an additional factor $(1-4m_L^2/M^2)^{1/2}\times(1+2m_L^2/M^2)$. This is discussed in detail in Sec. V.

Within the framework of QCD there are additional contributions to dilepton production, such as the elementary process

$$g+q\rightarrow(\gamma \text{ or } Z^0)+q \\ \qquad\qquad \hookrightarrow l^+l^- , \tag{4.23}$$

as well as strong-interaction corrections to the basic Drell-Yan mechanism. Although these do not alter our conclusions qualitatively, they do have interesting consequences for the rate, the transverse momentum distribution, event topology, and other features. The state of the art is summarized in the workshop proceedings edited by Berger *et al.* (1983).

B. Intermediate boson production

The intermediate bosons of the standard model, which set the scale for the current generation of colliders, will still be of interest at a supercollider for calibration and backgrounds, and for the study of rare decays. The conventional expectations for the discovery of the intermediate bosons were set out in detail in papers by Quigg (1977) and by Okun and Voloshin (1977). An up-to-date review has been given by Ellis *et al.* (1982). The first observations of the $W^{\pm}$ and Z^0 have been reported by Arnison *et al.* (1983a,1983c), Banner *et al.* (1983), and Bagnaia *et al.* (1983b).

We recall that in the standard model the mass of the charged intermediate boson is given in lowest order by

$$M_W^2=\frac{\pi\alpha}{G_F\sqrt{2}x_W} \\ =\frac{(37.3\ \text{GeV}/c^2)^2}{x_W} , \tag{4.24}$$

where $x_W=\sin^2\theta_W$ is the weak mixing angle. The leptonic decay rate is

$$\Gamma(W\rightarrow l\nu)=G_F M_W^3/6\pi\sqrt{2} . \tag{4.25}$$

The partial widths for nonleptonic $W^{\pm}$ decays may be related at once to the leptonic width as, for example,

$$\Gamma(W^+\rightarrow u\bar{d})=3\cos^2\theta_c\Gamma(W\rightarrow l\nu) , \\ \Gamma(W^+\rightarrow u\bar{s})=3\sin^2\theta_c\Gamma(W\rightarrow l\nu) , \tag{4.26}$$

where the factor of 3 accounts for quark colors. More generally, if D_q is the number of color-triplet SU(2) doublets of quarks into which the intermediate boson can decay, and D_l is the number of energetically accessible lepton doublets, then the total width is given by

$$\Gamma(W\rightarrow\text{all})=(D_l+3D_q)\Gamma(W\rightarrow l\nu) . \tag{4.27}$$

Here we have ignored quark masses and mixing angles.

For the weak mixing parameter

$$x_W=0.22 , \tag{4.28}$$

a plausible value, we find

$$M_W\approx 81\ \text{GeV}/c^2 \tag{4.29}$$

and

$$\Gamma(W\rightarrow l\nu)\approx 250\ \text{MeV} . \tag{4.30}$$

Consequently, for three doublets of quarks and leptons we anticipate a total width of

$$\Gamma(W\rightarrow\text{all})\approx 2.8\ \text{GeV} . \tag{4.31}$$

There are radiative corrections to these masses and widths in the standard model which depend upon the masses of quarks and leptons (Marciano, 1979; Antonelli, Consoli, and Corbo, 1980; Veltman, 1980; Sirlin and Marciano, 1981; Wheater and Llewellyn Smith, 1982; Marciano and Senjanovic, 1982; Marciano and Sirlin, 1984). In particular, the ratio $\rho=M_W^2/M_Z^2(1-x_W)$ deviates slightly from one (Veltman, 1977; Marciano, 1979); this is used to constrain extra generations of quarks and leptons in Sec. V. The resulting values for the radiatively corrected masses are (Marciano and Parsa, 1982) $M_W=83.9^{+5.5}_{-4.7}$ GeV/c^2 and $M_Z=93.8^{+2.5}_{-2.4}$ GeV/c^2.

The normalized angular distribution of the decay fermion is

$$\frac{dN}{d\Omega}=\begin{cases}\frac{3}{16\pi}(1-\cos\theta)^2 , & \lambda_W=1 \\ \frac{3}{8\pi}\sin^2\theta , & \lambda_W=0 \\ \frac{3}{16\pi}(1+\cos\theta)^2 , & \lambda_W=-1 ,\end{cases} \tag{4.32}$$

where λ_W is the helicity of the $W^{\pm}$ and θ is the angle between the lepton direction and the W spin quantization axis in the W rest frame.

The cross section for the reaction

$$a+b\rightarrow W^{\pm}+\text{anything} \tag{4.33}$$

can be computed directly in the Drell-Yan picture. In this case the elementary reactions are

$$u+\bar{d}_\theta\rightarrow W^+ , \\ \bar{u}+d_\theta\rightarrow W^- , \tag{4.34}$$

where $d_\theta=d\cos\theta_c+s\sin\theta_c$. The differential cross section is given by

$$\frac{d\sigma}{dy}=G_F\pi\sqrt{2}\tau W^{(\pm)}(\sqrt{\tau}e^y,\sqrt{\tau}e^{-y},M_W^2) , \tag{4.35}$$

where $\tau=M_W^2/s$ and

$$W^{(+)}(x_a,x_b,Q^2)=\tfrac{1}{3}\{[f_u^{(a)}(x_a,Q^2)f_{\bar{d}}^{(b)}(x_b,Q^2)+f_{\bar{d}}^{(a)}(x_a,Q^2)f_u^{(b)}(x_b,Q^2)]\cos^2\theta_c$$
$$+[f_u^{(a)}(x_a,Q^2)f_{\bar{s}}^{(b)}(x_b,Q^2)+f_{\bar{s}}^{(a)}(x_a,Q^2)f_u^{(b)}(x_b,Q^2)]\sin^2\theta_c\} . \quad (4.36)$$

Quarks and antiquarks are interchanged for W^- production. The integrated $W^\pm$ cross section is[5]

$$\sigma_{W^\pm}=G_F\pi\sqrt{2}\tau\int_\tau^1\frac{dx\,W^{(\pm)}(x,\tau/x,M_W^2)}{x}$$
$$=\frac{G_F\pi\sqrt{2}}{3}\left[\tau\frac{d\mathcal{L}_{u\bar{d}}}{d\tau}\cos^2\theta_c+\tau\frac{d\mathcal{L}_{u\bar{s}}}{d\tau}\sin^2\theta_c\right]$$
$$\approx 6.3\text{ nb}\,\tau\frac{d\mathcal{L}_{u\bar{d}}}{d\tau} . \quad (4.37)$$

Integrated cross sections for $W^\pm$ production in pp and $\bar{p}p$ collisions are shown in Figs. 110 and 111 as functions of the c.m. energy $\sqrt{s}$. The figures also show the cross sections for production of $W^\pm$ in the rapidity interval between -1.5 and $+1.5$. In pp collisions the production of W^- is suppressed relative to W^+ by a factor of 2 or so because of the smaller momentum fraction carried by down quarks compared with up quarks. The cross sections for W^+ and W^- production are necessarily equal in $\bar{p}p$ collisions. As in the case of dilepton production, the competitive advantage of antiproton beams is important only for $\sqrt{\tau}\geq 0.1$.

The angular distribution of the produced W's is of great importance for the design of experiments. At supercollider energies, many intermediate bosons will be produced within a narrow angular cone about the beam direction. Special-purpose detectors deployed near the forward direction may have significant advantages for the study of rare decays.[6] To illustrate this point we show in Fig. 112(a) the rapidity distribution $d\sigma/dy$ for W^+ production in proton-proton collisions at 40 TeV. The mapping from rapidity to c.m. angles is given in Fig. 113. In a machine with an average luminosity of $10^{33}\text{ cm}^{-2}\text{sec}^{-1}$, there will be a flux of approximately 10 W^+/sec emitted within 2° of the beam direction, in each hemisphere. Similar results for $\bar{p}p$ collisions are shown in Fig. 114(a). The nearly complete alignment of W spins, which provided a dramatic charge asymmetry in the CERN $S\bar{p}pS$ experiments at $\sqrt{s}=540$ GeV, is considerably diluted at these high energies, where much of the cross section is provided by annihilations of sea quarks and sea antiquarks. [Compare, for example, Fig. 16 of Quigg (1977).] Figures 112(b) and 114(b) show the net helicity of the produced W^+ at $\sqrt{s}=40$ TeV.

The analysis of single Z^0 production proceeds along similar lines, and is implicit in our discussion of dilepton production where the expectations of the standard model for mass and widths were given. The reaction

$$a+b\to Z^0+\text{anything} \quad (4.38)$$

proceeds via the elementary processes $u\bar{u}\to Z^0$, $d\bar{d}\to Z^0$, etc. The differential cross section may be written as

$$\frac{d\sigma}{dy}=\frac{G_F\pi\tau}{\sqrt{2}}Z(\sqrt{\tau}e^y,\sqrt{\tau}e^{-y},M_Z^2) , \quad (4.39)$$

where $\tau=M_Z^2/s$ and

$$Z(x_a,x_b,Q^2)=\tfrac{1}{3}\sum_{\substack{\text{quark}\\ \text{flavors } q}}\{[f_q^{(a)}(x_a,Q^2)f_{\bar{q}}^{(b)}(x_b,Q^2)$$
$$+f_{\bar{q}}^{(a)}(x_a,Q^2)f_q^{(b)}(x_b,Q^2)]$$
$$\times(L_q^2+R_q^2)\} . \quad (4.40)$$

The neutral current couplings L_q and R_q have been given in (4.16). The integrated Z^0 cross section is

$$\sigma_{Z^0}=\frac{G_F\pi\tau}{\sqrt{2}}\int_\tau^1\frac{dx\,Z(x,\tau/x,M_Z^2)}{x}$$
$$=\frac{G_F\pi}{3\sqrt{2}}\sum_q\frac{\tau d\mathcal{L}_{q\bar{q}}}{d\tau}(L_q^2+R_q^2)$$
$$\approx 3.3\text{ nb}\left[0.59\tau\frac{d\mathcal{L}_{u\bar{u}}}{d\tau}+0.75\tau\frac{d\mathcal{L}_{d\bar{d}}}{d\tau}\right] . \quad (4.41)$$

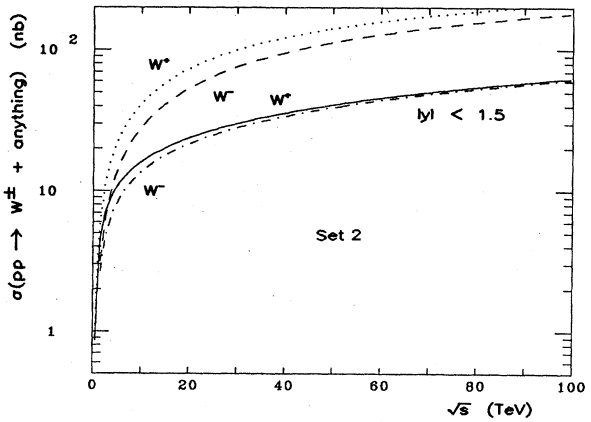

FIG. 110. Cross sections for $W^\pm$ production in pp collisions in the Drell-Yan picture. Also shown are the cross sections for $W^\pm$ produced in the rapidity interval $-1.5<y<+1.5$. Set 2 of parton distributions was used.

[5]The subsequent formulas are given for only two generations of quarks and leptons. The complete formulas are a trivial extension and were used in generating the figures.

[6]We thank F. Sciulli for raising this possibility.

Integrated cross sections for Z^0 production in pp and $\bar{p}p$ collisions are shown in Fig. 115 for the distributions of Set 2 and in Fig. 116 for those of Set 1. Again the cross section if the Z is restricted to rapidity between $+1.5$ and -1.5 is also shown. The $\bar{p}p$ cross section is larger by a factor of 5 at $\sqrt{s}=0.54$ TeV, but the advantage of $\bar{p}p$ over pp diminishes rapidly with increasing energy. It is only a 15% effect at $\sqrt{s}=10$ TeV. The rapidity distributions are similar to those anticipated for $W^{\pm}$ production.

The transverse momentum of the W's and Z's produced in the processes discussed so far is small. There are higher-order QCD processes which can produce a W (or Z) with large transverse momentum ($p_\perp$), the $p_\perp$ being balanced by a hadronic jet. The processes $g+q\to W+q$ and $q+\bar{q}\to W+g$ are shown in Fig. 117. The cross sections are given by Halzen and Scott (1978). The cross section for producing a W^+ with rapidity y is given by

$$\frac{d\sigma}{dp_\perp dy}=2p_\perp\sum_{ij}\int_{x_{\min}}^{1}dx_a\frac{f_i^{(a)}(x_a,Q^2)f_j^{(b)}(x_b,Q^2)\hat{\sigma}_{ij}(\hat{s},\hat{t},\hat{u})}{x_a s+u-M_W^2}\,, \tag{4.42}$$

where

$$\begin{aligned}
t&=-\sqrt{s}m_\perp e^{-y}+M_W^2\,,\\
u&=-\sqrt{s}m_\perp e^{y}+M_W^2\,,\\
\hat{s}&=x_a x_b s\,,\\
\hat{t}&=-\sqrt{s}x_a m_\perp e^{-y}+M_W^2\,,\\
\hat{u}&=-\sqrt{s}x_b m_\perp e^{y}+M_W^2\,,
\end{aligned} \tag{4.43}$$

with

$$\begin{aligned}
m_\perp^2&=p_\perp^2+M_W^2\,,\\
x_b&=\frac{-x_a t-(1-x_a)M_W^2}{x_a s+u-M_W^2}\,,\\
x_{\min}&=-u/(s+t-M_W^2)\,,
\end{aligned} \tag{4.44}$$

and the partonic cross-sections are for $q+\bar{q}\to W+g$

$$\hat{\sigma}_{ij}(\hat{s},\hat{t},\hat{u})=\frac{2\pi\alpha\alpha_s(Q^2)}{9x_W}\frac{(\hat{t}-M_W^2)^2+(\hat{u}-M_W^2)^2}{\hat{s}\hat{t}\hat{u}} \tag{4.45}$$

and for $q+g\to W+q$ or $\bar{q}+g\to W+\bar{q}$

$$\hat{\sigma}(\hat{s},\hat{t},\hat{u})=\frac{\pi\alpha\alpha_s(Q^2)}{12x_W}\frac{\hat{s}^2+\hat{u}^2+2M_W^2\hat{t}}{-\hat{s}^2\hat{u}}+(\hat{t}\leftrightarrow\hat{u})\,. \tag{4.46}$$

We have used $Q^2=p_\perp^2$ in generating Fig. 118, which shows $d\sigma/dp_\perp dy\,|_{y=0}$ as a function of $p_\perp$ for various energies. For a recent thorough treatment, with specific applications to $S\bar{p}pS$ experiments, see Altarelli *et al.* (1984).

The number of intermediate bosons produced at a high luminosity supercollider is impressively large. At a c.m. energy of 40 TeV, for example, a run with an integrated luminosity of 10^{40} cm^{-2} would yield approximately 6×10^8 Z^0's and 2×10^9 $W^{\pm}$'s. For comparison, in a high luminosity Z^0 factory such as the Large Electron-Positron Collider (LEP) at CERN ($\mathcal{L}\approx2\times10^{31}$ cm^{-2}sec^{-1}) the number of Z^0's expected in a year of running is approximately 10^7. While LEP is expected to operate at least five years before a multi-TeV hadron collider, there are conceivably some advantages in the high-

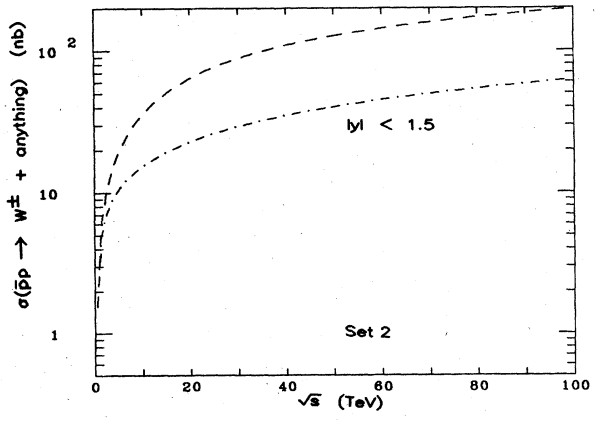

FIG. 111. Cross section for W^+ production in $p\bar{p}$ collisions evaluated using the parton distributions of Set 2. The W^- cross sections are equal. Also shown are the cross sections for W^+ produced in the rapidity interval $-1.5<y<1.5$.

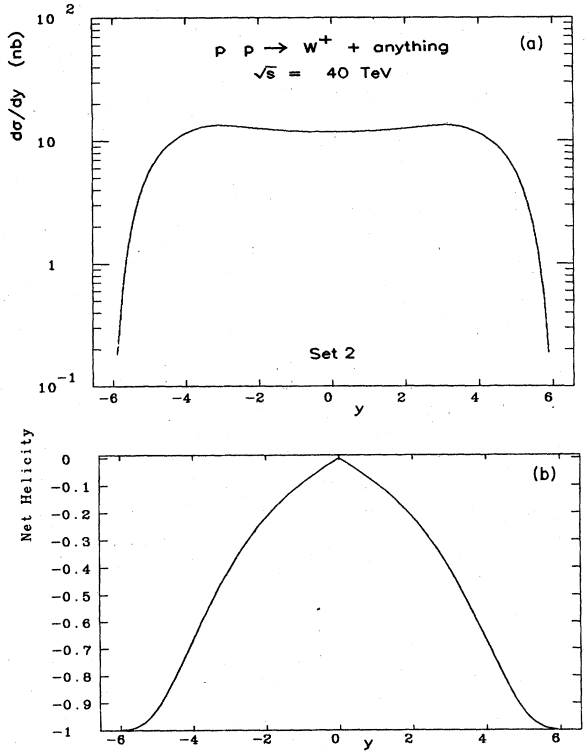

FIG. 112. (a) Rapidity distribution for W^+ produced in pp collisions at $\sqrt{s}=40$ TeV; (b) the net helicity of the W^+ as a function of rapidity. Parton distributions of Set 2 were used.

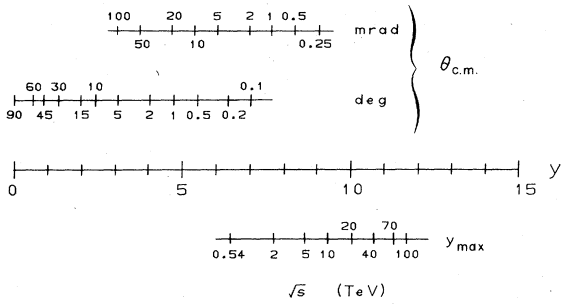

FIG. 113. Correspondence of angles to the c.m. rapidity scale used in other figures. Also shown is the maximum rapidity, $y_{max}=\ln(\sqrt{s}/M_{proton})$ accessible for light secondaries.

energy kinematics for some special purposes. This is an issue that deserves further study in the context of specific detectors and physics goals. In the case of charged intermediate bosons, there is no comparable source in prospect, but again there the question of how and why to study W decays in various regions of phase space must be examined in detail. The physics interest of rare decays of $W^{\pm}$ and Z^0 has been considered by Axelrod (1982). Further discussion of the decays of W and Z into exotic modes will be given in Sec. VI.

The signature for W and Z will now be discussed briefly. The decay $Z\to e^+e^-$ or $\mu^+\mu^-$ each with a 3% branching ratio should produce a clear signal with essentially no background apart from instrumental problems, such as e/π separation. The leptonic decay $W\to\nu e,\nu\mu$ will enable the W momentum to be reconstructed if the missing transverse momentum in the event (carried off by the neutrino) can be measured. This method cannot be used clearly in events with other sources of missing $p_\perp$, such as a W pair event where both W's decay leptonically.

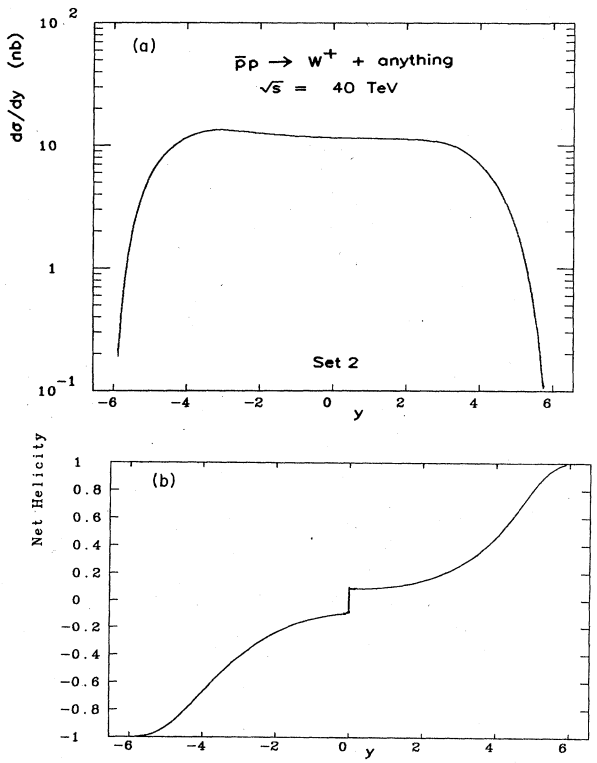

FIG. 114. (a) Rapidity distribution for W^+ produced in $\bar{p}p$ collisions at $\sqrt{s}=40$ TeV; (b) the net helicity of the produced W^+ as a function of rapidity. For W^- production replace $y\to -y$. Parton distributions of Set 2 were used.

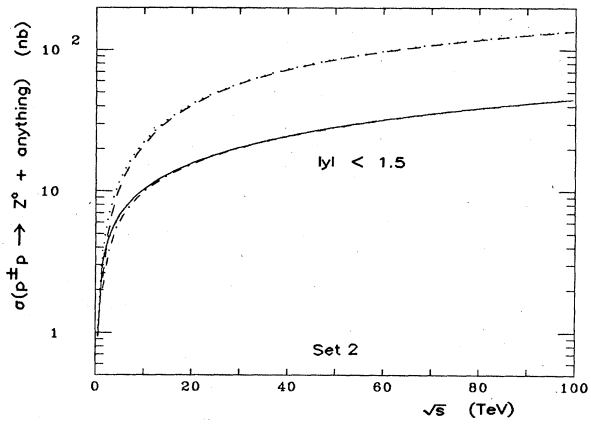

FIG. 115. Cross sections for Z^0 production in $p\bar{p}$ (dotted line) and pp (dashed line) collisions evaluated using Set 2 of distributions. Also shown are the cross sections for Z^0 produced in the rapidity interval $-1.5<y<1.5$: $\bar{p}p$ (solid line); pp (dotted-dashed line).

An important question is whether one can identify $W\to q\bar{q}$ by looking at hadronic jets. For low-momentum W's where the opening angle between the jets is large this method may be applicable. One would hope to see a peak in the jet pair mass. The background is, of course, from multijet QCD events, which are difficult to estimate reliably (see Sec. III). For a high-momentum W the two jets will be close together and may not be clearly distinguished and one may have to measure the invariant mass of a single jet. The relevant background is now a single QCD jet with large invariant mass (M). For a jet of energy E, the distribution in $\xi=M/E$ is given roughly by $dN/d\xi \approx 0.25e^{-4\xi}$ (Paige, 1984), as predicted by the ISAJET Monte Carlo (Paige and Protopopescu, 1981), using our Set 1 of distributions. The formula is applicable for $E=5$ TeV, but the dependence on E is rather weak. The distribution is rather broad and the average value of M is of order $0.15E$. This background is potentially serious and a more detailed study is needed.[7] In any case it seems that it will be difficult to distinguish W and Z from their hadronic decays, but such a separation would be extremely useful.

C. Pair production of gauge bosons

Incisive tests of the structure of the electroweak interactions may be achieved in detailed measurements of

[7]We are grateful to Frank Paige, M. Shochet, and Pierre Darriulat for a discussion of these issues.

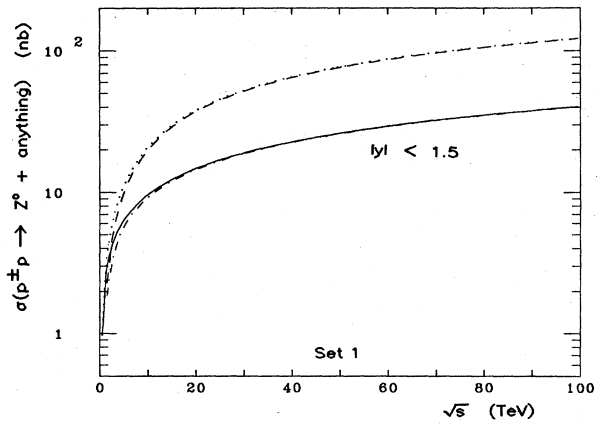

FIG. 116. Cross sections for Z^0 production in $p\bar{p}$ (dotted line) and pp (dashed line) collisions evaluated using Set 1 of the parton distributions. Also shown are the cross sections for Z^0 produced in the rapidity interval $-1.5<y<1.5$: $\bar{p}p$ (solid line); pp (dotted-dashed line).

the cross sections for production of W^+W^-, $W^\pm Z^0$, Z^0Z^0, $W^\pm\gamma$, and $Z\gamma$ pairs. The rate for $W^\pm\gamma$ production is sensitive to the magnetic moment of the intermediate boson. In the standard model there are important cancellations in the amplitudes for W^+W^- and $W^\pm Z^0$ production which rely on the gauge structure of the WWZ trilinear coupling. The Z^0Z^0 and $Z^0\gamma$ reactions do not probe trilinear couplings in the standard model, but are sensitive to nonstandard interactions such as might arise if the gauge bosons were composite. In addition, the W^+W^- and Z^0Z^0 final states may be significant backgrounds to the detection of heavy Higgs bosons and possible new degrees of freedom (see Sec. VI).

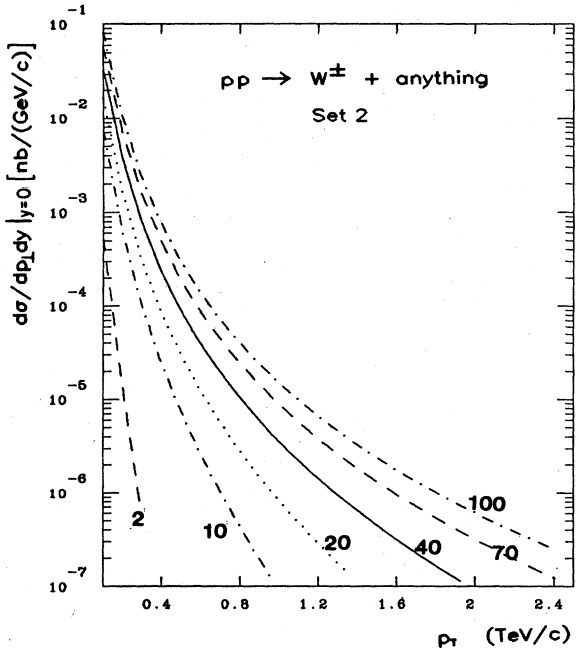

FIG. 118. Differential cross section $d\sigma/dp_\perp dy\,|_{y=0}$ for the production of a $W^\pm$ as a function of the $W^\pm$ transverse momentum ($p_\perp$), at $\sqrt{s}=2$, 10, 20, 40, 70, and 100 TeV. Set 2 of distributions was used.

1. Production of W^+W^- pairs

The Feynman diagrams for the process

$$q_i\bar{q}_i\rightarrow W^+W^- \tag{4.47}$$

are shown in Fig. 119. The intrinsic interest in this pro-

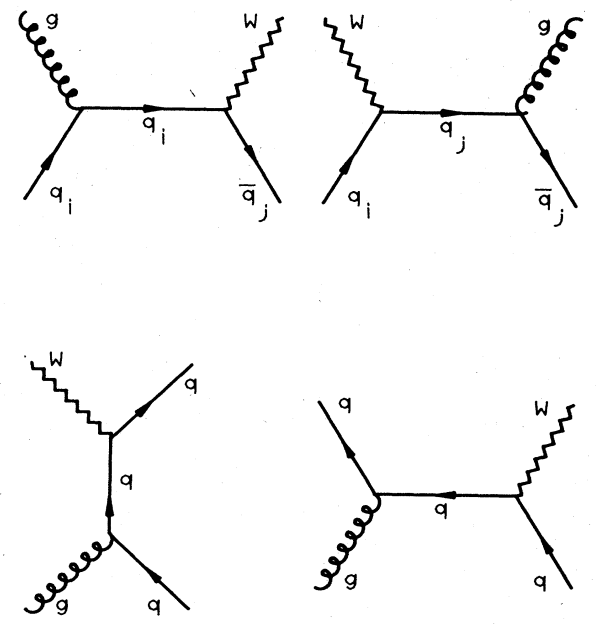

FIG. 117. Lowest-order Feynman graphs for the reactions $q\bar{q}\rightarrow W+g$ and $g+q\rightarrow W+q$.

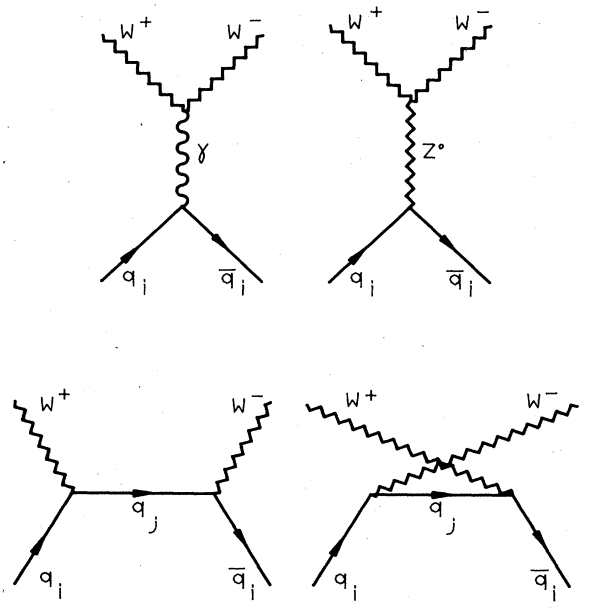

FIG. 119. Lowest-order Feynman diagrams for the reaction $q_i\bar{q}_i\rightarrow W^+W^-$. A direct-channel Higgs boson diagram vanishes because the quarks are idealized as massless.

cess, which accounts in part for plans to study e^+e^- annihilations at c.m. energies around 180 GeV at LEP, is owed to the sensitivity of the cross section to the interplay among the γ-, Z^0-, and quark-exchange contributions. As is well known, in the absence of the Z^0-exchange term, the cross section for production of a pair of longitudinally polarized intermediate bosons is proportional to s, in gross violation of unitarity. It is important to verify that the amplitude is damped as expected. Whether this direct measurement or the study of quantities sensitive to electroweak radiative corrections ultimately provides the best probe of the gauge structure of the interactions cannot be foretold with certainty.

The differential cross section for the elementary process (4.47) (Brown and Mikaelian, 1979), averaged over quark colors, is conveniently written as

$$\frac{d\sigma}{dz}(q_i\bar{q}_i\to W^+W^-)=\frac{\hat{s}\beta_W}{2}\frac{d\sigma}{d\hat{t}}$$

$$=\frac{\pi\alpha^2\beta_W}{24x_W^2\hat{s}}\left\{\left[\frac{\hat{u}\hat{t}-M_W^4}{\hat{s}^2}\right]\left[3-\left[\frac{\hat{s}-6M_W^2}{\hat{s}-M_Z^2}\right]\frac{L_i}{\tau_{3i}(1-x_W)}+\left[\frac{\hat{s}}{\hat{s}-M_Z^2}\right]^2\left[\beta_W^2+\frac{12M_W^4}{\hat{s}^2}\right]\left[\frac{L_i^2+R_i^2}{4(1-x_W)^2}\right]\right]\right.$$

$$-4\left[\frac{M_Z^2}{\hat{s}-M_Z^2}\right]\frac{L_i}{\tau_{3i}}+\frac{M_Z^2\hat{s}\beta_W^2}{(\hat{s}-M_Z^2)^2}\left[\frac{L_i^2+R_i^2}{1-x_W}\right]$$

$$+\Theta(-e_i)\left[2\left[1+\frac{M_Z^2}{\hat{s}-M_Z^2}\frac{L_i}{\tau_{3i}}\right]\left[\frac{\hat{u}\hat{t}-M_W^4}{\hat{s}\hat{t}}-\frac{2M_W^2}{\hat{t}}\right]+\frac{\hat{u}\hat{t}-M_W^4}{\hat{t}^2}\right]$$

$$\left.+\Theta(e_i)\left[2\left[1+\frac{M_Z^2}{\hat{s}-M_Z^2}\frac{L_i}{\tau_{3i}}\right]\left[\frac{\hat{u}\hat{t}-M_W^4}{\hat{s}\hat{u}}-\frac{2M_W^2}{\hat{u}}\right]+\frac{\hat{u}\hat{t}-M_W^4}{\hat{u}^2}\right]\right\}, \tag{4.48}$$

where again $\hat{t}$ ($\hat{u}$) measures the momentum transfer between q_i and W^- (W^+), e_i is the electric charge of q_i, and

$$\beta_W=(1-4M_W^2/\hat{s})^{1/2}. \tag{4.49}$$

In order to impose experimental cuts on the produced W's, it is convenient to decompose the rapidity of a product in the hadron-hadron c.m. frame in terms of the rapidity y^* of the product in the parton-parton c.m. frame and the motion of the parton-parton system with respect to the overall c.m., as characterized by y_{boost}:

$$y=y_{\text{boost}}+y^* \tag{4.50}$$

where y_{boost} is related to the parton momentum fractions x_a and x_b by

$$y_{\text{boost}}=\tfrac{1}{2}\ln(x_a/x_b). \tag{4.51}$$

The rapidity of the product in the parton-parton c.m. frame is simply

$$y^*=\tanh^{-1}(\beta z), \tag{4.52}$$

where $z=\cos\theta^*$ measures the c.m. scattering angle and

$$\beta=(1-4M_W^2/s)^{1/2}. \tag{4.53}$$

The cross section to produce a W^+W^- pair of invariant mass $M=\sqrt{s\tau}$ such that both intermediate bosons lie in the rapidity interval $(-Y,Y)$ is then

$$\frac{d\sigma}{dM}(ab\to W^+W^-+\text{anything})=\frac{2M}{s}\sum_i\int_{-Y}^{Y}dy_{\text{boost}}[f_i^{(a)}(x_a,M^2)f_{\bar{i}}^{(b)}(x_b,M^2)+f_{\bar{i}}^{(a)}(x_a,M^2)f_i^{(b)}(x_b,M^2)]$$

$$\times\int_{-z_0}^{z_0}dz\frac{d\sigma}{dz}(q_i\bar{q}_i\to W^+W^-), \tag{4.54}$$

where as usual

$$x_a=\sqrt{\tau}e^{y_{\text{boost}}},$$

$$x_b=\sqrt{\tau}e^{-y_{\text{boost}}}, \tag{3.27}$$

and

$$\frac{d\sigma}{dz}=\frac{\beta\hat{s}}{2}\frac{d\sigma}{d\hat{t}} . \tag{4.55}$$

The limit of the angular integration is given by

$$z_0=\min[\beta^{-1}\tanh(Y-y_{\text{boost}}),1] . \tag{4.56}$$

The result of the angular integration is

$$\int_{-z_0}^{z_0}dz\frac{d\sigma}{dz}=\frac{\pi\alpha^2}{12x_W^2\hat{s}}\left\{\tfrac{1}{4}\beta_W^3 z_0(1-z_0^2/3)\left[3-\left[\frac{\hat{s}-6M_W^2}{\hat{s}-M_Z^2}\right]\frac{L_i}{\tau_{3i}(1-x_W)}+\left[\frac{\hat{s}}{\hat{s}-M_Z^2}\right]^2\left[\beta_W^2+\frac{12M_W^4}{\hat{s}^2}\right]\left[\frac{L_i^2+R_i^2}{4(1-x_W)^2}\right]\right]\right.$$

$$+\beta_W z_0\left[\frac{M_Z^2\hat{s}\beta_W^2}{(\hat{s}-M_Z^2)^2}\left[\frac{L_i^2+R_i^2}{1-x_W}\right]-4\left[\frac{M_Z^2}{\hat{s}-M_z^2}\right]\frac{L_i}{\tau_{3i}}\right]$$

$$+\frac{1}{\hat{s}^2}\left[1+\frac{M_Z^2}{\hat{s}-M_Z^2}\frac{L_i}{\tau_{3i}}\right][\hat{t}_+^2-\hat{t}_-^2-2M_W^2(M_W^2+2\hat{s})\ln(\hat{t}_+/\hat{t}_-)]$$

$$\left.+\left[\frac{\hat{t}_++\hat{t}_-}{\hat{s}}\right]\ln(\hat{t}_+/\hat{t}_-)-\frac{\hat{t}_+-\hat{t}_-}{\hat{s}}-\frac{M_W^4(\hat{t}_+-\hat{t}_-)}{\hat{s}\hat{t}_+\hat{t}_-}\right\}, \tag{4.57}$$

where

$$\hat{t}_\pm\equiv\hat{t}(\pm z_0)=M_W^2-\tfrac{1}{2}\hat{s}(1\mp\beta_W z_0) . \tag{4.58}$$

The rate of W^+W^- pair production in pp and $\bar{p}p$ collisions is presented in Figs. 120 and 121, where we show the total yields as well as the cross sections for W's satisfying rapidity cuts of $|y|<1.5$ or 2.5. Ideally, of course, one would like to impose instrumental cuts on the final decay products. However, at the energies we are discussing, the intermediate bosons are relatively light particles and their decay products have limited mobility of about ±1 unit of rapidity. This means that a detector with angular coverage down to a few degrees from the beam direction should capture essentially all the decay products of an intermediate boson with $|y|<2.5$.

The yield of W^+W^- pairs is quite substantial at high energies. For example, a run with integrated luminosity $\int\mathcal{L}\,dt=10^{40}$ cm^{-2} would result in approximately 10^6 pairs. The key to exploiting this potential sample lies in reconstructing the intermediate bosons from their nonleptonic decays, which account for 75% of the total decay rate.

Of greater interest both for the verification of gauge cancellations and for the assessment of backgrounds to heavy Higgs boson decays is the mass spectrum of W^+W^- pairs. This is shown for intermediate bosons satisfying $|y|<2.5$ in Figs. 122 and 124 for pp and $\bar{p}p$ collisions. The mass spectrum for $pp\to W^+W^-$ with $|y|<1.5$ is shown in Fig. 123. Again the number of pairs produced at high energies seems adequate for a test of the gauge cancellations, provided that the intermediate

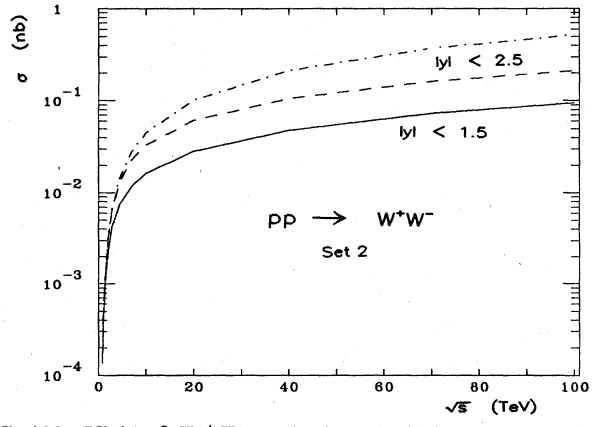

FIG. 120. Yield of W^+W^- pairs in pp collisions, according to the parton distributions of Set 2. Both W's must satisfy the rapidity cuts indicated.

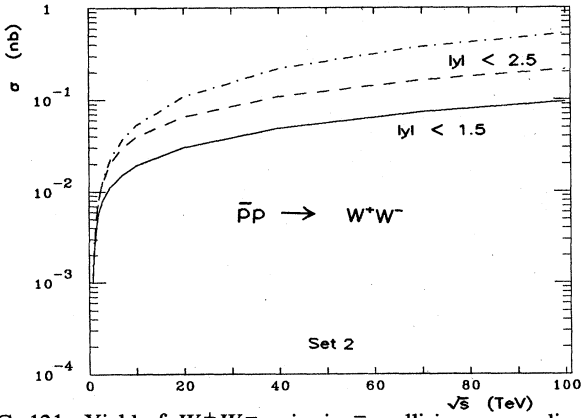

FIG. 121. Yield of W^+W^- pairs in $\bar{p}p$ collisions, according to the parton distributions of Set 2. Both W's must satisfy the rapidity cuts indicated.

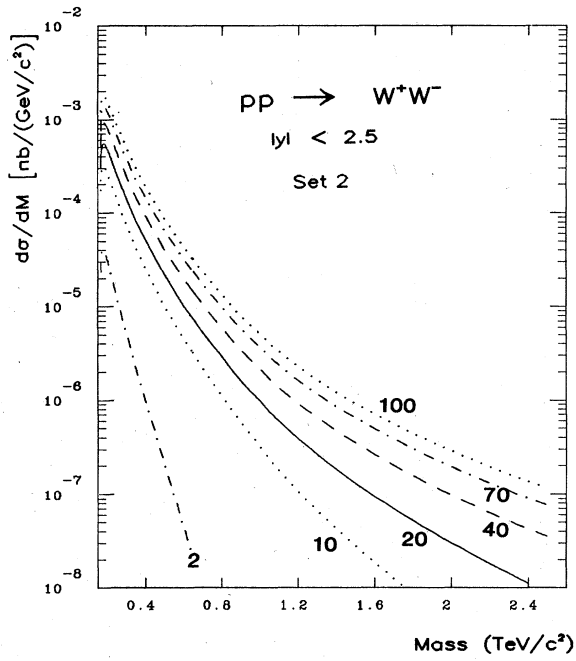

FIG. 122. Mass spectrum of W^+W^- pairs produced in pp collisions, according to the parton distributions of Set 2. Both W^+ and W^- must satisfy $|y|<2.5$.

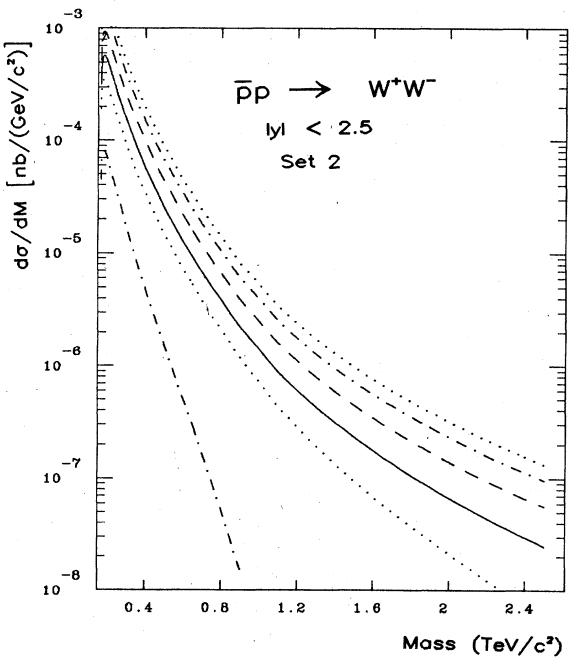

FIG. 124. Mass spectrum of W^+W^- pairs produced in $p\bar{p}$ collisions, according to the parton distributions of Set 2. Both W^+ and W^- must satisfy $|y|<2.5$.

bosons can be detected. We shall discuss the signal-to-noise ratio for heavy Higgs decays in Sec. IV.D below. In models in which the interactions among W bosons become strong, the scale of interest is an invariant mass of around 1 TeV/c^2. In the standard model we anticipate a few hundred events in a 10-GeV/c^2 bin around 1 TeV/c^2 at a c.m. energy of 40 TeV. The yield could be enhanced by an order of magnitude if nonstandard interactions are present (Robinett, 1983b). An example of a factor of 2 enhancement will be given in our discussion of technicolor models in Sec. VI.B.

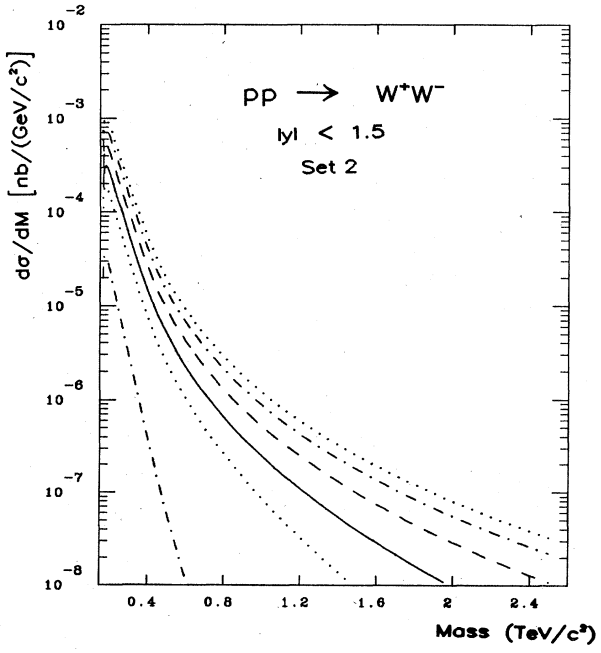

FIG. 123. Mass spectrum of W^+W^- pairs produced in pp collisions, according to the parton distributions of Set 2. Both W^+ and W^- must satisfy $|y|<1.5$.

2. Production of $W^{\pm}Z^0$ pairs

The Feynman diagrams for the process

$$q_i\bar{q}_j \rightarrow W^{\pm}Z^0 \tag{4.59}$$

are shown in Fig. 125. This process is also of interest as a probe of the gauge structure of the electroweak interactions. The differential cross section for reaction (4.59) (Brown, Sahdev, and Mikaelian, 1979), averaged over quark colors, is given by

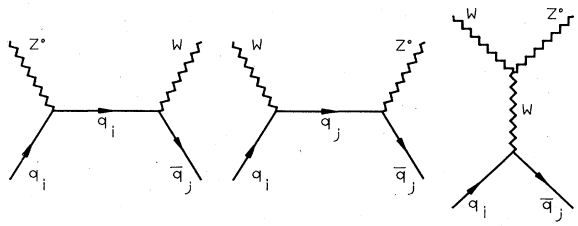

FIG. 125. Lowest-order Feynman diagrams for the reaction $q_i\bar{q}_j \rightarrow W^{\pm}Z^0$.

$$\frac{d\sigma}{d\hat{t}}=\frac{\pi\alpha^2|U_{ij}|^2}{6\hat{s}^2x_W^2}\left\{\left[\frac{1}{\hat{s}-M_W^2}\right]^2\left[\left[\frac{9-8x_W}{4}\right](\hat{u}\hat{t}-M_W^2M_Z^2)+(8x_W-6)\hat{s}(M_W^2+M_Z^2)\right]\right.$$

$$+\left[\frac{\hat{u}\hat{t}-M_W^2M_Z^2-\hat{s}(M_W^2+M_Z^2)}{\hat{s}-M_W^2}\right]\left[\frac{L_j}{\hat{t}}-\frac{L_i}{\hat{u}}\right]$$

$$\left.+\frac{(\hat{u}\hat{t}-M_W^2M_Z^2)}{4(1-x_W)}\left[\frac{L_j^2}{\hat{t}^2}+\frac{L_i^2}{\hat{u}^2}\right]+\frac{\hat{s}(M_W^2+M_Z^2)}{2(1-x_W)}\frac{L_iL_j}{\hat{t}\hat{u}}\right\}. \tag{4.60}$$

The cross section to produce a $W^{\pm}Z^0$ pair of invariant mass $M=\sqrt{s\tau}$ such that both intermediate bosons lie in the

$$\frac{d\sigma}{d\mathcal{M}}(ab\to W^{\pm}Z^0+\text{anything})=\frac{2\mathcal{M}}{s}\sum_{ij}\int_{-Y}^{Y}dy_{\text{boost}}[f_i^{(a)}(x_a,\mathcal{M}^2)f_{\bar{j}}^{(b)}(x_b,\mathcal{M}^2)+f_{\bar{j}}^{(a)}(x_a,\mathcal{M}^2)f_i^{(b)}(x_b,\mathcal{M}^2)]$$

$$\times\int_{-z_0}^{z_0}dz\frac{d\sigma}{dz}(q_i\bar{q}_j\to W^{\pm}Z), \tag{4.61}$$

where x_a and x_b are given by (4.54) and

$$\frac{d\sigma}{dz}=\frac{\beta\hat{s}}{2}\frac{d\sigma}{d\hat{t}}, \tag{4.62}$$

where in this case

$$\beta=\left[\left[1-\frac{M_W^2+M_Z^2}{\hat{s}}\right]^2-\frac{4M_W^2M_Z^2}{\hat{s}^2}\right]^{1/2}. \tag{4.63}$$

The result of the angular integration is

$$\int_{-z_0}^{z_0}dz\frac{d\sigma}{dz}=\frac{\pi\alpha^2\beta}{6x_W^2\hat{s}}\left[\frac{z_0}{4(1-M_W^2/\hat{s})^2}\left[\frac{(9-8x_W)\beta^2(1-z_0^2/3)}{4}+(4x_W-3)\varepsilon'\right]\right.$$

$$+2(1-x_W)\left[\frac{(\varepsilon'/2+M_W^2M_Z^2/\hat{s}^2)}{\beta}\mathbb{L}-z_0(1-\varepsilon'/2)\right]$$

$$\left.-\frac{L_i^2+L_j^2}{4(1-x_W)}\left[z_0+\frac{(1-\varepsilon'/2)}{\beta}\mathbb{L}-\frac{4M_W^2M_Z^2z_0}{\hat{s}^2[(1-\varepsilon'/2)^2-\beta^2z_0^2]}\right]+\frac{L_iL_j\varepsilon'\mathbb{L}}{(1-x_W)\beta(1-\varepsilon'/2)}\right], \tag{4.64}$$

where

$$\varepsilon'=(M_W^2+M_Z^2)/s, \tag{4.65}$$

and

$$\mathbb{L}=\ln\left[\frac{1-\varepsilon'+\beta z_0}{1-\varepsilon'-\beta z_0}\right], \tag{4.66}$$

with

$$z_0=\min[\beta_W^{-1}\tanh(Y-y_{\text{boost}}),1],$$
$$\beta_W=\beta\Big/\left[1+\frac{M_W^2-M_Z^2}{\hat{s}}\right]. \tag{4.67}$$

The rate of W^+Z^0 and W^-Z^0 pair production in pp and $\bar{p}p$ collisions is presented in Figs. 126 and 127, where we show the total yields as well as the cross sections for intermediate bosons satisfying rapidity cuts of $|y|<1.5$ or 2.5. The yield of WZ pairs is approximately a factor of 5 smaller, for each charge, than the W^+W^- yield shown in Figs. 120 and 121.

The mass spectrum of $W^{\pm}Z^0$ pairs in pp collisions is shown in Figs. 128 and 129 for gauge bosons satisfying the cuts $|y|<2.5$ and $|y|<1.5$. Here we expect, in a run with integrated luminosity $\int dt\,\mathcal{L}=10^{40}$ cm^{-2}, about a hundred events per 10-GeV/c^2 bin in the interesting region around 1 TeV.

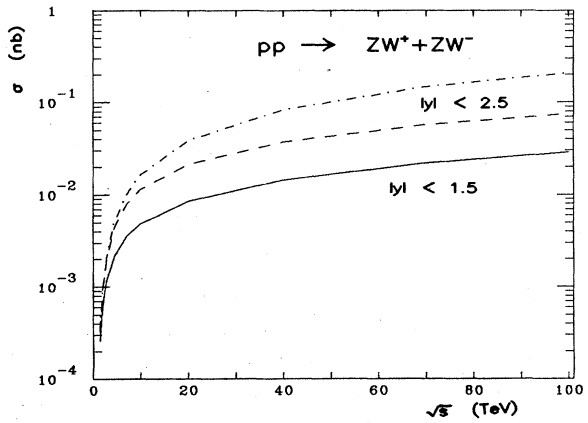

FIG. 126. Yield of $W^{\pm}Z^0$ pairs in pp collisions, according to the parton distributions of Set 2. Both intermediate bosons must satisfy the rapidity cuts indicated.

3. Production of Z^0Z^0 pairs

The Feynman diagrams for the process

$$q_i\bar{q}_i \rightarrow Z^0Z^0 \tag{4.68}$$

are shown in Fig. 130. This process is of interest as a background to the production and decay of heavy Higgs bosons, and as a channel in which to search for unorthodox interactions. The differential cross section for reaction (4.68) (Brown and Mikaelian, 1979) may be written in the form

$$\frac{d\sigma}{d\hat{t}}(q_i\bar{q}_i \rightarrow Z^0Z^0) = \frac{\pi\alpha^2(L_i^4+R_i^4)}{96x_W^2(1-x_W)^2\hat{s}^2} \times \left[\frac{\hat{t}}{\hat{u}}+\frac{\hat{u}}{\hat{t}}+\frac{4M_Z^2\hat{s}}{\hat{t}\hat{u}} - M_Z^4\left[\frac{1}{\hat{t}^2}+\frac{1}{\hat{u}^2}\right]\right], \tag{4.69}$$

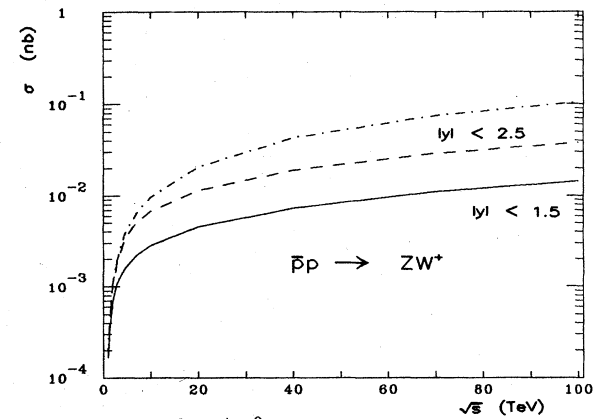

FIG. 127. Yield of W^+Z^0 pairs in $\bar{p}p$ collisions, according to the parton distributions of Set 2. Both intermediate bosons must satisfy the rapidity cuts indicated. The W^-Z^0 yield is identical.

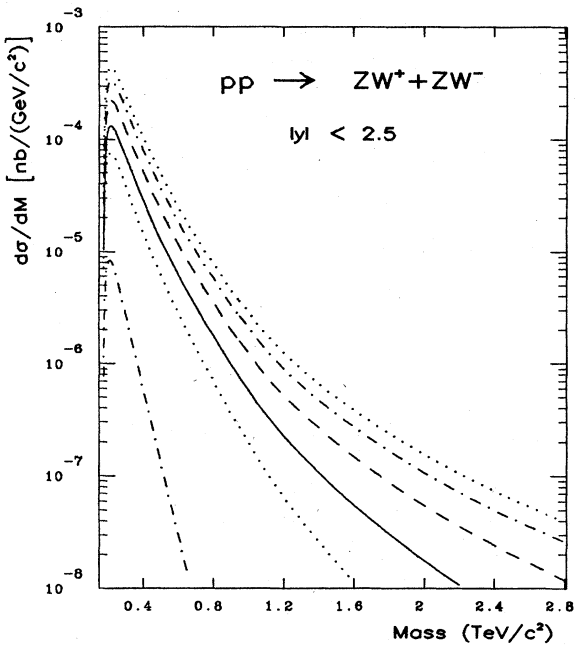

FIG. 128. Mass spectrum of $W^{\pm}Z^0$ pairs produced in pp collisions, according to the parton distributions of Set 2. Both $W^{\pm}$ and Z^0 must satisfy $|y|<2.5$.

where we have averaged over the initial quark colors and included a statistical factor of $\frac{1}{2}$ for the identical particles in the final state.

The cross section for production of a Z^0Z^0 pair of invariant mass $M=\sqrt{s\tau}$ such that both intermediate bosons lie in the rapidity interval $(-Y,Y)$ is

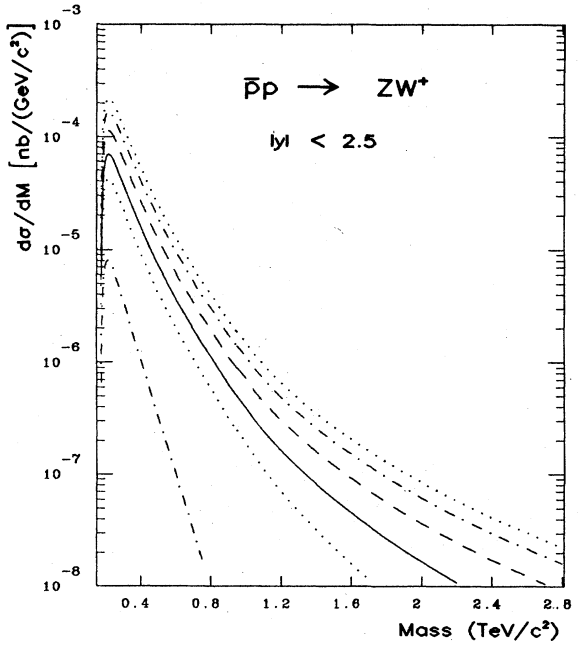

FIG. 129. Mass spectrum of W^+Z^0 pairs produced in $p\bar{p}$ collisions, according to the parton distributions of Set 2. Both W^+ and Z^0 must satisfy $|y|<2.5$. The W^-Z^0 yield is identical.

$$\frac{d\sigma}{d\mathcal{M}}(ab\to Z^0Z^0+\text{anything})=\frac{2\mathcal{M}}{s}\sum_i\int_{-Y}^{Y}dy_{\text{boost}}[f_i^{(a)}(x_a,\mathcal{M}^2)f_{\bar{i}}^{(b)}(x_b,\mathcal{M}^2)+f_{\bar{i}}^{(a)}(x_a,\mathcal{M}^2)f_i^{(b)}(x_b,\mathcal{M}^2)]$$
$$\times\int_{-z_0}^{z_0}dz\frac{d\sigma}{dz}(q_i\bar{q}_i\to Z^0Z^0)\ , \tag{4.70}$$

where

$$\frac{d\sigma}{dz}=\frac{\beta\hat{s}}{2}\frac{d\sigma}{d\hat{t}} \tag{4.71}$$

with

$$\beta=(1-4M_Z^2/\hat{s})^{1/2}\ . \tag{4.72}$$

The integrated cross section is

$$\int_{-z_0}^{z_0}dz\frac{d\sigma}{dz}=\frac{\pi\alpha^2}{48x_W^2(1-x_W)^2}\frac{\beta}{\hat{s}}(L_i^4+R_i^4)$$
$$\times\left[\frac{4+\varepsilon^2}{2\beta(2-\varepsilon)}\ln\left[\frac{1-\varepsilon/2+\beta z_0}{1-\varepsilon/2-\beta z_0}\right]\right.$$
$$\left.-2z_0\frac{\varepsilon^2+2\beta^2(1-z_0^2)}{\varepsilon^2+4\beta^2(1-z_0^2)}\right]\ , \tag{4.73}$$

where as usual

$$z_0=\min[\beta^{-1}\tanh(Y-y_{\text{boost}})\ ,1]\ ,$$
$$\varepsilon=4M_Z^2/\hat{s}\ . \tag{4.74}$$

The rate of Z^0Z^0 pair production in pp and $\bar{p}p$ collisions is presented in Figs. 131 and 132, where we show the total yields as well as the cross sections for intermediate bosons satisfying the rapidity cuts of $|y|<1.5$ or 2.5. The yield of Z^0Z^0 pairs is smaller by a factor of 5—10 than that of W^+W^- pairs. At $\sqrt{s}=40$ TeV and for $\int\mathcal{L}\,dt=10^{40}$ cm^{-2} there are approximately 2×10^5 Z pair events with $|y|<2.5$. If the Z's are detected only in their leptonic modes, there will be approximately 700 reconstructed events. Again, high detection efficiency is a prerequisite to detailed study.

The mass spectrum of Z^0Z^0 pairs in pp collisions is shown in Figs. 133 and 134 for gauge bosons satisfying the cuts $|y|<2.5$ and $|y|<1.5$. We shall return to these spectra in our discussion of the observability of heavy Higgs bosons in Sec. IV.D. For now, let us remark that in the standard model we expect about 50 events in a 10-GeV/c^2 bin around 1 TeV/c^2 at a c.m. energy of 40 TeV, for a run with integrated luminosity of 10^{40} cm^{-2}.

4. $W^\pm\gamma$ production

The elementary process which operates in the reaction

$$p^\pm p\to W^\pm\gamma+\text{anything} \tag{4.75}$$

is

$$q_i\bar{q}_j\to W^\pm\gamma\ , \tag{4.76}$$

for which the Feynman diagrams are given in Fig. 135. The differential cross section has been calculated by Brown, Sahdev, and Mikaelian (1979) and Mikaelian, Samuel, and Sahdev (1979). The result, averaged over initial quark colors, is

$$\frac{d\sigma}{d\hat{t}}(q_i\bar{q}_j\to W^\pm\gamma)=\frac{\pi\alpha^2}{6\hat{s}^2}\frac{|U_{ij}|^2}{x_W}\left[\left[\frac{1}{1+\hat{t}/\hat{u}}-\frac{1}{3}\right]^2\frac{\hat{t}^2+\hat{u}^2+2M_W^2\hat{s}}{\hat{t}\hat{u}}\right]\ , \tag{4.77}$$

where U_{ij} is an element of the (Kobayashi and Maskawa, 1973) quark mixing matrix and $\hat{t}$ measures the momentum transfer between q_i and W^-. The same expression holds for $W^+\gamma$ production, with $\hat{t}$ reinterpreted as the momentum transfer between q_j and W^+. The invariant mass of the $W\gamma$ pair is given by $\sqrt{s\tau}$. The vanishing of

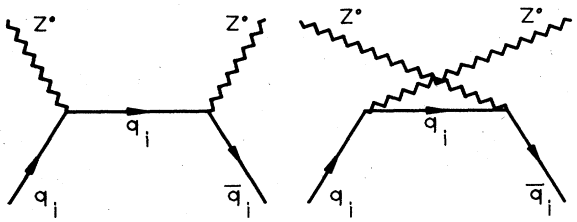

FIG. 130. Lowest-order Feynman diagrams for the reaction $q_i\bar{q}_i\to Z^0Z^0$.

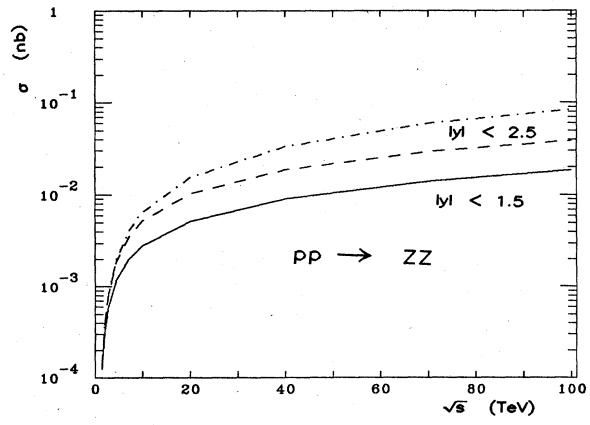

FIG. 131. Yield of Z^0Z^0 pairs in pp collisions, according to the parton distributions of Set 2. Both intermediate bosons must satisfy the rapidity cuts indicated.

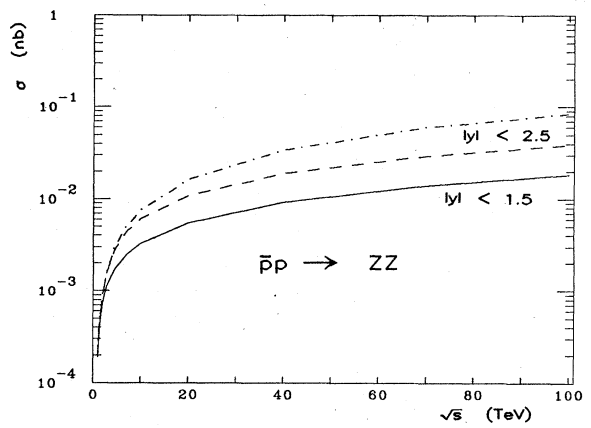

FIG. 132. Yield of Z^0Z^0 pairs in $\bar{p}p$ collisions, according to the parton distributions of Set 2. Both intermediate bosons must satisfy the rapidity cuts indicated.

the differential cross section at $\hat{t}/\hat{u}=2$ (which corresponds to $\cos\theta_{\text{c.m.}}=-\frac{1}{3}$) has been understood (Brodsky and Brown, 1982; Samuel, 1983; Brown, Kowalski, and Brodsky, 1983) in terms of classical radiation zeroes.

The total rate observable in experiments depends sensitively upon the $W\gamma$ invariant mass and consequently on the minimum detectable energy of a photon. Figure 136 shows the total cross section for $pp\to W^{\pm}\gamma$ when the invariant mass of the W and the photon is restricted to be more than 200 GeV/c^2. This cut removes the infrared divergence when the photon energy vanishes. The cross sections are constrained so that both the W and the photon have rapidity between $+2.5$ and -2.5. A tighter rapidity cut of $y<|1.5|$ is also shown. The total cross section is, of course, formally infinite, since the expression (4.77) has a $\hat{t}$ channel pole. Figure 137 shows the distribution in $\cos\theta$, at $\sqrt{s}=40$ TeV, where θ is the angle between the photon and the beam in the $W\gamma$ center of mass frame. We have applied a cut on the transverse momentum of the photon of 20, 50, and 100 GeV/c. The distribution is sensitive to the details of the $WW\gamma$ coupling and in particular to the magnetic moment of the W. Departures can be expected in nonstandard models such as composite gauge boson theories (Robinett, 1983a).

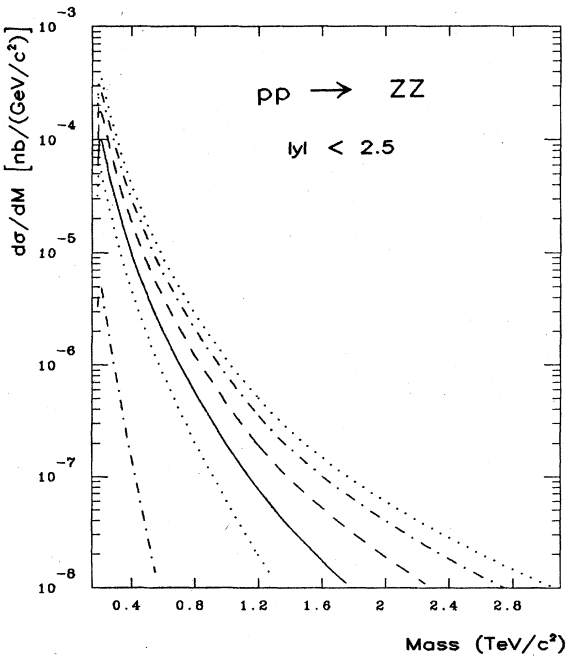

FIG. 133. Mass spectrum of Z^0Z^0 pairs produced in pp collisions, according to the parton distributions of Set 2. Both Z^0's must satisfy $|y|<2.5$.

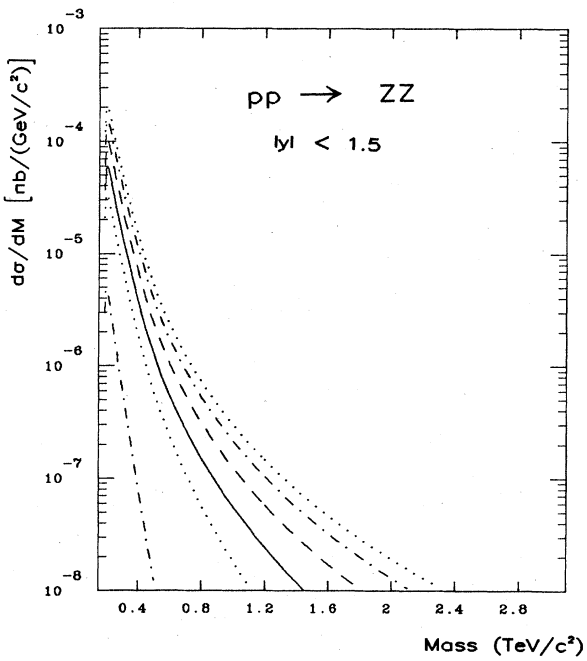

FIG. 134. Mass spectrum of Z^0Z^0 pairs produced in pp collisions, according to the parton distributions of Set 2. Both Z^0's must satisfy $|y|<1.5$.

5. $Z^0\gamma$ production

The Feynman diagrams for the process

$$q_i\bar{q}_i\to Z^0\gamma \tag{4.78}$$

are shown in Fig. 138. This process is chiefly of interest as a channel in which to search for unorthodox interactions. For example, Leurer, Harari, and Barbieri (1984) have shown that in a composite Z^0 scheme the process $q+\bar{q}\to Z^0+\gamma$ may yield large $p_\perp$ photons at a rate substantially greater than predicted by the standard model. In the standard model, the differential cross section for reaction (4.76) is (Renard, 1982)

$$\frac{d\sigma}{d\hat{t}}(q_i\bar{q}_i\to Z^0\gamma)=\frac{\pi\alpha^2(L_i^2+R_i^2)}{6x_W(1-x_W)\hat{s}^2}\left[\frac{\hat{s}^2+M_Z^4}{2\hat{t}\,\hat{u}}-1\right], \tag{4.79}$$

where we have averaged over the initial quark colors.

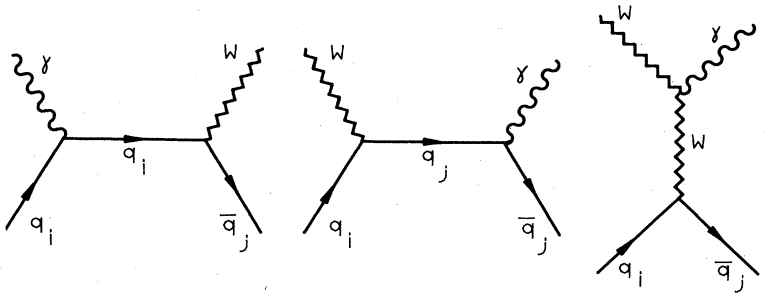

FIG. 135. Lowest-order Feynman diagrams for the reaction $q_i\bar{q}_j \to W^{\pm}\gamma$.

Figure 139 shows the total cross section in pp collisions where we have required that the Z and photon have invariant mass of more than 200 GeV/c^2, and that they satisfy rapidity cuts of $|y|<2.5$ and $|y|<1.5$. Figure 140 shows the distribution in $\cos\theta$ at $\sqrt{s}=40$ TeV (see preceding section); again the transverse momentum of the photon is restricted to be greater than 20, 50, and 100 GeV/c.

D. Production of Higgs bosons

In the standard electroweak theory, a single neutral scalar particle remains as a vestige of the spontaneous breakdown of the $SU(2)_L \otimes U(1)_Y$ gauge symmetry. As we have already noted in Sec. I.B, the mass of this Higgs boson is not specified by the theory, but consistency arguments suggest (Linde, 1976; Weinberg, 1976a; Veltman, 1977; Lee, Quigg, and Thacker, 1977)

$$7\ \text{GeV}/c^2 \lesssim M_H \lesssim 1\ \text{TeV}/c^2\ . \tag{4.80}$$

The interactions of the Higgs boson are of course prescribed by the gauge symmetry. It is therefore straightforward to write down the partial widths for kinematically allowed decays. The partial width for decay into a fermion-antifermion pair is

$$\Gamma(H\to f\bar{f}) = \frac{G_F m_f^2 M_H N_c}{4\pi\sqrt{2}}(1-4m_f^2/M_H^2)^{3/2}\ , \tag{4.81}$$

where N_c is the number of fermion colors. For $M_H \leq 2M_W$, the preferred decay of the Higgs boson is into the heaviest accessible pair of quarks or leptons.

In contrast, a Higgs boson with $M_H \geq 2M_W$ has the striking property that it will decay into pairs of gauge bosons. For the intermediate boson decay modes, the partial widths are given in perturbation theory by (Lee, Quigg, and Thacker, 1977)

$$\Gamma(H\to W^+W^-) = \frac{G_F M_H^3}{32\pi\sqrt{2}}(4-4a_W+3a_W^2)(1-a_W)^{1/2}\ , \tag{4.82}$$

$$\Gamma(H\to Z^0Z^0) = \frac{G_F M_H^3}{64\pi\sqrt{2}}(4-4a_Z+3a_Z^2)(1-a_Z)^{1/2}\ , \tag{4.83}$$

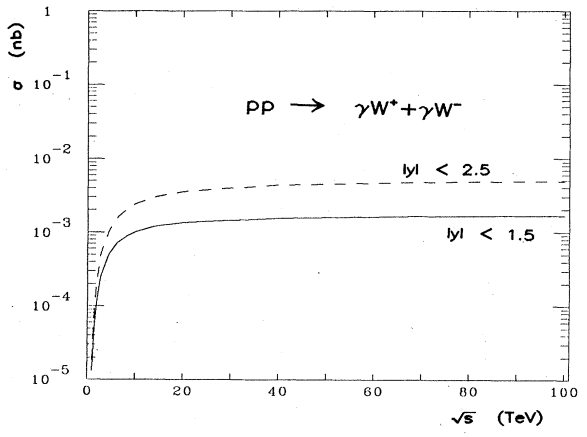

FIG. 136. Total cross section for the reaction $pp\to W^{\pm}\gamma$ + anything as a function of $\sqrt{s}$. The invariant mass of the $W^{\pm}\gamma$ pair is more than 200 GeV/c^2: Both $W^{\pm}$ and γ must satisfy $|y|<1.5$ or $|y|<2.5$, as indicated. Set 2 of the distributions was used.

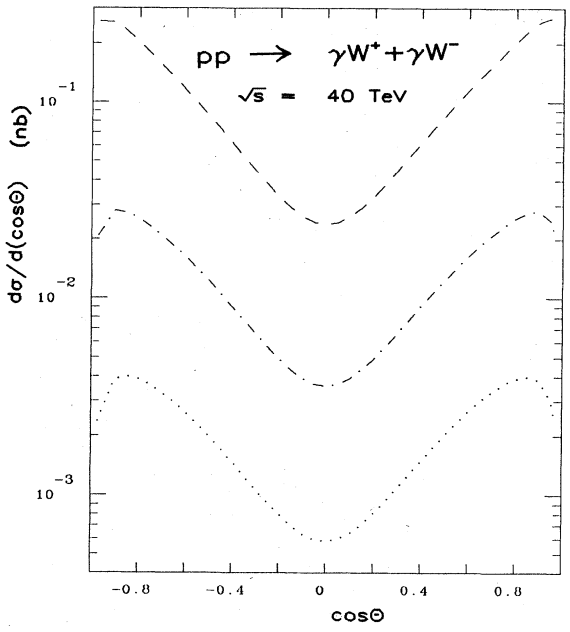

FIG. 137. Distribution in $\cos\theta$, where θ is the angle between the photon and the beam in the $W\gamma$ c.m. frame, for the process $pp\to W^{\pm}\gamma$ + anything at $\sqrt{s}=40$ TeV. The transverse momentum of the photon is restricted to be greater than 20 (dashed line), 50 (dotted-dashed line), or 100 (dotted line) GeV/c. Set 2 of the distributions was used.

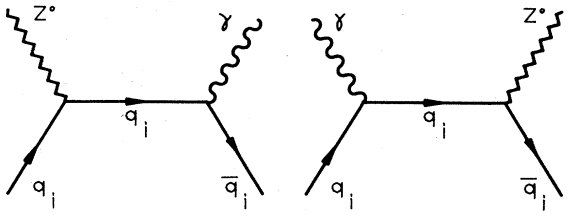

FIG. 138. Lowest-order Feynman diagrams for the reaction $q_i\bar{q}_i \to \gamma Z^0$.

where $a_W = 4M_W^2/M_H^2$ and $a_Z = 4M_Z^2/M_H^2$. The resulting partial decay widths are shown in Fig. 141. There we also show the partial widths for the decay $H \to Q\bar{Q}$ for heavy-quark masses of 30 and 70 GeV/c^2. The decay into pairs of intermediate bosons is dominant. If the perturbatively estimated width can be trusted, it will be difficult to establish a Higgs boson heavier than about 600 GeV/c^2.

The expected properties of light Higgs bosons have been reviewed by Ellis, Gaillard, and Nanopoulos (1976), and by Vainshtein, Zakharov, and Shifman (1980). The heavy Higgs alternative has been explored by Lee, Quigg, and Thacker (1977), and by Gordon *et al.* (1982).

A number of production mechanisms for Higgs bosons has been considered. Here we discuss the production of Higgs bosons in isolation; associated production of Higgs bosons and intermediate bosons will be treated in Sec. IV.E.

The direct production of a Higgs boson in the reaction

$$q_i\bar{q}_i \to H \tag{4.84}$$

is depicted in Fig. 142. The differential cross section for the reaction

$$a + b \to H + \text{anything} \tag{4.85}$$

is given by

$$\frac{d\sigma}{dy} = \frac{G_F\pi}{3\sqrt{2}} \sum_i \left[\frac{m_i^2}{M_H^2}\right] \tau [f_i^{(a)}(x_a, M_H^2) f_{\bar{i}}^{(b)}(x_b, M_H^2) + f_{\bar{i}}^{(a)}(x_a, M_H^2) f_i^{(b)}(x_b, M_H^2)] , \tag{4.86}$$

where $\tau = M_H^2/s$ and $x_{a,b}$ are given by (4.10). The integrated cross section is then given by[8]

$$\sigma(ab \to H + \text{anything}) = \frac{G_F\pi}{3\sqrt{2}} \sum_i \left[\frac{m_i^2}{M_H^2}\right] \tau \frac{d\mathcal{L}_{i\bar{i}}}{d\tau} \approx 3.36 \text{ nb} \sum_i \left[\frac{m_i^2}{M_H^2}\right] \tau \frac{d\mathcal{L}_{i\bar{i}}}{d\tau} . \tag{4.87}$$

[8]All our production cross sections are given in zero-width approximation for the Higgs boson. This approximation will underestimate the production rate when the Higgs width becomes very large.

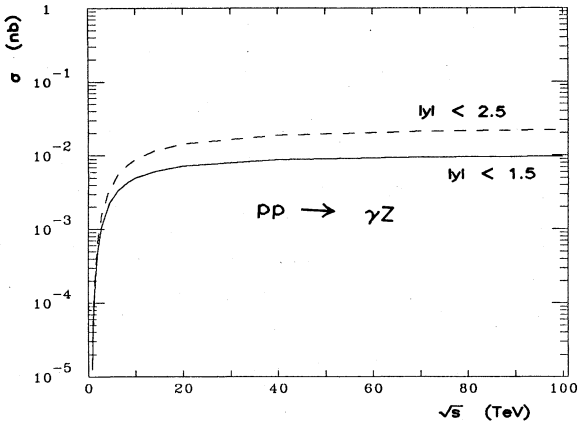

FIG. 139. Total cross section for the reaction $pp \to Z\gamma$ + anything as a function of $\sqrt{s}$. The invariant mass of the $Z\gamma$ pair is more than 200 GeV/c^2. Both the Z and γ must satisfy $|y| < 1.5$ or $|y| < 2.5$, as indicated. Set 2 of the distributions was used.

For light quarks this is negligibly small even for rather light Higgs bosons because of the (m_i^2/M_H^2) factor. For heavy quarks this contribution is small because of the small parton luminosity. Figure 143 shows the Higgs production cross section via this mechanism for $m_t = 30$ GeV/c^2 as a function of M_H. The pp and $\bar{p}p$ rates are equal. In particular, the cross section due to the reaction $t\bar{t} \to H$ for $M_H = 100$ GeV/c^2 and $m_t = 30$ GeV/c^2 is only 9 pb at $\sqrt{s} = 40$ TeV.

A more promising source of Higgs bosons in hadron

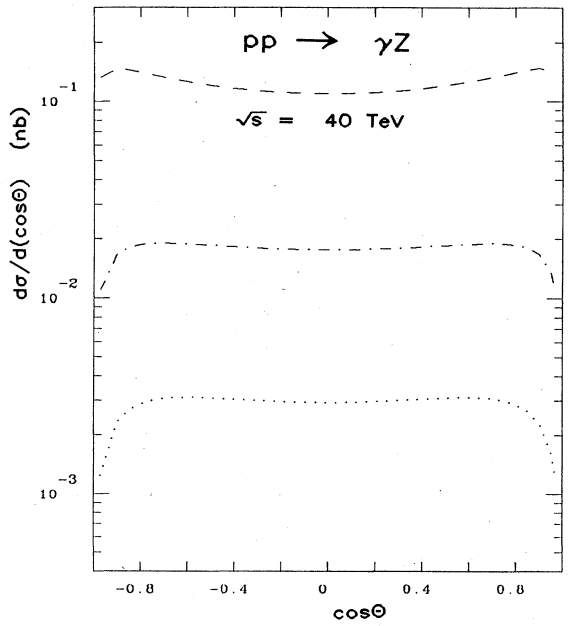

FIG. 140. Distribution in $\cos\theta$, where θ is the angle between the photon and the beam in the $Z\gamma$ c.m. frame, for the process $pp \to Z\gamma$ + anything at $\sqrt{s} = 40$ TeV. The transverse momentum of the photon is restricted to be greater than 20 (dashed line), 50 (dotted-dashed line), or 100 (dotted line) GeV/c. Set 2 of the distributions was used.

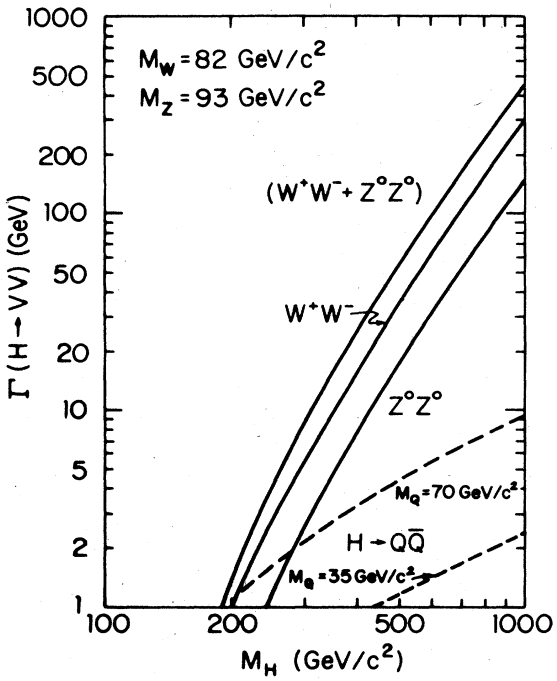

FIG. 141. Partial decay widths of the Higgs boson into intermediate boson pairs vs the Higgs-boson mass. For this illustration we have taken $M_W = 82$ GeV/c^2 and $M_Z = 93$ GeV/c^2.

collisions is the gluon fusion mechanism indicated in Fig. 144 (Georgi *et al.*, 1978). This process makes a contribution to the differential cross section for Higgs production of

$$\frac{d\sigma}{dy}(ab \to H + \text{anything}) = \frac{G_F \pi}{32\sqrt{2}} \left[\frac{\alpha_s}{\pi}\right]^2 \tau |\eta|^2 \times f_g^{(a)}(x_a, M_H^2) f_g^{(b)}(x_b, M_H^2) , \tag{4.88}$$

where (Resnick, Sundaresan, and Watson, 1973)

$$\eta = \sum_i \int_0^1 dx \int_0^{1-x} \frac{dy(1-4xy)}{1-(xyM_H^2/m_i^2)} , \tag{4.89}$$

and the strong coupling constant is evaluated at M_H^2.

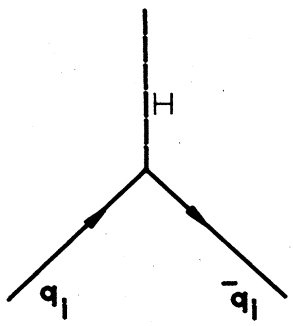

FIG. 142. Feynman diagram for the production of a Higgs boson in $q\bar{q}$ collisions.

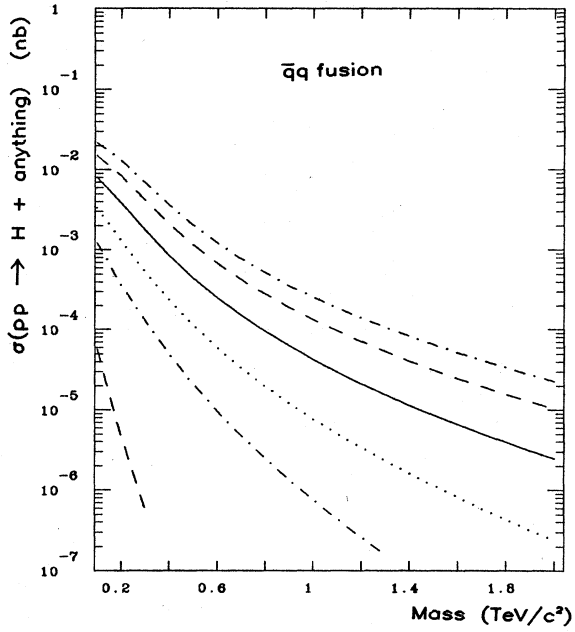

FIG. 143. Total cross section for Higgs boson production by $q\bar{q}$ fusion in pp collisions as a function of the Higgs boson mass at $\sqrt{s} = 2$, 10, 20, 40, 70, and 100 TeV, according to the parton distributions of Set 2.

Consequently the integrated cross section is

$$\sigma(ab \to H + \text{anything}) = \frac{G_F \pi}{32\sqrt{2}} \left[\frac{\alpha_s}{\pi}\right]^2 |\eta|^2 \tau \frac{d\mathcal{L}_{gg}}{d\tau} . \tag{4.90}$$

A quark with $m_i \geq M_H$ gives $\eta \approx \frac{1}{3}$. For $4m_i^2 < M_H^2$, η is complex. Defining

$$\varepsilon = 4m_i^2/M_H^2 , \tag{4.91}$$

we may write

$$\eta = \frac{\varepsilon}{2}[1 + (\varepsilon - 1)\varphi(\varepsilon)] , \tag{4.92}$$

with

$$\varphi(\varepsilon) = \begin{cases} -[\sin^{-1}(1/\sqrt{\varepsilon})]^2 , & \varepsilon > 1 \\ \frac{1}{4}[\ln(\zeta_+/\zeta_-) + i\pi]^2 , & \varepsilon < 1 , \end{cases} \tag{4.93}$$

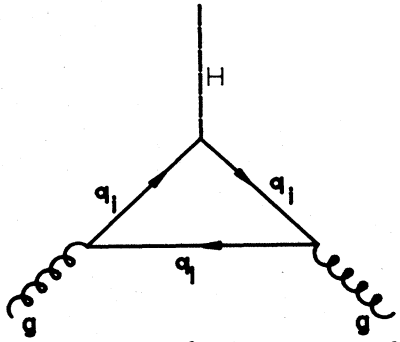

FIG. 144. Feynman diagram for the production of a Higgs boson in gluon-gluon fusion.

where

$$\zeta_{\pm}=1\pm\sqrt{1-\varepsilon}\ . \tag{4.94}$$

We plot $|\eta(\varepsilon)|^2$ as a function of ε in Fig. 145. For quark masses $m_i \lesssim 70$ GeV/c^2 and Higgs boson masses $m_H > 200$ GeV/c^2 the parameter ε is less than 0.5. In this region $|\eta(\varepsilon)|^2$ may be approximated by

$$|\eta(\varepsilon)|^2 \approx 0.7\varepsilon\ ,\quad \varepsilon < 0.5\ . \tag{4.95}$$

Consequently the production rate from this mechanism is proportional to m_i^2 and light quarks are ineffective.

The total cross sections for Higgs boson production by this gluon fusion process are shown in Fig. 146 for $m_t=30$ GeV/c^2 and in Fig. 147 for $m_t=70$ GeV/c^2. The sensitivity to the top quark mass is apparent. Differential cross sections for $\sqrt{s}=40$ TeV are plotted in Fig. 148. They show the expected behavior, with light Higgs bosons produced uniformly in rapidity and heavy Higgs bosons produced more centrally. The number of events is not large. In the case of the ZZ final state, the requirement that both Z's decay leptonically will result in only nine events for $m_H \approx 500$ GeV/c^2 and $m_t=30$ GeV/c^2 at $\sqrt{s}=40$ TeV and for $\int \mathcal{L}\,dt = 10^{40}$ cm^{-2}. This small number of events may be sufficient in the absence of background (see below).

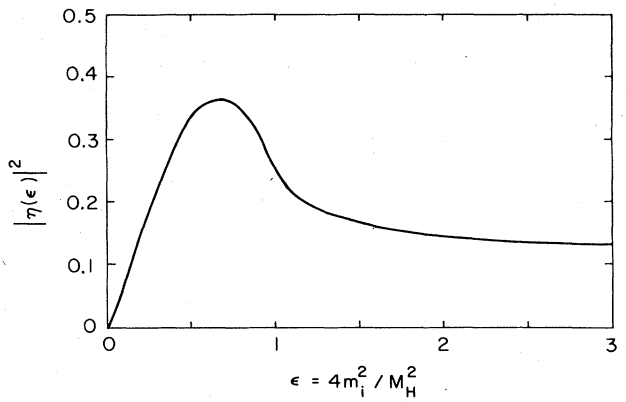

FIG. 145. Function $|\eta(\epsilon)|^2$ defined in Eqs. (4.93) and (4.94).

Another mechanism for the production of heavy Higgs bosons earlier discussed by Petcov and Jones (1979) has recently been studied by Cahn and Dawson (1984). This is the intermediate boson fusion mechanism depicted in Fig. 149, which becomes important at large Higgs boson masses, because the coupling of the Higgs boson to longitudinal W's and Z's is proportional to M_H. Useful approximate forms for the cross sections are (Chanowitz and Gaillard, 1984; Cahn and Dawson, 1984)

$$\sigma_{WWH}(ab\to H+\text{anything}) \approx \frac{1}{16M_W^2}\left[\frac{\alpha}{x_W}\right]^3 [(1+M_H^2/\hat{s})\ln(\hat{s}/M_H^2)-2+2M_H^2/\hat{s}] \times \sum_{i,k} f_i^{(a)}(x_a,M_H^2) f_k^{(b)}(x_b,M_H^2)\theta(-e_i e_k)\ , \tag{4.96}$$

and

$$\sigma_{ZZH}(ab\to H+\text{anything}) \approx \frac{1}{64M_W^2}\left[\frac{\alpha}{x_W(1-x_W)}\right]^3 [(1+M_H^2/\hat{s})\ln(\hat{s}/M_H^2)-2+2M_H^2/\hat{s}] \times \sum_{i,k} [(L_i^2+R_i^2)(L_k^2+R_k^2) f_i^{(a)}(x_a,M_H^2) f_k^{(b)}(x_b,M_H^2)]\ . \tag{4.97}$$

These approximations assume that the gauge bosons are emitted at zero angle. The total cross sections for Higgs boson production by intermediate boson fusion are shown in Fig. 150. This contribution exceeds that from gluon fusion for Higgs boson masses in excess of about 300 GeV/c^2 if $m_t=30$ GeV/c^2, as may be seen by comparison with Fig. 146. For a top quark mass of 70 GeV/c^2, the gluon fusion mechanism dominates for Higgs boson masses up to 550 GeV/c^2.

To assess the observability of Higgs bosons we must discuss the signal and the background. We will first consider the case in which the Higgs boson is heavier than $2M_W$ so that it decays almost exclusively into states of W^+W^- or ZZ (see Fig. 141). We display in Fig. 151 the cross section for the production and decay

$$pp\to H+\text{anything},\quad H\to W^+W^- \tag{4.98}$$

at $\sqrt{s}=40$ TeV. We have restricted the rapidity of the W so that $|y_W|<2.5$ and have assumed $m_t=30$ GeV/c^2. As discussed in Sec. IV.B, this cut will ensure that the decay products of the W's are not confused with the forward-going beam fragments. The contributions from gluon fusion [Eq. (4.90)] and gauge boson fusion [Eqs. (4.96) and (4.97)] are shown separately.

Assuming that the W's can be identified, the background comes from W pair production [Eq. (4.47)]. We have estimated this background by taking $d\sigma/dM$ for W pair production with $|y_W|<2.5$ (Fig. 122), evaluating it at W pair mass M equal to M_H and multiplying by the Higgs width or 10 GeV, whichever is larger (see Fig. 141). It can be seen that the signal exceeds the background for $M_H < 630$ GeV/c^2. Figure 152 shows the same result for $m_t=70$ GeV/c^2. For large Higgs masses this change is unimportant, since the gluon fusion mechanism is not dominant. A tighter rapidity cut of $|y_W|<1.5$ is shown in Fig. 153. The effect on signal and background of a

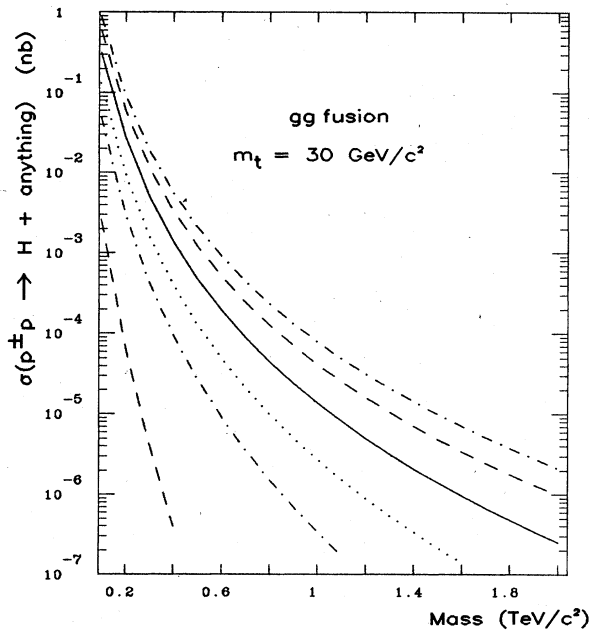

FIG. 146. Integrated cross sections for Higgs-boson production by gluon fusion in $p^{\pm}p$ collisions, for $m_t=30$ GeV/c^2 at $\sqrt{s}=2$, 10, 20, 40, 70, and 100 TeV, according to Set 2 of the distributions.

change in the beam energy can be seen by comparing Fig. 154 ($\sqrt{s}=10$ TeV) with Fig. 151. At this lower energy, the signal and background become equal at $M_H=320$ GeV/c^2.

The Higgs production rate is almost the same in $p\bar{p}$ collisions, but the background is larger (compare Figs. 122 and 124). At $\sqrt{s}=40$ TeV and $M_H=400$ GeV/c^2 the background is larger by approximately a factor of 4 in $\bar{p}p$ than in pp collisions.

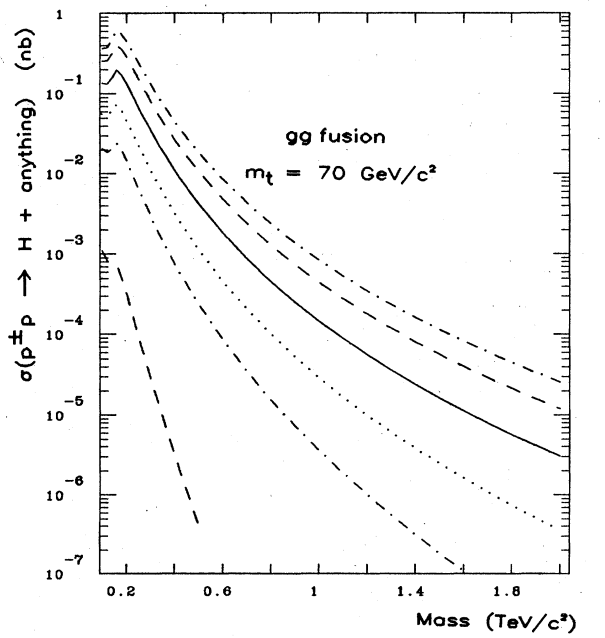

FIG. 147. Integrated cross sections for Higgs-boson production by gluon fusion in $p^{\pm}p$ collisions, for $m_t=70$ GeV/c^2 at $\sqrt{s}=2$, 10, 20, 40, 70, and 100 TeV, according to Set 2 of the distributions.

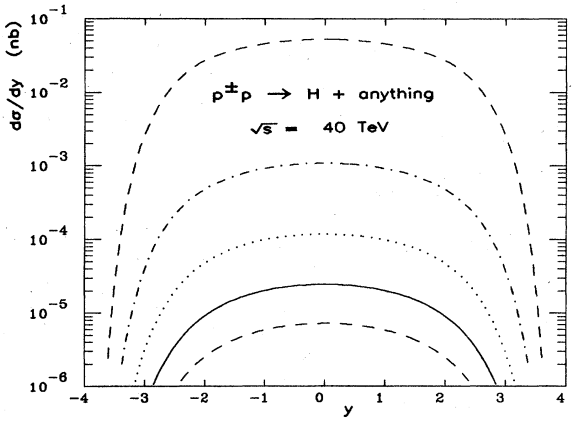

FIG. 148. Differential cross sections for Higgs-boson production by gluon fusion in $p^{\pm}p$ collisions at $\sqrt{s}=40$ TeV. The top quark mass is taken to be 30 GeV/c^2, and the gluon distributions of Set 2 are used. $M_H=100$, 300, 500, 700, and 900 GeV/c^2.

We can also attempt to observe the Higgs in its Z-pair decay mode. The signal is less by a factor of 2 [see Eqs. (4.82) and (4.83)], but the background is less significant, as can be seen by comparing Figs. 122 and 133. Figure 155 shows the signal and background in the Z-pair final state at $\sqrt{s}=40$ TeV in pp collisions with $|y_Z|<2.5$ and $m_t=30$ GeV/c^2. The signal exceeds the background for $M_H<1$ TeV/c^2.

In order to estimate the reach of various machines we have adopted the following criterion to establish the existence of a Higgs boson. There must be at least 5000 events, and the signal must stand above the background by five standard deviations. The 5000 events should be adequate even if we are restricted to the leptonic modes of the W's or Z's. In particular, 18 detected events would remain from a sample of 5000 Z pairs where both Z's decay into e^-e^+ or $\mu^+\mu^-$. Figure 156 shows the maximum detectable Higgs mass in the W-pair final state,

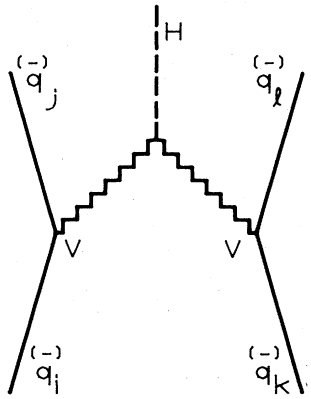

FIG. 149. Intermediate-boson fusion mechanism for Higgs-boson formation.

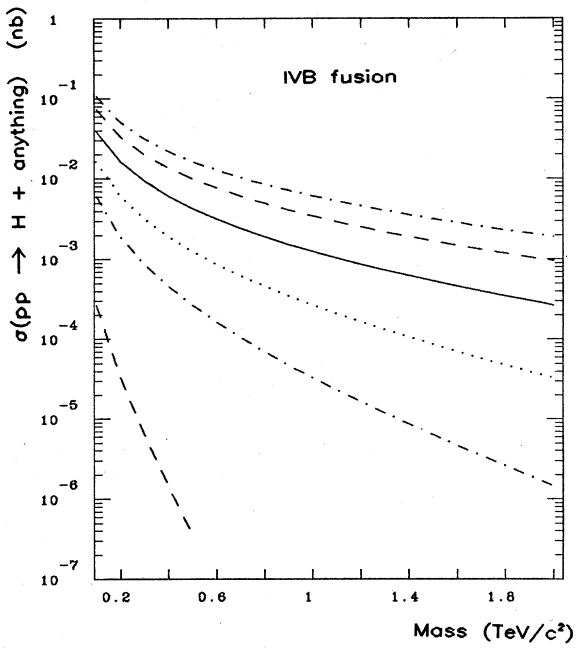

FIG. 150. Integrated cross sections for Higgs-boson production by intermediate-boson fusion in pp collisions, according to the parton distributions of Set 2.

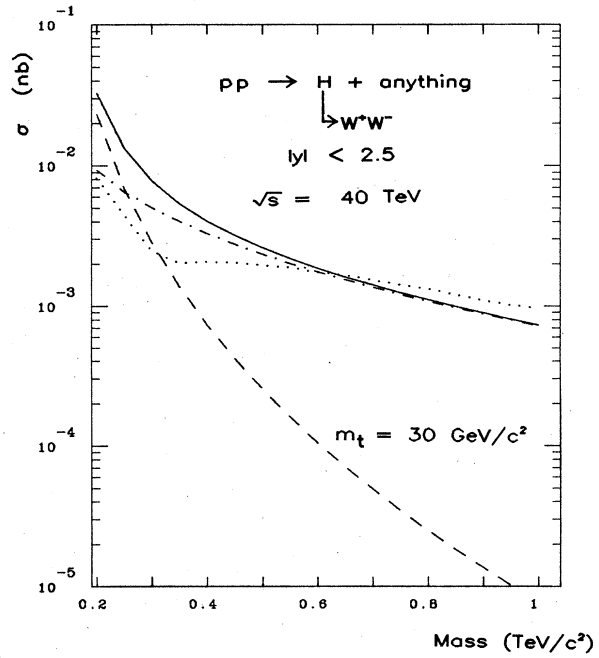

FIG. 151. Cross section for the reaction $pp \to (H \to W^+W^-) +$ anything, with $m_t = 30$ GeV/c^2, according to the parton distributions of Set 2, for $\sqrt{s} = 40$ TeV. The intermediate bosons must satisfy $|y_W| < 2.5$. The contributions of gluon fusion [dashed line, Eq. (4.90)] and WW/ZZ fusion [dotted-dashed line, Eqs. (4.96) and (4.97)] are shown separately. Also shown (dotted line) is $\Gamma d\sigma(pp \to W^+W^- + X)/dM$, with $|y_W| < 2.5$ and $M = M_H$, where $\Gamma = \max(\Gamma_H, 10\text{ GeV})$. (See Fig. 122.)

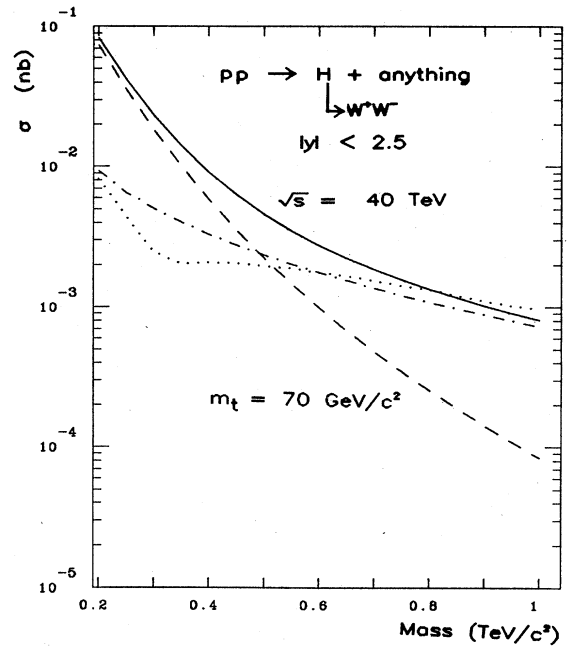

FIG. 152. Cross section for the reaction $pp \to (H \to W^+W^-) +$ anything, with $m_t = 70$ GeV/c^2, according to the parton distributions of Set 2, for $\sqrt{s} = 40$ TeV. The intermediate bosons must satisfy $|y_W| < 2.5$. The contributions of gluon fusion [dashed line, Eq. (4.90)] and WW/ZZ fusion [dotted-dashed line, Eqs. (4.96) and (4.97)] are shown separately. Also shown (dotted line) is $\Gamma d\sigma(pp \to W^+W^- + X)/dM$, with $|y_W| < 2.5$ and $M = M_H$, where $\Gamma = \max(\Gamma_H, 10\text{ GeV})$. (See Fig. 122.)

with $|y_W| < 2.5$, and $m_t = 30$ GeV/c^2 as a function of $\sqrt{s}$ for various integrated luminosities. The criteria applied to the ZZ final state do not yield significantly different results. It may be possible to distinguish a W or a Z from QCD jets if the W or Z decays hadronically. If this is the case and one cannot distinguish between a W and Z in their hadronic modes, then one must add the ZZ and WW final states. In this case, the background is increased, since it receives a contribution from WZ final states (Fig. 128).

If we apply the criterion to $p\bar{p}$ collisions, we shall obtain results very similar to those in pp. At $\sqrt{s} = 40$ TeV the limiting factor is the width of the Higgs as well as the production rate. An extremely wide resonance is difficult to establish. However, as we have already remarked, there should be sufficient W pair events to see some structure in the W^+W^- channel indicative of a heavy Higgs. At $\sqrt{s} = 10$ TeV the production rates are lower and a heavy Higgs is consequently more difficult to observe.

If the Higgs mass is less than $2M_W$, then we must attempt to observe its decay into a pair of t quarks,

$$pp \to H + \text{anything} \quad \Big\lfloor \to t\bar{t}\,, \tag{4.99}$$

for which only the gluon fusion production mechanism is important (see Figs. 146 and 150). The cross section for

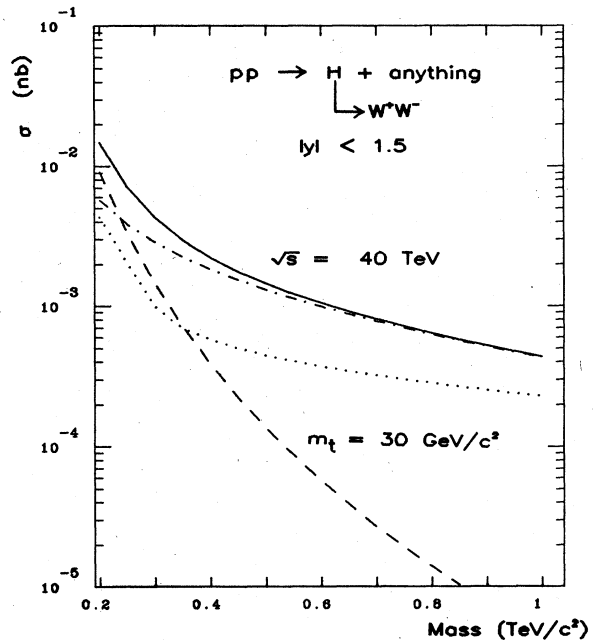

FIG. 153. Cross section for the reaction $pp \to (H \to W^+W^-) +$ anything, with $m_t = 30$ GeV/c^2, according to the parton distributions of Set 2, for $\sqrt{s} = 40$ TeV. The intermediate bosons must satisfy $|y_W| < 1.5$. The contributions of gluon fusion [dashed line, Eq. (4.90)] and WW/ZZ fusion [dotted-dashed line, Eqs. (4.96) and (4.97)] are shown separately. Also shown (dotted line) is $\Gamma d\sigma(pp \to W^+W^- + X)/dM$, with $|y_W| < 1.5$ and $M = M_H$, where $\Gamma = \max(\Gamma_H, 10\text{ GeV})$. (See Fig. 122.)

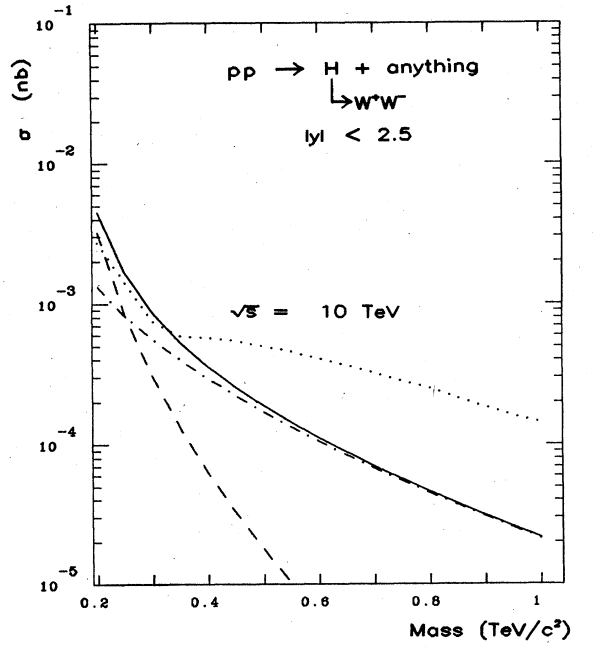

FIG. 154. Cross section for the reaction $pp \to (H \to W^+W^-) +$ anything, with $m_t = 30$ GeV/c^2, according to the parton distributions of Set 2, for $\sqrt{s} = 10$ TeV. The intermediate bosons must satisfy $|y_W| < 2.5$. The contributions of gluon fusion [dashed line, Eq. (4.90)] and WW/ZZ fusion [dotted-dashed line, Eqs. (4.96) and (4.97)] are shown separately. Also shown (dotted line) is $\Gamma d\sigma(pp \to W^+W^- + X)/dM$, with $|y_W| < 2.5$ and $M = M_H$, where $\Gamma = \max(\Gamma_H, 10\text{ GeV})$. (See Fig. 122.)

production of a Higgs boson, with subsequent emission of both t and $\bar{t}$ with $|y| < 1.5$ is plotted as a function of Higgs boson mass in Fig. 157. Although the cross sections are substantial and lead to the expectation of many events, the anticipated backgrounds make prospects for observation seem discouraging.

In the absence of any highly selective topological cut, the background to this signal arises from two-jet events due to hard scattering of partons. Such events were discussed in some detail in Sec. III. We showed in Figs. 90—92 the spectrum of two-jet invariant masses arising from the reaction

$$pp \to \text{jet}_1 + \text{jet}_2 + \text{anything} , \tag{4.100}$$

where the rapidity of each jet satisfies $|y| < 1.5$. The rate exceeds the Higgs boson production cross section by many orders of magnitude.

At the other extreme, we may imagine identifying t quarks in an experimental trigger. The t-quark lifetime is estimated to be

$$\tau(t) \approx 10^{-19}\text{ sec} \left[\frac{30\text{ GeV}/c^2}{m_t} \right]^5 , \tag{4.101}$$

and is consequently too short to be observed. However, the chain $t \to b$ results in a b quark with a relatively long lifetime (Fernandez *et al.*, 1983; Lockyer *et al.*, 1983),

$$\tau(b) = (1.6 \pm 0.4 \pm 0.3) \times 10^{-12}\text{ sec} . \tag{4.102}$$

A vertex detector could be used to tag this. We show in Fig. 158 the cross section for $t\bar{t}$ production via the process

$$gg \to Q\bar{Q} \tag{4.103}$$

which is discussed at length in Sec. V. Even this background dwarfs the Higgs signal of reaction (4.99).

We conclude this section with a few general comments. Our estimates of Higgs cross sections are conservative; in particular, we have concentrated on the case $m_t = 30$ GeV/c^2 and have assumed no additional generations of quarks. If m_t is larger, or if there are heavier flavors, then the Higgs production rates will increase considerably. We have seen that a machine with $\mathcal{L} = 10^{32}$ cm^{-2}sec^{-1} and $\sqrt{s} = 40$ TeV should be able to establish the existence of a Higgs if $M_H > 2M_W$ or will have sufficient event rate to be able to see structure in the W^+W^- channel in the event that M_H is very large, provided at least one of the intermediate bosons can be observed in its hadronic decay modes. If only the leptonic decays can be observed, $\mathcal{L} = 10^{33}$ cm^{-2}sec^{-1} will be required. If $M_H < 2M_W$, the discovery of a Higgs boson in $p^{\pm}p$ collisions seems more problematical. [For further details on the case $m_t = 45$ GeV/c^2, see Eichten *et al.* (1984).]

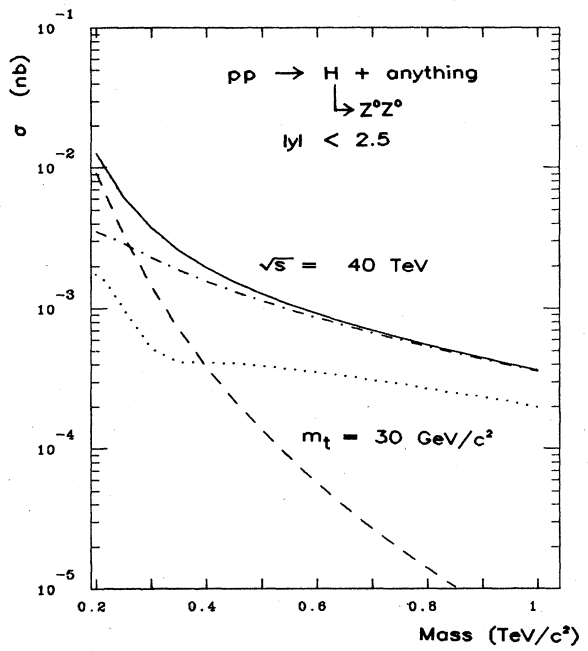

FIG. 155. Cross section for the reaction $pp \to (H \to ZZ) +$ anything, with $m_t = 30$ GeV/c^2, according to the parton distributions of Set 2, for $\sqrt{s} = 40$ TeV. The intermediate bosons must satisfy $|y_Z| < 2.5$. The contributions of gluon fusion (dashed line) and ZZ/WW fusion (dotted-dashed line) are shown separately. Also shown (dotted line) is $\Gamma d\sigma(pp \to ZZ + X)/dM$ with $|y_Z| < 2.5$ and $M = M_H$, where $\Gamma = \max(\Gamma_H, 10\text{ GeV})$. (See Fig. 133.)

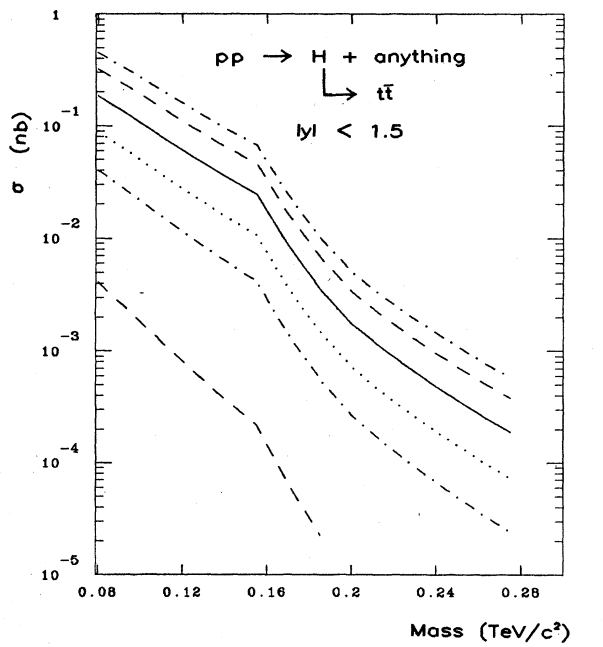

FIG. 157. Cross section for the reaction $pp \to (H \to t\bar{t}) +$ anything as a function of M_H with $m_t = 30$ GeV/c^2, according to the parton distributions of Set 2 at $\sqrt{s} = 2$, 10, 20, 40, 70, and 100 TeV. The t and $\bar{t}$ must satisfy $|y_t| < 1.5$.

E. Associated production of Higgs bosons and gauge bosons

In electron-positron collision, a favored reaction for Higgs boson production is

$$e^+e^- \to HZ\ , \tag{4.104}$$

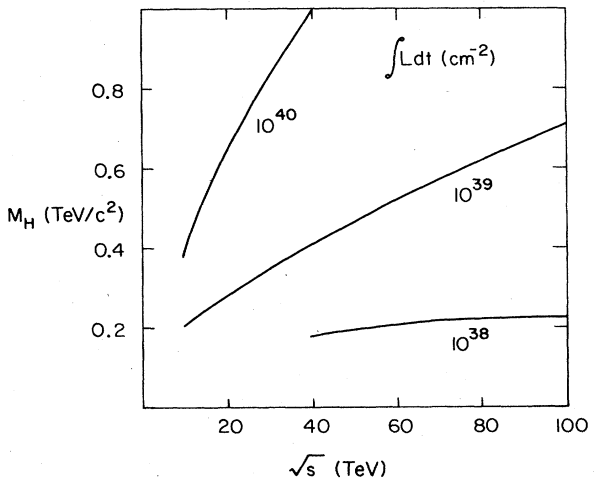

FIG. 156. "Discovery limit" of M_H as a function of $\sqrt{s}$ in $pp \to (H \to W^+W^-) +$ anything for integrated luminosities of 10^{38}, 10^{39}, and 10^{40} cm^{-2}, according to the criteria explained in the text.

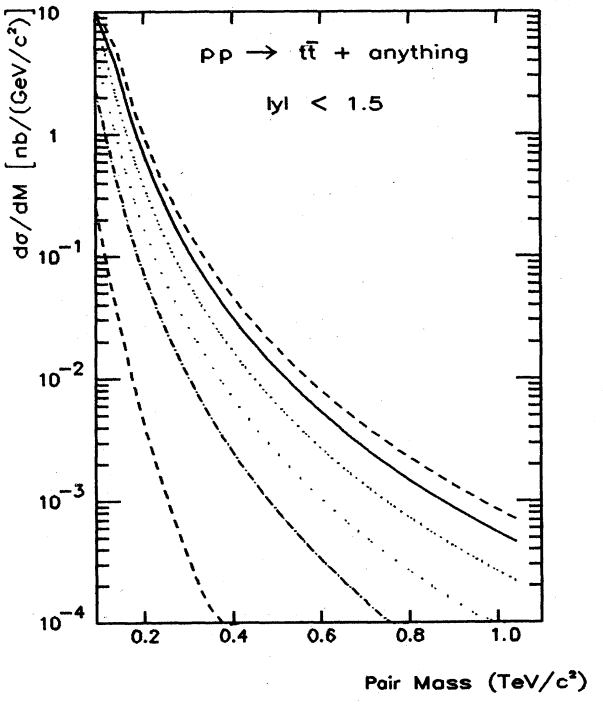

FIG. 158. Mass spectrum of $t\bar{t}$ pairs produced in proton-proton collisions, according to the parton distributions of Set 2. The rapidity of each produced quark is constrained to satisfy $|y_t| < 1.5$.

which proceeds by the direct-channel formation and decay of a virtual intermediate boson. Its advantage, in terms of a favorable cross section, arises from the fact that the HZZ coupling is of unsuppressed semiweak strength. The corresponding elementary processes that operate in hadron collisions are

$$q_i\bar{q}_j \to HW^{\pm} \tag{4.105}$$

and

$$q_i\bar{q}_i \to HZ\ . \tag{4.106}$$

The cross sections, averaged over initial quark colors, are

$$\frac{d\sigma}{d\Omega}(q_i\bar{q}_j \to HW^{\pm}) = \frac{\alpha^2 |\, U_{ij}\,|^2}{48x_W^2}\left[\frac{2K}{\sqrt{\hat{s}}}\right] \times \frac{1}{(\hat{s}-M_W^2)^2}\left[M_W^2+\frac{K^2}{2}\sin^2\theta\right] \tag{4.107}$$

and

$$\frac{d\sigma}{d\Omega}(q_i\bar{q}_i \to HZ) = \frac{\alpha^2(L_i^2+R_i^2)}{96x_W^2(1-x_W)^2}\left[\frac{2K}{\sqrt{\hat{s}}}\right] \times \frac{1}{(\hat{s}-M_Z^2)^2}\left[M_Z^2+\frac{K^2}{2}\sin^2\theta\right], \tag{4.108}$$

where K is the c.m. momentum of the emerging particles. Equation (4.107) holds for $W^{\pm}$ production when $e_i+e_{\bar{j}}=\pm 1$. The corresponding total cross sections are

$$\sigma(q_i\bar{q}_j \to W^{\pm}H) = \frac{\pi\alpha^2 |\, U_{ij}\,|^2}{36x_W^2}\left[\frac{2K}{\sqrt{\hat{s}}}\right] \times \frac{1}{(\hat{s}-M_W^2)^2}(K^2+3M_W^2) \tag{4.109}$$

and

$$\sigma(q_i\bar{q}_i \to HZ) = \frac{\pi\alpha^2(L_i^2+R_i^2)}{72x_W^2(1-x_W)^2}\left[\frac{2K}{\sqrt{\hat{s}}}\right] \times \frac{1}{(\hat{s}-M_Z^2)^2}(K^2+3M_Z^2)\ . \tag{4.110}$$

The cross sections for the reactions

$$p^{\pm}p \to W^{\pm}H + \text{anything} \tag{4.111}$$

and

$$p^{\pm}p \to HZ + \text{anything} \tag{4.112}$$

are shown in Figs. 159–162. Although they are significantly smaller than the cross sections for production of a single Higgs boson by gluon fusion, the annual production rates for $M_H=400$ GeV/c^2 still run to approximately 10^3 HV pairs at $\sqrt{s}=40$ TeV, assuming $\int dt\,\mathcal{L}=10^{40}$ cm^{-2}. Whether this number is sufficient for discovery is a question of detection efficiency. The final state has three gauge bosons. If all those decay hadronically this will produce six jets. A detailed Monte Carlo study is needed in order to know whether this state can be reconstructed. The event rate is so low that only one boson can probably be detected in its leptonic mode.

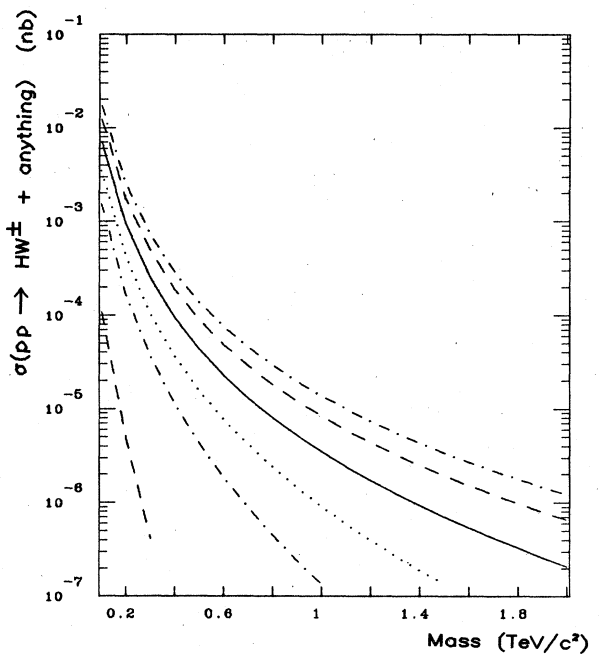

FIG. 159. Integrated cross sections for associated $HW^{\pm}$ production in pp collisions, according to the parton distributions of Set 2.

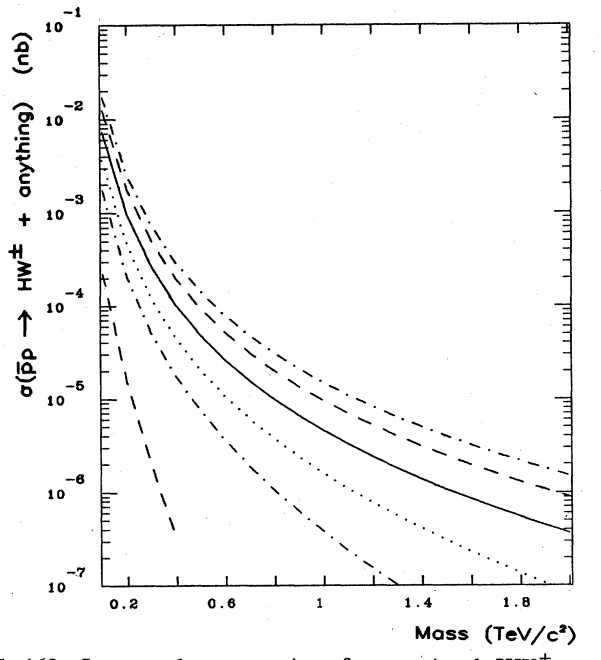

FIG. 160. Integrated cross sections for associated $HW^{\pm}$ production in $\bar{p}p$ collisions, according to the parton distributions of Set 2.

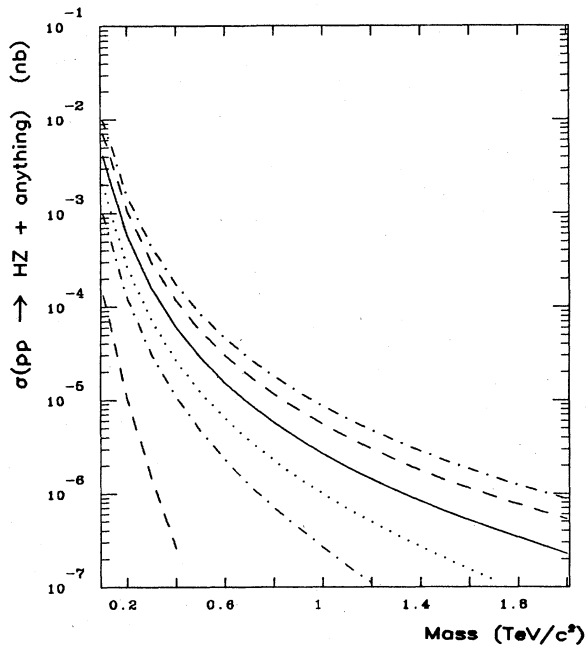

FIG. 161. Integrated cross sections for associated HZ production in pp collisions, according to the parton distributions of Set 2.

F. Summary

In this section we have shown how a high-energy, high-luminosity hadron-hadron collider may be exploited to extensively test the structure of the minimal model of electroweak interactions. The rate for production of W and Z bosons is extremely large (see Figs. 110, 111, 115, and 116). In particular, a 40-TeV collider capable of experiments with an integrated luminosity of 10^{39} cm^{-2} will generate approximately 6×10^{7} W's in a range of rapidity ($|y_W|<1.5$), where the decay products should be well separated from the beam fragments. Such a large sample cannot be obtained from any other foreseeable source and provides an opportunity to study rare W decays.

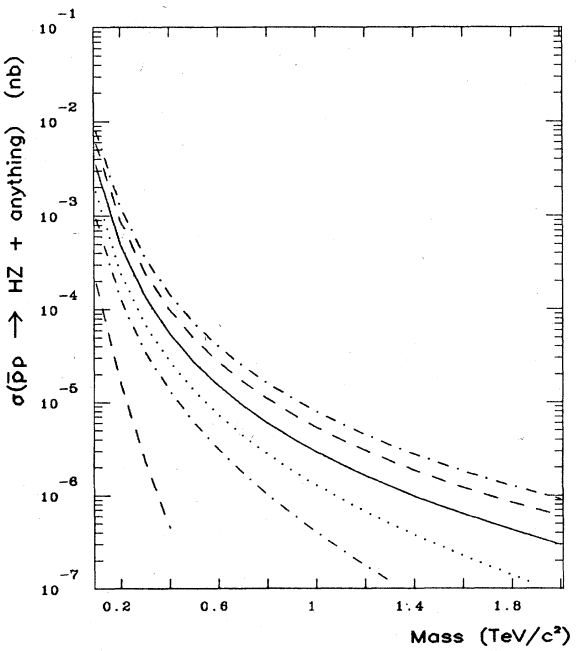

FIG. 162. Integrated cross sections for associated HZ production in $\bar{p}p$ collisions, according to the parton distributions of Set 2.

Of great importance is the detection and study of a Higgs boson. We have shown that if $M_H>2M_W$, the study of final states with W^+W^- or ZZ at $\sqrt{s}=40$ TeV should be able to reveal the presence of a Higgs boson, provided that its mass is less than 0.8 TeV/c^2 and provided that a luminosity of 10^{32} cm^{-2}sec^{-1} can be achieved and exploited. This requires detecting at least one intermediate boson in its hadronic decay modes. If both intermediate bosons must be observed in the leptonic modes, a luminosity of 10^{33} cm^{-2} sec^{-1} is necessary to reach above $M_H=400$ GeV/c^2. For a Higgs boson having a mass larger than this, the large width makes a resonance difficult to establish. In this case perturbative calculations become unreliable and the precise signals unclear. A search for structure in the W^+W^- invariant mass distribution should reveal deviations from those predicted in Figs. 122 and 123. An example of such a structure will be given in Sec. VI. In this case luminosity and the ability to reconstruct W^+W^- final states efficiently are critical.

V. MINIMAL EXTENSIONS OF THE STANDARD MODEL

In this section we discuss the production rates and experimental signatures of new quarks, leptons, and intermediate bosons that may arise in straightforward generalizations of the minimal $SU(2)_L\otimes U(1)_Y$ electroweak theory for three fermion generations. The new quarks and leptons we shall consider are "sequential" replicas of the known fermions. The generalization to exotic color charges or electroweak quantum numbers is elementary, and need not be treated explicitly. Additional gauge bosons beyond $W^{\pm}$ and Z^0 arise in many theories based on expanded gauge groups. We shall deal with representative examples.

One minimal extension of the standard model that we shall not consider here in detail is the enlargement of the Higgs sector to include more than a single complex doublet. This would imply the existence of charged physical Higgs scalars $H^{\pm}$ as well as additional neutrals $H^{0\prime}$. If the masses of these particles were less than about 40 GeV/c^2, the problem of producing and detecting them would be very similar to that of the light technipions discussed in Secs. VI.C and VI.D. For neutral Higgs bosons with $M(H^{0\prime})\gtrsim 2M_W$, the search for structure in the W^+W^- and Z^0Z^0 channels, described for the conventional Higgs boson in Sec. IV.D, is appropriate. The production and detection of heavy charged Higgs bosons is more problematical. These cannot be produced in association with $W^{\pm}$ or Z^0, because the $W^{\pm}H^{\mp}Z^0$ coupling is forbidden for physical Higgs scalars that belong to weak-

isospin doublets. Unless the $H^{\pm}$ coupling to light quarks is unexpectedly large, the rate for $q\bar{q}' \to H^{\pm}$ will be negligible. The reaction $gg \to H^+H^-$ via a quark loop will also occur at a tiny rate unless there are very heavy quarks in the loop. A production mechanism which does not entail small (Yukawa) couplings is the Drell-Yan process,

$$q\bar{q} \to \gamma \to H^+H^- . \tag{5.1}$$

The cross section, including the contribution of the direct-channel Z^0 pole, is given by Eqs. (4.3)—(4.12), with the factor e_i^2 in (4.7) replaced by (Lane, 1982)

$$e_i^2 \to \frac{\beta^3}{4}\left[e_i^2 - \frac{M^2(M^2-M_Z^2)(1-2x_W)(L_q+R_q)}{2x_W(1-x_W)[(M^2-M_Z^2)^2+M_Z^2\Gamma_Z^2]}e_i + \frac{M^4(1-2x_W)^2(L_q^2+R_q^2)}{16x_W^2(1-x_W)^2[(M^2-M_Z^2)^2+M_Z^2\Gamma_Z^2]}\right], \tag{5.2}$$

with the chiral couplings L_q and R_q given by (4.16), and

$$\beta=(1-4M_{H^{\pm}}^2/M^2)^{1/2} . \tag{5.3}$$

Thus the cross section approaches $\frac{1}{4}$ the lepton-pair cross section for high pair masses, modulo the differences in the neutral-current contribution to (5.2) and (4.14). Yields may be judged from Fig. 108 and Eq. (4.22). The most prominent decay of $H^{\pm}$ will be into a pair of hadron jets. The signature is similar to that for the pair production of technipions, which is addressed in Sec. VI.E.

A. Pair production of heavy quarks

Because we do not understand the pattern of fermion generations or masses, we must be alert to the possible existence of new flavors. We shall analyze the case in which new quarks occur in sequential $SU(2)_L$ doublets of color triplets, and specifically the case of quarks heavier than the intermediate boson.

Little can be said on general theoretical grounds about the masses of new flavors, but interesting constraints arise from consistency requirements and from phenomenological relationships. Imposing the requirement that partial-wave unitarity be respected at tree level in the reactions

$$F\bar{F} \to \begin{cases} W^+W^- \\ Z^0Z^0 \\ HZ^0 \\ HH , \end{cases} \tag{5.4}$$

where F denotes a heavy fermion, leads to restrictions on the heavy-fermion masses M_F, which set the scale $(G_FM_F^2\sqrt{2})^{1/2}$ of the $HF\bar{F}$ couplings (Veltman 1977b; Chanowitz, Furman, and Hinchliffe, 1979). For a new doublet $\binom{U}{D}$ of heavy quarks, this amounts to

$$|M_U-M_D| \lesssim 550 \text{ GeV}/c^2 , \tag{5.5}$$

while for a new lepton doublet $\binom{N^0}{L^-}$, it is

$$|M_L-M_N| \lesssim 1 \text{ TeV}/c^2 . \tag{5.6}$$

The difference between quark and lepton inequalities is due to color factors.

Heavy-fermion loops contribute to the renormalization of low-energy observables such as

$$\rho \equiv \frac{M_W^2}{M_Z^2(1-x_W)} \approx 1+\frac{G_FM_F^2N_c}{8\pi^2\sqrt{2}} , \tag{5.7}$$

where N_c is the number of colors of the heavy fermion F. The approximate form (5.7) holds when the mass of fermion F is large compared to the mass of its $SU(2)_L$ partner. A recent compilation (Marciano and Sirlin, 1983) of neutral-current cross-section measurements yields the value

$$\rho=1.02\pm0.02 . \tag{5.8}$$

This suggests the bounds

$$M_L \lesssim 620 \text{ GeV}/c^2 \tag{5.9}$$

for a charged sequential lepton accompanied by a massless neutrino, and

$$|M_U^2-M_D^2|^{1/2} \lesssim 350 \text{ GeV}/c^2 \tag{5.10}$$

for the mass splitting within a new quark doublet. Interesting bounds in the context of unified theories have been derived by Cabibbo *et al.* (1979).

The principal decays of heavy fermions will involve the emission of a real W boson. If $M_U > M_D$ [as suggested by the $\binom{c}{s}$ and $\binom{t}{b}$ generations], we anticipate

$$U \to \begin{cases} q^{-1/3}+W^+ & \text{(5.11a)} \\ D+W^+ & \text{(5.11b)} \end{cases}$$

and

$$D \to q^{+2/3}+W^- \tag{5.12}$$

for the quarks, and

$$L^- \to N^0+W^- \tag{5.13}$$

for the heavy lepton. In a theory with an expanded Higgs sector, decays such as $U \to D+H^+$ may compete favorably with W emission. We shall not consider these potentially interesting charged Higgs modes any further.

We now turn to estimates of the production cross sections in $p^{\pm}p$ collisions. In contrast to the c and b quarks, which were signalled by the dilepton decays of the $\psi/J(c\bar{c})$ and $\Upsilon(b\bar{b})$ states, the existence of a heavy quark Q will not be signalled by the chain

$$p^{\pm}p \to {}^3S_1(Q\bar{Q})+\text{anything}, \quad {}^3S_1(Q\bar{Q}) \to l^+l^- , \tag{5.14}$$

because the weak decay rate for the constituents $Q,\bar{Q}$ ($\propto M_Q^5$) greatly exceeds the leptonic decay rate of heavy quarkonium ($\propto M_Q$). Therefore, we must rely on inclusive $Q\bar{Q}$ production.

In lowest contributing order in the strong interactions, the elementary reactions leading to the $Q\bar{Q}$ final state are

$$gg \to Q\bar{Q} \tag{5.15}$$

and

$$q\bar{q} \to Q\bar{Q}\ , \tag{5.16}$$

for which the Feynman graphs appear in Figs. 74 and 71. The gluon fusion cross section is (Combridge, 1979)

$$\frac{d\sigma}{d\hat{t}}(gg\to Q\bar{Q}) = \frac{\pi\alpha_s^2}{8\hat{s}^2}\left\{\frac{6}{\hat{s}^2}(\hat{t}-M_Q^2)(\hat{u}-M_Q^2)+\left[\left[\frac{4}{3}\frac{(\hat{t}-M_Q^2)(\hat{u}-M_Q^2)-2M_Q^2(\hat{t}+M_Q^2)}{(\hat{t}-M_Q^2)^2} + \frac{3(\hat{t}-M_Q^2)(\hat{u}-M_Q^2)+M_Q^2(\hat{u}-\hat{t})}{\hat{s}(\hat{t}-M_Q^2)}\right]+[t\leftrightarrow u]\right] - \frac{M_Q^2(\hat{s}-4M_Q^2)}{3(\hat{t}-M_Q^2)(\hat{u}-M_Q^2)}\right\}. \tag{5.17}$$

In numerical calculations, we evaluate the strong coupling constant α_s at $Q^2=4M_Q^2$. The cross section for $Q\bar{Q}$ production in $q\bar{q}$ annihilations is

$$\frac{d\sigma}{d\hat{t}}(q\bar{q}\to Q\bar{Q}) = \frac{4\pi\alpha_s^2}{9\hat{s}^2}\left[\frac{(\hat{t}-M_Q^2)^2+(\hat{u}-M_Q^2)^2+2M_Q^2\hat{s}}{\hat{s}^2}\right]. \tag{5.18}$$

If the proton acquires its $Q\bar{Q}$ content perturbatively, in the manner described in Sec. II.B, the reaction

$$gQ \to gQ \tag{5.19}$$

will occur with a negligible cross section. We shall therefore not include diffractive production of heavy flavors. We are open to the possibility that diffraction is an important mechanism, although it may lie outside the realm of perturbative QCD. For a recent discussion of the production of a fourth quark generation in the context of a specific model for the diffractive component, see Barger *et al.* (1984).

The integrated cross sections for the reactions $p^{\pm}p\to Q\bar{Q}+$anything, evaluated using the parton distributions of Set 2, are shown as functions of the heavy quark mass M_Q in Fig. 163. The parton distributions of Set 1 lead to cross sections which are smaller by 10—20% over the range of interest. Proton-antiproton collisions enjoy a competitive advantage only for

$$2M_Q/\sqrt{s} \gtrsim 0.1\ ; \tag{5.20}$$

exploitation of this advantage requires high luminosities.

To better determine the detectability of the heavy quark pairs, we plot in Fig. 164 the cross section for production of heavy quarks in the rapidity interval $|y|<1.5$. Since $Q\bar{Q}$ production is dominated by gluon fusion, the pp and $\bar{p}p$ cross sections are approximately equal except at very large values of $\hat{s}$, where there are very few events.

The signature for heavy quark pairs will be events containing two W bosons and two quark jets. This should be relatively free of conventional backgrounds. Typically the mobility of products in the decays (5.11) and (5.12) will be approximately one unit of rapidity. The same is true for the products of intermediate boson decay,

$$W^{\pm}\to \begin{cases} q\bar{q}' \\ l\nu\ . \end{cases} \tag{5.21}$$

Consequently, all the ultimate products of heavy quarks produced with $|y|<1.5$ should be contained in a detector with angular coverage down to 2°.

To assess the capabilities of various colliders, we define an observable cross section to be one that yields at least fifty detected $Q\bar{Q}$ *pairs* in a run of 10^7 sec. (This could well be an unnecessarily stringent criterion; it may suffice in practice to impose a topology cut and to reconstruct one heavy quark per event.) The maximum quark mass that can be reached in a collider of given energy and luminosity depends sensitively upon the efficiency ε for identi-

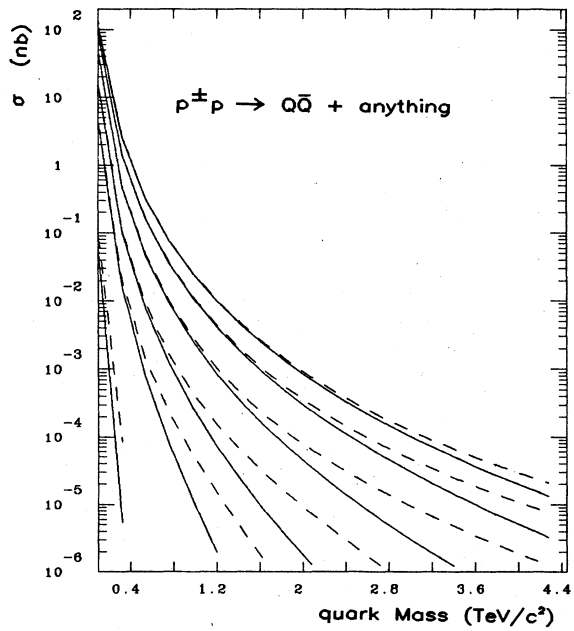

FIG. 163. Integrated cross sections for pair production of heavy quarks in proton-proton (solid lines) and proton-antiproton (dashed lines) collisions, according to the parton distributions of Set 2, at $\sqrt{s}=2$, 10, 20, 40, 70, and 100 TeV.

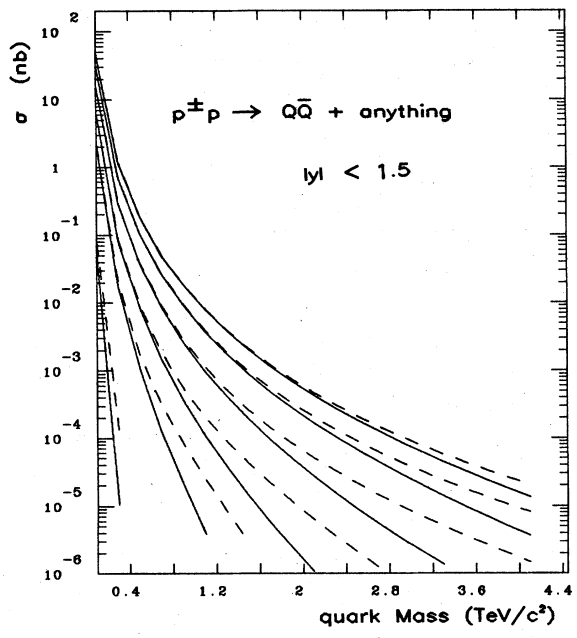

FIG. 164. Integrated cross sections for pair production of heavy quarks satisfying $|y_Q|, |y_{\bar{Q}}| < 1.5$ in proton-proton (solid lines) and proton-antiproton (dashed lines) collisions, according to the parton distributions of Set 2.

fying and measuring the products. Note, for example, that if the intermediate boson can be identified only in its electronic and muonic decays, the efficiency cannot exceed $\sim 15\%$ per heavy quark, or $\sim 2\%$ per $Q\bar{Q}$ pair. Bearing these numbers in mind, we plot in Fig. 165 the maximum quark masses accessible for specified values of the *effective* integrated luminosity

$$\mathscr{L}_{\text{eff}} \equiv \varepsilon \int dt\, \mathscr{L} \tag{5.22}$$

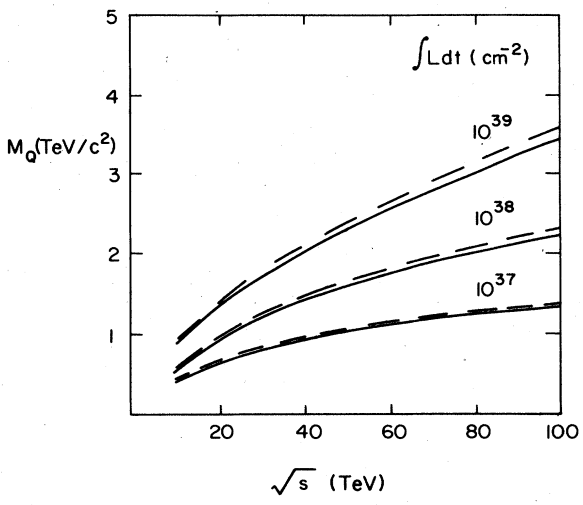

FIG. 165. Maximum quark mass M_Q accessible in pp (solid lines) and $\bar{p}p$ (dashed lines) collisions for specified values of the *effective* luminosity. Both quark and antiquark are restricted to $|y| < 1.5$. The actual collider luminosity required will be larger by a factor of 1/(efficiency for identification and measurement of the final state).

in either pp or $\bar{p}p$ collisions. Again there is little difference between pp and $\bar{p}p$ collisions in the regime of potential experimental interest.

If the mass difference between members of a heavy quark doublet is large,

$$M_U - M_D > M_W\ , \tag{5.23}$$

then the decay chain

$$\begin{aligned} U &\rightarrow D + W^+ \\ &\hookrightarrow q^{2/3} + W^- \end{aligned} \tag{5.24}$$

will lead to a signature of $W^+W^-W^+W^- + 2$ jets for the production of $U\bar{U}$ pairs. This sort of possibility emphasizes the benefits to be derived from the ability to identify intermediate bosons with high efficiency.

If the U-D mass difference is indeed large, a favorable production mechanism for the heavier partner may be

$$\begin{aligned} p^{\pm}p &\rightarrow W^{+}_{\text{virtual}} + \text{anything} \\ &\hookrightarrow U\bar{D}\ , \end{aligned} \tag{5.25}$$

which leads to a final state containing three intermediate bosons and two jets. Monte Carlo studies of specific examples should be quite revealing.

B. Pair production of heavy leptons

We next consider the pair production of charged sequential leptons (L^+L^-). We assume that

$$M_L - M_N > M_W\ , \tag{5.26}$$

and that the neutral lepton N^0 is effectively stable and noninteracting. This includes the most conventional case in which N^0 is essentially massless.

The pair production of charged heavy leptons proceeds by the Drell-Yan (1970,1971) mechanism reviewed in Sec. IV.A. As noted there, the differential and total cross sections are given by Eqs. (4.3), (4.11), and (4.12) times the kinematic suppression factor $(1-4M_L^2/M^2)^{1/2} \times (1+2M_L^2/M^2)$, where M is the invariant mass of the pair. We show in Fig. 166 the cross section

$$\left.\frac{d\sigma}{dy}\right|_{y=0} = \int dM \left.\frac{d\sigma}{dM\,dy}\right|_{y=0} \tag{5.27}$$

for the production of heavy-lepton pairs in the reaction

$$pp \rightarrow L^+L^- + \text{anything} \tag{5.28}$$

as a function of the lepton mass M_L. The same quantity is shown for $\bar{p}p$ collisions in Fig. 167. At large lepton masses, $\bar{p}p$ enjoys a considerable advantage over pp in the production rate. Whether this can be exploited depends upon backgrounds in the two cases and the number of events required to establish a signal.

One may search for a heavy-lepton (L^+L^-) signal in two ways: by observing an excess in the W^+W^- production rate, or by selecting events in which W^+W^- appear on opposite sides of the beam, with transverse momenta that do not balance. For the first case, the conventional

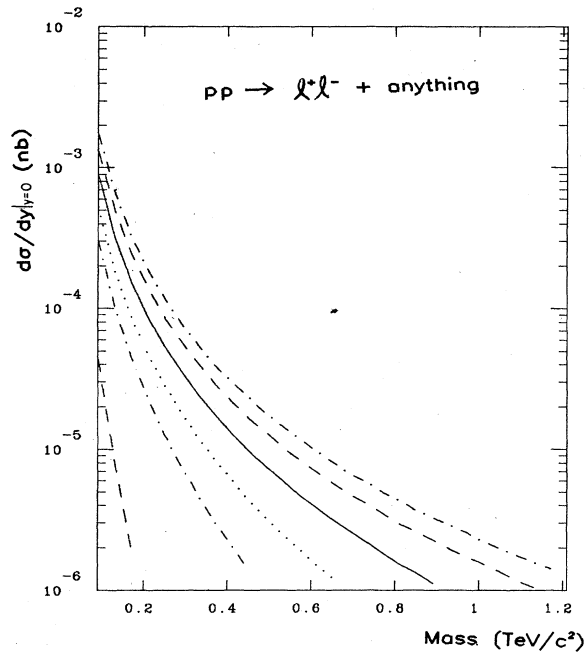

FIG. 166. Cross section $d\sigma/dy\,|_{y=0}$ for the production of (L^+L^-) heavy-lepton pairs in pp collisions. The contributions of both γ and Z^0 intermediate states are included, and the calculation is carried out using the parton distributions of Set 2.

W^+W^- pair production treated in Sec. IV.C.2 presents a severe background. Comparison of the rates for the conventional electroweak process shown in Figs. 120—124 with the rates implied by Figs. 166 and 167 shows that if this signal can be used, a large number of events will be required to establish an effect. This means that only

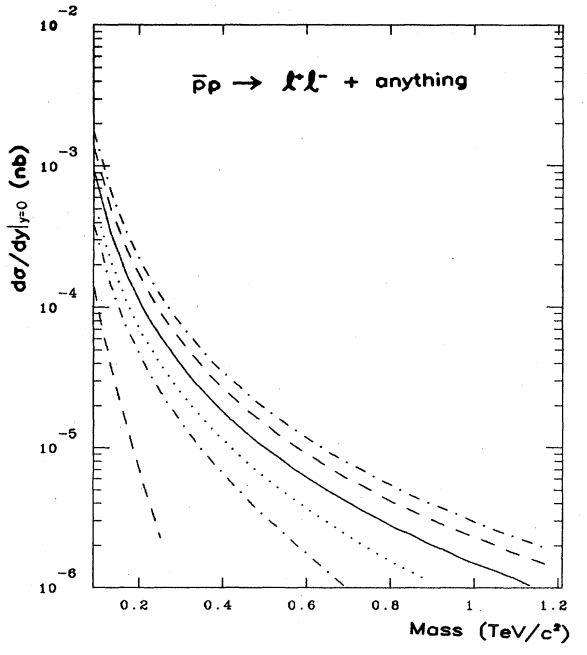

FIG. 167. Cross section $d\sigma/dy\,|_{y=0}$ for the production of (L^+L^-) heavy-lepton pairs in $\bar{p}p$ collisions. Calculational details are as for Fig. 166.

modest lepton masses $[O(100\ \text{GeV}/c^2)]$ are likely to be accessible. A realistic simulation will be required to make any precise statement.

The unbalanced transverse momentum signature relies on the fact that in the sequence

$$p^{\pm}p \rightarrow L^+L^- + \text{anything}, \quad L^- \rightarrow W^- + N^0, \quad L^+ \rightarrow W^+ + \bar{N}^0 \tag{5.29}$$

the heavy leptons may emit the decay products out of the production plane. If both W^+ and W^- are emitted up, for example, the event will have a large imbalance in visible $p_\perp$, because the neutral leptons N^0 will go undetected. This topology should be both characteristic and free of conventional background. Evidently the $W^\pm$ must be detected in nonleptonic channels. To assess the utility of this signature requires a Monte Carlo simulation. The following rough exercise will serve to show why a detailed simulation might be interesting and worthwhile.

We assume, as in the discussion of heavy quarks in Sec. V.B, that the ultimate decay products of heavy leptons produced in the rapidity interval $-1.5 < y < 1.5$ will be captured in a standard "4π" collider detector. Some fraction of these will survive the topological cut imposed by the requirement of significant transverse momentum imbalance. A reasonable guess for this fraction is $\frac{1}{6}$. The maximum lepton mass for which 25 such events will be detected is shown for various values of *effective* luminosity in Fig. 168. For effective luminosities in the range of 10^{38}—10^{39} cm^2, which correspond to thinkable combinations of detection efficiency and collider luminosity, a 40-TeV collider would be sensitive to heavy leptons with masses up to 250 GeV/c^2. This possibility deserves more serious study.

Another mechanism for the production of heavy lep-

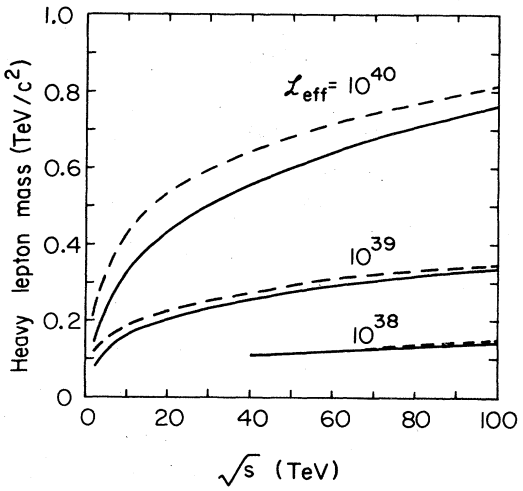

FIG. 168. Maximum-charged lepton mass M_L accessible in L^+L^- production in pp (solid lines) and $\bar{p}p$ (dashed lines) collisions for specified values of the *effective* luminosity. The actual collider luminosity required will be larger by a factor of 1/(efficiency for identification and measurement of the final state).

tons is the reaction

$$p^{\pm}p \to L^{\pm}N^0 + \text{anything} , \tag{5.30}$$

which proceeds by the elementary process

$$q_i\bar{q}_j \to W^{\pm}_{\text{virtual}} \to L^{\pm}N^0 . \tag{5.31}$$

The differential cross section is

$$\frac{d\hat{\sigma}_{ij}}{d\hat{t}} = \frac{\pi\alpha^2 \mid U_{ij} \mid^2}{12x_W^2\hat{s}^2} \frac{(\hat{u}-M_L^2)(\hat{u}-M_N^2)}{(\hat{s}-M_W^2)^2+M_W^2\Gamma_W^2} , \tag{5.32}$$

where U_{ij} is an element of the Kobayashi and Maskawa (1973) quark mixing matrix, and the total cross section is

$$\hat{\sigma}_{ij} = \frac{\pi\alpha^2 \mid U_{ij} \mid^2}{48x_W^2} \frac{\beta\hat{s}}{(\hat{s}-M_W^2)^2+M_W^2\Gamma_W^2} \times \left[1+\frac{\beta^2}{3}-\left[\frac{M_L^2-M_N^2}{\hat{s}}\right]^2\right] , \tag{5.33}$$

with

$$\beta = \left[1-2\left[\frac{M_L^2+M_N^2}{\hat{s}}\right]+\left[\frac{M_L^2-M_N^2}{\hat{s}}\right]^2\right]^{1/2} . \tag{5.34}$$

We show in Fig. 169 the cross section

$$\left.\frac{d\sigma}{dy}\right|_{y=0} = \int d\sqrt{\hat{s}} \left.\frac{d\sigma}{d\sqrt{\hat{s}}\,dy}\right|_{y=0} \tag{5.35}$$

for the production of $(L^{\pm}N^0)$ pairs in pp collisions as a function of the heavy-lepton mass M_L. The same quantity is shown for $\bar{p}p$ collisions in Fig. 170. In these examples, we have assumed the mass of the neutral partner N^0 to be negligible. The yields are considerably larger, for a given value of M_L, than those for L^+L^- pairs, because of the accessibility of lower $L^{\pm}N^0$ pair masses. For large values of M_L, $\bar{p}p$ collisions display the familiar advantage of valence quark—valence antiquark collisions.

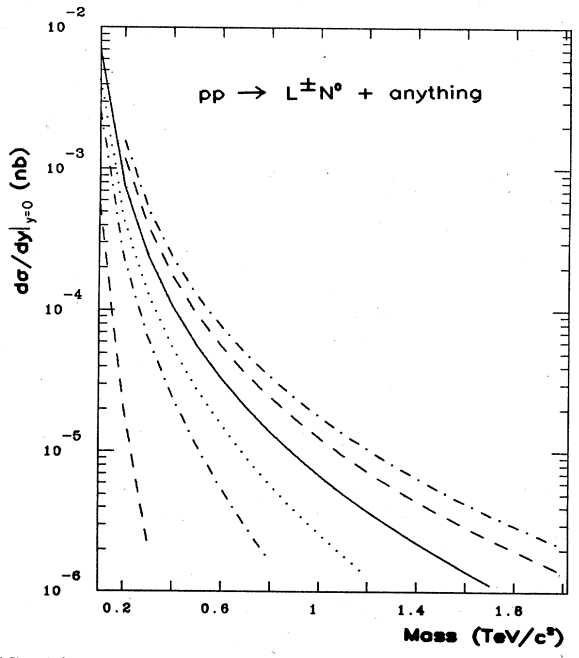

FIG. 169. Cross section $d\sigma/dy\,|_{y=0}$ for the production of $(L^{\pm}N^0)$ pairs in pp collisions. The N^0 is assumed to be massless, and the parton distributions are those of Set 2.

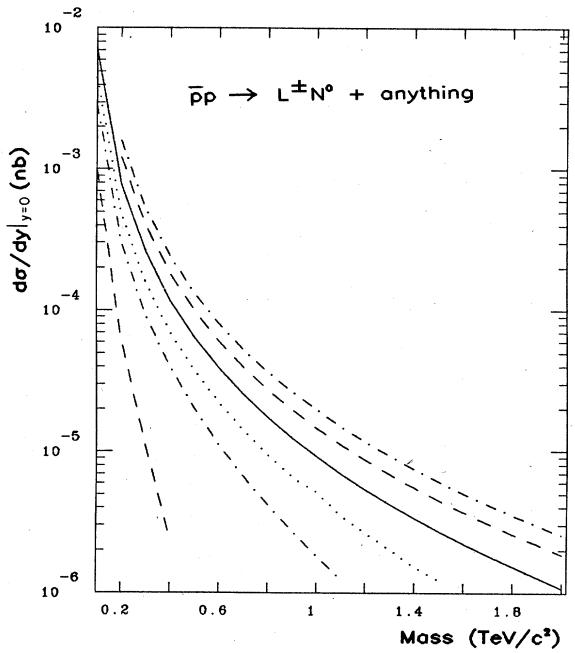

FIG. 170. Cross section $d\sigma/dy\,|_{y=0}$ for the production of $(L^{\pm}N^0)$ pairs in $\bar{p}p$ collisions. Calculational details are as in Fig. 169.

To estimate the discovery reach of high-energy colliders, we determine the effective luminosity required to establish a 5σ excess of

$$\begin{array}{l} L^{\pm}N^0 \\ \quad\llcorner\, W^{\pm}N^0 \end{array} \tag{5.36}$$

final states, in which the neutral leptons escape undetected. For this purpose, we compare the yield of $L^{\pm}N^0$ events in the rapidity interval $-1.5 < y < 1.5$ with the background from the process

$$\begin{array}{l} p^{\pm}p \to W^{\pm}Z^0 \\ \qquad\quad\llcorner\, \nu\bar{\nu} , \end{array} \tag{5.37}$$

where the gauge bosons both lie in the rapidity interval $-2.5 < y < 2.5$. The larger bin for the background is chosen to match the mobility of $W^{\pm}$ from $L^{\pm}$ decay.

We show in Fig. 171 the maximum lepton mass for which a 5σ excess can be established for various values of *effective* luminosity. As usual, these effective luminosities must be divided by the efficiency ε_W for W detection to obtain the collider luminosity. For effective luminosities in the range 10^{38}–10^{39} cm^{-2}, the reach in M_L is typically two times as large in the $L^{\pm}N^0$ channel as in the L^+L^- channel.

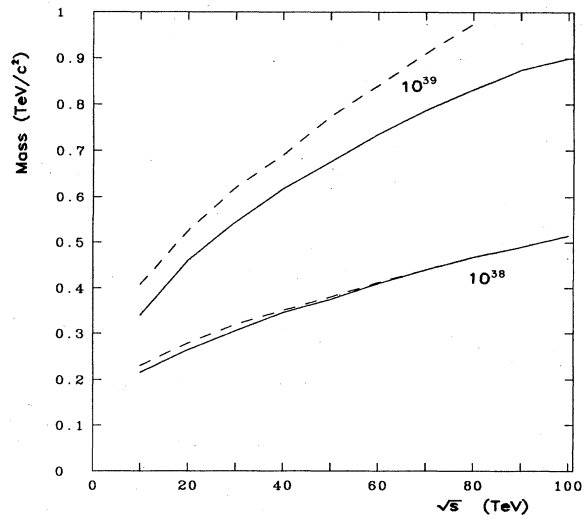

FIG. 171. Maximum-charged lepton mass M_L accessible in $L^{\pm}N^0$ production in pp (solid lines) and $\bar{p}p$ (dashed lines) for specified values of the *effective* luminosity. The actual collider luminosity required will be larger by a factor of 1/(efficiency for the identification and measurement of the final state).

C. New electroweak gauge bosons

A number of proposals have been advanced for enlarging the electroweak gauge group beyond the $SU(2)_L \otimes U(1)_Y$ of the standard model. One class contains the "left-right symmetric" models (Pati and Salam, 1974; Mohapatra and Pati, 1975; Mohapatra and Senjanovic, 1981; Mohapatra, 1983) based on the gauge group

$$SU(2)_L \otimes SU(2)_R \otimes U(1)_Y , \tag{5.38}$$

which restores parity invariance at high energies. Other models, notably the electroweak sector derived from the SO(10) unified theory, exhibit additional U(1) invariances. These will contain extra neutral gauge bosons. A general discussion was given by Georgi and Weinberg (1978). Prospects for detecting a second Z^0 have been analyzed recently by Leung and Rosner (1983).

All of these models have new gauge coupling constants which are of the order of the $SU(2)_L$ coupling constant of the standard model. They imply the existence of new gauge bosons with masses of a few hundred GeV/c^2 or more. In most interesting models, these new gauge bosons decay to the ordinary quarks and leptons (perhaps augmented by right-handed neutrinos). Roughly speaking, the decay rates of a W' will correspond to those of the familiar W, times $M_{W'}/M_W$. The heavier gauge bosons will therefore also be relatively narrow and prominent objects. To obtain a reasonable estimate of the cross sections for the production of additional W or Z bosons, we assume that the new bosons have the same gauge couplings to light leptons and quarks as do the familiar $W^{\pm}$ and Z^0.

The differential and total cross sections for $W'^{\pm}$ production are then given by (4.35) and (4.37) times $M_W^2/M_{W'}^2$, and with the scaling variable $\tau = M_{W'}^2/s$. We show in Figs. 172 and 173 the cross sections for W'^{+} and W'^{-} produced in pp and $\bar{p}p$ collisions in the rapidity interval $-1.5 < y_{W'} < 1.5$. At the largest masses, this restriction does not appreciably reduce the yield. As we have seen in other similar circumstances, the advantage of $\bar{p}p$ collisions over pp collisions becomes significant for $\sqrt{\tau} \gtrsim 0.1$.

There are two possibilities for detection: the leptonic decay modes

$$W' \rightarrow \begin{cases} e\nu_e \\ \mu\nu_\mu , \end{cases} \tag{5.39}$$

which occur with branching ratios

$$\Gamma(W' \rightarrow l\nu)/\Gamma(W' \rightarrow \text{all}) = 1/4n_g , \tag{5.40}$$

where n_g is the number of fermion generations, or the nonleptonic decays

$$W' \rightarrow \text{jet} + \text{jet} , \tag{5.41}$$

for which the branching ratio is

$$\Gamma(W' \rightarrow \text{jet} + \text{jet})/\Gamma(W' \rightarrow \text{all}) = \tfrac{3}{4} . \tag{5.42}$$

In the case of the $W^{\pm}$ and Z^0 of the Weinberg-Salam model, the QCD two-jet background is about an order of magnitude larger than the expected signal. Whether this circumstance continues for intermediate bosons in the TeV/c^2 regime depends, *inter alia,* upon the two-jet mass resolution that can be achieved. This is another question that is well suited for detailed simulations.

We adopt as a discovery criterion the requirement that

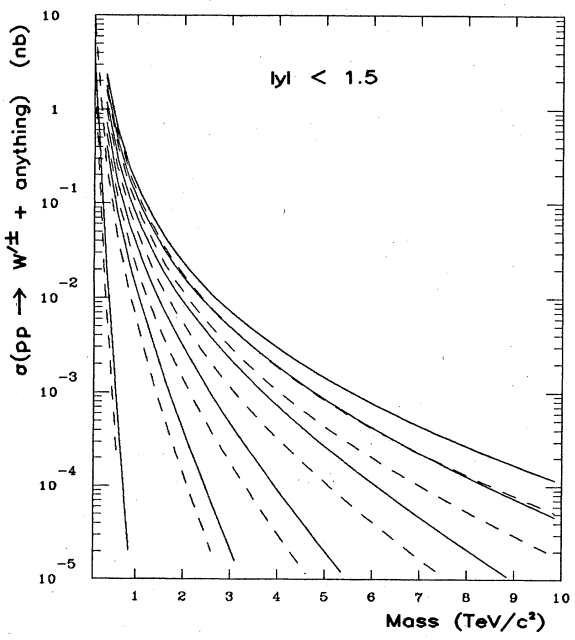

FIG. 172. Integrated cross sections for the production of W'^{+} (solid lines) or W'^{-} (dashed lines) with rapidities $|y_{W'}| < 1.5$ in proton-proton collisions, according to the parton distributions of Set 2, at $\sqrt{s} = 2$, 10, 20, 40, 70 and 100 TeV.

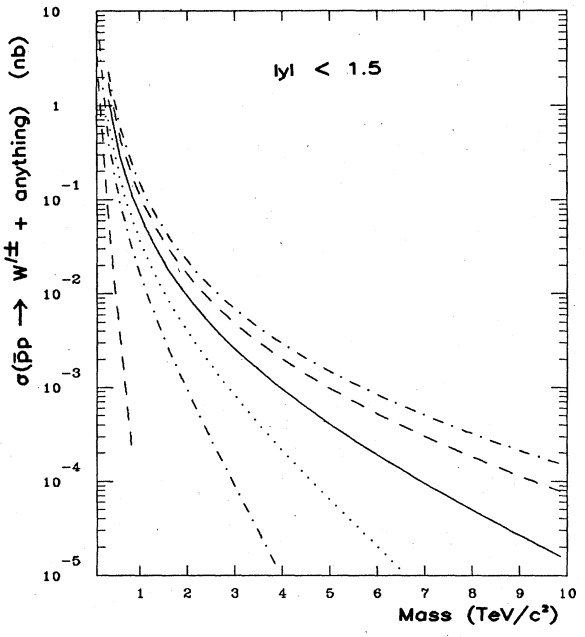

FIG. 173. Integrated cross sections for the production of W'^{+} or W'^{-} with rapidities $|y_{W'}|<1.5$ in proton-antiproton collisions, according to the parton distributions of Set 2.

1000 gauge bosons be produced in the rapidity interval $|y_{W'}|<1.5$. Unless the branching ratio for leptonic decay is much smaller than for the ordinary $W^{\pm}$, this should allow the establishment of a convincing signal in either the electron channel or the muon channel. The resulting discovery limits are shown in Fig. 174. The larger production rate for heavy gauge bosons in $\bar{p}p$ collisions makes itself apparent for integrated luminosities in excess of about 10^{39} cm^{-2}. For example, a 40-TeV pp collider can reach masses of 2.3, 4.1, and 6.5 TeV/c^2 for integrated luminosities of 10^{38}, 10^{39}, and 10^{40} cm^{-2}. A $\bar{p}p$ machine of the same energy can attain 2.4, 4.7, and 8.0 TeV/c^2.

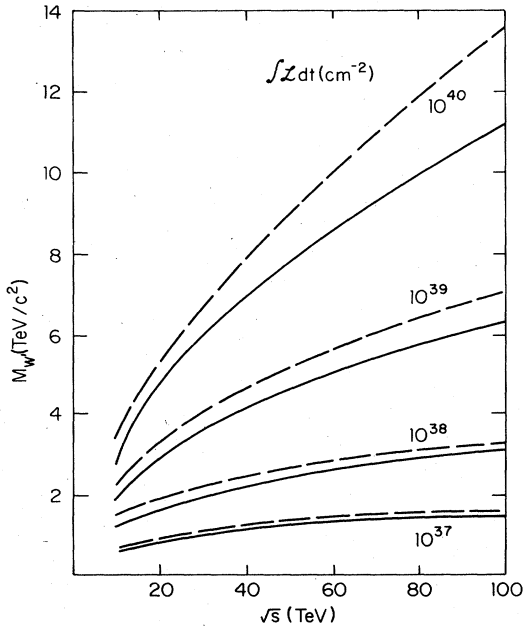

FIG. 174. Maximum mass of a new charged intermediate boson for which 10^3 events are produced with $|y_{W'}|<1.5$ at the stated integrated luminosities in proton-proton collisions (solid lines) and in proton-antiproton collisions (dashed lines).

The situation is rather similar for the production and detection of neutral gauge bosons. In this case we estimate the differential and integrated cross sections from Eqs. (4.39) and (4.41) times $M_Z^2/M_{Z'}^2$, with the scaling variable $\tau=M_{Z'}^2/s$. The resulting cross sections for $Z^{0\prime}$ production in the rapidity interval $|y_{Z'}|<1.5$ in pp and $\bar{p}p$ collisions are shown in Figs. 175 and 176. Again, the advantage of $\bar{p}p$ collisions is significant only for $\sqrt{\tau}\gtrsim 0.1$.

For a neutral gauge boson with couplings identical to those of the standard model Z^0, the leptonic decays

$$Z^{0\prime}\rightarrow\begin{cases}e^+e^-\\ \mu^+\mu^-\end{cases} \tag{5.43}$$

each occur with branching fraction

$$\Gamma(Z^{0\prime}\rightarrow l^+l^-)/\Gamma(Z^{0\prime}\rightarrow\text{all})\simeq 9\%/n_g\ , \tag{5.44}$$

where n_g is the number of fermion generations. The branching ratio for the nonleptonic decays

$$Z^{0\prime}\rightarrow\text{jet}+\text{jet} \tag{5.45}$$

is

$$\Gamma(Z^{0\prime}\rightarrow\text{jet}+\text{jet})/\Gamma(Z^{0\prime}\rightarrow\text{all})\approx\tfrac{3}{4}\ . \tag{5.46}$$

As for the $W'^{\pm}$, we regard 1000 neutral gauge bosons produced in $|y_{Z'}|<1.5$ as the minimum number required for discovery. The discovery limits implied by this requirement are displayed in Fig. 177. Once again, the

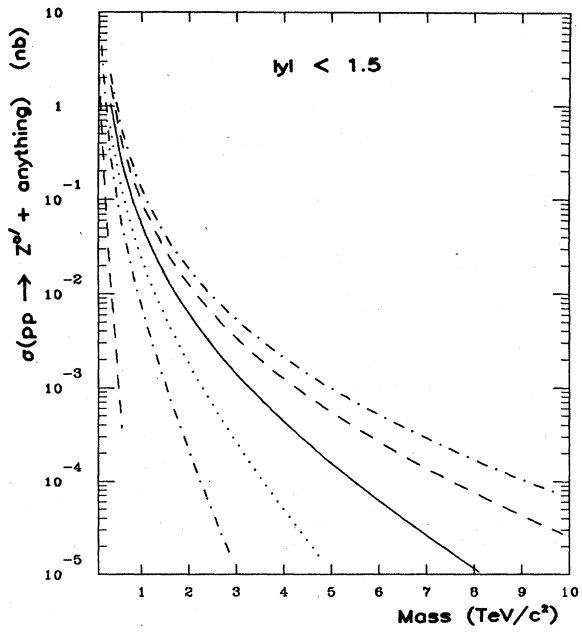

FIG. 175. Integrated cross sections for the production of $Z^{0\prime}$ with rapidity $|y_{Z'}|<1.5$ in proton-proton collisions, according to the parton distributions of Set 2.

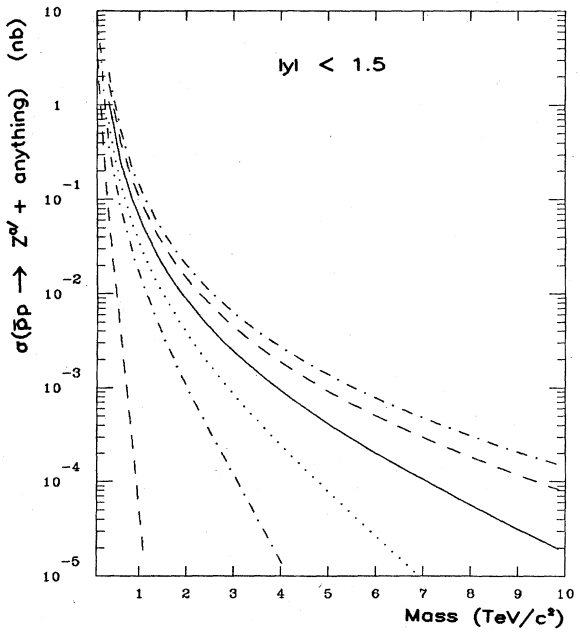

FIG. 176. Integrated cross sections for the production of $Z^{0\prime}$ with rapidity $|y_{Z'}| < 1.5$ in proton-antiproton collisions, according to the parton distributions of Set 2.

advantage of $\bar{p}p$ collisions in $q\bar{q}$ luminosity becomes apparent for integrated luminosities greater than 10^{39} cm^{-2}. At 40 TeV, a pp collider can reach 1.7, 3.3, and 5.5 TeV/c^2 for integrated luminosities of 10^{38}, 10^{39}, and 10^{40} cm^{-2}, whereas a $\bar{p}p$ collider can reach 1.9, 3.8, and 7.1 TeV/c^2. We may expect the same relative performance whatever the precise structure of the $Z^{0\prime}$ couplings to light fermions, so long as they are of universal (gauge) strength.

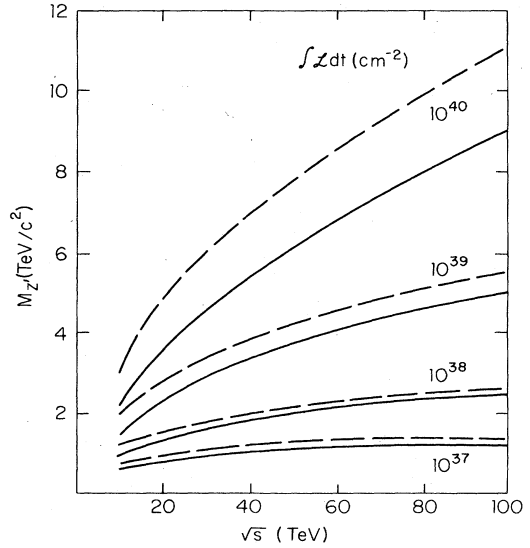

FIG. 177. Maximum mass of a new neutral intermediate boson for which 10^3 events are produced with $|y_{Z'}| < 1.5$ at the stated integrated luminosities in proton-proton collisions (solid lines) and in proton-antiproton collisions (dashed lines).

D. Summary

We have already given an assessment of the capabilities of multi-TeV colliders for the discovery of new quarks, leptons, and gauge bosons in Figs. 165, 168, 171, 174, and 177. Roughly speaking, the discovery limits lie in the range 1—2 TeV/c^2 for quarks, 0.1—0.7 TeV/c^2 for sequential charged leptons, and 4—5 TeV/c^2 for new gauge bosons, for colliders with c.m. energies and luminosities of the magnitudes being contemplated. Within the range of collider parameters under consideration, the reach of a 40-TeV collider is about twice that of a 10-TeV collider at the same luminosity. Increasing the collider energy to 100 TeV extends its reach by a factor of about 1.5 over that of the 40-TeV machine. These gains are somewhat smaller at low luminosities, and somewhat larger at high luminosities. For the minimal extensions we have discussed, a $\bar{p}p$ machine holds little advantage in production rates over a pp machine of the same energy and luminosity. More complicated comparisons, such as the physics tradeoff between a pp machine of given energy and luminosity versus a $\bar{p}p$ machine of higher energy but lower luminosity can be drawn from the summary figures 165, 168, 171, 174, and 177. Not for the last time, we note that there are significant benefits attached to detecting intermediate bosons in their nonleptonic modes. Detailed studies of the observability of heavy leptons in the final state

$$W^+W^- + \text{missing } p_\perp \tag{5.47}$$

and of new gauge bosons in the two-jet channel are required. For the leptonic decays of very massive $W'^{\pm}$, the consequences of the expected charge asymmetry [see, e.g., Rosner *et al.* (1984)] are worth pursuing.

VI. TECHNICOLOR

A. Motivation

In the standard electroweak model, the $SU(2)_L \otimes U(1)_Y$ local gauge symmetry is spontaneously broken to $U(1)_{em}$ through the medium of auxiliary, elementary scalar fields known as Higgs bosons. The self-interactions of the Higgs scalars select a vacuum, or minimum energy state, which does not manifest the full gauge symmetry of the Lagrangian. In so doing, they endow the gauge bosons and the elementary fermions of the theory with masses. Indeed, three of the four auxiliary scalars introduced in the minimal model become the longitudinal components of W^+, W^-, and Z^0. The fourth emerges as the physical Higgs boson, which has been the object of our attention in Sec. IV.D.

In spite of, or indeed because of, the phenomenological successes of the standard model, the elementary scalar solution to spontaneous symmetry breaking may be criticized as arbitrary, ambiguous, or even (Wilson, 1971) theoretically inconsistent. The principal objections concern the multitude of arbitrary parameters associated with

the Higgs potential and the Yukawa couplings that generate fermion masses, and the instability of the masses of elementary scalars in interacting field theory. One hopes for a better, more restrictive solution, with greater predictive power.

A promising approach is suggested by another manifestation of spontaneous symmetry breaking in nature, the superconducting phase transition. The macroscopic Ginzburg-Landau (1950) order parameter which acquires a nonzero vacuum expectation value in the superconducting state corresponds to the wave function of superconducting charges. In the microscopic Bardeen-Cooper-Schrieffer (1962) theory, the dynamical origin of the order parameter is identified with the formation of bound states of elementary fermions, the Cooper pairs of electrons. The hope of the general approach known as dynamical symmetry breaking[9] is that the dynamics of the fundamental gauge interactions will generate scalar bound states, and that these will assume the role heretofore assigned to the Higgs fields.

Could this occur for the electroweak theory without the introduction of any new interactions or fundamental constituents? It is quite instructive to see how QCD may act to hide the $SU(2)_L \otimes U(1)_Y$ gauge symmetry. Consider the conventional $SU(3)_{color} \otimes SU(2)_L \otimes U(1)_Y$ gauge theory applied to massless up and down quarks, and assume that the electroweak sector may be treated as a perturbation. The QCD Lagrangian has an exact chiral $SU(2)_L \otimes SU(2)_R$ symmetry.

It is generally supposed that the strong color forces spontaneously break the chiral symmetry $SU(2)_L \otimes SU(2)_R \rightarrow SU(2)$. As usual, the spontaneous breaking of a global continuous symmetry is accompanied by the appearance of massless Goldstone bosons, one for each broken generator of the global symmetry. In the case at hand, these are the three pions. (We attribute their nonzero masses in the real world to small quark masses in the Lagrangian.) The electroweak gauge bosons couple to broken generators of the chiral $SU(2)_L \otimes SU(2)_R$ symmetry group. These broken generators correspond to axial currents whose coupling to the pions is measured by the pion decay constant f_π. Consequently the electroweak gauge bosons acquire masses of order gf_π, where g is the coupling constant of the $SU(2)_L$ gauge symmetry. The massless pions disappear from the physical spectrum, having become the longitudinal components of W^+, W^-, and Z^0.

This is summarized by a mass matrix (Weinstein, 1973; Weinberg, 1979a; Susskind, 1979)

$$\mathcal{M}^2 = \begin{pmatrix} g^2 & 0 & 0 & 0 \\ 0 & g^2 & 0 & 0 \\ 0 & 0 & g^2 & gg' \\ 0 & 0 & gg' & g'^2 \end{pmatrix} f_\pi^2/4 , \tag{6.1}$$

in which rows and columns are labeled by the $SU(2)_L$ and $U(1)_Y$ gauge bosons (W^+, W^-, W^0, B), and $g'/2$ is the coupling constant for the weak-hypercharge group $U(1)_Y$. The mass matrix of the conventional Weinberg-Salam theory has precisely the form of (6.1), with $f_\pi \approx 93$ MeV replaced by the vacuum expectation value

$$v = (G_F\sqrt{2})^{-1/2} \approx 247 \text{ GeV} . \tag{6.2}$$

The spectrum of physical gauge bosons therefore includes the massless photon and the neutral intermediate boson Z^0, with

$$M_Z^2 = (g^2+g'^2)f_\pi^2/4 , \tag{6.3}$$

as well as the charged intermediate bosons $W^\pm$, with

$$M_W^2 = g^2 f_\pi^2/4 . \tag{6.4}$$

The conventional mass ratio

$$M_Z^2/M_W^2 = (g^2+g'^2)/g^2 = 1/\cos^2\theta_W \tag{6.5}$$

is preserved, but the masses themselves,

$$M_W \approx 30 \text{ MeV}/c^2 , \quad M_Z \approx 34 \text{ MeV}/c^2 , \tag{6.6}$$

are scaled down by a factor

$$f_\pi/v \approx 1/2650 . \tag{6.7}$$

The chiral symmetry breaking of QCD thus cannot be the source of electroweak symmetry breaking. Let us also note that one of the tasks of the Higgs scalars, the generation of fermion (including lepton) masses, is not addressed at all by this mechanism.

Although this simplest implementation of dynamical symmetry breaking does not succeed, it points the way to more realistic models. One natural response to the quantitative failure of the scheme described above is to postulate a new set of elementary fermions with interactions governed by a new strong-interaction gauge group. The term *technicolor* has come to stand both for this style of dynamical symmetry breaking and for the specific gauge group underlying the new dynamics. In the next section (VI.B) we introduce the minimal technicolor model of Weinberg (1976,1979) and Susskind (1979). This model shows how the generation of intermediate boson masses could arise without fundamental scalars or unnatural adjustments of parameters. However, it offers no explanation for the origin of quark and lepton masses.

We introduce in Sec. VI.C a nonminimal "extended technicolor" model due to Farhi and Susskind (1979) which shows how fermion masses might realistically be generated. Although this model is not rich enough to describe the real world, it has many observable consequences which would have to be present in any complete model of this type.

Sections VI.D and VI.E are devoted to some of the prominent experimental signatures for technicolor. There we discuss specifically the production and detection of single technihadrons (VI.D) and of technihadron pairs

[9] A convenient summary and reprint collection appears in Farhi and Jackiw (1982).

(VI.E). A summary of collider capabilities is given in Sec. VI.F.

Additional background material on technicolor, its phenomenology, and comparison with models involving elementary scalars may be found in the reviews by Farhi and Susskind (1981), Lane (1982), and Kaul (1983).

B. The minimal technicolor model

The minimal model of Weinberg (1976b,1979a) and Susskind (1979) is built of a chiral doublet of massless technifermions U and D which are taken for simplicity to be color singlets. Under the technicolor gauge group $G_{\rm TC}$, the technifermions transform according to a complex representation. It is convenient for illustrative purposes to choose $G_{\rm TC}=\mathrm{SU}(N)_{\rm TC}$, and to assign the technifermions to the fundamental N representation. With these assignments the technicolor, or TC, Lagrangian exhibits an exact chiral $\mathrm{SU}(2)_L\otimes\mathrm{SU}(2)_R$ symmetry. At an energy scale of order $\Lambda_{\rm TC}=O(1\ \mathrm{TeV})$, the technicolor interactions become strong and the chiral symmetry is spontaneously broken down to (vector) SU(2), the isospin group of the technifermions.

As a consequence of the spontaneous symmetry breaking, three Goldstone bosons appear. These are the massless technipions, $J^{\rm PC}=0^{-+}$ isovector states designated π_T^+,π_T^0,π_T^-.

The couplings of the technifermions to the electroweak gauge bosons are specified by the conventional $\mathrm{SU}(2)_L\otimes\mathrm{U}(1)_Y$ assignments, namely, a single left-handed weak-isospin doublet

$$\begin{bmatrix} U \\ D \end{bmatrix}_L \tag{6.8}$$

with weak hypercharge

$$Y(Q_L)=0\ , \tag{6.9}$$

and two right-handed weak-isospin singlets

$$U_R,\ D_R\ , \tag{6.10}$$

with weak hypercharge

$$\begin{aligned} &Y(U_R)=1\ , \\ &Y(D_R)=-1\ . \end{aligned} \tag{6.11}$$

With these assignments, the technifermion charges are given by the Gell-Mann-Nishijima formula

$$Q=I_3+\tfrac{1}{2}Y \tag{6.12}$$

as

$$\begin{aligned} &Q(U)=\tfrac{1}{2}\ , \\ &Q(D)=-\tfrac{1}{2}\ , \end{aligned} \tag{6.13}$$

and the electroweak sector is free of anomalies.

If the technicolor scale $\Lambda_{\rm TC}$ is chosen so that the technipion decay constant is

$$F_\pi=(G_F\sqrt{2})^{-1/2}\ , \tag{6.14}$$

then after the electroweak interaction is turned on, the $W^\pm$ and Z^0 will acquire the canonical masses

$$M_W^2=g^2/4G_F\sqrt{2}=\pi\alpha/G_F\sin^2\theta_W\ , \tag{6.15}$$

$$M_Z^2=M_W^2/\cos^2\theta_W\ . \tag{6.16}$$

The massless technipions disappear from the physical spectrum, having assumed the role of the longitudinal components of the intermediate bosons.

Knowing the spectrum of ordinary hadrons, and attributing its character to QCD, we may infer the remaining spectrum of technihadrons. It will include

an isotopic triplet of $J^{\rm PC}=1^{--}$ technirhos, $\rho_T^+,\rho_T^0,\rho_T^-$, with $M(\rho_T)=O(1\ \mathrm{TeV}/c^2)$,
an isoscalar $J^{\rm PC}=1^{--}$ techniomega, ω_T, with $M(\omega_T)=O(1\ \mathrm{TeV}/c^2)$,
an isoscalar pseudoscalar technieta, η_T, with $M(\eta_T)=O(1\ \mathrm{TeV}/c^2)$,
an isoscalar $J^{\rm PC}=0^{++}$ technisigma, σ_T, with $M(\sigma_T)=O(1\ \mathrm{TeV}/c^2)$,

plus other massive scalars, axial vectors, and tensors. The σ_T is the analog of the physical Higgs scalar in the Weinberg-Salam model. In addition to these $(T\bar{T})$ technimesons, there will be a rich spectrum of (T^N) technibaryons. Some of these might well be stable against decay, within technicolor.

In the absence of coupling to the electroweak sector, this techniworld mimics the QCD spectrum with two quark flavors. Large N arguments for the mass and width of the technirho (Dimopoulos, 1980; Dimopoulos, Raby, and Kane, 1981) give the estimates

$$M(\rho_T)=M(\rho)\frac{F_\pi}{f_\pi}\left[\frac{3}{N}\right]^{1/2}\approx(2\ \mathrm{TeV}/c^2)\left[\frac{3}{N}\right]^{1/2} \tag{6.17}$$

and

$$\begin{aligned} \Gamma(\rho_T\to\pi_T\pi_T)&=\Gamma(\rho\to\pi\pi)\left[\frac{3}{N}\right]\left[\frac{M(\rho_T)}{M(\rho)}\right] \\ &\quad\times[1-4M(\pi)^2/M(\rho)^2]^{-3/2} \\ &\approx(0.5\ \mathrm{TeV})\left[\frac{3}{N}\right]^{3/2}\ , \end{aligned} \tag{6.18}$$

where the technipion mass has been neglected compared to $M(\rho_T)$. For the popular choice $N=4$, we find

$$\begin{aligned} &M(\rho_T)\simeq 1.77\ \mathrm{TeV}/c^2\ , \\ &\Gamma(\rho_T\to\pi_T\pi_T)\simeq 325\ \mathrm{GeV}\ . \end{aligned} \tag{6.19}$$

The techniomega is expected to have approximately the same mass as the technirho, and to decay principally into three technipions.

We have already remarked that this minimal technicolor model does not account for the masses of the ordinary fermions. This shortcoming may be remedied by the extended technicolor strategy (Dimopoulos and Susskind, 1979; Eichten and Lane, 1980) to be explained below. Since the additional complication of extended technicolor is of little observational import in the framework of the minimal model, we shall not discuss it further in this context.

In hadron-hadron collisions, the technifermions of the minimal model will be pair produced by electroweak processes. One possible experimental signature is the creation of stable technibaryons, which for all odd values of N would carry half-integer charges. We are not confident in estimating the production rate for these states, except to note that it cannot exceed the overall rate of technifermion pair production, which will be minuscule—on the order of the Drell-Yan cross section. The signature is nevertheless an important one to bear in mind.

Less dependent on details, and thus more characteristic of the minimal technicolor scheme, are the expected modifications to electroweak processes in the 1-TeV regime. The most prominent of these are the contributions of the s-channel technirho to the pair production of gauge bosons. Because of the strong coupling of technirhos to pairs of longitudinal W's or Z's (the erstwhile technipions), the processes (Susskind, 1979)

$$q_i\bar{q}_i \to (\gamma \text{ or } Z^0) \to \rho_T^0 \to W_0^+ W_0^- \tag{6.20}$$

and

$$q_i\bar{q}_j \to W^\pm \to \rho_T^\pm \to W_0^\pm Z_0^0 , \tag{6.21}$$

where the subscript 0 denotes longitudinal polarization, will lead to significant enhancements in the pair-production cross sections.

Including the s-channel technirho enhancement, the differential cross sections for production of W^+W^- and $W^\pm Z^0$ are given by (4.48) for W^+W^-, with the coefficient of $(\hat{u}\hat{t}-M_W^4)/\hat{s}^2$ replaced by

$$2+\left[\frac{6M_W^2}{\hat{s}-M_Z^2}\right]\frac{L_i}{\tau_{3i}(1-x_W)}+\left[\frac{\hat{s}}{\hat{s}-M_Z^2}\right]^2\left[\beta_W^2-1+\frac{12M_W^4}{\hat{s}^2}\right]\left[\frac{L_i^2+R_i^2}{4(1-x_W)^2}\right]$$
$$+\left[1-\left[\frac{\hat{s}}{\hat{s}-M_Z^2}\right]\frac{L_i}{\tau_{3i}(1-x_W)}+\left[\frac{\hat{s}}{\hat{s}-M_Z^2}\right]^2\left[\frac{L_i^2+R_i^2}{4(1-x_W)^2}\right]\right]\frac{M_{\rho_T}^4}{(\hat{s}-M_{\rho_T}^2)^2+M_{\rho_T}^2\Gamma_{\rho_T}^2} , \tag{6.22}$$

and by (4.60) for WZ, with

$$(9-8x_W)\to\frac{M_{\rho_T}^4}{(\hat{s}-M_{\rho_T}^2)^2+M_{\rho_T}^2\Gamma_{\rho_T}^2}+8(1-x_W) , \tag{6.23}$$

where the notation is that of Sec. IV.

We show in Fig. 178 the mass spectrum of W^+W^- pairs produced in pp collisions at 20, 40, and 100 TeV, with and without the technirho enhancement. Both intermediate bosons are required to satisfy $|y|<1.5$. For this example, we have adopted the technirho parameters given in (6.19), and used the parton distributions of Set 2. The rates are substantially unchanged if the parton distributions of Set 1 are substituted. The yields are slightly higher in the neighborhood of the ρ_T enhancement in $\bar{p}p$ collisions. This is a 25% effect at 40 TeV and a 10% effect at 100 TeV.

The technirho enhancement amounts to nearly a doubling of the cross section in the resonance region. However, because the absolute rates are small, the convincing observation of this enhancement makes nontrivial demands on both collider and experiment. Let us now see this quantitatively.

The cross sections for W^+W^- pair production integrated over the resonance region

$$1.5 \text{ TeV}/c^2 \le \mathcal{M} \le 2.1 \text{ TeV}/c^2 \tag{6.24}$$

amount to

$$\int d\mathcal{M}\frac{d\sigma}{d\mathcal{M}}=\begin{cases}1.1\times10^{-5}\text{ nb}\\2.1\times10^{-5}\text{ nb}\end{cases} \tag{6.25}$$

at $\sqrt{s}=20$ TeV,

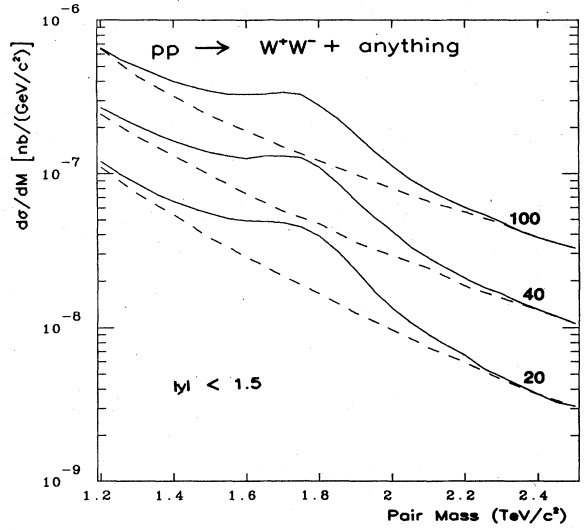

FIG. 178. Mass spectrum of W^+W^- pairs produced in pp collisions, according to the parton distributions of Set 2. Both W^+ and W^- must satisfy $|y|<1.5$. The cross sections are shown with (solid lines) and without (dashed lines) the technirho enhancement of Eq. (6.22). The technirho parameters are those of Eq. (6.19).

$$\int d\mathcal{M}\frac{d\sigma}{d\mathcal{M}}=\begin{cases}3.0\times10^{-5}\text{ nb}\\5.4\times10^{-5}\text{ nb}\end{cases}\tag{6.26}$$

at $\sqrt{s}=40$ TeV, and

$$\int d\mathcal{M}\frac{d\sigma}{d\mathcal{M}}=\begin{cases}8.0\times10^{-5}\text{ nb}\\14\times10^{-5}\text{ nb}\end{cases}\tag{6.27}$$

at $\sqrt{s}=100$ TeV. In each case the larger number includes the technirho contribution. In this channel the enhancement is relatively modest, because the ρ_T pole multiplies a term in (6.22) that is numerically small.

In a standard run with integrated luminosity of 10^{40} cm^{-2}, the number of excess events will be 100 on a background of 110 at 20 TeV, 240 on a background of 300 at 40 TeV, and 600 on a background of 800 at 100 TeV. We require that the enhancement consist of a least 25 detected events, and that the signal represent a five standard deviation excess over the background. This criterion means that each W must be detected with an efficiency of

$$\epsilon_W\geq\begin{cases}0.52, & \sqrt{s}=20\text{ TeV}\\0.36, & \sqrt{s}=40\text{ TeV}\\0.24, & \sqrt{s}=100\text{ TeV}\,.\end{cases}\tag{6.28}$$

This is clearly quite demanding, and in particular precludes reliance on leptonic decay modes except perhaps at the very highest energies. The requirements are relaxed somewhat if the rapidity cuts are softened to $|y|<2.5$, and if a lower statistical significance is accepted. All these conclusions of course depend strongly upon the assumed ρ_T parameters.

The situation is somewhat more encouraging for the $\rho_T^{\pm}$ enhancement in the $W^{\pm}Z$ channel. The mass spectrum of W^+Z plus W^-Z pairs produced in pp collisions at 10, 20, 40, and 100 TeV is shown with and without the $\rho_T^{\pm}$ contribution in Fig. 179. The same remarks about structure functions and the pp vs $\bar{p}p$ comparison apply as before.

In the charged channels, the technirho enhancement results in a cross section that is about four times the standard-model rate in the resonance region. The cross sections for W^+Z^0 plus W^-Z^0 pair production integrated over the resonance region (6.24) are

$$\int d\mathcal{M}\frac{d\sigma}{d\mathcal{M}}=\begin{cases}1.0\times10^{-6}\text{ nb}\\3.8\times10^{-6}\text{ nb}\end{cases}\tag{6.29}$$

at $\sqrt{s}=10$ TeV,

$$\int d\mathcal{M}\frac{d\sigma}{d\mathcal{M}}=\begin{cases}4.8\times10^{-6}\text{ nb}\\2.0\times10^{-5}\text{nb}\end{cases}\tag{6.30}$$

at $\sqrt{s}=20$ TeV,

$$\int d\mathcal{M}\frac{d\sigma}{d\mathcal{M}}=\begin{cases}1.3\times10^{-5}\text{ nb}\\5.5\times10^{-5}\text{ nb}\end{cases}\tag{6.31}$$

at $\sqrt{s}=40$ TeV, and

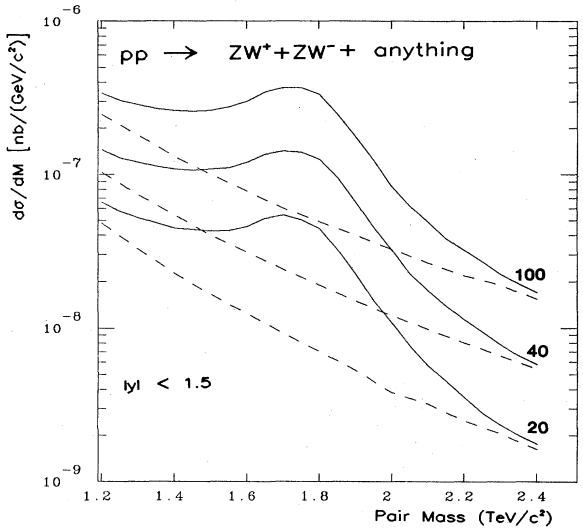

FIG. 179. Mass spectrum of W^+Z^0 and W^-Z^0 pairs produced in pp collisions, according to the parton distributions of Set 2. Both intermediate bosons must satisfy $|y|<1.5$. The cross sections are shown both with (solid lines) and without (dashed lines) the technirho enhancement of Eq. (6.23). The technirho parameters are those of Eq. (6.19).

$$\int d\mathcal{M}\frac{d\sigma}{d\mathcal{M}}=\begin{cases}3.2\times10^{-5}\text{ nb}\\14\times10^{-5}\text{ nb}\end{cases}\tag{6.32}$$

at $\sqrt{s}=100$ TeV. In each case the larger number includes the $\rho_T^{\pm}$ enhancement.

In a standard run with integrated luminosity of 10^{40} cm^{-2}, the number of excess events will be 28 on a background of 10 at 10 TeV, 150 on a background of 50 at 20 TeV, 420 on a background of 130 at 40 TeV, and 1080 on a background of 320 at 100 TeV. To establish the enhancement at the 5σ level therefore requires efficiencies ϵ_W and ϵ_Z for detection of W^+ and Z^0 of

$$(\epsilon_W\epsilon_Z)^{1/2}\geq\begin{cases}1, & \sqrt{s}=10\text{ TeV}\\0.41, & \sqrt{s}=20\text{ TeV}\\0.24, & \sqrt{s}=40\text{ TeV}\\0.15, & \sqrt{s}=100\text{ TeV}\,.\end{cases}\tag{6.33}$$

These are less demanding than the requirements (6.28) for observation of the technirho enhancement in the neutral channel.

If it should be necessary to rely on detection of the nonleptonic decay modes of the intermediate bosons, we must face the possibility that the $W^{\pm}$ and Z^0 cannot be separated in the two-jet invariant mass distribution. In this case, the quantity of interest is the sum of the W^+W^-, W^+Z^0, W^-Z^0, and Z^0Z^0 cross sections. The last of these receives no technirho enhancement, but is a small background. The resulting required detection efficiencies are comparable to those obtained in the discussion of $\rho_T^{\pm}$, and the same general conclusions apply. In this case, one will not be able to establish that the tech-

nirho occurs with charges $+1$, 0, and -1.

As in our treatment of gauge boson pair production in the standard electroweak theory, a key remaining question is whether the four-jet QCD background will compromise the detection of nonleptonic W and Z decays.

C. The Farhi-Susskind model

The minimal model just presented illustrates the general strategy and some of the consequences of a technicolor implementation of dynamical electroweak symmetry breaking. In a number of respects, it is not sufficiently rich to describe the world as we know it.

In any of the more nearly realistic technicolor models produced so far, there are at least four flavors of technifermions. As a consequence, the chiral flavor group is larger than $SU(2)_L \otimes SU(2)_R$, so that more than three massless technipions result from the spontaneous breakdown of chiral symmetry. Just as before, three of these will be incorporated into the electroweak gauge bosons. The others remain as physical spinless particles. Of course, these cannot and do not remain massless. Color-nonsinglet technimesons, if any, acquire most of their mass from QCD contributions (Dimopoulos, 1980; Peskin, 1980; Preskill, 1981; Dimopoulos, Raby, and Kane, 1981). The color-singlet technipions acquire mass from electroweak effects and from extended technicolor interactions (Eichten and Lane, 1980).

Extended technicolor provides a mechanism for endowing the ordinary quarks and leptons with masses. This is accomplished by embedding the technicolor gauge group G_{TC} into a larger extended technicolor gauge group $G_{ETC} \supset G_{TC}$ which couples quarks and leptons to the techifermions. It is assumed that the breakdown $g_{ETC} \rightarrow G_{TC}$ occurs at the energy scale

$$\Lambda_{ETC} \sim 30\text{—}300 \text{ TeV} \tag{6.34}$$

and that massive ETC gauge boson exchange generates quark and lepton bare masses of order

$$m \sim \Lambda_{TC}^3 / \Lambda_{ETC}^2 . \tag{6.35}$$

ETC gauge boson exchange also induces contact interactions of the kind discussed in Sec. VIII on compositeness. Unfortunately, no one has succeeded in constructing an extended technicolor model which is at all realistic.

Whichever of these mechanisms is responsible for the generation of technipion masses, the expected masses all are considerably less than the characteristic 1-TeV scale of technicolor. Equally important, the couplings of technipions to $SU(3)_c \otimes SU(2)_L \otimes U(1)_Y$ gauge bosons is known fairly reliably within any given model, and almost all of them will be copiously produced in a multi-TeV hadron collider. The challenge, as we shall see, lies in detecting these particles in the collider environment.

In this section we introduce a simple toy technicolor model due to Farhi and Susskind (1979), which has quite a rich spectrum of technipions and technivector mesons. The version of the model we consider has been developed in detail by Dimopoulos (1980), Peskin (1980), Preskill (1981), and Dimopoulos, Raby, and Kane (1981). This model cannot be correct in detail, but many of the observable consequences are typical of all quasirealistic technicolor models. We now discuss in turn the technifermion content, the spectrum and properties of the technipions and technirhos, the interactions of technimesons with $SU(3)_c \otimes SU(2)_L \otimes U(1)_Y$ gauge bosons (i.e., the means of producing technimesons), and the interactions of technimesons with quarks and leptons (which determine the means of detection).

The elementary technifermions in this model are a pair of color-triplet techniquarks $Q=(U,D)$, and a pair of color-singlet technileptons $L=(N,E)$. Both left-handed and right-handed components of the technifermions are assigned to the same complex representation of the technicolor group G_{TC}. For specific numerical estimates, we shall assume that $G_{TC}=SU(N)_{TC}$, with $N=4$, and that the $n_f = 2\times 3 + 2 = 8$ "flavors" of technifermions lie in the fundamental **4** representation. Under $SU(3)_c \otimes SU(2)_L \otimes U(1)_Y$, the technifermions transform as follows:

$$\begin{aligned} Q_L = (U,D)_L &: (3,2,Y) \begin{matrix} U_R : (3,1,Y+1) \\ D_R : (3,1,Y-1) \end{matrix} \\ L_L = (N,E)_L &: (1,2,-3Y) \begin{matrix} N_R : (1,1,-3Y+1) \\ E_R : (1,1,-3Y-1) \end{matrix} . \end{aligned} \tag{6.36}$$

The weak hypercharge assignments ensure the absence of anomalies in all gauge currents. For the choice $Y=\frac{1}{3}$, the techniquark and technilepton charges [compare (6.12)] are those of the ordinary quarks and leptons.

To determine the chiral flavor symmetry group G_f of the technimesons, we need only notice that all but the TC interactions themselves are feeble at the technicolor scale of about 1 TeV. In first approximation, QCD may be ignored by virtue of its asymptotic freedom, while the broken extended technicolor interactions are suppressed by at least $(\Lambda_{TC}/\Lambda_{ETC})^2$. (We note in passing that the asymptotic freedom of QCD is actually lost above the technifermion threshold ~ 1 TeV in such a theory. We shall not explore here the consequences of this fact.) Because both left-handed and right-handed technifermions belong to the same complex representation of G_{TC}, it follows that the techniflavor group is

$$G_f = SU(8)_L \otimes SU(8)_R \otimes U(1)_V . \tag{6.37}$$

This symmetry is spontaneously broken down to $SU(8)_V \otimes U(1)_V$. The breakdown is accompanied by the appearance of $8^2 - 1$ massless technipions which belong to the adjoint, or **63**-dimensional representation of the residual $SU(8)_V$ flavor symmetry group. So far as the technicolor interactions are concerned, these are all pseudoscalars. The technimesons are enumerated in Table II. There are seven color singlets, of which three $(\pi_T^+, \pi_T^0, \pi_T^-)$ become the longitudinal components of the electroweak gauge bosons. The remaining four are denoted P^+, P^0, P^-, and $P^{0\prime}$. At least these color-singlet technipions

TABLE II. Technipions and technivector mesons in the model of Farhi and Susskind (1979). [See also Peskin (1980) and Preskill (1981).] For unit normalization, the technifermion states should be divided by $\sqrt{N}$. The SU(8)$_V$ matrices are 8×8 matrices written in 4×4 block form. The λ_a are the 15 orthonormal generators of SU(4). The SU(3)$_c$ indices α,β run over 1,2,3 for color triplets; the index a runs over 1, . . . , 8 for color octets. Repeated indices are to be summed. The symbol $\lambda_{a\pm}$ denotes $\lambda_a \pm i\lambda_{a+1}$ for $a=9$, 11, and 13. The weak hypercharge parameter Y is given in (6.36).

States	Technifermion wave function	Color	(I,I_3)	Charge	SU(8)$_V$ matrices
π_T^+,ρ_2^+	$1/2 \mid U_\alpha\bar{D}_\alpha+N\bar{E}\rangle$	1	(1,1)	1	$1/\sqrt{8}\begin{bmatrix}0 & I\\ 0 & 0\end{bmatrix}$
π_T^0,ρ_2^0	$(1/\sqrt{8}) \mid U_\alpha\bar{U}_\alpha-D_\alpha\bar{D}_\alpha+N\bar{N}-E\bar{E}\rangle$	1	(1,0)	0	$1/4\begin{bmatrix}I & 0\\ 0 & -I\end{bmatrix}$
π_T^-,ρ_2^-	$1/2 \mid D_\alpha\bar{U}_\alpha+E\bar{N}\rangle$	1	(1,−1)	−1	$1/\sqrt{8}\begin{bmatrix}0 & 0\\ I & 0\end{bmatrix}$
P^+,ρ_1^+	$(1/\sqrt{12}) \mid U_\alpha\bar{D}_\alpha-3N\bar{E}\rangle$	1	(1,1)	1	$1/2\begin{bmatrix}0 & \lambda_{15}\\ 0 & 0\end{bmatrix}$
P^0,ρ_1^0	$(1/\sqrt{24}) \mid U_\alpha\bar{U}_\alpha-D_\alpha\bar{D}_\alpha-3(N\bar{N}-E\bar{E})\rangle$	1	(1,0)	0	$1/\sqrt{8}\begin{bmatrix}\lambda_{15} & 0\\ 0 & -\lambda_{15}\end{bmatrix}$
P^-,ρ_1^-	$(1/\sqrt{12}) \mid D_\alpha\bar{U}_\alpha-3E\bar{N}\rangle$	1	(1,−1)	−1	$1/2\begin{bmatrix}0 & 0\\ \lambda_{15} & 0\end{bmatrix}$
$P^{0'},\rho^{0'}$	$(1/\sqrt{24}) \mid U_\alpha\bar{U}_\alpha+D_\alpha\bar{D}_\alpha-3(N\bar{N}+E\bar{E})\rangle$	1	(0,0)	0	$1/\sqrt{8}\begin{bmatrix}\lambda_{15} & 0\\ 0 & \lambda_{15}\end{bmatrix}$
η_T',ω_T	$(1/\sqrt{8}) \mid U_\alpha\bar{U}_\alpha+D_\alpha\bar{D}_\alpha+N\bar{N}+E\bar{E}\rangle$	1	(0,0)	0	$1/4\begin{bmatrix}I & 0\\ 0 & I\end{bmatrix}$
P_3^1,ρ_3^1	$\mid U_\alpha\bar{E}\rangle$	3	(1,1)	$2Y+1$	$1/\sqrt{8}\begin{bmatrix}0 & \lambda_{a+}\\ 0 & 0\end{bmatrix}$
P_3^0,ρ_3^0	$(1/\sqrt{2} \mid U_\alpha\bar{N}-D_\alpha\bar{E}\rangle$	3	(1,0)	$2Y$	$1/4\begin{bmatrix}\lambda_{a+} & 0\\ 0 & -\lambda_{a+}\end{bmatrix}$
P_3^{-1},ρ_3^{-1}	$\mid D_\alpha\bar{N}\rangle$	3	(1,−1)	$2Y-1$	$1/\sqrt{8}\begin{bmatrix}0 & 0\\ \lambda_{a+} & 0\end{bmatrix}$
$\bar{P}_3^{-1},\bar{\rho}_3^{-1}$	$\mid N\bar{D}_\alpha\rangle$	3	(1,1)	$1-2Y$	$1/\sqrt{8}\begin{bmatrix}0 & \lambda_{a-}\\ 0 & 0\end{bmatrix}$
$\bar{P}_3^0,\bar{\rho}_3^0$	$(1/\sqrt{2}) \mid N\bar{U}_\alpha-E\bar{D}_\alpha\rangle$	3	(1,0)	$-2Y$	$1/4\begin{bmatrix}\lambda_{a-} & 0\\ 0 & -\lambda_{a-}\end{bmatrix}$
$\bar{P}_3^1,\bar{\rho}_3^1$	$\mid E\bar{U}_\alpha\rangle$	3	(1,−1)	$-1-2Y$	$1/\sqrt{8}\begin{bmatrix}0 & 0\\ \lambda_{a-} & 0\end{bmatrix}$
P_3',ρ_3'	$(1/\sqrt{2}) \mid U_\alpha\bar{N}+D_\alpha\bar{E}\rangle$	3	(0,0)	$2Y$	$1/4\begin{bmatrix}\lambda_{a+} & 0\\ 0 & \lambda_{a+}\end{bmatrix}$
$\bar{P}_3',\bar{\rho}_3'$	$(1/\sqrt{2}) \mid N\bar{U}_\alpha+E\bar{D}_\alpha\rangle$	3	(0,0)	$-2Y$	$1/4\begin{bmatrix}\lambda_{a-} & 0\\ 0 & \lambda_{a-}\end{bmatrix}$
P_8^+,ρ_8^+	$(\lambda_a/\sqrt{2})_{\alpha\beta} \mid U_\alpha\bar{D}_\beta\rangle$	8	(1,1)	1	$1/2\begin{bmatrix}0 & \lambda_a\\ 0 & 0\end{bmatrix}$
P_8^0,ρ_8^0	$(\lambda_a/2)_{\alpha\beta} \mid U_\alpha\bar{U}_\beta-D_\alpha\bar{D}_\beta\rangle$	8	(1,0)	0	$1/\sqrt{8}\begin{bmatrix}\lambda_a & 0\\ 0 & -\lambda_a\end{bmatrix}$
P_8^-,ρ_8^-	$(\lambda_a/\sqrt{2})_{\alpha\beta} \mid D_\beta\bar{U}_\alpha\rangle$	8	(1,−1)	−1	$1/2\begin{bmatrix}0 & 0\\ \lambda_a & 0\end{bmatrix}$
$P_8^{0'}=\eta_T,\rho_8^{0'}$	$(\lambda_a/2)_{\alpha\beta} \mid U_\alpha\bar{U}_\beta+D_\alpha\bar{D}_\beta\rangle$	8	(0,0)	0	$1/\sqrt{8}\begin{bmatrix}\lambda_a & 0\\ 0 & \lambda_a\end{bmatrix}$

occur in all nonminimal technicolor models. The Farhi-Susskind model contains in addition 24 color-triplet $Q\bar{L}$ and $\bar{Q}L$ bound states designated P_3 (sometimes called leptoquarks), and 32 color-octet $Q\bar{Q}$ bound states P_8^+, P_8^0, P_8^-, and $P_8^{0\prime}$ (also known as η_T). All of these are classified in Table II according to their quantum numbers in the natural SU(4)⊗SU(2) decomposition of SU(8). Here SU(4) is the Q-L symmetry group of which $SU(3)_c$ is a subgroup. The SU(2) refers to the total weak-isospin group which reflects the family symmetries among U and D on the one hand and N and E on the other. The pseudoscalar decay constant for these states is

$$F_\pi=(G_F n_f/\sqrt{2})^{-1/2}\approx 124\ \text{GeV}\ . \tag{6.38}$$

The color-singlet technipions are the closest analogs in this model to the charged and neutral Higgs bosons in nonminimal electroweak models with elementary scalars. The P^+ and P^- acquire mass from both electroweak and extended technicolor interactions, while the P^0 and $P^{0\prime}$ masses arise from ETC alone. These masses have been estimated as (Eichten and Lane, 1980)

$$\begin{aligned} &8\ \text{GeV}/c^2<M(P^\pm)<40\ \text{GeV}/c^2\ , \\ &2\ \text{GeV}/c^2<M(P^0,P^{0\prime})<40\ \text{GeV}/c^2\ ; \end{aligned} \tag{6.39}$$

the estimates are fairly independent of detailed assumptions. It is worth noting that the upper end of the range, namely, 40 GeV/c^2, is considerably higher than the value of 14 GeV/c^2 sometimes quoted in the literature (Barbiellini *et al.*, 1981). The lower value is the basis for experimental claims (Althoff *et al.*, 1983) that technicolor has been ruled out, a verdict we regard as premature.

The color-triplet and color-octet technipions also receive electroweak and ETC contributions to their masses, but these are much smaller than the expected QCD contribution (Peskin, 1980; Preskill, 1981),

$$\begin{aligned} M(P_3)&=160\ \text{GeV}/c^2\left[\frac{4}{N}\frac{n_f}{8}\right]^{1/2}, \\ M(P_3)&=240\ \text{GeV}/c^2\left[\frac{4}{N}\frac{n_f}{8}\right]^{1/2}. \end{aligned} \tag{6.40}$$

These estimates are of course specific to the color-SU(3) representations, to the $SU(N)_{TC}$ group, and to the flavor group (6.37).

If the weak hypercharge parameter Y [cf. Eq. (6.36)] satisfies

$$2Y=\tfrac{2}{3}+\text{integer}\ , \tag{6.41}$$

as it will for the canonical choice $Y=\frac{1}{3}$, then the color-triplet technipions will decay as

$$P_3\rightarrow\begin{cases} q\bar{l}+\cdots \\ \text{or} \\ q\bar{q}+\cdots\ . \end{cases} \tag{6.42}$$

If the condition (6.41) is not met, the lightest P_3's will be absolutely stable.

In this model there are also 64 massive technivector mesons, also listed in Table II. The 63 which lie in the adjoint representation of $SU(8)_V$ are called technirhos. They have the same $SU(3)_c$ quantum numbers as the technipions, and have a common mass given up to QCD corrections by (6.17) with F_π given by (6.38),

$$M(\rho_T)\approx 885\ \text{GeV}/c^2\left[\frac{4}{N}\right]^{1/2}\left[\frac{8}{n_f}\right]^{1/2}. \tag{6.43}$$

The decay modes and branching ratios of the neutral technirhos are listed in Table III, where the partial decay rates are estimated as (Dimopoulos, 1980; Peskin, 1980; Preskill, 1981; Dimopoulos, Raby, and Kane, 1981; Ellis, Gaillard, Nanopoulos, and Sikivie, 1981)

$$\Gamma(\rho_c\rightarrow P_A P_B)=\frac{g_{\rho_T}^2}{6\pi}\{2\,\text{Tr}([t_A,t_B]t_c)\}^2\frac{p^3}{M(\rho_T)^2}\ , \tag{6.44}$$

where g_{ρ_T} is related to the $\rho\rightarrow\pi\pi$ coupling constant g_ρ ($g_\rho^2/4\pi=2.98$) by

$$g_{\rho_T}^2=g_\rho^2(3/N)\ , \tag{6.45}$$

p is the momentum of the technipions in the ρ_T rest frame, and the t_A are the SU(8) generators given in Table II.

Like the ρ_T of the minimal model, the ρ_2 of the Farhi-Susskind model decays into $\pi_T\pi_T$ (W_0W_0 or W_0Z_0) pairs, and will give rise to an enhancement in the cross section for pair production of gauge bosons. Because ρ_2 is only half the mass of the ρ_T of the minimal model, the expected event rate is larger than that discussed in Sec. VI.B. However, the greater width of ρ_2 and the small branching ratio for the W^+W^- decay reduce the effect in the neutral channel to an enhancement of 20—25%. We therefore illustrate in Fig. 180 the more prominent enhancement in the $W^\pm Z^0$ channel, which will be somewhat easier to observe than the corresponding effect in the minimal model.

Of more interest in the context of the Farhi-Susskind model is the role of the technirhos in producing other technipion species. The most important technirho for this purpose is $\rho_8^{0\prime}$, which has the quantum numbers of the gluon, and so can enhance technipion production through technivector meson dominance. We shall address this possibility below.

The sixty-fourth technivector meson, ω_T, is a singlet under flavor SU(8), and so decays only into three technipions. It does not couple to the photon or Z^0 or to two gluons, and therefore does not significantly enhance the already rather small production of three technipions. We shall not discuss it further.

The interactions of technipions with the $SU(3)_c\otimes SU(2)_L\otimes U(1)_Y$ gauge bosons occur dynamically through technifermion loops. At subenergies well below the characteristic technicolor scale, the technipions may be regarded as pointlike. Their couplings to gauge bosons

TABLE III. Decay modes, branching ratios, and widths of neutral technirho mesons in the Farhi-Susskind model. Partial widths are computed from Eq. (6.44), with $M(\rho_T)=885$ GeV/c^2, $M(P_3)=160$ GeV/c^2, $M(P_8)=240$ GeV/c^2. For each decay $\rho_A \to P_B P_C$, the top number is the weight $\{2\,\mathrm{Tr}([t_B,t_C]t_A)\}^2$ and the second is the branching fraction.

Decay mode	Technirho $\rho_8^{0\prime}$	ρ_8^0	$\rho^{0\prime}$	ρ_1^0	ρ_2^0
$P_8^+P_8^-$	$\frac{3}{2}$	$\frac{5}{6}$		$\frac{2}{3}$	2
	0.34	0.18		0.12	0.41
$P_8^0P_8^0+P_8^{0\prime}P_8^{0\prime}$	$\frac{3}{2}$				
	0.34				
$P_3^1\bar{P}_3^1+P_3^{-1}\bar{P}_3^{-1}$	$\frac{1}{2}$	$\frac{1}{2}$	2	$\frac{1}{2}$	$\frac{3}{2}$
	0.16	0.15	0.50	0.13	0.42
$P_3^0\bar{P}_3^0+P_3'\bar{P}_3'$	$\frac{1}{2}$		2		
	0.16		0.50		
$P_8^0P_8^{0\prime}$		$\frac{3}{2}$			
		0.33			
$P_3^0\bar{P}_3'+P_3'\bar{P}_3^0$		$\frac{1}{2}$		2	
		0.15		0.50	
$P_8^+P^-+P_8^-P^+$		$\frac{1}{6}$			
		0.05			
$P_8^+\pi_T^-+P_8^-\pi_T^+$		$\frac{1}{2}$			
		0.14			
P^+P^-				$\frac{1}{3}$	$\frac{1}{4}$
				0.10	0.09
$P^+\pi_T^-+P^-\pi_T^+$				$\frac{1}{2}$	
				0.15	
$\pi_T^+\pi_T^-$					$\frac{1}{4}$
					0.08
Total width (GeV)	440	460	550	550	490

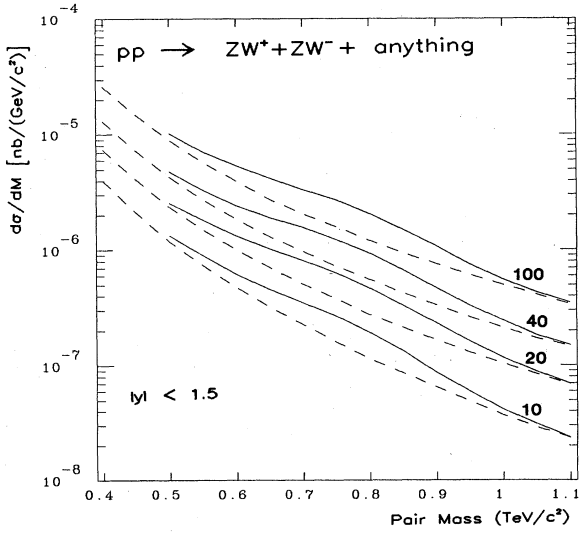

FIG. 180. Mass spectrum of $W^{\pm}Z^0$ pairs produced in pp collisions, according to the Farhi-Susskind model. The parton distributions of Set 2 have been used. Both $W^{\pm}$ and Z^0 must satisfy $|y|<1.5$. The cross sections are shown with (solid lines) and without (dashed lines) the ρ_2^0 enhancement.

may therefore be calculated reliably, using well-known techniques of current algebra or effective Lagrangian methods (Chadha and Peskin, 1981a,1981b). At higher subenergies (≥ 1 TeV), we shall improve this pointlike approximation by using technirho dominance.

The production of a single-technipion P is governed by its coupling to a pair of gauge bosons, B_1 and B_2. This coupling arises from a triangle (anomaly) graph analogous to the one responsible for the decay $\pi^0 \to \gamma\gamma$. The amplitude for the PB_1B_2 coupling is (Dimopoulos, 1980; Dimopoulos, Raby, and Kane, 1981; Ellis *et al.*, 1981)

$$\mathscr{A}_{PB_1B_2}=\frac{S_{PB_1B_2}}{8\pi^2\sqrt{2}F_\pi}\varepsilon_{\mu\nu\lambda\rho}\varepsilon_1^\mu\varepsilon_2^\nu p_1^\lambda p_2^\rho\ , \tag{6.46}$$

where the triangle anomaly factor is

$$S_{PB_1B_2}=\frac{g_1g_2}{2}\,\mathrm{Tr}(Q_P\{Q_1,Q_2\})\ . \tag{6.47}$$

Here g_1 and g_2 are the gauge coupling constants, Q_1 and Q_2 are the gauge charges, or generators, corresponding to the gauge bosons, and Q_P is the chiral SU(8) generator of the technipion given in Table II. The contributions from different gauge boson helicity states are summed separate-

ly in the trace. These results lead to the following approximate decay rates valid when the product masses are negligible:

$$\Gamma(B_1\to PB_2)=\frac{M(B_1)^3}{96\pi}\left[\frac{S_{PB_1B_2}}{8\pi^2\sqrt{2}F_\pi}\right]^2, \tag{6.48}$$

$$\Gamma(P\to B_1B_2)=(1+\delta_{B_1B_2})\frac{M(P)^3}{32\pi}\left[\frac{S_{PB_1B_2}}{8\pi^2\sqrt{2}F_\pi}\right]^2. \tag{6.49}$$

The PB_1B_2 channel is of experimental interest only for neutral technipions, because the charged technipions are more easily produced in pairs. Therefore, we list in Table IV only the anomaly factors for neutrals. Models other than the Farhi-Susskind model yield similar results.

One may infer from Table IV and Eq. (6.48) that the rates for the processes (Bjorken, 1976; Glashow, Nanopoulos, and Yildiz, 1978)

$$\begin{aligned} &Z^0\to Z^0\ (P^0 \text{ or } P^{0\prime}),\\ &W^\pm\to W^\pm\ (P^0 \text{ or } P^{0\prime}), \end{aligned} \tag{6.50}$$

involving a virtual Z^0 or $W^\pm$ are 4 or 5 orders of magnitude smaller than the corresponding standard-model rates for the decays

$$\begin{aligned} &Z^0\to Z^0H,\\ &W^\pm\to W^\pm H. \end{aligned} \tag{6.51}$$

Consequently if a neutral Higgs-type scalar is found at the levels discussed in Sec. IV.E, the technicolor scenario would seem to be ruled out.

More interesting from the experimental point of view are the couplings of a single gauge boson to a pair of technipions. These provide access to nearly all the technipions, with cross sections that are generally quite large. The BPP' couplings may be read off from an $SU(3)_c\otimes SU(2)_L\otimes U(1)_Y$-invariant effective Lagrangian for the technipions (Peskin, 1980; Preskill, 1981; Lane, 1982). The results for the Farhi-Susskind model are given in Table V.

A parenthetical note of caution about model dependence is in order here. In models more general than this one, mixing usually occurs among technipions with the same color and electric charge. Such mixing can occur even in the Farhi-Susskind model between P^0 and $P^{0\prime}$ and P_8^0 and $P_8^{0\prime}$. The only entry in Table V that would be affected is that involving $W^\pm$. The modification takes the form of model-dependent factors from the unitary matrices that diagonalize the technipion mass matrices. The cross section summed over all channels with the same color and charge should therefore still be given reliably by the couplings tabulated.

The extended technicolor interaction couples technifermions to quarks and leptons, and so governs the decays of technipions into ordinary matter. For light color-singlet technipions, these are the dominant decay modes. If, like Higgs bosons, these couple to mass, the decays occur at a rate of approximately

$$\Gamma(P\to f_i\bar{f}_j)\approx\frac{G_Fp(M_i^2+M_j^2)}{16\pi}C_{ij}, \tag{6.52}$$

where G_F is the Fermi constant, p is the momentum of the products in the technipion rest frame, and C_{ij} is a color factor which is equal to 3 for the decay of a color singlet into quarks and 1 otherwise. The only possible exception to the dominance of $f\bar{f}$ modes is the decay of $P^{0\prime}$ into two gluons, for which the partial width is

$$\begin{aligned}\Gamma(P^{0\prime}\to gg)&\approx\frac{\alpha_s^2}{6\pi^3}\frac{M(P^{0\prime})^3}{F_\pi^2}\left[\frac{N}{4}\right]^2\\&\approx 14\text{ eV}\left[\frac{N}{4}\right]^2\left[\frac{M(P^{0\prime})}{1\text{ GeV}/c^2}\right]^3,\end{aligned} \tag{6.53}$$

TABLE IV. Anomaly factors $S_{PB_1B_2}$ in the Farhi-Susskind model as defined in Eq. (6.47).

Vertex PB_1B_2	$S_{PB_1B_2}$
$P^0\gamma\gamma$	$e^2(4N)/\sqrt{6}$
$P^0Z^0Z^0$	$-e^2(2N/\sqrt{6})(2x_W-1)^2/(1-x_W)$
$P^0Z^0\gamma^0$	$e^2(N/\sqrt{6})(1-4x_W)/[x_W(1-x_W)]^{1/2}$
$P^0W^+W^-$	0
$P^{0\prime}g_ag_b$	$g_s^2(N/\sqrt{6})\delta_{ab}$
$P^{0\prime}\gamma\gamma$	$-e^2(4N/3\sqrt{6})$
$P^{0\prime}Z^0\gamma$	$e^2(4N/3\sqrt{6})[x_W/(1-x_W)]^{1/2}$
$P^{0\prime}Z^0Z^0$	$-e^2(4N/3\sqrt{6})x_W/(1-x_W)$
$P^{0\prime}W^+W^-$	0
$P_{8a}^0\gamma g_b$	$eg_sN\delta_{ab}$
$P_{8a}^0Z^0g_b$	$-eg_s(N/2)\delta_{ab}(2x_W-1)/[x_W(1-x_W)]^{1/2}$
$P_8^{0\prime}g_bg_c$	$g_s^2Nd_{abc}$
$P_{8a}^{0\prime}\gamma g_b$	$eg_s(N/3)\delta_{ab}$
$P_{8a}^{0\prime}Z^0g_b$	$-eg_s(N/3)\delta_{ab}[x_W/(1-x_W)]^{1/2}$

TABLE V. Amplitudes for the coupling of gauge bosons to pairs of technipions. Three-point amplitudes are given by the factors tabulated times $(p_1-p_2)\cdot\varepsilon$, where the p_i are technipion momenta and ε is the polarization vector of the gauge boson. Four-point amplitudes involving two gluons are given by $\varepsilon\cdot\varepsilon'$ times the tabulated factors. The 3×3 Gell-Mann matrices λ_c are the generators of SU(3); the f_{abc} are the antisymmetric structure constants. The hypercharge parameter Y is given in (6.36).

	Gauge bosons				
Technipions	$\gamma(e)$	$Z^0\{e/2[x_W(1-x_W)]^{1/2}\}$	$W^{\pm}(e/2\sqrt{x_w})$	$g_c(g_s)$	$g_c g_d(g_s^2)$
P^+P^-	1	$-(2x_W-1)$	0	0	0
$P^+_{8a}P^-_{8b}$	δ_{ab}	$-(2x_W-1)\delta_{ab}$	0	f_{abc}	$2(f_{ace}f_{bde}+f_{ade}f_{bce})$
$P^0_{8a}P^0_{8b}$	0	0	0	$(1/2)f_{abc}$	$(f_{ace}f_{bde}+f_{ade}f_{bce})$
$P^{0'}_{8a}P^{0'}_{8b}$	0	0	0	$(1/2)f_{abc}$	$(f_{ace}f_{bde}+f_{ade}f_{bce})$
$P'_{3\alpha}\bar{P}'_{3\beta}$	$2Y\delta_{\alpha\beta}$	$-4Yx_W\delta_{\alpha\beta}$	0	$i(\lambda_c/2)_{\alpha\beta}$	
$P^1_{3\alpha}\bar{P}^1_{3\beta}$	$(2Y+1)\delta_{\alpha\beta}$	$[1-2(2Y+1)x_W]\delta_{\alpha\beta}$	0	$i(\lambda_c/2)_{\alpha\beta}$	$(\frac{1}{4})\{\lambda_c,\lambda_d\}_{\alpha\beta}$
$P^0_{3\alpha}\bar{P}^0_{3\beta}$	$2Y\delta_{\alpha\beta}$	$-4Yx_W\delta_{\alpha\beta}$	0	$i(\lambda_c/2)_{\alpha\beta}$	
$P^{-1}_{3\alpha}\bar{P}^{-1}_{3\beta}$	$(2Y-1)\delta_{\alpha\beta}$	$-[1+2(4Y-1)x_W]\delta_{\alpha\beta}$	0	$i(\lambda_c/2)_{\alpha\beta}$	
$P^{\pm}P_0$	0	0	1	0	0

where the numerical estimate applies for $\alpha_s=0.2$. This becomes comparable to the rate for $P^{0\prime}\to b\bar{b}$ for $M(P^{0\prime})\approx 40\ \mathrm{GeV}/c^2$.

It is also expected that heavy colored technipions decay predominantly to fermion pairs. The principal exception to this rule would be the decay of $P_8^{0\prime}$ into two gluons, for which the partial width is

$$\Gamma(P_8^{0\prime}\to gg)\approx\frac{5\alpha_s^2}{24\pi^3}\frac{M(P_8^{0\prime})^3}{F_\pi^2}\left[\frac{N}{4}\right]^2. \tag{6.54}$$

Because of the anticipated dominance of $f\bar{f}$ decay modes, it is of great importance to know what the extended technicolor interactions are. It is just in this regard that the existing models, including that of Farhi and Susskind, cannot be relied upon (Lane, 1982).

One statement that is known to be generally true about technipion couplings to light fermions is that they are parity violating (Eichten and Lane, 1980), and probably CP violating as well (Eichten, Lane, and Preskill, 1980). This fact may lead to many interesting investigations if technipions are ever found. We put aside such questions and focus on the initial search. According to the conventional wisdom, which is inspired by analogy with the minimal electroweak model, the technipions couple essentially to fermion mass. Bearing in mind that this tendency to couple to mass can be evaded even in the case that there are two or more elementary Higgs doublets, we list in Table VI the expected major decay modes of technipions. In the interest of brevity, we shall base most of our discussion of signals on this most obvious possibility.

D. Single production of technipions

The production of single technipions is in many respects analogous to the production of Higgs bosons treated in Secs. IV.D and IV.E. It may proceed by two-gluon fusion or by quark-antiquark fusion. The most important process is the production of the neutral technipions $P^{0\prime}$ and $P_8^{0\prime}$ in gluon-gluon fusion, which leads to equal cross sections in $p^{\pm}p$ collisions. Ignoring any mixing with P^0 and P_8^0, we may write the differential cross sections as [compare (4.86)]

TABLE VI. Principal decay modes of technipions if Pf_1f_2 couplings are proportional to fermion mass.

Technipion	Principal decay modes
P^+	$t\bar{b},c\bar{b},c\bar{s},\tau^+\bar{\nu}_\tau$
P^0	$b\bar{b},c\bar{c},\tau^+\tau^-$
$P^{0\prime}$	$b\bar{b},c\bar{c},\tau^+\tau^-;gg$
P_3,P_3'	$t\tau^+,t\bar{\nu}_\tau,b\tau^+,\ldots$
(if unstable)	or $\bar{t}\,t,\bar{t}\,b,\ldots$
P_8^+	$(t\bar{b})_8$
P_8^0	$(t\bar{t})_8$
$P_8^{0\prime}$	$(t\bar{t})_8;gg$

$$\frac{d\sigma}{dy}(ab\to P'+\text{anything})=\frac{\pi^2\Gamma(P'\to gg)}{8M^3}\tau f_g^{(a)}(x_a,M^2)\times f_g^{(b)}(x_b,M^2)\ , \tag{6.55}$$

where we have abbreviated $M(P')$ as M and as usual

$$x_a=\sqrt{\tau}e^{y}\qquad x_b=\sqrt{\tau}e^{-y}\ , \tag{6.56}$$

with

$$\tau=M^2/s\ . \tag{6.57}$$

The partial widths $\Gamma(P'\to gg)$ are given in (6.53) and (6.54).

The differential cross section for $P^{0\prime}$ production at $y=0$ is shown as a function of the technipion mass in Fig. 181. According to (6.52) and (6.53), the principal decays will be into

$$P^{0\prime}\to\begin{cases}gg\\ b\bar{b}\\ \tau^+\tau^-\ ,\end{cases} \tag{6.58}$$

with branching ratios indicated in Fig. 182. Comparing with the two-jet mass spectra shown in Figs. 90—94, we see that there is no hope of finding $P^{0\prime}$ as a narrow peak in the two-jet invariant mass distribution. The background from $b\bar{b}$ pairs, estimated using (5.17) and (5.18), is shown in Fig. 183. It is 3 orders of magnitude larger than the anticipated signal. The background to the $\tau^+\tau^-$ mode is the Drell-Yan process, for which the appropriate cross sections have been given in Figs. 108 and 109. Even when the small ($\sim 2\%$) branching ratio into τ pairs is taken into account, the signal is approximately equal to or an order of magnitude larger than the background. The signal-to-background ratio is crucially dependent upon the experimental resolution in the invariant mass of the pair. It seems questionable that taus can be identified with high efficiency and measured with sufficient precision to make this a useful signal.

The differential cross section for color-octet ($P_8^{0\prime}$) technipion production at $y=0$ is shown as a function of the

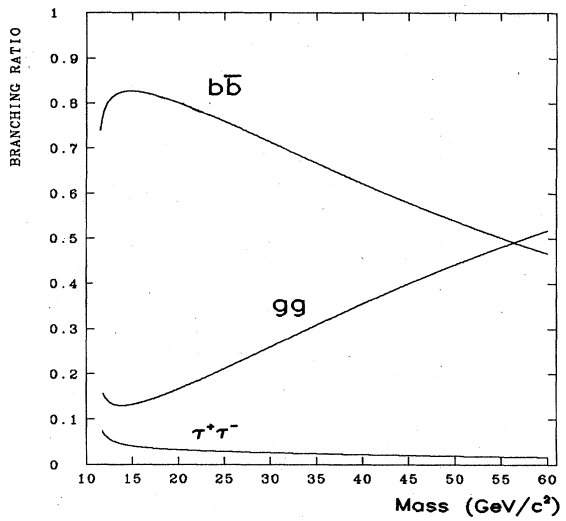

FIG. 182. Approximate branching ratios for $P^{0\prime}$ decay. In Eq. (6.53) we choose $N=4$ and use the running coupling $\alpha_s(M_P^2)$.

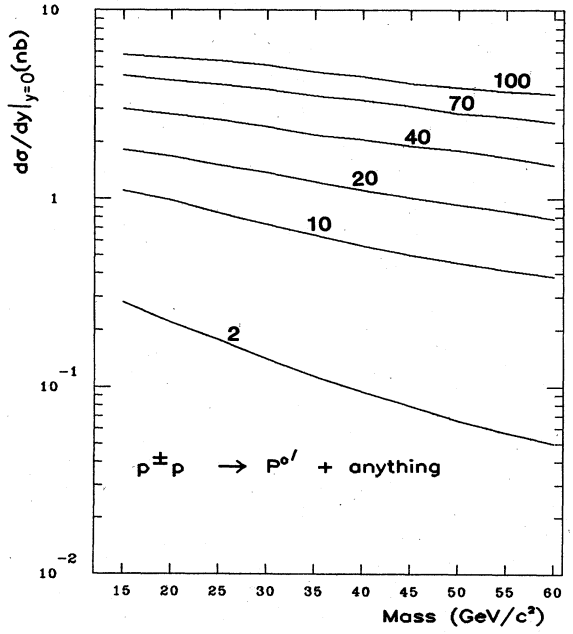

FIG. 181. Differential cross section for production of the color-singlet technipion $P^{0\prime}$ at $y=0$ in pp or $\bar{p}p$ collisions, according to the parton distributions of Set 2.

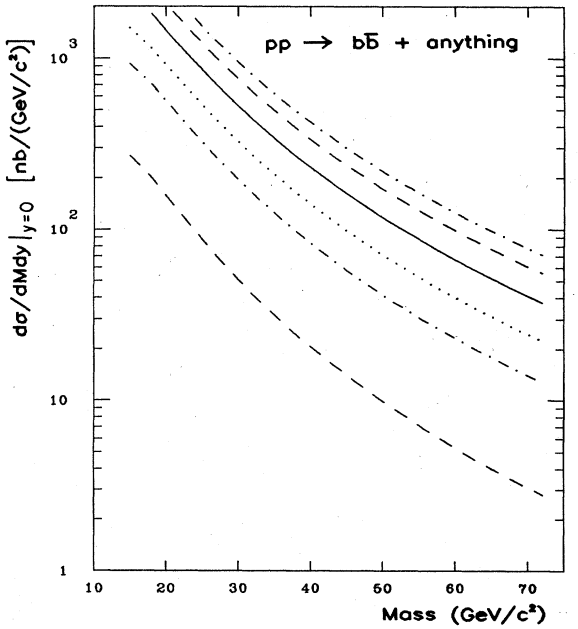

FIG. 183. Cross section $d\sigma/d\mathcal{M}\,dy\,|_{y=0}$ for the production of $b\bar{b}$ pairs in pp collisions, according to the parton distributions of Set 2. $\sqrt{s}=2$, 10, 20, 40, 70, and 100 TeV.

technipion mass in Fig. 184. The dominant decay modes will be

$$P_8^{0\prime} \to \begin{cases} gg \\ t\bar{t} \end{cases} . \tag{6.59}$$

The expected branching ratios depend upon the top quark mass. Representative estimates are shown in Fig. 185. The background expected from $t\bar{t}$ production by conventional mechanisms is plotted in Fig. 158, for a top quark mass of 30 GeV/c^2. When the branching ratios are taken into account, the signal and background are roughly comparable, and the expected number of events is quite large at supercollider energies. The signal-to-background ratio improves somewhat with increasing $P_8^{0\prime}$ mass. The main issues for detection are the identification of t quarks and the resolution in invariant mass of the reconstructed pairs. This is an appropriate topic for Monte Carlo studies.

In the two-gluon channel, the signal will be comparable to the $t\bar{t}$ signal or (for large $P_8^{0\prime}$ masses) somewhat larger. The expected background, which may be judged from Figs. 90–94, is very large compared to the signal except at the highest $P_8^{0\prime}$ masses considered.

To sum up, the neutral technipions $P^{0\prime}$ and $P_8^{0\prime}$ will be produced copiously in high-luminosity multi-TeV colliders. However, within the conventional scenario for their decays, detection requires the ability to identify and measure top quarks and tau leptons with high efficiency and high precision. Extraction of a convincing signal will mightily test experimental technique.

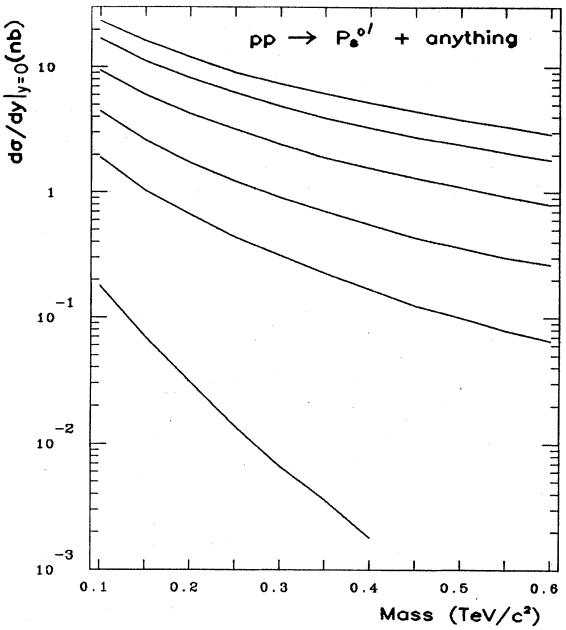

FIG. 184. Differential cross section for production of the color-octet technipion $P_8^{0\prime}$ at $y=0$ in pp or $\bar{p}p$ collisions, according to the parton distributions of Set 2. The expected mass, according to (6.40), is approximately 240 GeV/c^2.

E. Pair production of technipions

We now discuss the production of pairs of color-singlet technipions through the chains

$$\begin{array}{l} p^{\pm}p \to W^{\pm} + \text{anything} \\ \qquad\quad \hookrightarrow P^{\pm}P^0 \end{array} \tag{6.60}$$

and

$$\begin{array}{l} p^{\pm}p \to Z^0 + \text{anything} \\ \qquad\quad \hookrightarrow P^+P^- , \end{array} \tag{6.61}$$

as well as the production of pairs of color-triplet or color-octet technipions in gg and $q\bar{q}$ collisions.

According to the mass estimates (6.39), both charged and neutral color-singlet technipions are expected to be lighter than 40 GeV/c^2. Consequently, both species should be produced in intermediate boson decays (Lane, 1982,1984). From the couplings given in Table V, we may estimate the branching ratios in the Farhi-Susskind model to be

$$\frac{\Gamma(W^{\pm}\to P^{\pm}P^0)}{\Gamma(W^{\pm}\to \text{all})} = \frac{\alpha M_W \left[1-\dfrac{(M_0+M_{\pm})^2}{M_W^2}\right]^{3/2}\left[1-\dfrac{(M_0-M_{\pm})^2}{M_W^2}\right]^{3/2}}{48 x_W \Gamma(W^{\pm}\to \text{all})}$$

$$\approx 0.02\left[1-\frac{(M_0+M_{\pm})^2}{M_W^2}\right]^{3/2}\left[1-\frac{(M_0-M_{\pm})^2}{M_W^2}\right]^{3/2} \tag{6.62}$$

and

$$\frac{\Gamma(Z^0\to P^+P^-)}{\Gamma(Z^0\to \text{all})} = \frac{\alpha M_Z (1-2x_W)^2\left[1-\dfrac{4M_{\pm}^2}{M_Z^2}\right]^{3/2}}{48 x_W (1-x_W)\Gamma(Z^0\to \text{all})}$$

$$\approx 0.01\left[1-\frac{4M_{\pm}^2}{M_Z^2}\right]^{3/2} , \tag{6.63}$$

where $x_W = \sin^2\theta_W$. The estimate (6.63) for the technipion branching ratio of Z^0 is model independent. The estimate (6.62) for the W branching ratio may be modified by mixing angles in more complicated models. The very large samples of intermediate bosons anticipated in high-energy pp and $\bar{p}p$ collisions (compare Figs. 110–112 and 114–116) may make possible the study of these rare decays. The prospects have been considered by Kagan

(1982) and Lane (1982).

The elementary processes for pair-production of colored technipions are depicted in Fig. 186. The differential cross sections for neutral channels are

$$\frac{d\sigma}{d\hat{t}}(gg\to PP)=\frac{2\pi\alpha_s^2 T(R)}{\hat{s}^2}\left[\left[\frac{T(R)}{d(R)}-\frac{3}{32}\right](1-2V+2V^2)+\tfrac{3}{32}\beta^2 z^2(|X|^2-2V\,\mathrm{Re}X+2V^2)\right], \tag{6.65}$$

where $z=\cos\theta^*$ measures the c.m. scattering angle,

$$\beta^2=1-4M(P)^2/\hat{s}\,, \tag{6.66}$$

$$V=1-\frac{1-\beta^2}{1-\beta^2 z}\,, \tag{6.67}$$

and the $\rho_8^{0\prime}$ enhancement factor is

$$X=\frac{M(\rho_8^{0\prime})^2}{M(\rho_8^{0\prime})^2-\hat{s}-iM(\rho_8^{0\prime})\Gamma(\hat{s})}\,, \tag{6.68}$$

where the energy-dependent width of $\rho_8^{0\prime}$ is

$$M(\rho_8^{0\prime})\Gamma(\hat{s})=\frac{g_{\rho_T}^2\hat{s}}{48\pi}[\beta_3^3\theta(\beta_3)+3\beta_8^3\theta(\beta_8)]\,. \tag{6.69}$$

The color factors are

$$T(R)=\begin{cases}\frac{1}{2} & \text{for } P_3\\ 3 & \text{for } P_8\end{cases} \tag{6.70}$$

and

$$d(R)=\begin{cases}3 & \text{for } P_3\\ 8 & \text{for } P_8\,.\end{cases} \tag{6.71}$$

In writing (6.64) and (6.65) we have summed over all charges and colors. The individual charge states

$$P_3^1\bar{P}_3^1,\quad P_3^{-1}\bar{P}_3^{-1},\quad P_3^0\bar{P}_3^0,\quad P_3'\bar{P}_3' \tag{6.72}$$

$$\frac{d\sigma}{d\hat{t}}(q\bar{q}\to PP)=\frac{2\pi\alpha_s^2}{9\hat{s}^2}T(R)\beta^2|X|^2(1-z^2)\,, \tag{6.64}$$

and

or

$$P_8^+P_8^-,\quad P_8^0P_8^0+P_8^{0\prime}P_8^{0\prime} \tag{6.73}$$

occur with equal cross sections.

As is the case for the pair production of heavy quarks, the gluon fusion mechanism is the more important at collider energies, so that the cross sections in pp and $p\bar{p}$ collisions are nearly equal. The integrated cross section for the reaction

$$pp\to P_3\bar{P}_3+\text{anything}\,, \tag{6.74}$$

summed over the charge states (6.72), is shown as a function of $M(P_3)$ in Fig. 187 with and without the $\rho_8^{0\prime}$ enhancement. For the purposes of this calculation, we adopted the canonical value (6.43) $M(\rho_8^{0\prime})=885$ GeV/c^2 of the technirho mass and evaluated the mass-dependent technirho width, using (6.44) with $M(P_8)$ fixed at its nominal value of 240 GeV/c^2, as given by (6.40). The cross sections are substantial. The same cross sections are shown in Fig. 188 for technipions satisfying the rapidity cut $|y|<1.5$. We have also computed these cross sections using the parton distributions of Set 1; they differ by no more than 10%.

Comparing Figs. 187 and 188, we find that the degree of $\rho_8^{0\prime}$ enhancement is not much affected by the rapidity cuts. The enhancement is generally not so dramatic that measurement of the $P_3\bar{P}_3$ production rate would confirm or deny the existence of $\rho_8^{0\prime}$, much less determine its pa-

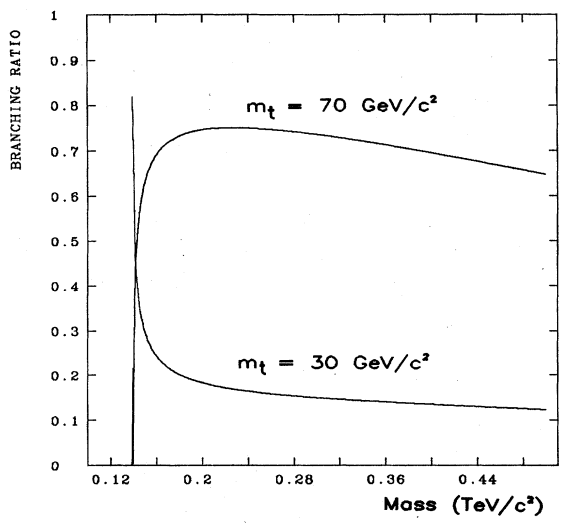

FIG. 185. Branching fractions for $P_8^{0\prime}\to t\bar{t}$. The remaining decays are into the two-gluon channel.

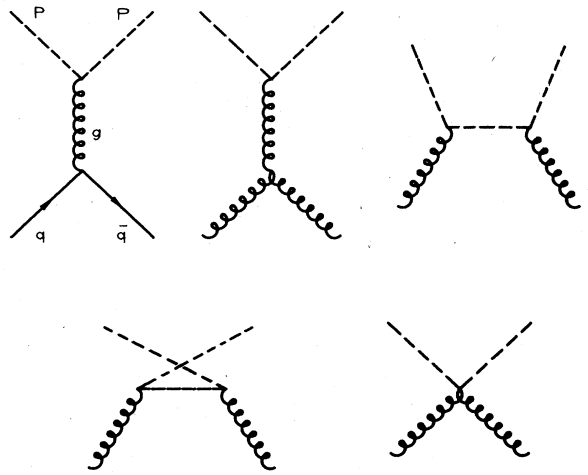

FIG. 186. Feynman graphs for the production of pairs of colored technipions. The curly lines are gluons, solid lines are quarks, and dashed lines are technipions. The graphs with s-channel gluons include the $\rho_8^{0\prime}$ enhancement.

rameters. For example, at $\sqrt{s}=40$ TeV, the $P_3\bar{P}_3$ cross section (with rapidity cuts) is enhanced by a factor of 1.3 at the canonical technipion mass, $M(P_3)=160$ GeV/c^2 (6.40), by a factor of 2 at $M(P_3)=280$ GeV/c^2, and by a factor of 1.4 at $M(P_3)=400$ GeV/c^2.

If the technipions are stable, which will be the case if (6.41) is not satisfied, the signatures should be quite striking and essentially background free. Each event will appear as a pair of extremely narrow jets consisting of the very massive P_3 core (plus a quark or antiquark to neutralize its color), together with relatively soft $q\bar{q}$ pairs and gluons.[10] The decay of unstable technipions into $q+\bar{l}+\cdots$ should also provide a characteristic signature: a jet and an isolated lepton on each side of the beam. In this case the only comparable conventional background would be from the pair production of heavy quarks, with the subsequent decay

$$Q\to qW \quad (W\to l\nu). \tag{6.75}$$

For such events one expects equal numbers of electrons, muons, and taus. In contrast, the technipion decays are expected to favor taus.

We conclude that the identification of $P_3\bar{P}_3$ pair production at supercollider energies should be possible even at quite modest luminosities ($\int \mathcal{L}\,dt \geq 10^{38}$ cm^{-2}) for technipions of the canonical mass. Reconstruction of an invariant mass peak may be quite demanding because of the difficulty of measuring the momenta of heavy quarks and leptons.

We turn next to the pair production of octet technipions. The integrated cross section for the reaction

$$pp\to P_8\bar{P}_8+\text{anything} \tag{6.76}$$

is plotted in Fig. 189 with and without the $\rho_8^{0\prime}$ enhancement. These are typically ~ 15 times the cross sections for color-triplet technipion production, because of the larger color factors in (6.65), and comparable to the cross sections for single-$P_8^{0\prime}$ production. The effect of the restriction $|y|<1.5$ on the technipion rapidities is illustrated in Fig. 190. In this case, we have computed the mass-dependent $\rho_8^{0\prime}$ width, using (6.44) with $M(P_3)$ fixed at its nominal value (6.40) of 160 GeV/c^2. The technirho enhancement is less effective in the octet technipion channel because of the large color factor in the first term in (6.65).

The expected decays of octet technipions are

$$P_8^+\to t\bar{b}\,, \qquad P_8^0\to t\bar{t}\,, \tag{6.77}$$

and

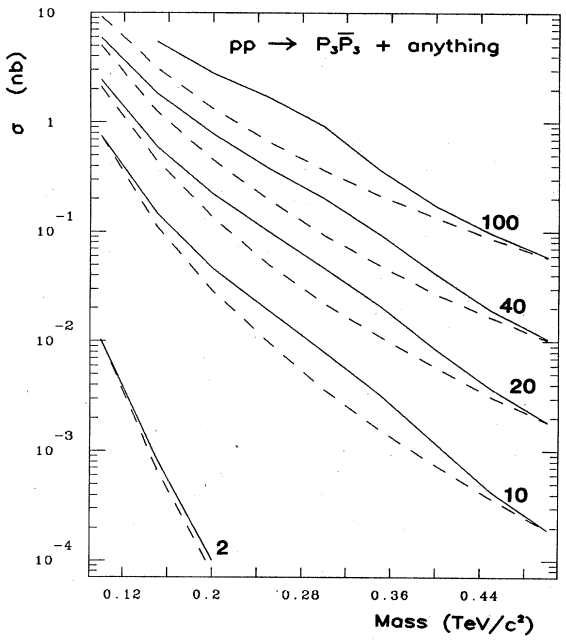

FIG. 187. Integrated cross section for the production of $P_3\bar{P}_3$ pairs in pp collisions, according to the parton distributions of Set 2. All charge states are summed. The cross sections are shown with (solid lines) and without (dashed lines) the technirho ($\rho_8^{0\prime}$) enhancement of Eq. (6.68). The technirho parameters are given in the text. The canonical value of the technipion mass is $M(P_3)=160$ GeV/c^2.

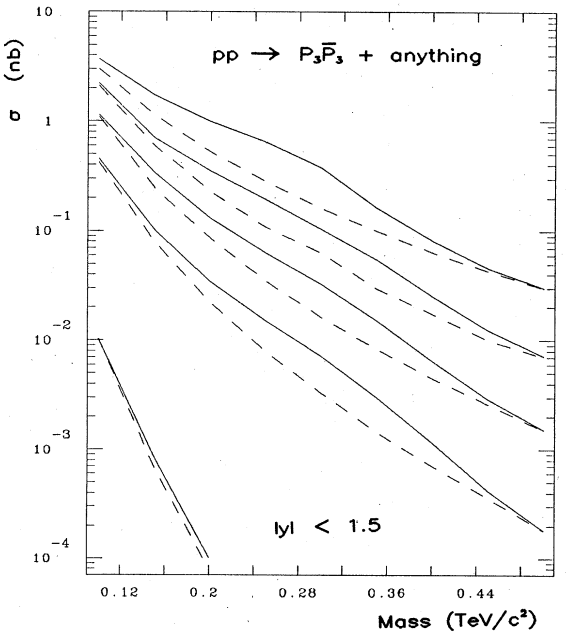

FIG. 188. Cross section for the production of $P_3\bar{P}_3$ pairs in pp collisions. Rapidities of the technipions must satisfy $|y|<1.5$. The cross sections are shown with (solid lines) and without (dashed lines) the $\rho_8^{0\prime}$ enhancement of Eq. (6.68). Parameters are as in Fig. 187.

[10]Time-of-flight methods for heavy-particle detection have been explored by Baltay *et al.* (1982).

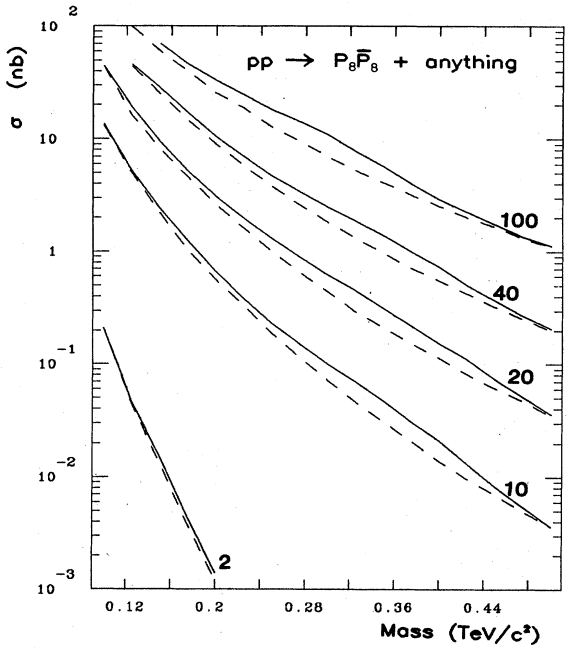

FIG. 189. Integrated cross section for the production of $P_8\bar{P}_8$ pairs in pp collisions, according to the parton distributions of Set 2. Both charge states are summed. The cross sections are shown with (solid lines) and without (dashed lines) the technirho ($\rho_8^{0\prime}$) enhancement of Eq. (6.68). The technirho parameters are given in the text. The canonical value of the technipion mass is $M(P_8)=240$ GeV/c^2.

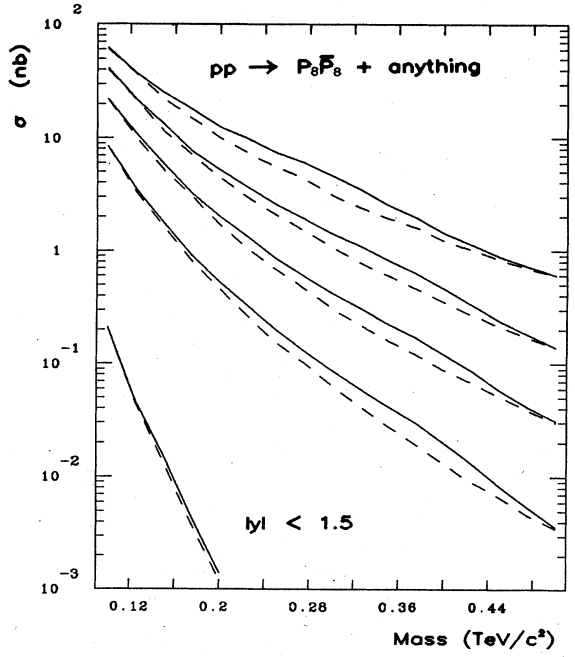

FIG. 190. Cross section for the production of $P_8\bar{P}_8$ pairs in pp collisions. Rapidities of the technipions must satisfy $y<1.5$. The cross sections are shown with (solid lines) and without (dashed lines) the $\rho_8^{0\prime}$ enhancement of Eq. (6.68). Parameters are as in Fig. 189.

$$P_8^{0\prime}\rightarrow\begin{cases}t\bar{t}\\ gg\end{cases}, \tag{6.59}$$

with branching fractions given earlier in Fig. 185. The signature for the $P_8^+P_8^-$ channel is therefore $t\bar{b}$ on one side of the beam and $\bar{t}b$ on the other. If the heavy flavors can be tagged with high efficiency, we know of no significant conventional backgrounds. If it is necessary to rely on the four-jet signal, the QCD background must be considered. At present, this can neither be calculated nor reliably estimated. Similar conclusions apply for the neutral octet technipions.

The charged-octet technipion can also decay by means of the triangle anomaly mechanism [compare Eqs. (6.46) and (6.47)] into two gauge bosons,

$$P_8^+\rightarrow gW^+ . \tag{6.78}$$

The estimates (6.49) and (6.52) of the decay rate would suggest that

$$\frac{\Gamma(P_8^+\rightarrow gW^+)}{\Gamma(P_8^+\rightarrow t\bar{b})}\approx\frac{1}{5}-\frac{1}{10} . \tag{6.79}$$

The signal of a jet and an intermediate boson opposite two jets or of a jet and an intermediate boson should be rather characteristic. Again, the pair production of heavy quarks is a background to the $(gW^+)(gW^-)$ signal.

F. Summary

If the technicolor scenario correctly describes the breakdown of the electroweak gauge symmetry, there will be a number of spinless technipions, all with masses much smaller than the TC scale of about 1 TeV. We have analyzed the simple but, we believe, representative model of Farhi and Susskind (1979), in which color-singlet technipions lie between 5 and 40 GeV/c^2 and colored technipions occur between 100 and 300 GeV/c^2. Other models will have similar spectra.

The couplings of technipions to the $SU(3)_c\otimes SU(2)_L\otimes U(1)_Y$ gauge bosons are reliably known, so the production cross sections can be estimated with confidence. The technipion couplings to quarks and leptons are not known with comparable certainty. All our comments about the signals for technipion production must therefore be regarded as tentative.

For any hypothesis about technipion decay, careful Monte Carlo studies will be required to ascertain more accurately the signal and background levels. In the absence of such information, we have tried to be sensibly conservative in estimating the capabilities of multi-TeV hadron colliders to search for signs of technicolor. A rough appraisal of these capabilities is given in Table VII, where we have collected the minimum *effective* luminosities required for the observation of technihadrons. In constructing the table, we have required that for a given charge state, the enhancement consist of at least 25 events, and that the signal represent a five-standard-deviation excess over background in the rapidity interval

TABLE VII. Minimum *effective* integrated luminosities in cm^{-2} required to establish signs of technicolor in $p^{\pm}p$ colliders. To arrive at the required integrated luminosities, divide by the efficiencies ϵ_i to identify and adequately measure the products.

Channel	Collider energy: 2 TeV $\bar{p}p$	10 TeV	20 TeV	40 TeV	100 TeV
Minimal model:					
$\rho_T^0 \to W_0^+ W_0^-$			3.4×10^{39}	1×10^{39}	6×10^{38}
$\rho_T^{\pm} \to W_0^{\pm} Z^0$		10^{40}	1.6×10^{39}	6×10^{38}	2×10^{38}
Farhi-Susskind model:					
$P^{0\prime} \to \tau^+\tau^-$	5×10^{36}	8×10^{35}	3×10^{35}	2×10^{35}	10^{35}
$P_8^{0\prime} \to t\bar{t}$ (240 GeV/c^2)	2×10^{36}	7×10^{34}	3×10^{34}	10^{34}	3×10^{33}
$P_3\bar{P}_3$(160 GeV/c^2)	2×10^{38}	2×10^{36}	4×10^{35}	2×10^{35}	7×10^{34}
(400 GeV/c^2)		10^{38}	2×10^{37}	4×10^{36}	10^{36}
$P_8\bar{P}_8$(240 GeV/c^2)	10^{38}	2×10^{35}	5×10^{34}	2×10^{34}	7×10^{33}
(400 GeV/c^2)		2×10^{36}	4×10^{35}	10^{35}	3×10^{34}
$\rho_T^{\pm} \to W_0^{\pm} Z^0$		2×10^{39}	7×10^{38}	3×10^{38}	1.5×10^{38}

$-1.5 < y < 1.5$. The effective luminosities quoted must be adjusted for the finite efficiency to identify and measure the decay products. We have used the branching ratios of Fig. 182 for $P^0 \to \tau^+\tau^-$, and Fig. 185 for $P_8^0 \to t\bar{t}$, with $m_t = 30$ GeV/c^2, and have assumed that all P_3's produced in the rapidity bin are detectable. We remind the reader one last time that we have assumed the conventional wisdom for the decay modes of these particles, and that the exploitation of some of these decay modes will require advances in detector technology. With that final caveat, we conclude that a 40-TeV $p^{\pm}p$ collider with a luminosity of at least 10^{39} cm^{-2} will be able to confirm or rule out technicolor.

VII. SUPERSYMMETRY

The fermion-boson connection known as supersymmetry (Gol'fand and Likhtman, 1971; Volkov and Akulov, 1973; Wess and Zumino, 1974a,1974b,1974c; Salam and Strathdee, 1974a,1974b; Fayet and Ferrara, 1977; Wess and Bagger, 1983) is a far-reaching idea which may play a role in the resolution of the Higgs problem. It is natural to hope that supersymmetry might reduce or even eliminate the freedom surrounding fermions and scalars in existing theories by linking the fermions to the vectors and the scalars to the fermions.

We have already discussed in Secs. IV and VI the naturalness problem of the Higgs sector of the standard $SU(2)_L \otimes U(1)_Y$ electroweak theory, which has been posed most sharply by 't Hooft (1980). Technicolor provides one possible solution, with the proposal that the scalars are composite particles, with the compositeness scale a few times the electroweak scale. The consequences were elaborated in Sec. VI. Supersymmetry, in contrast, provides the only natural framework in which to formulate spontaneously broken gauge theories involving *elementary* scalars. The implications of the supersymmetry alternative for experimentation at supercollider energies will be explored in this section.

In the minimal ($N=1$) supersymmetric theory, every particle is related to a superpartner that differs by $\frac{1}{2}$ unit of spin and otherwise carries identical quantum numbers. Among the known particles there are no satisfactory candidates for pairs related by supersymmetry. Consequently we must anticipate doubling the spectrum by associating to every known particle a new superpartner. If supersymmetry were exact, each particle would be degenerate in mass with its superpartner. This is plainly not the case. For theories in which supersymmetry is broken, the mass degeneracy is lifted. The masses acquired by the superpartners are highly model dependent. However, if supersymmetry is to contribute to a resolution of the hierarchy problem (Gildener, 1976; Weinberg, 1979b), the mass splittings should not greatly exceed the electroweak scale. This suggests that the low-energy artifacts of supersymmetry, including the superpartners, should occur on a scale of ~ 1 TeV or below.

No superpartners have yet been found. However, some useful bounds on superpartner masses have been derived from studies of electron-positron annihilations, from hadronic beam-dump experiments, and from cosmological constraints. The current experimental situation has been summarized by Savoy-Navarro (1984), Dawson, Eichten, and Quigg (1984), and Haber and Kane (1984). In addition, Dawson *et al.* have presented a collection of all the relevant formulas for the production of superpartners in hadron collisions. We adopt their conventions and notation.

This section is organized as follows. In Sec. VII.A we review the expectations for the superparticle spectrum in a minimal supersymmetric theory and summarize the elementary cross sections for superpartner production. Section VII.B contains the estimated rates for the production of superpartners of quarks and gluons in high-energy $p^{\pm}p$ collisions, and a discussion of experimental signatures. A similar treatment of the supersymmetric partners of elec-

troweak gauge bosons and leptons takes up Sec. VII.C. Some general conclusions about the prospects for the observation of superpartners at supercollider energies appear in Sec. VII.D.

A. Superpartner spectrum and elementary cross sections

In this paper we shall examine the simplest ($N=1$) supersymmetric extension of the $SU(3)_c \otimes SU(2)_L \otimes U(1)_Y$ model of the strong and electroweak interactions. To every known quark or lepton we associate a new scalar superpartner to form a chiral supermultiplet. Similarly, we group a gauge fermion ("gaugino") with each of the gauge bosons of the standard model to form a vector supermultiplet. The couplings in the Lagrangian are then completely specified by the gauge symmetry and the supersymmetry algebra (Wess and Bagger, 1983).

Some theories in which supersymmetry is respected at low energies naturally possess a global U(1) variance, usually called R invariance (Fayet, 1975; Salam and Strathdee, 1975; Fayet and Ferrara, 1977). In such theories there is, in addition to the standard quantum numbers, a new fermionic quantum number R associated with the U(1) symmetry. Quantum number assignments for the conventional particles and their supersymmetric partners are given in Table VIII (from Dawson *et al.*, 1984), where $\chi=\pm 1$ is a chirality index. R invariance is undoubtedly broken by the vacuum expectation values of the Higgs scalars, which break the electroweak $SU(2)_L \otimes U(1)_Y$ symmetry and endow the $W^{\pm}$ and Z^0 with masses. The phenomenological consequences of various possibilities for residual or broken R invariance have been analyzed by Farrar and Weinberg (1983). In writing cross sections, we have assumed that no continuous R invariance remains. This is generally required to give Majorana masses to the gauginos.

We do not choose any particular model of supersymmetry breaking or make any explicit assumptions about the Higgs structure of the theory. However, in any supersymmetric theory at least two scalar doublets are required to give masses to the fermions with weak isospin of both $I_3=\pm\frac{1}{2}$. As a result, there will be charged scalars in addition to the familiar neutral Higgs boson. The signatures of the charged scalars would resemble those of the technipions $P^{\pm}$ discussed in Sec. VI. In general, mixing may occur between the gauge fermions associated with $W^{\pm}$, Z^0, and γ and supersymmetric partners of the Higgs bosons (Ellis *et al.*, 1983; Frère and Kane, 1983), so that the mass eigenstates are linear combinations of the two species. This would introduce mixing angles in the electroweak gaugino sector. In our calculations we ignore such mixing, as well as the direct production of Higgsinos. The latter approximation would seem quite justified in hadron-hadron collisions because of the small Yukawa couplings of Higgsinos to light quarks. Our discussion can easily be extended to include the appropriate mixing angles. These issues are treated more fully by Dawson *et al.* (1984). When global supersymmetry is spontaneously broken, a massless Goldstone fermion, the Goldstino, appears. Because the couplings of the Goldstino to quarks and gluons are quite small, we do not calculate cross sections for its direct production. The Goldstino will, however, appear as a possible decay product of the other superparticles. In locally supersymmetric models, the Goldstino becomes the helicity $\pm\frac{1}{2}$ com-

TABLE VIII. Supersymmetric partners of $SU(3)_c \otimes SU(2)_L \otimes U(1)_Y$ particles.

Particle		Spin	Color	Charge	R number
g	gluon	1	8	0	0
$\tilde{g}$	gluino	$\frac{1}{2}$	8	0	$\|1\|$
γ	photon	1	0	0	0
$\tilde{\gamma}$	photino	$\frac{1}{2}$	0	0	$\|1\|$
$W^{\pm},Z^0$	intermediate bosons	1	0	$\pm 1,0$	0
$\tilde{W}^{\pm},\tilde{Z}^0$	wino, zino	$\frac{1}{2}$	0	$\pm 1,0$	$\|1\|$
q	quark	$\frac{1}{2}$	3	$\frac{2}{3},-\frac{1}{3}$	0
$\tilde{q}$	squark	0	3	$\frac{2}{3},-\frac{1}{3}$	$-\chi=\pm 1$
e	electron	$\frac{1}{2}$	0	-1	0
$\tilde{e}$	selectron	0	0	-1	$-\chi=\pm 1$
ν	neutrino	$\frac{1}{2}$	0	0	0
$\tilde{\nu}$	sneutrino	0	0	0	1
Higgs bosons	$\begin{pmatrix} H^+ \\ H^0 \end{pmatrix} \begin{pmatrix} H'^0 \\ H^- \end{pmatrix}$	0	0	$\pm 1,0$	0
Higgsinos	$\begin{pmatrix} \tilde{H}^+ \\ \tilde{H}^0 \end{pmatrix} \begin{pmatrix} \tilde{H}'^0 \\ \tilde{H}^- \end{pmatrix}$	$\frac{1}{2}$	0	$\pm 1,0$	$\|1\|$

ponents of the massive, spin-$\frac{3}{2}$ gravitino (Deser and Zumino, 1976). In such models, the photino is often the lightest superpartner. For the remainder of this section, Goldstino will refer to either case.

The usual Yukawa couplings of scalars to quarks or leptons generalize in a supersymmetric theory to include Higgs-squark and Higgs-slepton couplings, as well as Higgsino-quark-squark and Higgsino-lepton-slepton transitions. Just as there is a Kobayashi-Maskawa matrix which mixes quark flavors and introduces a CP-violating phase, so, too, will there be mixing matrices in the quark-squark and squark-squark interactions. Mixing may also occur in principle in the lepton-slepton and slepton-slepton interactions. While there is no general theoretical reason for the mixing angles to be small, the requirement that a supersymmetric Glashow-Iliopoulos-Maiani (1970) mechanism operate to suppress flavor-changing neutral currents places some restrictions on squark mass splittings and on mixing angles. For an up-to-date assessment of these constraints, see Baulieu, Kaplan, and Fayet (1984). For simplicity, we will assume that there is no mixing outside the quark-quark sector. As a result, each quark (or lepton) of given chirality will couple to a single squark (or slepton) flavor. The general case is treated in Dawson *et al.* (1984).

Once we have stated the ground rules, it is straightforward to calculate the elementary cross sections for the production of superparticles in collisions of quarks and gluons. We summarize the results of Dawson *et al.* (1984).

1. Gaugino pair production

The differential cross section for the production of two gauge fermions in quark-antiquark collisions is given by

$$\begin{aligned}\frac{d\sigma}{d\hat{t}}(q\bar{q}'\to\text{gauginos})=\frac{\pi}{\hat{s}^2}\Bigg[&A_s\frac{(\hat{t}-m_1^2)(\hat{t}-m_2^2)+(\hat{u}-m_1^2)(\hat{u}-m_2^2)+2m_1m_2\hat{s}}{(\hat{s}-M_s^2)^2}\\&+A_t\frac{(\hat{t}-m_1^2)(\hat{t}-m_2^2)}{(\hat{t}-M_t^2)^2}+A_u\frac{(\hat{u}-m_1^2)(\hat{u}-m_2^2)}{(\hat{u}-M_u^2)^2}\\&+A_{st}\frac{(\hat{t}-m_1^2)(\hat{t}-m_2^2)+m_1m_2\hat{s}}{(\hat{s}-M_s^2)(\hat{t}-M_t^2)}+A_{tu}\frac{m_1m_2\hat{s}}{(\hat{t}-M_t^2)(\hat{u}-M_u^2)}\\&+A_{su}\frac{(\hat{u}-m_1^2)(\hat{u}-m_2^2)+m_1m_2\hat{s}}{(\hat{s}-M_s^2)(\hat{u}-M_u^2)}\Bigg],\end{aligned}\tag{7.1}$$

where m_1 and m_2 are the masses of the produced gauginos, and M_s, M_t, and M_u are the masses of the particles exchanged in the s, t, and u channels, respectively. The coefficients A_x are collected in Table IX for all possible pairs of gauginos.

The total cross section is

$$\begin{aligned}\sigma(q\bar{q}'\to\text{gauginos})=\frac{\pi}{(1+I)\hat{s}^2}\Bigg[&\frac{A_s\mathcal{S}}{3(\hat{s}-M_s^2)^2}\{2\hat{s}^2+\hat{s}[6m_1m_2-(m_1^2+m_2^2)]-(m_1^2-m_2^2)^2\}\\&+\Bigg\{A_t\Bigg[\mathcal{S}+(\Delta_{t1}+\Delta_{t2})\Lambda_t+\frac{\mathcal{S}\Delta_{t1}\Delta_{t2}}{M_t^4+m_1^2m_2^2+M_t^2(\hat{s}-m_1^2-m_2^2)}\Bigg]\\&+\frac{A_{st}}{\hat{s}-M_s^2}\Bigg[\mathcal{S}\Bigg[M_t^2-\frac{\hat{s}+m_1^2+m_2^2}{2}\Bigg]+(\Delta_{t1}\Delta_{t2}+m_1m_2\hat{s})\Lambda_t\Bigg]+(t\leftrightarrow u)\Bigg\}\\&-A_{tu}\frac{m_1m_2\hat{s}}{\hat{s}+\Delta_{t1}+\Delta_{u2}}(\Lambda_t+\Lambda_u)\Bigg].\end{aligned}\tag{7.2}$$

The quantity $1/(1+I)$ is a symmetry factor for identical particles. $I=1$ for identical gauginos $\tilde{g}\tilde{g}$, $\tilde{\gamma}\tilde{\gamma}$, and $\tilde{Z}\tilde{Z}$; in all other cases, $I=0$. We have also introduced the convenient quantities

$$\mathcal{S}=[\hat{s}-(m_1+m_2)^2]^{1/2}[\hat{s}-(m_1-m_2)^2]^{1/2},\tag{7.3}$$

$$\Delta_{ai}=M_a^2-m_i^2,\tag{7.4}$$

and

$$\Lambda_a=\ln\left[\frac{\hat{s}+\Delta_{a1}+\Delta_{a2}-\mathcal{S}}{\hat{s}+\Delta_{a1}+\Delta_{a2}+\mathcal{S}}\right].\tag{7.5}$$

TABLE IX. Coefficients[a] for the reaction $q_i\bar{q}_j \to \text{gaugino}_1 + \text{gaugino}_2$.

		Exchanged Particle								
gaugino$_1$	gaugino$_2$	s	t	u	A_s	A_t	A_u	A_{st}	A_{su}	A_{tu}
$\tilde{\gamma}$	$\tilde{\gamma}$		$\tilde{q}$	$\tilde{q}$	0	$\frac{2\alpha^2 e_q^4}{3}\delta_{qq'}$	A_t	0	0	$-2A_t$
$\tilde{\gamma}$	$\tilde{g}$		$\tilde{q}$	$\tilde{q}$	0	$\frac{8\alpha_s \alpha e_q^2}{9}\delta_{qq'}$	A_t	0	0	$-2A_t$
$\tilde{\gamma}$	$\tilde{Z}$		$\tilde{q}$	$\tilde{q}$	0	$\frac{\alpha^2 e_q^2}{12x_W}\left(\frac{L^2+R^2}{1-x_W}\right)\delta_{qq'}$	A_t	0	0	$-2A_t$
$\tilde{Z}$	$\tilde{Z}$		$\tilde{q}$	$\tilde{q}$	0	$\frac{\alpha^2}{48x_W^2}\left(\frac{L^4+R^4}{(1-x_W)^2}\right)\delta_{qq'}$	A_t	0	0	$-2A_t$
$\tilde{Z}$	$\tilde{g}$		$\tilde{q}$	$\tilde{q}$	0	$\frac{\alpha_s \alpha}{9x_W}\left(\frac{L^2+R^2}{1-x_W}\right)\delta_{qq'}$	A_t	0	0	$-2A_t$
$\tilde{g}$	$\tilde{g}$	g	$\tilde{q}$	$\tilde{q}$	$\frac{8\alpha_s^2}{3}\delta_{qq'}$	$\frac{32\alpha_s^2}{27}\delta_{qq'}$	A_t	$\frac{8\alpha_s^2}{3}\delta_{qq'}$	A_{st}	$\frac{8\alpha_s^2}{27}\delta_{qq'}$
$\tilde{W}^+$	$\tilde{W}^-$	γ AND Z	$\tilde{q}$		$\frac{2\alpha^2}{3}\left(e_q^2+\frac{e_q(L_q+R_q)}{2x_W(1-\frac{M_Z^2}{s})}+\frac{(L_q^2+R_q^2)}{8x_W^2(1-\frac{M_Z^2}{s})^2}\right)\delta_{qq'}$	$\frac{\alpha^2}{12x_W^2}\delta_{qq'}\delta_{qu}$	$\frac{\alpha^2}{12x_W^2}\delta_{qq'}\delta_{qd}$	$\frac{\alpha^2}{3x_W}\left(e_q+\frac{L_q}{2x_W(1-\frac{M_Z^2}{s})}\right)\times\delta_{qq'}\delta_{qu}$	$\frac{\alpha^2}{3x_W}\left(e_q+\frac{L_q}{2x_W(1-\frac{M_Z^2}{s})}\right)\times\delta_{qq'}\delta_{qd}$	0
$\tilde{W}^+$	$\tilde{Z}$	W	$\tilde{q}'$	$\tilde{q}$	$\alpha^2\frac{(1-x_W)}{6x_W^2}\delta_{qu}\delta_{q'd}$	$\frac{\alpha^2}{24x_W^2}\left(\frac{L_{q'}^2}{1-x_W}\right)\delta_{qu}\delta_{q'd}$	$\frac{\alpha^2}{24x_W^2}\left(\frac{L_q^2}{1-x_W}\right)\delta_{qu}\delta_{q'd}$	$\frac{-\alpha^2 L_{q'}}{6x_W^2}\delta_{qu}\delta_{q'd}$	$\frac{\alpha^2 L_q}{6x_W^2}\delta_{qu}\delta_{q'd}$	$\frac{-\alpha^2}{12x_W^2}\frac{L_{q'}L_q}{(1-x_W)}\times\delta_{qu}\delta_{q'd}$
$\tilde{W}^+$	$\tilde{\gamma}$	W	$\tilde{q}'$	$\tilde{q}$	$\frac{\alpha^2}{6x_W}\delta_{qu}\delta_{q'd}$	$\frac{\alpha^2 e_{q'}^2}{6x_W}\delta_{qu}\delta_{q'd}$	$\frac{\alpha^2 e_q^2}{6x_W}\delta_{qu}\delta_{q'd}$	$\frac{-\alpha^2 e_{q'}}{3x_W}\delta_{qu}\delta_{q'd}$	$\frac{\alpha^2 e_q}{3x_W}\delta_{qu}\delta_{q'd}$	$\frac{-\alpha^2 e_q e_{q'}}{3x_W}\times\delta_{qu}\delta_{q'd}$
$\tilde{W}^+$	$\tilde{g}$		$\tilde{q}'$	$\tilde{q}$	0	$\frac{2\alpha_s\alpha}{9x_W}\delta_{qu}\delta_{q'd}$	$\frac{2\alpha_s\alpha}{9x_W}\delta_{qu}\delta_{q'd}$	0	0	$\frac{-4\alpha_s\alpha}{9x_W}\times\delta_{qu}\delta_{q'd}$

[a]Here $x_W=\sin^2\theta_W$. The neutral-current couplings are defined in Eqs. (7.22) and (7.23).

The production of gluino pairs also occurs in gluon-gluon collisions, with the differential cross section

$$\frac{d\sigma}{d\hat{t}}(gg\to\tilde{g}\tilde{g})=\frac{9\pi\alpha_s^2}{4\hat{s}^2}\left\{\frac{2(\hat{t}-m_{\tilde{g}}^2)(\hat{u}-m_{\tilde{g}}^2)}{\hat{s}^2}+\left[\left[\frac{(\hat{t}-m_{\tilde{g}}^2)(\hat{u}-m_{\tilde{g}}^2)-2m_{\tilde{g}}^2(\hat{t}+m_{\tilde{g}}^2)}{(\hat{t}-m_{\tilde{g}}^2)^2}+\frac{(\hat{t}-m_{\tilde{g}}^2)(\hat{u}-m_{\tilde{g}}^2)+m_{\tilde{g}}^2(\hat{u}-\hat{t})}{\hat{s}(\hat{t}-m_{\tilde{g}}^2)}\right]+[t\leftrightarrow u]\right]+\frac{m_{\tilde{g}}^2(\hat{s}-4m_{\tilde{g}}^2)}{(\hat{t}-m_{\tilde{g}}^2)(\hat{u}-m_{\tilde{g}}^2)}\right\}, \tag{7.6}$$

where $m_{\tilde{g}}$ is the gluino mass. An elementary integration gives the total cross section

$$\sigma(gg\to\tilde{g}\tilde{g})=\frac{3\pi\alpha_s^2}{4\hat{s}}\left[3\left[1+\frac{4m^2}{\hat{s}}-\frac{4m^4}{\hat{s}^2}\right]\ln\left[\frac{\hat{s}+\mathscr{S}}{\hat{s}-\mathscr{S}}\right]-\left[4+\frac{17m^2}{\hat{s}}\right]\frac{\mathscr{S}}{\hat{s}}\right]. \tag{7.7}$$

2. Associated production of squarks and gauginos

The differential cross section for the production of squarks and gauginos in collisions of quarks and gluons is

$$\frac{d\sigma}{d\hat{t}}(gq_i\to\text{gaugino}+\tilde{q}_i)=\frac{\pi}{\hat{s}^2}\left[B_s\frac{\mu^2-\hat{t}}{\hat{s}}+B_t\frac{(\mu^2-\hat{t})\hat{s}+2\mu^2(m_i^2-\hat{t})}{(\hat{t}-\mu^2)^2}\right.$$
$$+\frac{B_u(\hat{u}-\mu^2)(\hat{u}+m_i^2)}{(\hat{u}-m_i^2)^2}+\frac{B_{st}[(\hat{s}-m_i^2+\mu^2)(\hat{t}-m_i^2)-\mu^2\hat{s}]}{\hat{s}(\hat{t}-\mu^2)}$$
$$+B_{su}\frac{\hat{s}(\hat{u}+\mu^2)+2(m_i^2-\mu^2)(\mu^2-\hat{u})}{\hat{s}(\hat{u}-m_i^2)}$$
$$\left.+B_{tu}\frac{(m_i^2-\hat{t})(\hat{t}+2\hat{u}+\mu^2)+(\hat{t}-\mu^2)(\hat{s}+2\hat{t}-2m_i^2)+(\hat{u}-\mu^2)(\hat{t}+\mu^2+2m_i^2)}{2(\hat{t}-\mu^2)(\hat{u}-m_i^2)}\right], \tag{7.8}$$

where μ is the mass of the gauge fermion and m_i is the mass of the squark. The coefficients B_x for each of the final states are tabulated in Table X. Upon integration we obtain the total cross section

$$\sigma(gq_i\to\text{gaugino}+\tilde{q}_i)=\frac{\pi}{\hat{s}^2}\left[B_s\frac{\mathcal{S}}{2}(1-\Delta/\hat{s})+B_t[2\Delta\mathcal{S}/\hat{s}+(\hat{s}+2\mu^2)\tilde{\Lambda}]\right.$$
$$+B_u[\mathcal{S}(1+2\Lambda/\hat{s})+(3m_i^2-\mu^2)\Lambda]+B_{st}[\mathcal{S}(1-\Delta/\hat{s})+(m_i^2-\Delta^2/\hat{s})\tilde{\Lambda}]$$
$$+B_{su}[\mathcal{S}(1-2\Delta/\hat{s})+(\mu^2+m_i^2-2\Delta^2/\hat{s})\Lambda]$$
$$\left.+B_{tu}\{-[m_i^2+\mu^2+2(m_i^4-\mu^4)/\hat{s}]\Lambda+[-2m_i^2+2(m_i^4-\mu^4)/\hat{s}]\tilde{\Lambda}-\mathcal{S}\}\right], \tag{7.9}$$

where

$$\Delta=m_i^2-\mu^2\,, \tag{7.10}$$

$$\Lambda=\ln\left[\frac{\Delta+\hat{s}-\mathcal{S}}{\Delta+\hat{s}+\mathcal{S}}\right], \tag{7.11}$$

and

$$\tilde{\Lambda}=\ln\left[\frac{\Delta-\hat{s}-\mathcal{S}}{\Delta-\hat{s}+\mathcal{S}}\right]. \tag{7.12}$$

3. Squark pair production

The production of pairs of squarks in hadron collisions can occur in quark-quark, quark-antiquark, or gluon-gluon collisions. For the first two cases we shall include only the gluino exchange contributions. The differential cross sec-

TABLE X. Coefficients[a] for the reaction $gq_i\to\text{gaugino}+\tilde{q}_j$.

Gaugino	s	Exchanged particle t	u	B_s	B_t	B_u	B_{st}	B_{su}	B_{tu}
$\tilde{\gamma}$	q		$\tilde{q}$	$\frac{\alpha_s\alpha e_q^2}{3}\delta_{ij}$	0	B_s	0	$-B_s$	0
$\tilde{W}^+$	q		$\tilde{q}$	$\frac{\alpha_s\alpha}{12x_W}\delta_{iu}\delta_{jd}$	0	B_s	0	$-B_s$	0
$\tilde{Z}$	q		$\tilde{q}$	$\frac{\alpha_s\alpha}{24x_W}\left[\frac{L_q^2+R_q^2}{1-x_W}\right]\delta_{ij}$	0	B_s	0	$-B_s$	0
$\tilde{g}$	q	$\tilde{g}$	$\tilde{q}$	$\frac{4\alpha_s^2}{9}\delta_{ij}$	$\alpha_s^2\delta_{ij}$	$\frac{4\alpha_s^2}{9}\delta_{ij}$	$-\alpha_s^2\delta_{ij}$	$\frac{\alpha_s^2}{18}\delta_{ij}$	$\frac{\alpha_s^2}{2}\delta_{ij}$

[a]Here $x_W=\sin^2\theta_W$. The neutral-current couplings are defined in Eqs. (7.22) and (7.23).

tions for these cases are

$$\frac{d\sigma}{d\hat{t}}(q_iq_j\to\tilde{q}_i\tilde{q}_j)=\frac{4\pi\alpha_s^2}{9\hat{s}^2}\left[-\frac{(\hat{t}-m_i^2)(\hat{t}-m_j^2)+\hat{s}\hat{t}}{(\hat{t}-m_{\tilde{g}}^2)^2}-\delta_{ij}\frac{(\hat{u}-m_i^2)(\hat{u}-m_j^2)+\hat{s}\hat{u}}{(\hat{u}-m_{\tilde{g}}^2)^2}\right]$$
$$+\left[\frac{\hat{s}m_{\tilde{g}}^2}{(\hat{t}-m_{\tilde{g}}^2)^2}+\frac{\hat{s}m_{\tilde{g}}^2}{(\hat{u}-m_{\tilde{g}}^2)^2}\delta_{ij}-\frac{2\hat{s}m_{\tilde{g}}^2}{3(\hat{t}-m_{\tilde{g}}^2)(\hat{u}-m_{\tilde{g}}^2)}\delta_{ij}\right], \tag{7.13}$$

and

$$\frac{d\sigma}{d\hat{t}}(q_i\bar{q}_j\to\tilde{q}_i\tilde{q}_j^*)=\frac{4\pi\alpha_s^2}{9\hat{s}^2}\left\{\left[\frac{\hat{u}\hat{t}-m_i^2m_j^2}{\hat{s}^2}\right]\left[\delta_{ij}\left[2-\frac{2}{3}\frac{\hat{s}}{\hat{t}-m_{\tilde{g}}^2}\right]+\frac{\hat{s}^2}{(\hat{t}-m_{\tilde{g}}^2)^2}\right]+\frac{m_{\tilde{g}}^2\hat{s}}{(\hat{t}-m_{\tilde{g}}^2)^2}\right\}. \tag{7.14}$$

where m_i and m_j are the masses of the produced squarks and $m_{\tilde{g}}$ is the gluino mass. In the case of gluon-gluon collisions, the differential cross section is given by

$$\frac{d\sigma}{d\hat{t}}(gg\to\tilde{q}_i\tilde{q}_i^*)=\frac{\pi\alpha_s^2}{\hat{s}^2}\left[\frac{7}{48}+\frac{3(\hat{u}-\hat{t})^2}{16\hat{s}^2}\right]\left[1+\frac{2m^2\hat{t}}{(\hat{t}-m^2)^2}+\frac{2m^2\hat{u}}{(\hat{u}-m^2)^2}+\frac{4m^4}{(\hat{t}-m^2)(\hat{u}-m^2)}\right], \tag{7.15}$$

where m is the common mass of the produced squarks.

The total cross sections are easily computed as

$$\sigma(q_iq_j\to\tilde{q}_i\tilde{q}_j)=\frac{4\pi\alpha_s^2}{9\hat{s}^2}\left[\left[-2\mathscr{S}-(\hat{s}+\Delta_{ti}+\Delta_{tj})\Lambda_t+\frac{1}{1+\delta_{ij}}\frac{\mathscr{S}\hat{s}m_{\tilde{g}}^2}{\Delta_{ti}\Delta_{tj}+\hat{s}m_{\tilde{g}}^2}\right.\right.$$
$$\left.\left.+\frac{1}{3}\delta_{ij}\frac{\hat{s}m_{\tilde{g}}^2}{\hat{s}+\Delta_{ti}+\Delta_{tj}}\Lambda_t\right]+\delta_{ij}(t\to u)\right], \tag{7.16}$$

$$\sigma(q_i\bar{q}_j\to\tilde{q}_i\tilde{q}_j^*)=\frac{4\pi\alpha_s^2}{27\hat{s}^2}\left[\delta_{ij}\left[\frac{\mathscr{S}^3}{\hat{s}^2}+\frac{\mathscr{S}(\hat{s}+\Delta_{ti}+\Delta_{tj})}{\hat{s}}+\frac{2(\Delta_{ti}\Delta_{tj}+m_{\tilde{g}}^2\hat{s})}{\hat{s}}\Lambda_t\right]\right.$$
$$\left.+3\left[-2\mathscr{S}-(\hat{s}+\Delta_{ti}+\Delta_{tj})\Lambda_t+\frac{\mathscr{S}\hat{s}m_{\tilde{g}}^2}{\hat{s}m_{\tilde{g}}^2+\Delta_{ti}\Delta_{tj}}\right]\right], \tag{7.17}$$

and

$$\sigma(gg\to\tilde{q}_i\tilde{q}_i^*)=\frac{\pi\alpha_s^2}{3\hat{s}^2}\left[\left[\frac{5}{8}+\frac{31}{4}\frac{m^2}{\hat{s}}\right]\mathscr{S}+\left[4+\frac{m^2}{\hat{s}}\right]m^2\ln\left[\frac{\hat{s}-\mathscr{S}}{\hat{s}+\mathscr{S}}\right]\right]. \tag{7.18}$$

We shall also require the cross sections for the production of pairs of the supersymmetric partners of leptons in quark-antiquark collisions. These reactions proceed by the exchange of photons and Z^0's in the direct channel. The differential cross section is

$$\frac{d\sigma}{d\hat{t}}(q\bar{q}\to\tilde{l}\tilde{l}^*)=\frac{4\pi\alpha^2}{3\hat{s}^2}\left[e_q^2e_l^2+\frac{e_qe_l(L_q+R_q)(L_l+R_l)}{8x_W(1-x_W)(1-M_Z^2/\hat{s})}+\frac{(L_q^2+R_q^2)(L_l^2+R_l^2)}{64x_W^2(1-x_W)^2(1-M_Z^2/\hat{s})^2}\right]\left[\frac{\hat{u}\hat{t}-m_{\tilde{l}}^4}{\hat{s}^2}\right], \tag{7.19}$$

where $m_{\tilde{l}}$ is the slepton mass, and the total cross section is

$$\sigma(q\bar{q}\to\tilde{l}\tilde{l}^*)=\frac{2\pi\alpha^2\mathscr{S}^3}{9\hat{s}^4}\left[e_q^2e_l^2+\frac{e_qe_l(L_q+R_q)(L_l+R_l)}{8x_W(1-x_W)^2(1-M_Z^2/\hat{s})}+\frac{(L_q^2+R_q^2)(L_l^2+R_l^2)}{64x_W^2(1-x_W)^2(1-M_Z^2/\hat{s})^2}\right]. \tag{7.20}$$

Here the chiral neutral current couplings are

$$L_f=\tau_f^{(3)}-2e_fx_W\ ,$$
$$R_f=-2e_fx_W\ , \tag{7.21}$$

where $\tau_f^{(3)}$ is twice the (left-handed) weak isospin I_3 of fermion f, e_f is the fermion charge in units of the proton charge, and

$$x_W=\sin^2\theta_W \tag{7.22}$$

is the weak mixing parameter. After these preliminaries, we turn to the task of estimating supercollider cross sections.

B. Production and detection of strongly interacting superpartners

We now discuss the rates expected for squark and gluino production in high-energy hadron-hadron collisions. Gluino pair production arises in quark-antiquark collisions [Eq. (7.2)] and in gluon-gluon collisions [Eq. (7.7)]. Both elementary cross sections depend upon the gluino mass. The cross section for $q\bar{q}\to\tilde{g}\tilde{g}$ depends, in addition, upon the squark mass that appears in the t-channel and u-channel exchange diagrams. Neither the squark and gluino masses nor the relationship of $m_{\tilde{g}}$ and $m_{\tilde{q}}$ is fixed by theoretical considerations. For illustration, we have chosen the representative case of equal squark and gluino masses.

The cross sections for gluino pair production in pp collisions at $\sqrt{s}=2$, 10, 20, 40, and 100 TeV are shown in Fig. 191 as a function of the common squark and gluino mass. These estimates are based on the parton distributions of Set 2. Here and throughout this discussion, we require that the superpartners be emitted with rapidities $|y_i|<1.5$. The cross sections are quite large at supercollider energies. For example, at $\sqrt{s}=40$ TeV the cross section is 10 pb for $m_{\tilde{g}}=1$ TeV/c^2, a mass considerably greater than the value expected in typical models of low-energy supersymmetry. The cross sections for gluino pair production in $\bar{p}p$ collisions, calculated under the same assumptions, are shown in Fig. 192. The relatively small differences between the pp and $\bar{p}p$ cross sections reflect the dominance of the $gg\to\tilde{g}\tilde{g}$ process. The relative unimportance of the $q\bar{q}\to\tilde{g}\tilde{g}$ mechanism means that the cross sections will be rather insensitive to the value of the squark mass. This conclusion is supported by the cross sections for gluino production in pp collisions shown in Fig. 193, for which we have fixed the squark mass at $m_{\tilde{q}}=1$ TeV/c^2. Finally, the sensitivity of these results to the parton distributions is also mild, as shown by the cross sections plotted in Fig. 194, which were computed using the parton distributions of Set 1. Over the range of gluino masses from 50 GeV/c^2 to 1 TeV/c^2, these estimates differ from those of Fig. 191 by no more than 20%. Copious production of gluinos therefore seems assured for hadron colliders in the energy range between 10 and 100 TeV. We defer a discussion of how gluinos may be detected until we have completed this survey of production rates.

Associated production of squarks and gluinos provides a second source of gluinos. If the gluino is much heavier than the up or down squarks, then associated production is the dominant mechanism for gluino production. Similarly, if the gluino is much lighter than the up and down squarks, associated production will be the dominant mechanism for squark production. If the squark and gluino masses are comparable, associated production will be a significant contributor to both squark and gluino production.

The total cross section for associated production of squarks and gluinos is given by the elementary cross section (7.9). If we sum over $\tilde{g}\tilde{q}_u$, $\tilde{g}\tilde{q}_d$, $\tilde{g}\tilde{q}^*_u$, and $\tilde{g}\tilde{q}^*_d$ final

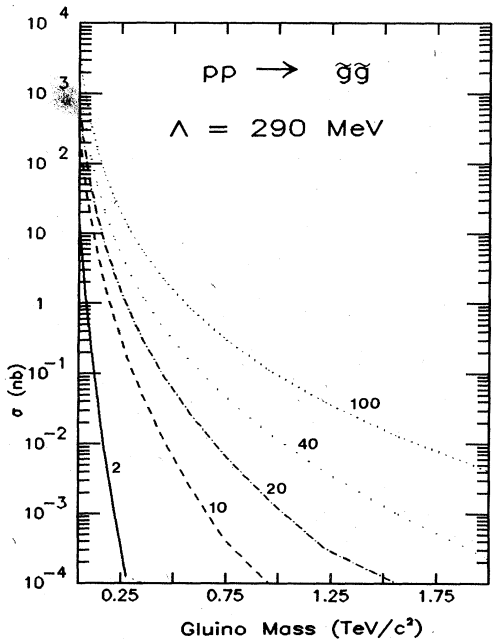

FIG. 191. Cross sections for the reaction $pp\to\tilde{g}\tilde{g}+$ anything as a function of gluino mass, for collider energies $\sqrt{s}=2$, 10, 20, 40, and 100 TeV, according to the parton distributions of Set 2. Both gluinos are restricted to the interval $|y_i|<1.5$. For this illustration, the squark mass is set equal to the gluino mass.

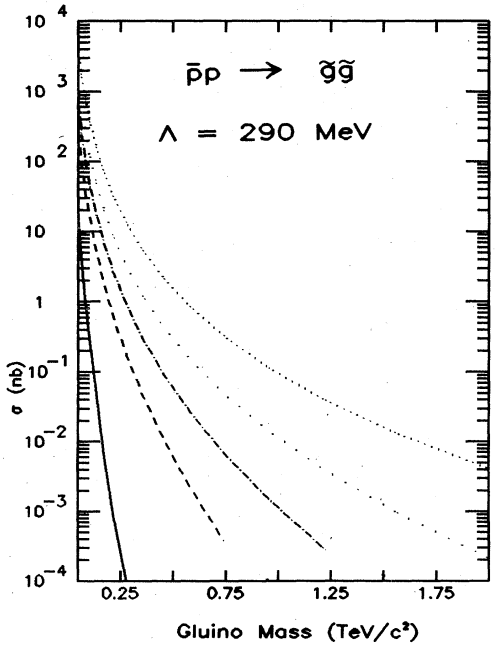

FIG. 192. Cross sections for the reaction $\bar{p}p\to\tilde{g}\tilde{g}+$ anything as a function of gluino mass, according to the parton distributions of Set 2. Cuts and parameters are as in Fig. 191.

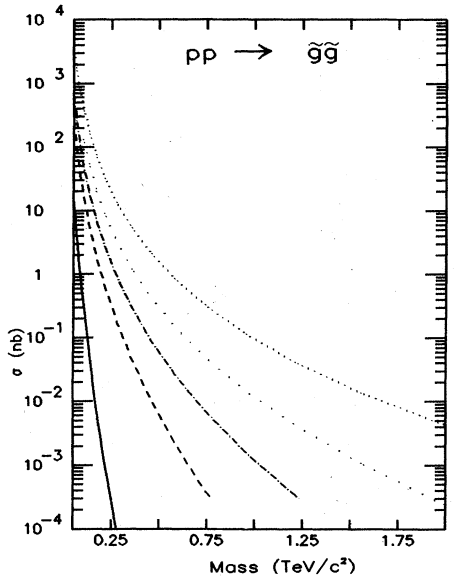

FIG. 193. Cross sections for the reaction $pp \to \tilde{g}\tilde{g} +$ anything as a function of gluino mass, according to the parton distributions of Set 2. Cuts are as in Fig. 191, but the squark mass is chosen as 0.5 TeV/c^2.

states, then the cross sections are equal in pp and $\bar{p}p$ collisions. The total cross section is shown in Fig. 195 for the case of equal squark and gluino masses and the parton distributions of Set 2.

We next consider the pair production of squarks in $p^{\pm}p$ collisions. In these considerations we shall assume for simplicity that the scalar partners of left- and right-handed quarks are degenerate in mass but distinguishable,

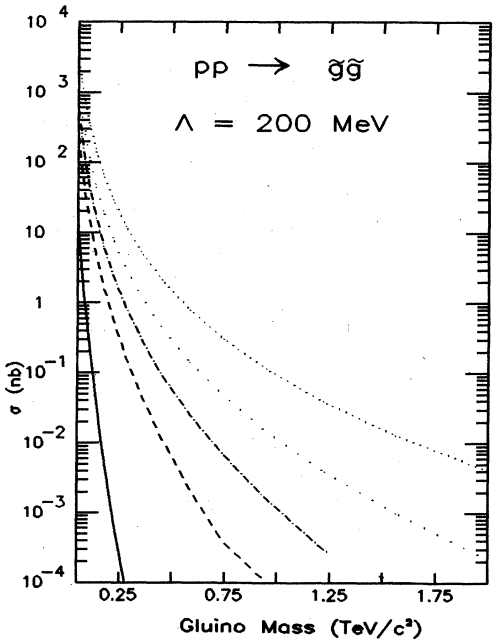

FIG. 194. Cross sections for the reaction $pp \to \tilde{g}\tilde{g} +$ anything as a function of gluino mass, according to the parton distributions of Set 1. Cuts and parameters are as in Fig. 191.

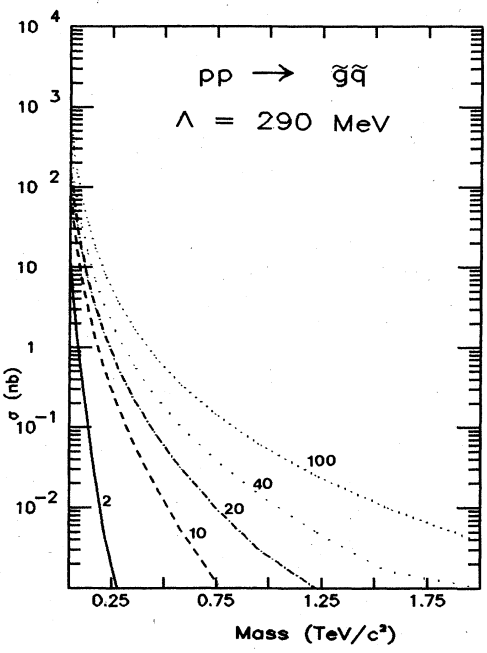

FIG. 195. Cross sections for the reaction $pp \to \tilde{g}$ ($\tilde{q}_u$ or $\tilde{q}_d$ or $\tilde{q}^*_u$ or $\tilde{q}^*_d$) + anything as a function of the superparticle mass, for collider energies $\sqrt{s} = 2$, 10, 20, 40, and 100 TeV, according to the parton distributions of Set 2. We have assumed equal mass for the squarks and gluino, and have included the partners of both left- and right-handed quarks. Both squark and gluino are restricted to the rapidity interval $|y_i| < 1.5$.

and that the up and down squarks have a common mass. The generalization to left- and right-"handed" squarks with unequal masses is explained in Dawson *et al.* (1984). Some restrictions on mass differences among squarks of different flavors have been deduced by Suzuki (1982). We further assume that there is no mixing between squarks, and that a quark of a given flavor and chirality couples only to the squark labeled by the same flavor and chirality. None of our general conclusions depends critically upon these assumptions.

The processes leading to the production of left- and right-handed up and down squarks in $p^{\pm}p$ collisions are

$$p^{\pm}p \to \tilde{q}_u\tilde{q}_d + \text{anything}\ , \tag{7.23}$$

$$p^{\pm}p \to (\tilde{q}_u\tilde{q}_u \text{ or } \tilde{q}_d\tilde{q}_d) + \text{anything}\ , \tag{7.24}$$

$$p^{\pm}p \to \tilde{q}^*_u\tilde{q}^*_d + \text{anything}\ , \tag{7.25}$$

$$p^{\pm}p \to (\tilde{q}^*_u\tilde{q}^*_u \text{ or } \tilde{q}^*_d\tilde{q}^*_d) + \text{anything}\ , \tag{7.26}$$

$$p^{\pm}p \to (\tilde{q}^*_u\tilde{q}_d \text{ or } \tilde{q}_u\tilde{q}^*_d) + \text{anything}\ , \tag{7.27}$$

$$p^{\pm}p \to (\tilde{q}_u\tilde{q}^*_u \text{ or } \tilde{q}_d\tilde{q}^*_d) + \text{anything}\ , \tag{7.28}$$

for which the elementary cross sections are given by Eqs. (7.13)—(7.18). Since it is nontrivial experimentally to distinguish $\tilde{q}_u$ jets, $\tilde{q}^*_u$ jets, $\tilde{q}_d$ jets, and $\tilde{q}^*_d$ jets, we combine all the above reactions and both chiralities for each initial state. The resulting inclusive cross section for the production of an up or down squark or antisquark with $|y| < 1.5$ in pp collisions is shown in Fig. 196. The larg-

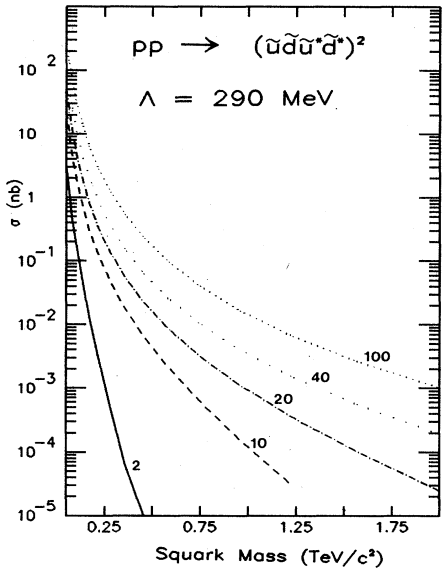

FIG. 196. Cross sections for the pair production in pp collisions of up and down squarks or antisquarks in the rapidity interval $|y_i| < 1.5$, as a function of the common squark mass, for collider energies $\sqrt{s} = 2$, 10, 20, 40, and 100 TeV. The parton distributions of Set 2 are used.

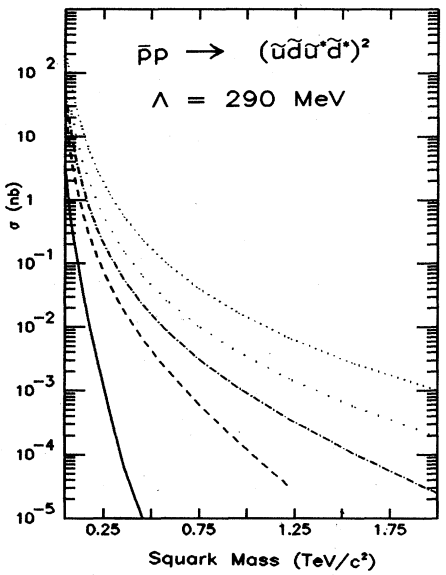

FIG. 197. Cross sections for the pair production of up and down squarks or antisquarks in $\bar{p}p$ collisions, according to the parton distributions of Set 2. Cuts and parameters are as in Fig. 196.

est contributions are associated with reaction (7.28), which has components from both $q\bar{q}$ and gg collisions, and with reactions (7.23) and (7.24), for which valence quarks enhance the cross sections at larger squark masses.

Apart from reaction (7.28), all the processes are mediated only by t-channel or u-channel gluino exchange, so the cross sections are sensitive to our assumptions about the gluino mass. For large gluino masses $m_{\tilde{g}}$, these cross sections scale approximately as $m_{\tilde{g}}^{-4}$.

The inclusive cross section for up and down squark and antisquark production in $\bar{p}p$ collisions is shown in Fig. 197. The same quantity, evaluated using the distribution functions of Set 1, is shown for pp collisions in Fig. 198. Both of these are quite similar to the pp cross section displayed in Fig. 196. As in the case of gluino pair production, the cross sections are quite substantial even for squark masses as large as 1 TeV/c^2.

In some supersymmetric models (e.g., Claudson, Hall, and Hinchliffe, 1983), the heaviest quark flavor is associated with the lightest squark. In such a model, the top squark would be the lightest of the squarks and thus would be the most copiously produced flavor at supercollider energies. The important production mechanisms for new squark flavors are $gg \to \tilde{q}\tilde{q}^* q\bar{q} \to \tilde{q}\tilde{q}^*$. If, as we have assumed, the heavy flavor component of the proton is induced only perturbatively, processes involving heavy quarks in the initial state may be safely neglected. The cross sections for the production of top squark pairs in pp and $\bar{p}p$ collisions are shown in Figs. 199 and 200. As before, we have set the gluino mass equal to the squark mass, and have used the parton distributions of Set 2. Above 20 TeV, the cross sections are ample even for squark masses of 1 TeV/c^2.

A comparison of the three mechanisms for the production of strongly interacting superpartners in 40-TeV pp collisions is shown in Fig. 201, for which we have taken the squark and gluino masses equal, required $|y_i| < 1.5$, and used the parton distributions of Set 2. A similar comparison for $\bar{p}p$ collisions at 40 TeV is given in Fig. 202. If squarks and gluinos are light, the gluino-gluino final state dominates the total cross section for production of colored superpartners. Squarks are then produced

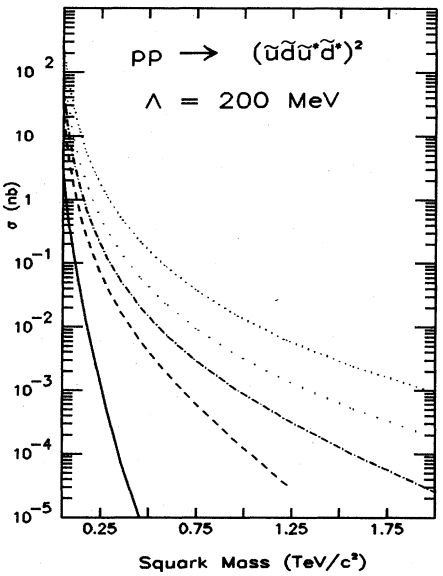

FIG. 198. Cross sections for the pair production of up and down squarks and antisquarks in pp collisions, according to the parton distributions of Set 1. Cuts and parameters are as in Fig. 196.

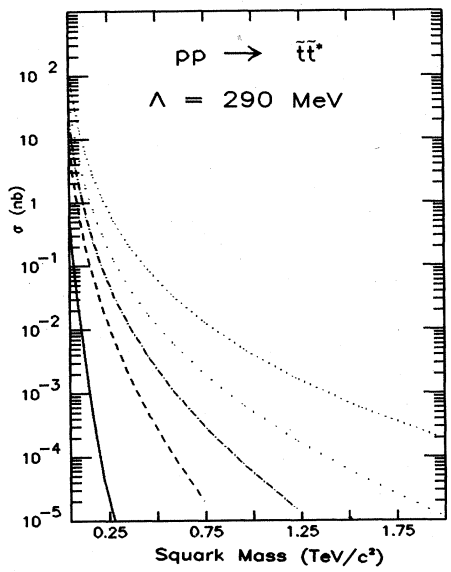

FIG. 199. Cross sections for the production of a "heavy" squark flavor in the reaction $pp \to \tilde{t}\tilde{t}^* +$ anything, according to the parton distributions of Set 2. Cuts and parameters are as in Fig. 196.

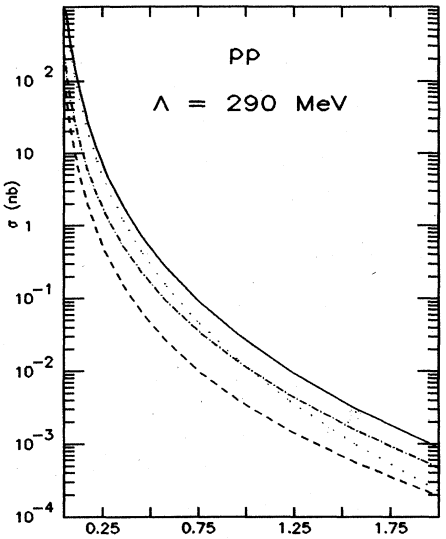

FIG. 201. Comparison of the cross sections for $\tilde{g}\tilde{g}$ (dotted line), $\tilde{g}\tilde{q}$ (dotted-dashed line), and $\tilde{q}\tilde{q}$ (dashed line) production in pp collisions at 40 TeV, according to the parton distributions of Set 2. Also shown is the total cross section for squark or gluino production (solid line). Cuts and parameters are as in Fig. 191.

most effectively in association with gluinos. For values of the common squark and gluino mass in excess of about 1 TeV/c^2, associated squark-gluino production becomes the most important reaction mechanism. As the preceding figures suggest, the importance of the squark-squark final state grows as the collider energy is reduced, for fixed superparticle masses. Raising the energy, in contrast, enhances the importance of the gluino-gluino final state.

Having examined the production rates, we now turn to the more difficult question of the detection of squarks and gluinos in the environment of a hadron collider. Any analysis of the signals for superpartners is complicated by the extreme model dependence of superparticle masses. All that can be said with certainty is that if supersymmetry is to solve the hierarchy problem, then the lightest superpartners of the quarks, leptons, and gauge bosons should not be much heavier than the electroweak scale, and that none of the superpartners should be heavier than

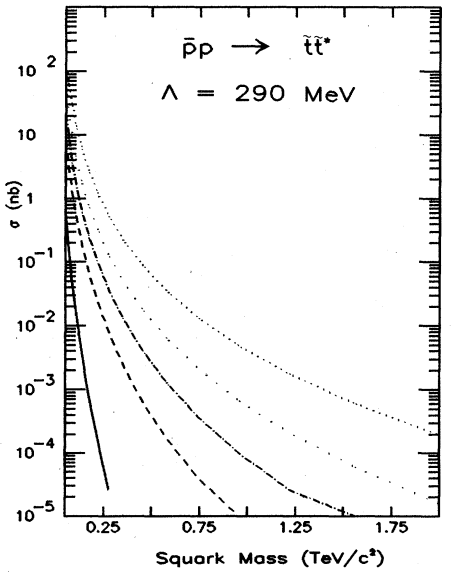

FIG. 200. Cross sections for the production of a "heavy" squark flavor in $\bar{p}p$ collisions, according to the parton distributions of Set 2. Cuts and parameters are as in Fig. 196.

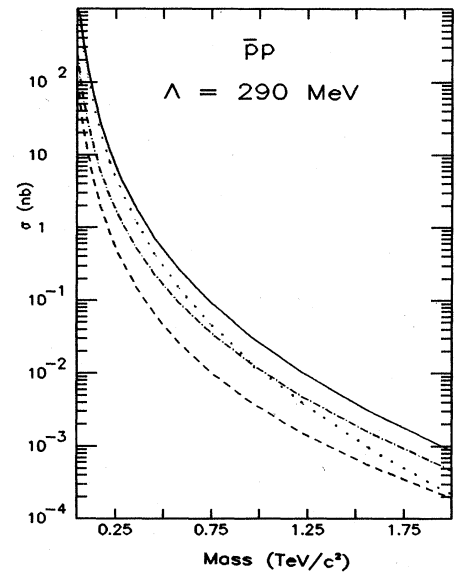

FIG. 202. Comparison of the cross sections for $\tilde{g}\tilde{g}$ (dotted line), $\tilde{g}\tilde{q}$ (dotted-dashed line), and $\tilde{q}\tilde{q}$ (dashed line) production in $\bar{p}p$ collisions at 40 TeV, according to the parton distributions of Set 2. Also shown is the total cross section for squark or gluino production (solid line). Cuts and parameters are as in Fig. 191.

a few TeV/c^2 (Fayet, 1982).

In the absence of reliable theoretical guidance it is a nearly impossible task to discuss all possible decay scenarios. We shall concentrate on a few of the more plausible schemes. The strengths of couplings are prescribed by supersymmetric models. Therefore, the possible decays depend solely on the kinematic constraints imposed by the unknown mass spectrum.

Possible decay schemes for the gluino are these, in increasing order of coupling strength.

(i) The gluino is stable or long lived, with $\tau_{\tilde{g}} \gtrsim 10^{-8}$ sec. In this case the gluino will combine with a gluon or a quark-antiquark pair to form hadrons with charges 0 and ± 1. MIT bag model estimates suggest (Chanowitz and Sharpe, 1983) that these states should have masses close to the gluino mass, if the gluino is massive.

(ii) The gluino decays into a gluon and a Goldstino. The experimental signature in this case would be a gluon jet and missing transverse energy, since the Goldstino will escape undetected.

(iii) The gluino is not the lightest gaugino, and decays into a quark-antiquark pair plus the lightest gaugino. In our analysis we shall assume that the lightest gaugino is the photino, as is true in many models (Fayet, 1981; Dine and Fischler, 1982; Ibañez and Ross, 1982; Nappi and Ovrut, 1982). The photino either is stable and weakly interacting (so that it escapes undetected) or decays into an undetected Goldstino and a hard photon. Thus the signature for this gluino decay mode is two jets, missing transverse momentum, and perhaps a hard photon.

(iv) The gluino decays into a squark and antiquark or quark and antisquark. The signature for this mode depends on the subsequent decay of the squark [cases (i)—(iii) below]. The dominant decay of the gluino will therefore be the last of these possibilities which is kinematically allowed.

For squarks the list of possible decays is nearly identical to the gluino list (again in increasing order of coupling strength).

(i) The squark is stable, so the experimental signature is a massive stable hadron ($\tilde{q}\bar{q}$ or $\tilde{q}^* q$).

(ii) The squark decays into a quark and a Goldstino. The experimental signature in this case would be a quark jet and missing transverse momentum.

(iii) The squark decays into the lightest gaugino (presumably a photino) and a quark. The resulting signature is one jet, missing transverse momentum, and possibly a hard photon.

(iv) The squark decays into a quark and a gluino. The signature for this model depends on the subsequent decay [cases (i)—(iii) above] of the gluino. The possibilities are thus one, two, or three jets and missing transverse momentum. In the three-jet case there may be an accompanying hard photon.

Since the signatures for gluino and squark decays are so similar, we can discuss them both at once. Given the copious production rates we expect, the signatures of (a) a new stable hadron, (b) jets, missing transverse momentum, and a hard photon, and (c) clearly separated multijets and missing transverse momentum are characteristic and should be relatively free of conventional backgrounds. The most pernicious of the backgrounds would seem to be heavy-quark semileptonic decays. A charged-lepton veto may thus be useful. The most difficult signature is the case in which the superpartner decays to a single jet, or coalesced multiple jets, with missing transverse momentum carried off by undetected particles. For such events the background associated with the semileptonic decays of heavy quarks produced in the hadronization of a standard QCD jet (in a two-jet event) may be quite severe. In the background events, energy and transverse momentum may be carried away with the undetected neutrino, while the charged lepton may be buried in a hadron jet. A preliminary study of the signal-to-background problem has been reported by Littenberg (1984). His Monte Carlo analysis suggests that for gluino and squark masses in excess of 100 GeV/c^2, approximately 3000 superparticle events are required to obtain an adequate rejection of the background by introducing a series of kinematic cuts. If it were possible to recognize leptons within jets with high efficiency, fewer events would be required to establish a squark or gluino signal. The whole area of extracting squark and gluino signatures from background can clearly benefit from much more extensive modeling.

C. Production and detection of color singlet superpartners

The fermionic partners $\tilde{\gamma}$, $\tilde{Z}^0$, and $\tilde{W}^{\pm}$ of the electroweak gauge bosons and the scalar partners $\tilde{e},\tilde{\mu},\tilde{\tau},\tilde{\nu}_i$ of the leptons are produced with typical electroweak strengths. As a consequence the production cross sections are considerably smaller than those for gluinos or squarks of the same mass.

The most favorable mechanism for production of $\tilde{\gamma}$, $\tilde{Z}^0$, or $\tilde{W}^{\pm}$ is in association with a gluino or squark. The cross sections for the elementary processes

$$\begin{aligned} &q_i\bar{q}_i \to \tilde{g}\tilde{\gamma}\ , \\ &q_i\bar{q}_i \to \tilde{g}\tilde{Z}^0\ , \\ &q_u\bar{q}_d \to \tilde{g}\tilde{W}^+\ , \end{aligned} \tag{7.29}$$

are given by Eqs. (7.1) and (7.2) and the coefficients listed in Table IX. The resulting cross sections for electroweak gaugino production in pp and $\bar{p}p$ collisions are presented in Figs. 203—211. The rapidities of the superpartners are restricted to $|y_i| < 1.5$. For the purpose of these examples, we have taken all the gaugino masses to be equal, and have set the squark mass equal to the gaugino masses. While this is unlikely to be an accurate assumption, it should reliably indicate the discovery reach of a collider for exploration of high masses, because the superpartner masses are likely to be similar in order of magnitude. In Figs. 205, 208, and 211, the squark mass has been fixed at 0.5 TeV/c^2.

We show in Figs. 203—205 the cross sections for gluino-photino associated production in pp collisions

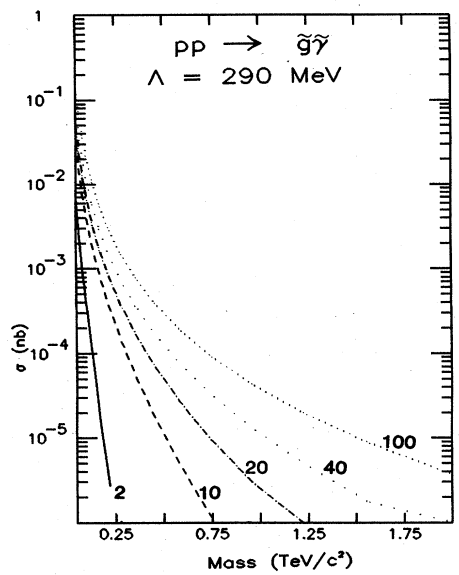

FIG. 203. Cross sections for the reaction $pp \to \tilde{g}\tilde{\gamma} +$ anything as a function of the photino mass, for collider energies $\sqrt{s} = 2$, 10, 20, 40, and 100 TeV, according to the parton distributions of Set 2. Both gluino and photino are restricted to the rapidity interval $|y_i| < 1.5$. For this illustration, all squark and gaugino masses are taken to be equal.

(based on the parton distributions of Set 2), in $\bar{p}p$ collisions, and in pp collisions ($M_{\tilde{q}} = 500$ GeV/c^2). Under the assumptions we have made here, the $\bar{p}p$ cross section significantly exceeds the pp cross section for gaugino masses larger than about $\sqrt{s}/20$. This corresponds to the familiar value of $\sqrt{\tau} \gtrsim 0.1$, which we have encountered in other reactions that proceed through $q\bar{q}$ interactions. There are no significant differences between the two sets of parton distributions in this case. Similar comments apply to the rates for $\tilde{g}\tilde{Z}^0$ production (Figs. 206–208) and for $\tilde{g}\tilde{W}^+ + \tilde{g}\tilde{W}^-$ production (Figs. 209–211). We note that the cross sections are substantial for a broad range of gaugino masses. We shall discuss observability below.

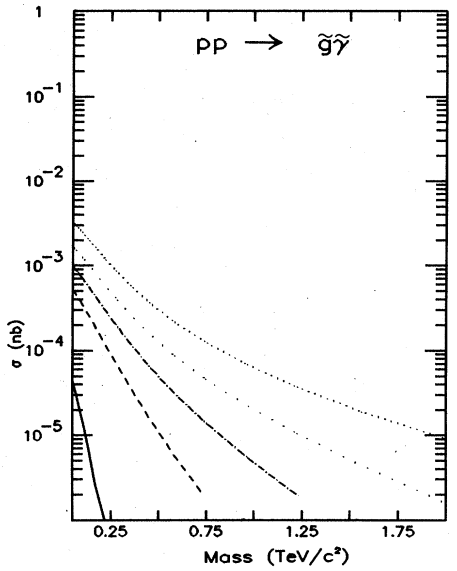

FIG. 205. Cross sections for the reaction $pp \to \tilde{g}\tilde{\gamma} +$ anything as a function of the photino mass, according to the parton distributions of Set 2. Cuts and parameters are as in Fig. 203, except that $M_{\tilde{q}} = 0.5$ TeV/c^2.

The elementary cross sections for associated production of gauginos and squarks in the reactions

$$gq \to \tilde{\gamma}\tilde{q}\,, \quad gq \to \tilde{Z}^0\tilde{q}\,, \quad gq \to \tilde{W}\tilde{q}\,, \tag{7.30}$$

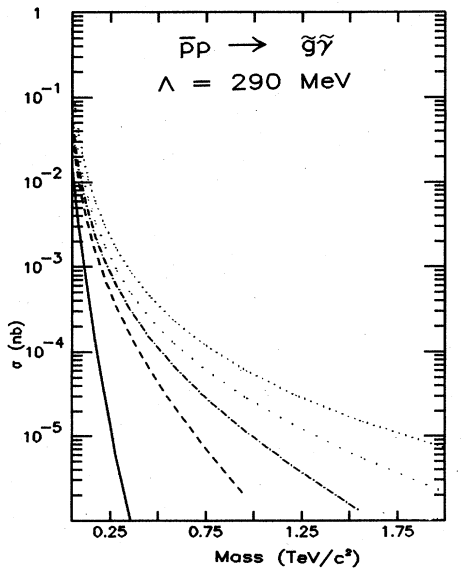

FIG. 204. Cross sections for the reaction $\bar{p}p \to \tilde{g}\tilde{\gamma} +$ anything as a function of the photino mass, according to the parton distributions of Set 2. Cuts and parameters are as in Fig. 203.

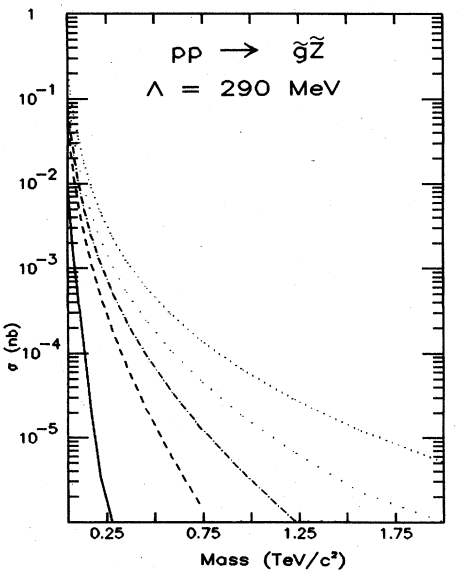

FIG. 206. Cross sections for the reaction $pp \to \tilde{g}\tilde{Z} +$ anything as a function of the zino mass, according to the parton distributions of Set 2. Cuts and parameters are as in Fig. 203.

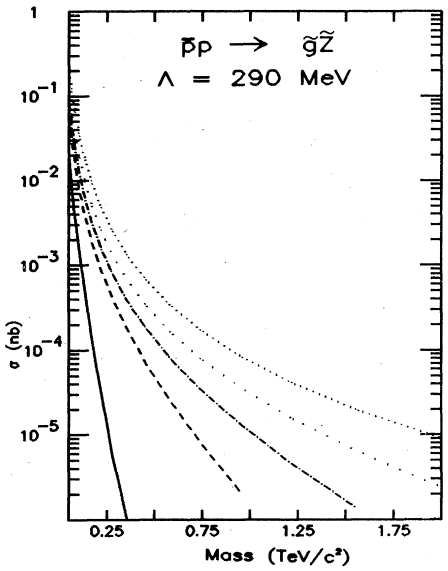

FIG. 207. Cross sections for the reaction $\bar{p}p \to \tilde{g}\tilde{Z} +$ anything as a function of the zino mass, according to the parton distributions of Set 2. Cuts and parameters are as in Fig. 203.

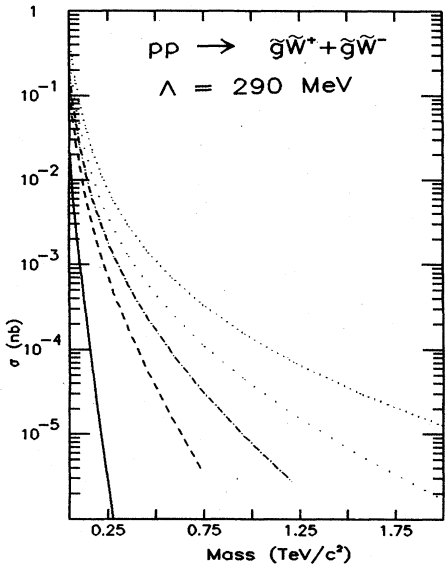

FIG. 209. Cross sections for the reaction $pp \to \tilde{g}\tilde{W}^{\pm} +$ anything as a function of the wino mass, according to the parton distributions of Set 2. Cuts and parameters are as in Fig. 203.

are given by Eq. (7.9) and Table X. To arrive at the total cross sections we sum over up and down squarks and antisquarks and continue to assume that all relevant squark and gaugino masses are equal. The resulting cross sections are shown for $pp \to \tilde{\gamma}\tilde{q}$ in Fig. 212, for $pp \to \tilde{Z}^0\tilde{q}$ in Fig. 213, and for $pp \to \tilde{W}^{\pm}\tilde{q}$ in Fig. 214. The cross sections in $\bar{p}p$ collisions are identical. These rates are somewhat larger than those for production of an electroweak gaugino in association with a gluino. For some values of the superparticle masses, gaugino-squark production is the more important process because of the additional s-channel quark-exchange diagram. In view of the similarity of the cross sections and the event signatures for the gluino-gaugino and squark-gaugino final states, it will suffice to consider only one case explicitly.

For our survey of decay modes and superparticle signatures we shall assume that the photino is the lightest of the superpartners. It will therefore either be stable or decay into a photon and a Goldstino. Since the photino decay will result in a hard photon plus missing transverse

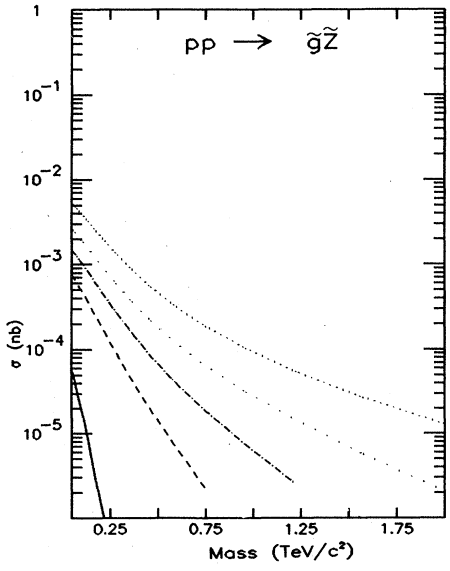

FIG. 208. Cross sections for the reaction $pp \to \tilde{g}\tilde{Z} +$ anything as a function of the zino mass, according to the parton distributions of Set 2. Cuts and parameters are as in Fig. 203, except that $M_{\tilde{q}} = 0.5$ TeV/c^2.

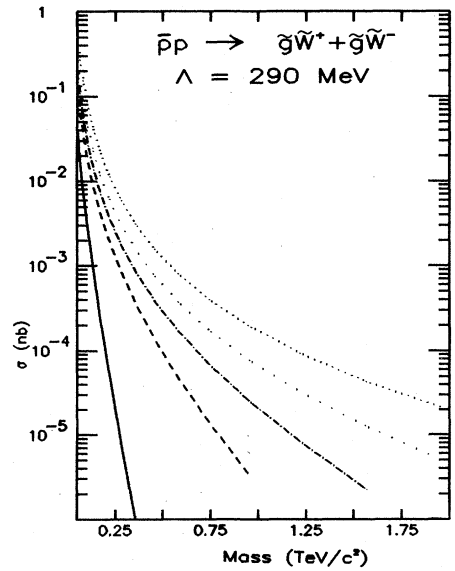

FIG. 210. Cross section for the reaction $\bar{p}p \to \tilde{g}\tilde{W}^{\pm} +$ anything as a function of the wino mass, according to the parton distributions of Set 2. Cuts and parameters are as in Fig. 203.

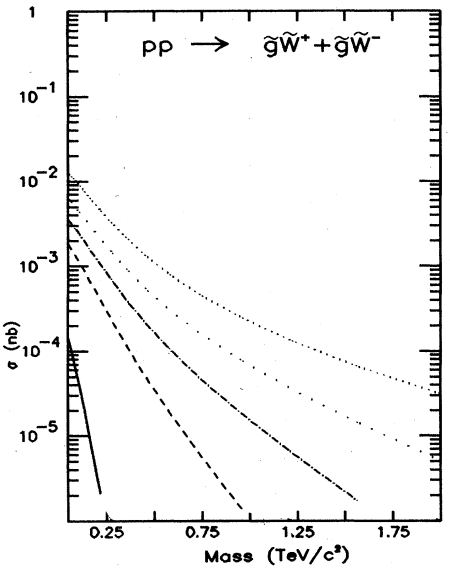

FIG. 211. Cross sections for the reaction $pp \to \tilde{g}\tilde{W}^{\pm}$ + anything as a function of the wino mass, according to the parton distributions of Set 2. Cuts and parameters are as in Fig. 203, except that $M_{\tilde{q}}=0.5$ TeV/c^2.

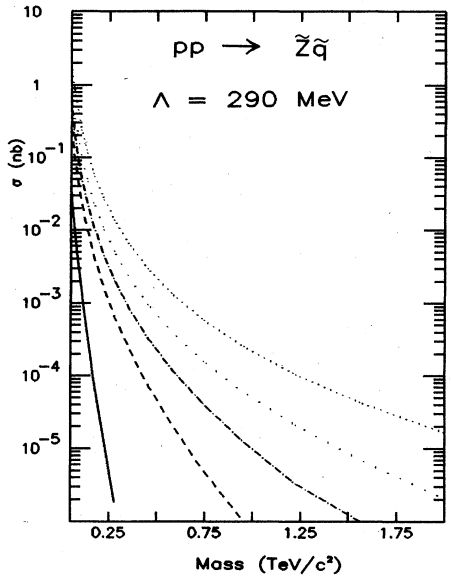

FIG. 213. Cross sections for associated production of a zino and a squark in $p^{\pm}p$ collisions as a function of the zino mass, according to the parton distributions of Set 2. Cuts and parameters are as in Fig. 212.

momentum, it should be detectable with high efficiency. We will focus our analysis on the more difficult signature of a stable photino.

Photino-gluino (or, equivalently, photino-squark) events will display a striking signature: they are one-sided events. The gluino (or squark) will produce one or more jets, possibly with missing transverse momentum, on one side of the beam axis, while the photino will escape undetected on the opposite side. Such events are essentially free of conventional background, so that 100 $\tilde{\gamma}\tilde{g}$ pairs should suffice to establish a signal. Confirmation that the signal represents the gluino-photino channel, as opposed to some other unexpected new phenomenon, may require an extended analysis.

The decay modes of $\tilde{W}^{\pm}$ and $\tilde{Z}^0$ are considerably more complex, and will not produce as striking a signa-

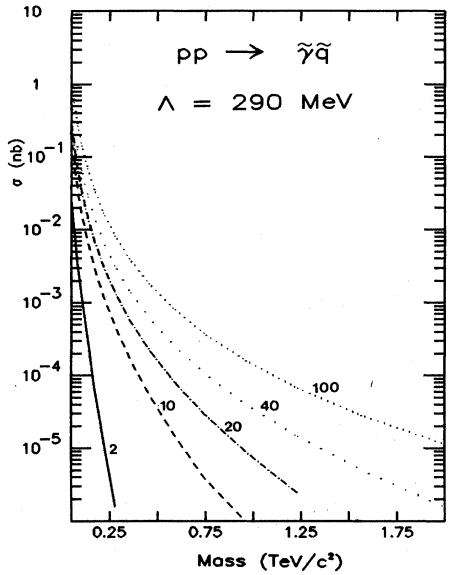

FIG. 212. Cross sections for associated production of a photino and up or down squark or antisquark in $p^{\pm}p$ collisions as a function of the photino mass, for collider energies $\sqrt{s}=2$, 10, 20, 40, and 100 TeV, according to the parton distributions of Set 2. For this illustration we set the squark mass equal to the gaugino mass. Both squark and photino are restricted to the rapidity interval $|y_i| < 1.5$.

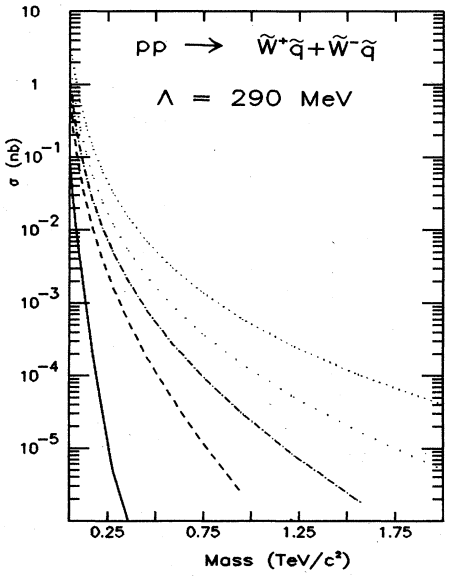

FIG. 214. Cross sections for associated production of a $\tilde{W}^+$ or $\tilde{W}^-$ and a squark in pp collisions as a function of the wino mass, according to the parton distributions of Set 2. Cuts and parameters are as in Fig. 212.

ture as a stable or unstable photino. The possible decay modes of the weak gauginos are

$$\tilde{W}^+ \rightarrow \begin{cases} l^+\tilde{\nu}_l \\ \tilde{l}^+\nu_l \\ q_u\tilde{\bar{q}}^*_d \\ \tilde{q}_u\bar{q}_d \\ W^+\tilde{\gamma} \\ W^+\tilde{Z} \end{cases} \tag{7.31}$$

and

$$\tilde{Z}^0 \rightarrow \begin{cases} l^\pm\tilde{l}^\mp \\ \nu\tilde{\bar{\nu}}^* \\ \bar{\nu}\tilde{\nu} \\ q\tilde{\bar{q}}^* \\ \bar{q}\tilde{q} \\ W^\pm\tilde{W}^\mp . \end{cases} \tag{7.32}$$

After the decays of all superpartners, the signatures for the $\tilde{W}^\pm$ and $\tilde{Z}^0$ involve missing transverse momentum in association with hadron jets, or leptons, or both. For the gaugino decays involving jets the important background processes are the same as in the case of squark and gluino production, but the signal is about 100 times smaller. Such decays will be very difficult to observe. However, the leptonic decays of $\tilde{W}^\pm$ and $\tilde{Z}^0$ may be more easily observable. In particular, the decay

$$\tilde{Z}^0 \rightarrow \tilde{l}^\pm l^\mp \\ \quad \hookrightarrow l^\pm\tilde{\gamma}$$

yields a pair of charged leptons and missing transverse momentum, while the decay

$$\tilde{W}^\pm \rightarrow \tilde{l}^\pm\nu \\ \quad \hookrightarrow l^\pm\tilde{\gamma}$$

leads to a single charged lepton and large missing transverse momentum.

Without a model for the masses of squarks, sleptons, and gauginos, it is not possible to know the branching ratios for these decays. If we assume that the squark and slepton masses are negligible compared to the weak gaugino masses, and that the decays $\tilde{W}^\pm \rightarrow W^\pm\tilde{Z}^0$ and $\tilde{Z}^0 \rightarrow \tilde{W}^\pm W^\mp$ are kinematically forbidden, then the branching ratio for the decay $\tilde{Z}^0 \rightarrow l^\pm\tilde{l}^\mp$ will be the same ($\sim 3\%$) as that for $Z^0 \rightarrow l^+l^-$. The decay rate for $\tilde{W}^\pm \rightarrow l^\pm\nu\tilde{\gamma}$ will receive contributions from $\tilde{l}^\pm\nu$ and $W^\pm\tilde{\gamma}$ channels. Consequently the branching ratio should lie in the range 4—8 % (for three fermion generations).

The conventional background to the signals for the $\tilde{g}\tilde{W}$ or $\tilde{q}\tilde{W}$ and $\tilde{g}\tilde{Z}$ or $\tilde{q}\tilde{Z}$ final states arises from the $W+$ jet and $Z+$ jet events that occur as QCD corrections to the Drell-Yan process. The anticipated rates for the $W+$ jet background have been given in Fig. 118. If the $\tilde{W}^\pm$ and $\tilde{Z}^0$ masses exceed about 150 GeV/c, it appears relatively straightforward to distinguish signal from background. It is worth examining this background in a little more detail for the wino-gluino and wino-squark final states.

A prominent characteristic of the $\tilde{W}^\pm\tilde{g}$ or $\tilde{W}^\pm\tilde{q}$ events in which the wino decays ultimately into a charged lepton, a neutrino, and an undetected superparticle is their large missing transverse momentum. If for illustration we assign to the wino and gluino or squark a common mass M, the events will consist of

(a) the jet arising from gluino or squark decay, with visible energy $E_\perp^{\text{jet}} \gtrsim M/2$;
(b) the charged lepton from wino decay, with energy $E_\perp^{\text{lepton}} \gtrsim M/2$;
(c) unbalanced or "missing" transverse momentum $p_\perp^u \gtrsim M/\sqrt{2}$.

The total energy inferred for these events is thus

$$E_\perp^{\text{total}} \gtrsim 1.7M . \tag{7.33}$$

The signal must be compared with background $W+$ jet events for which the inferred transverse energy

$$E_\perp = p_\perp + (p_\perp^2 + M_{\tilde{W}}^2)^{1/2} \tag{7.34}$$

exceeds the value (7.33). For $M > M_W$, this corresponds to events with

$$p_\perp^{\min} \gtrsim 0.8M . \tag{7.35}$$

The potential background given by

$$\int_{p_\perp^{\min}}^{\infty} dp_\perp \int_{-1.5}^{1.5} dy \frac{d\sigma}{dp_\perp dy}(p^\pm p \rightarrow W^\pm + \text{jet})$$

is typically a few hundred times larger than the signal defined by

$$\int_{-1.5}^{1.5} dy \frac{d\sigma}{dy}(p^\pm p \rightarrow \tilde{W}^\pm + \tilde{g} \text{ or } \tilde{q}) .$$

However, for $M > M_W$, a transverse mass cut should effectively eliminate the background events. We define the transverse mass by

$$M_\perp^2 = 2p_\perp^{\text{lepton}} p_\perp^u (1 - \cos\theta) , \tag{7.36}$$

where θ is the angle between the transverse momentum of the charged lepton and the missing transverse momentum. Apart from the effect of missing momentum due to heavy-quark semileptonic decays in the opposing jet, the transverse mass of the background events would be strictly bounded by M_W in an ideal detector:

$$M_\perp^2 \mid_{bgd} < M_W^2 , \tag{7.37}$$

and the transverse mass distribution would peak around $M_W/2$. Imposing a cut $M_\perp^2 \gtrsim M_W^2$ would thus eliminate the background, while preserving much of the signal for a wino more massive than the intermediate boson. Although this is clearly a case which calls for detailed

Monte Carlo simulation, it is plausible that for $M \gtrsim 2M_W$ a transverse mass cut will yield an extremely pure sample of wino events.

The cross sections for pair production of electroweak gauginos are smaller than the gluino plus electroweak gaugino cross sections by a factor of approximately α/α_s. We show in Figs. 215 and 216 the total cross sections for the reactions

$$pp \to \tilde{\gamma}\tilde{Z} + \text{anything} \tag{7.38}$$

and

$$pp \to \tilde{\gamma}\tilde{W}^{+} + \text{anything}\,, \tag{7.39}$$

respectively. These have the same sort of signature as the photino-gluino channel: they are one-sided events. If the $\tilde{W}^{\pm}$ or $\tilde{Z}$ decays into quarks and squarks, it will be quite difficult to distinguish these events from $\tilde{\gamma}\tilde{g}$ events. The leptonic decay modes of the gauginos should provide an extremely distinctive signature. A potential background to the lepton signal arises from γZ or $\gamma W^{\pm}$ events in which the photon escapes detection.

The total cross section for the reaction

$$pp \to \tilde{\gamma}\tilde{\gamma} + \text{anything} \tag{7.40}$$

is shown in Fig. 217. If the photino is stable, this process may well be unobservable in the collider environment. If instead the photino decays to a photon and Goldstino, the signature of two hard photons with missing (hence unbalanced) transverse momentum.

Figures 218–220 present the cross sections for the reactions

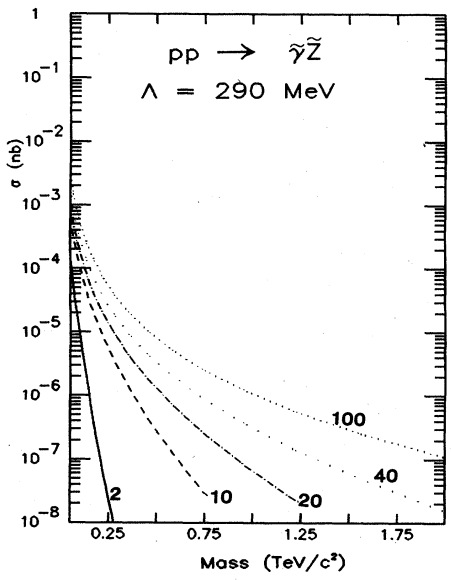

FIG. 215. Cross sections for associated production of a photino and zino in pp collisions as a function of the common gaugino mass, for collider energies $\sqrt{s} = 2$, 10, 20, 40, and 100 TeV, according to the parton distributions of Set 2. Both gauginos are restricted to the rapidity interval $|y_i| < 1.5$. For this illustration, the squarks and gauginos are assigned a common mass.

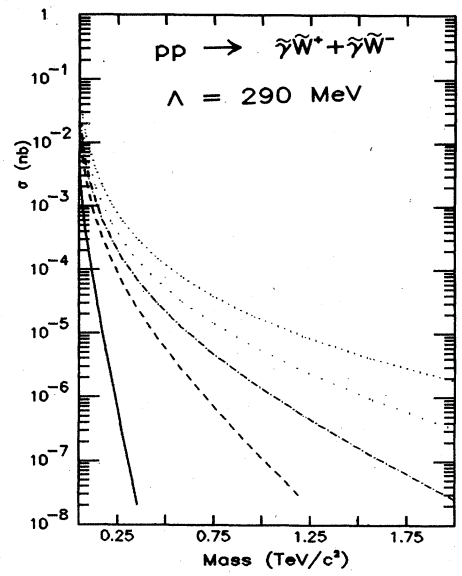

FIG. 216. Cross sections for associated production of a photino and $\tilde{W}^{+}$ or $\tilde{W}^{-}$ in pp collisions as a function of the common gaugino mass, according to the parton distributions of Set 2. Cuts and parameters are as in Fig. 215.

$$pp \to \tilde{Z}\tilde{Z} + \text{anything}\,, \tag{7.41}$$

$$pp \to \tilde{Z}\tilde{W}^{+} + \text{anything}\,, \tag{7.42}$$

and

$$pp \to \tilde{W}^{+}\tilde{W}^{-} + \text{anything}\,, \tag{7.43}$$

which are in general 10–20 times smaller than the corresponding associated production process with a gluino or

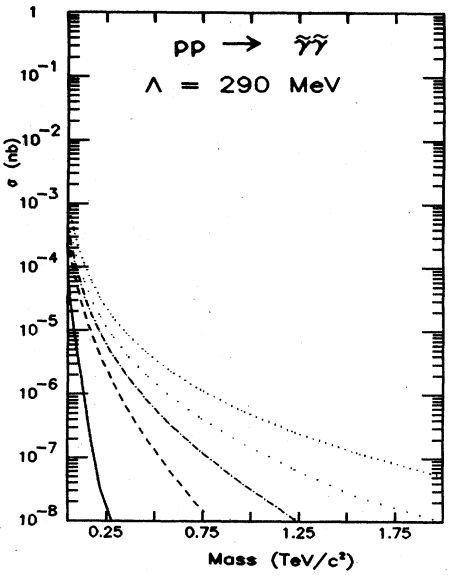

FIG. 217. Cross sections for pair production of photinos in pp collisions as a function of the photino mass, according to the parton distributions of Set 2. Cuts and parameters are as in Fig. 215.

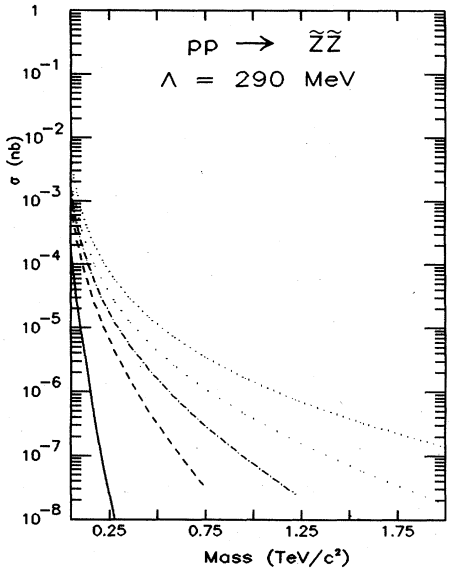

FIG. 218. Cross sections for pair production of zinos in *pp* collisions as a function of the zino mass, according to the parton distributions of Set 2. Cuts and parameters are as in Fig. 215.

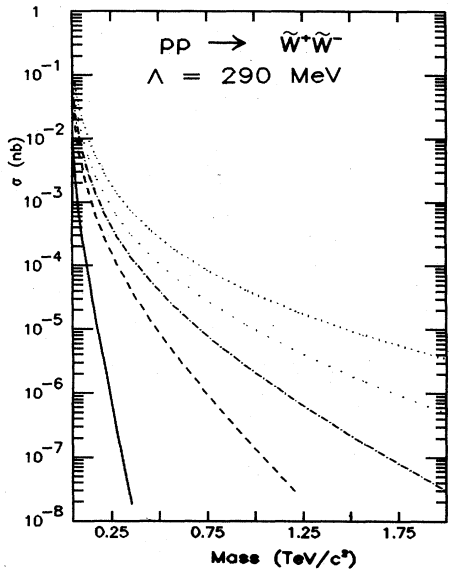

FIG. 220. Cross sections for $\tilde{W}^+\tilde{W}^-$ production in *pp* collisions as a function of the wino mass, according to the parton distributions of Set 2. Cuts and parameters are as in Fig. 215.

squark. Furthermore, to definitively identify these final states would require the observation of both gauginos in their leptonic decay modes, at the price of two branching ratios. Thus these processes do not appear to provide the most promising approach to the discovery of $\tilde{W}^{\pm}$ and $\tilde{Z}^0$.

Finally, we turn to the pair production of the scalar partners of leptons, for which the elementary reaction is a simple generalization of the usual Drell-Yan process. The cross section for the reaction

$$q\bar{q}\to\tilde{l}\tilde{l}^* , \tag{7.44}$$

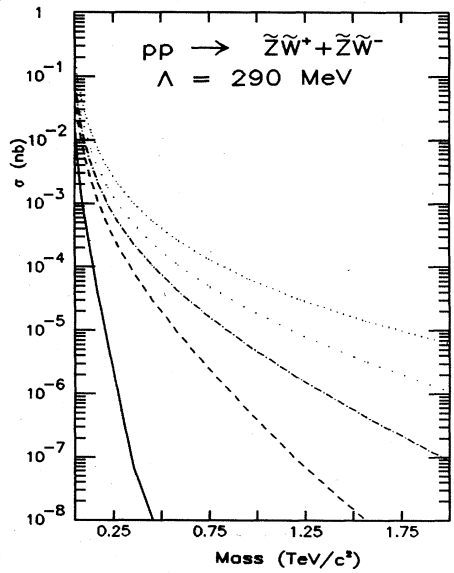

FIG. 219. Cross sections for $\tilde{W}^{\pm}Z^0$ production in *pp* collisions as a function of the common gaugino mass, according to the parton distributions of Set 2. Cuts and parameters are as in Fig. 215.

summed over left- and right-handed sleptons (assumed degenerate in mass) is given by (7.19)—(7.21). Some restrictions on the $\tilde{e}_L-\tilde{e}_R$ mass difference have been given by Hinchliffe and Littenberg (1982). The implied rates for the reactions

$$p^{\pm}p\to\tilde{l}\tilde{l}^*+\text{anything} \tag{7.45}$$

are displayed in Figs. 221 and 222, respectively, for the parton distributions of Set 2. The cross sections that fol-

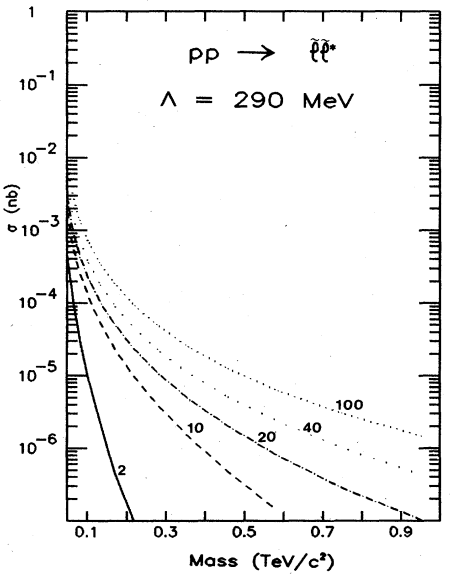

FIG. 221. Cross sections for the reaction $pp\to\tilde{l}\tilde{l}^*$ + anything as a function of the slepton mass, for collider energies $\sqrt{s}=2$, 10, 20, 40, and 100 TeV, according to the parton distributions of Set 2. Both sleptons are restricted to lie in the rapidity interval $|y_i|<1.5$.

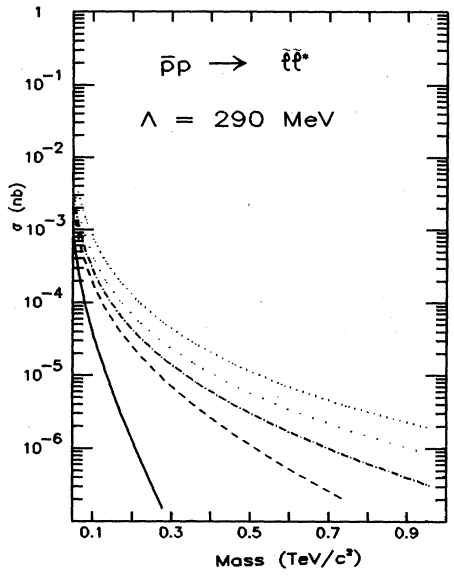

FIG. 222. Cross sections for the reaction $\bar{p}p \rightarrow \tilde{l}\tilde{l}^* +$ anything as a function of the slepton mass, according to the parton distributions of Set 2. Cuts and parameters are as in Fig. 221.

low from Set 1 are nearly identical. For the decay $\tilde{l}^{\pm} \rightarrow l^{\pm}\tilde{\gamma}$, where the photino goes unobserved, the upper limit on the mass of an observable slepton will be comparable to that inferred in Sec. V for sequential heavy leptons.

D. Summary

If supersymmetry is to be relevant to the solution of the hierarchy problem, and thus to the physics of the electroweak scale, then the supersymmetric partners of the known fundamental fields must have masses that are no more than a few times the scale $(G_F\sqrt{2})^{-1/2}=247$ GeV/c^2 of electroweak symmetry breaking. It is important that the supercollider permit a comprehensive search for evidence of supersymmetric particles.

Our estimates show that the supersymmetric partners of the quarks and gluons will be produced copiously, even for masses in excess of 1 TeV/c^2. Detection of squarks and gluinos is a more difficult consideration. For some of the most plausible gluino and squark decay modes there can be substantial backgrounds from conventional physics processes. A relatively large event sample will therefore be required for discovery. A rough analysis suggests (Littenberg, 1984) that 10^3—10^4 gluinos or squarks would be needed to establish a signal above these backgrounds. Adopting 10^4 events produced in the rapidity interval $-1.5 \leq y \leq 1.5$ as a reasonable discovery criterion for gluinos, we show in Fig. 223 the maximum gluino masses accessible in pp colliders of varying c.m. energies and integrated luminosities. The discovery limits for squarks deduced under the same assumptions, are shown in Fig. 224. In these two cases, we find no significant differences between pp and $\bar{p}p$ collisions at the same energy and luminosity. New analysis techniques and more effective experimental cuts may reduce considerably the number of events required to establish a signal.

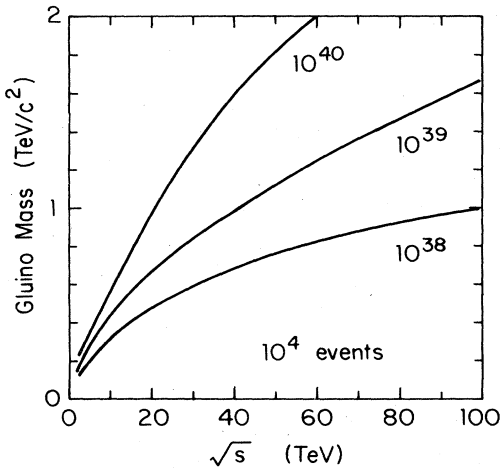

FIG. 223. "Discovery limits" for gluinos in pp and $\bar{p}p$ collisions. Contours show the largest mass for which 10^4 gluino pairs are produced with $|y_i| < 1.5$, for specified energy and integrated luminosity (in cm^{-2}). The parton distributions of Set 2 were used.

The smaller production cross sections of the electroweak gauge fermions are in general compensated for by cleaner signatures. The associated production of a photino and a squark or gluino has the most characteristic signature: a "one-sided" event. We estimate that fewer than 100 such events would be required for discovery. The rates for associated production of a zino or wino with a squark or gluino are comparable to the photino production rate, but detection is probably more challenging. The signature consists of leptons and missing $p_\perp$ in one hemisphere, with jets in the opposite hemisphere. We judge that 1000 events of this kind should suffice for discovery. Discovery limits for photinos, zinos, and winos are

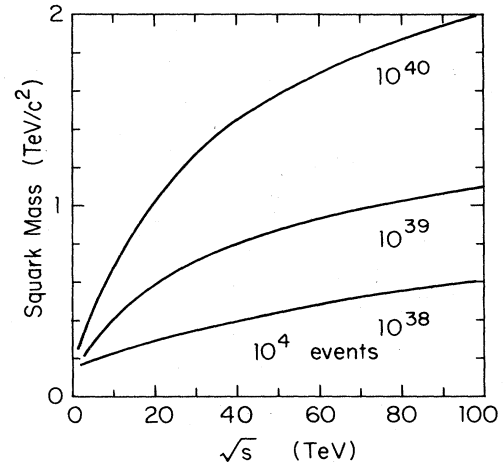

FIG. 224. "Discovery limits" for squarks in pp and $\bar{p}p$ collisions. Contours show the largest mass for which 10^4 squark pairs are produced with $|y_i| < 1.5$, for specified energy and integrated luminosity (in cm^{-2}). The parton distributions of Set 2 were used.

presented in Figs. 225–227 which are based on the gaugino-gluino cross sections with $M_{\tilde{q}}=M_{\text{gaugino}}$. In this case, there is at high luminosity a considerable advantage to proton-antiproton collisions because of the higher $q\bar{q}$ luminosity. The effect is largest for $\tilde{\gamma}$ production, which favors $u\bar{u}$ collisions, and smallest for $\tilde{Z}$ production, which favors $d\bar{d}$ collisions. This reflects the difference between the valence-parton distributions $u_v(x)$ and $d_v(x)$. The limits deduced from gaugino-squark–associated production are the same for pp and $\bar{p}p$ colliders. They are shown as dotted lines in Figs. 225–227. The limits are slightly better than those obtained from gaugino-gluino final states.

Finally, we considered the pair production of charged sleptons in hadron colliders. The production process is essentially the familiar Drell-Yan mechanism, and detection of the resulting acoplanar lepton pairs should be relatively straightforward. As few as 100 slepton pairs might suffice for discovery. However, because of the small production cross section, the discovery limits shown in Fig. 228 are only a few hundred GeV/c^2. Because of the relatively low masses involved, there are no significant differences between pp and $\bar{p}p$ collisions.

We infer from Figs. 223–228 that a 40-TeV $p^{\pm}p$ collider with integrated luminosity exceeding 10^{39} cm^{-2} should be adequate to establish the presence or absence of the superpartners predicted by models of low-energy supersymmetry.

VIII. COMPOSITE QUARKS AND LEPTONS

The proliferation of quarks and leptons has inspired the speculation that they are composite structures, bound states of more fundamental constituents often called preons. The basic assumption that underlies almost all composite model building is that the constituent preons interact by means of a new strong gauge interaction, sometimes called metacolor. According to current theoretical ideas, the non-Abelian metacolor theory should be asymptotically free and infrared confining. Below a characteristic energy scale Λ^*, the metacolor interaction becomes strong and binds the preons into metacolor-singlet states including the observed quarks and leptons. In this way, the idea of composite quarks and leptons may be seen as a natural extension of the technicolor strategy for composite Higgs scalars.

As we shall make precise below, there is no experimen-

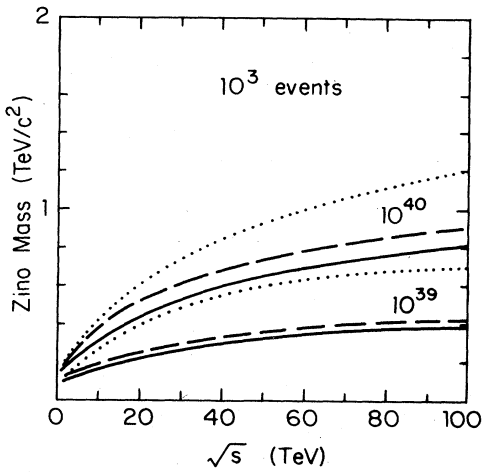

FIG. 226. "Discovery limits" for zinos produced in association with gluinos in pp (solid lines) or $\bar{p}p$ (dashed lines) collisions, or in association with squarks (dotted lines). Contours show the largest mass for which 10^3 zinos are produced with $|y_i|<1.5$, for specified energy and integrated luminosity (in cm^{-2}). The parton distributions of Set 2 were used.

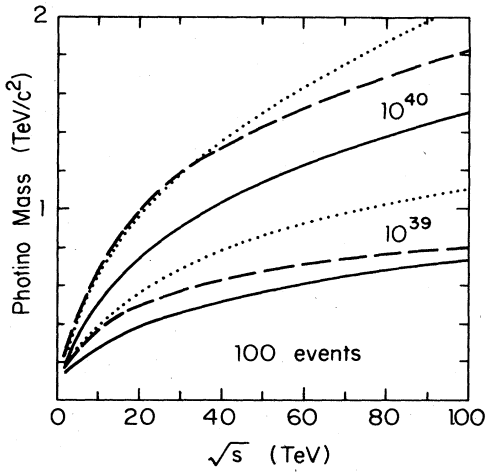

FIG. 225. "Discovery limits" for photinos produced in association with gluinos in pp (solid lines) or $\bar{p}p$ (dashed lines) collisions, or in association with squarks (dotted lines). Contours show the largest mass for which 100 photinos are produced with $|y_i|<1.5$, for specified energy and integrated luminosity (in cm^{-2}). The parton distributions of Set 2 were used.

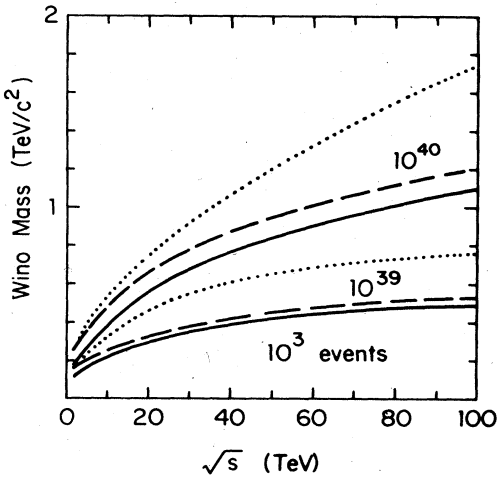

FIG. 227. "Discovery limits" for winos produced in association with gluinos in pp (solid lines) or $\bar{p}p$ (dashed lines) collisions, or in association with squarks (dotted lines). Contours show the largest mass for which 10^3 winos are produced with $|y_i|<1.5$, for specified energy and integrated luminosity (in cm^{-2}). The parton distributions of Set 2 were used.

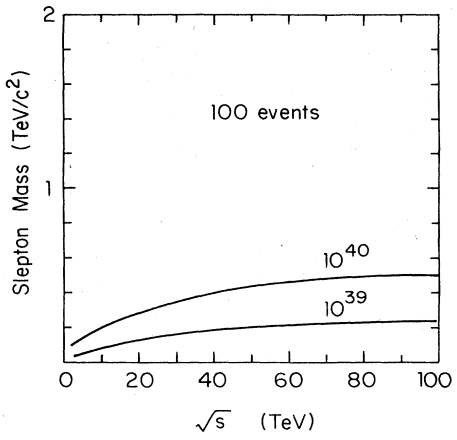

FIG. 228. "Discovery limits" for sleptons in pp and $\bar{p}p$ collisions. Contours show the maximum mass for which 100 slepton pairs are produced with $|y_i| < 1.5$, for specified energy and integrated luminosity (in cm^{-2}). The parton distributions of Set 2 were used.

tal indication of quark or lepton structure on a scale of 10^{-16} cm. As a consequence, the metacolor scale Λ^* cannot be much less than the electroweak scale $(G_F/\sqrt{2})^{-1/2}$. This means that the masses of the quarks and leptons are very much smaller than the characteristic scale of their compositeness.

In general, it is the scale Λ^* which determines the masses of composite states. However, there are special circumstances in which some composite states will be exactly or approximately massless compared to the scale Λ^*. The Goldstone (1961) theorem asserts that a massless spin-zero particle arises as a consequence of the spontaneous breakdown of a continuous global symmetry. For example, if the up and down quarks were massless, the ordinary $SU(3)_{color}$ strong interactions would be invariant under an exact $SU(2)_L \otimes SU(2)_R$ chiral symmetry. This symmetry is spontaneously broken down to a vectorial $SU(2)_V$ symmetry by the strong interactions, and massless pions appear as a consequence of the Goldstone theorem. In the real world, electromagnetic interactions as well as small bare masses of the up and down quarks explicitly break the chiral symmetries, so that the pions acquire small masses.

Recently, 't Hooft (1980) has pointed out that under certain special conditions, confining theories which possess global chiral symmetries may lead to the existence of massless composite fermions when the chiral symmetries are not spontaneously broken. We shall not discuss these conditions in detail here, but simply remark that 't Hooft's mechanism provides a consistent theoretical framework in which to understand how composite fermions can be massless. In analogy with the case of the pions, we may suppose that a small bare mass for the preons, or preon weak interactions that explicitly break the chiral symmetries, can account for the observed masses of quarks and leptons. Theoretical ideas on compositeness and the experimental implications of composite models have been reviewed recently by Peskin (1981), Abolins *et al.* (1982), Harari (1982), Lyons (1983a, 1983b), and Barbieri (1983).

For the ensuing analysis, we shall assume the standard $SU(3)_c \otimes SU(2)_L \otimes U(1)_Y$ gauge theory for quarks and leptons. We shall thus not consider the interesting possibility that the gluons and intermediate bosons are composite particles. The implications for collider physics of models in which $W^{\pm}$ and Z^0 are composite have been considered by Abbott, Farhi, and Tye (1982) and by Leurer, Harari, and Barbieri (1984).

The remainder of this section is organized as follows. In Sec. VIII.A we discuss the signals for compositeness in general terms. These signals take different forms, depending upon the subprocess energy $\sqrt{\hat{s}}$ relative to the characteristic compositeness scale Λ^*. When $\sqrt{\hat{s}}$ exceeds Λ^*, the manifestations of compositeness are very direct and need not be discussed at length. The consequences of compositeness are more subtle when $\sqrt{\hat{s}}$ is small compared with Λ^*. Therefore, we focus in Secs. VIII.B and VIII.C on the signals which will be prominent for $\sqrt{\hat{s}} \lesssim \Lambda^*$. Section VIII.B is devoted to composite effects in high transverse momentum jets, and Sec. VIII.C is concerned with modifications to the Drell-Yan process for the production of massive pairs of leptons. A summary of our results is given in Sec. VIII.D.

A. Manifestations of compositeness

No obviously correct or compelling model of composite quarks and leptons has yet emerged. Indeed, no consensus has been achieved even on the most fundamental aspect of substructure, the compositeness scale Λ^*. Within the context of the technicolor models discussed in Sec. VI, it is natural to extend the theory to allow for the possibility that quarks and leptons are composite, since a new strong interaction has already been introduced to account for a composite Higgs sector. In such models the scale Λ^* may lie not far above the electroweak scale. Nevertheless, there are nearly as many conjectures for the compositeness scale as there are proposals for composite models themselves (Peskin, 1981; Abolins *et al.*, 1982; Harari, 1982; Abbott, Farhi, and Tye, 1982; Barbieri, 1983). It is even conceivable that different compositeness scales apply to various fermion species. Therefore, it is important to consider those signals which are most sensitive to the presence of substructure in the widest possible variety of models. To begin to see how this may be done, let us catalog the major signals for compositeness of the light fermions.

The most striking indications that the quarks and leptons are composite would occur at subenergies $\sqrt{\hat{s}}$ of a few times the characteristic compositeness scale Λ^*. At these energies, multiple production processes would dominate over the familiar two-body parton-scattering processes. Examples of the sort of inelastic processes that may occur for a $u\bar{u}$ initial state are

$$u\bar{u}\rightarrow\begin{cases} u\bar{u}u\bar{u} \\ u\bar{u}l\bar{l} \\ b\bar{b}t\bar{t} \\ e^+e^-\mu^+\mu^- \\ q^*\bar{q}^* \ , \end{cases} \tag{8.1}$$

where q^* denotes an excited state with exotic color quantum numbers. Similar possibilities may exist for other quark-quark, quark-antiquark, or antiquark-antiquark initial states. Which processes actually occur is a highly model-dependent question. What can be said in general is that the cross section for the allowed inelastic processes will be geometrical in magnitude, of order $4\pi/\Lambda_*^2$. As a result, these unconventional events—multijets, jets with leptons, and multileptons—will completely dominate the standard $SU(3)_c\otimes SU(2)_L\otimes U(1)_Y$ processes, for which cross sections go roughly as $\pi\alpha_i^2/\hat{s}$.

If the compositeness scale lies just above the current bounds, spectacular signals of the kind we have just discussed may be expected at the supercollider. If instead the accessible subenergies $\sqrt{\hat{s}}$ are less than Λ^*, the departures from the standard model will be quantitative rather than qualitative. Several approaches are potentially of interest.

The classic test for substructure is to search for form factor effects, that is, deviations from the expected point-like behavior in gauge-field propagators and fermion vertices (Chanowitz and Drell, 1973). Such deviations would occur in any composite model, as a consequence of the vector dominance mechanism depicted in Fig. 229. In a favored parametrization of this effect, the gauge field propagator is modified by a factor

$$F(Q^2)=1+Q^2/\Lambda^{*2} \ , \tag{8.2}$$

where Q is the four momentum carried by the gauge field. Measurements of the reactions

$$e^+e^-\rightarrow\begin{cases} q\bar{q} \\ l^+l^- \end{cases} \tag{8.3}$$

at PETRA at c.m. energies up to 35 GeV have ruled out photon form factors for $\Lambda^*<100$—200 GeV (Branson, 1981; Brandelik *et al.*, 1982), and hence have excluded quark or lepton structure on or below this scale.

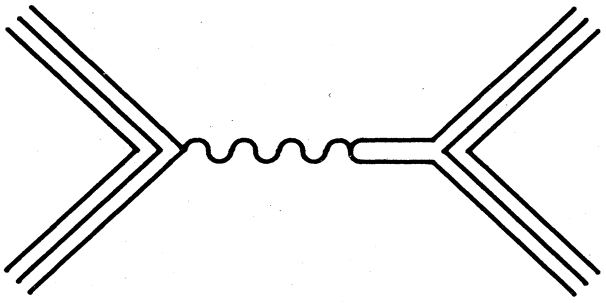

FIG. 229. Modification of gauge-boson interactions with fermions due to spin-1 bound states of preons.

Many other tests of compositeness can be carried out in the study of small effects or rare processes at low energies. For example, if a composite fermion f is naturally light because of 't Hooft's mechanism, there will arise a contribution to its anomalous magnetic moment of order $(m_f/\Lambda^*)^2$ (Barbieri, Maiani, and Petronzio, 1980; Brodsky and Drell, 1980). The agreement between the QED prediction and the measured value of $(g-2)_\mu$ (Calmet *et al.*, 1977; Combley, Farley, and Picasso, 1981) implies that

$$\Lambda^*\gtrsim 670 \text{ GeV} \tag{8.4}$$

for the muon. This is the only constraint on Λ^* from anomalous moments that improves the limits from reactions (8.3). A second class of tests relies on the existence in composite models of new effective four-fermion contact interactions at energies small compared to Λ^*. These effective point interactions are the low-energy manifestations of the constituent-interchange processes indicated in Fig. 230. If the contact interactions mediate flavor-changing transitions such as $K_L^0\rightarrow\mu e$ and $K^0-\bar{K}^0$ or $D^0-\bar{D}^0$ mixing, experimental constraints impose lower limits on Λ^*, ranging from 100 to 3000 TeV (Abolins *et al.*, 1982; Kane and Shrock, 1983). While these bounds are very impressive, the existence and form of flavor-changing contact terms is a highly model-dependent issue. It is possible (Bars, 1982) to construct models in which at least some of the dangerous flavor-changing interactions are absent. In such models, the bounds cited above lose their force.

Even if flavor-changing contact interactions are avoided, there is no way to eliminate all flavor-conserving contact terms, because identical quarks necessarily have common constituents. More precisely, in any model in which one or both chiral components of the fermion f is composite, there must occur flavor-diagonal contact interactions due to the strong metacolor forces of the form (Eichten, Lane, and Peskin, 1983)

$$\begin{aligned}\mathscr{L}_{ff}=(g^2/2\Lambda^{*2})(\ &\eta_{LL}\bar{f}_L\gamma^\mu f_L\bar{f}_L\gamma_\mu f_L \\ &+\eta_{RR}\bar{f}_R\gamma^\mu f_R\bar{f}_R\gamma_\mu f_R \\ &+2\eta_{LR}\bar{f}_L\gamma^\mu f_L\bar{f}_R\gamma_\mu f_R)\ ,\end{aligned} \tag{8.5}$$

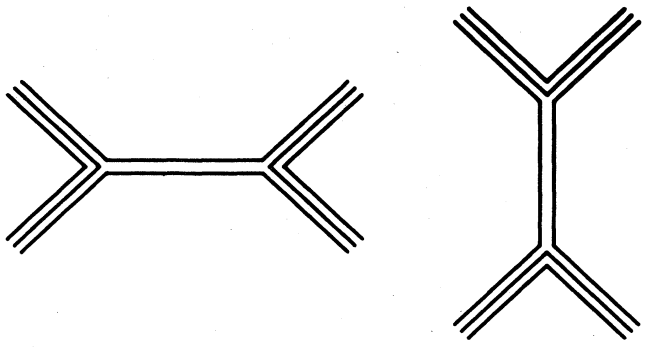

FIG. 230. Typical elastic interaction of composite fermions mediated by the exchange of preon bound states with masses of order Λ^*.

where $f_{L,R}$ are the left-handed and right-handed chiral components of f, respectively. In the construction of (8.5) it has been assumed that the $SU(3)_c \otimes SU(2)_L \otimes U(1)_Y$ description is correct (if incomplete), and that $\Lambda^* \gtrsim (G_F/\sqrt{2})^{-1/2}$. Above the scale of electroweak symmetry breaking the known interactions do not conserve parity, so there is no reason to assume that metacolor will be parity conserving. Indeed, the mechanism described by 't Hooft (1980) allows the possibility of massless composite fermions only in parity-violating gauge theories. We shall therefore regard f_L and f_R as distinct species, whereupon the compositeness of one does not necessarily imply the compositeness of the other. If both are composite, they need not have common constituents. Thus the LR term in (8.5) will be present only if both f_L and f_R are composite, and have at least one constituent in common. Finally, we define Λ^* for the purposes of (8.5) so that $g^2/4\pi = 1$ with the largest $|\eta_{ij}| = 1$. Color indices, if any, are suppressed here.

The $SU(3)_c \otimes SU(2)_L \otimes U(1)_Y$ invariance of $\mathscr{L}_{ff}$ generally implies the existence of additional contact interactions involving different fermion members of the same electroweak multiplet. In the absence of a complete theory, we do not know whether different fermions belonging to the same electroweak doublet should refer to mass eigenstates or weak eigenstates. One can argue that they should be the weak eigenstates. If that is so, there is the danger of the flavor-changing contact interactions we spoke of above. We shall have to assume here that any dangerous flavor-changing interactions are sufficiently suppressed by some unknown mechanism.

The flavor-diagonal contact interactions of Eq. (8.5) will modify cross sections for ff elastic scattering. If in the standard model this process is controlled by a gauge coupling $\alpha_f \ll 1$, then the helicity-preserving pieces of $\mathscr{L}_{ff}$ give rise to interference terms in the integrated cross section for ff scattering that are of order

$$\frac{\hat{s}}{\Lambda^{*2}} \frac{g^2}{4\pi\alpha_f} \equiv \frac{\hat{s}}{\alpha_f \Lambda^{*2}} \tag{8.6}$$

relative to the standard model contribution (Eichten, Lane, and Peskin, 1983). This modification to the conventional expectation is far more dramatic than the anticipated $O(\hat{s}/\Lambda^{*2})$ form factor effects. The direct contact term itself will dominate for subenergies satisfying

$$\hat{s} \gtrsim \alpha_f \Lambda^{*2} . \tag{8.7}$$

The approximation that the composite interactions can be represented by contact terms breaks down for $\hat{s} \approx \Lambda^{*2}$, so Eq. (8.5) becomes unreliable above these subenergies. The neglect of helicity-changing contact terms is justified in the energy range $\alpha_f \Lambda^{*2} \lesssim \hat{s} \lesssim \Lambda^{*2}$ by the fact that they will be suppressed by additional factors of $m_f^2/\hat{s}$ or $\hat{s}/\Lambda^{*2}$ relative to the helicity-conserving interactions (Eichten, Lane, and Peskin, 1983).

Searches for the effects of contact terms associated with electron compositeness have been carried out in Bhabha scattering measurements at PEP and PETRA. The studies summarized by Yamada (1983) lead to bounds on the scale of electron compositeness in the range of 1–2 TeV.

In hadron-hadron collisions, the process that is most sensitive to the presence of a flavor-diagonal contact term $\mathscr{L}_{ff}$ is the production of high-transverse momentum jets by the scattering of up or down quarks. This test of quark compositeness is of course independent of electron compositeness. We discuss in Sec. VIII.B the limits on light quark compositeness which are attainable in high-energy $p^{\pm}p$ collisions.

In addition to flavor-diagonal contact interactions, there can be flavor-conserving but nondiagonal interactions with strength comparable to the diagonal terms. This possibility is more model dependent, as it generally requires the two fermions to have a constituent in common. However, such an effective interaction may be generated by the metacolor gluon exchange mechanism[11] sketched in Fig. 231. At subenergies small compared with Λ^*, there is no reason to expect any inhibition of this sort of flavor mixing: the metacolor coupling constant is not small. An interaction mixing a light quark pair and a lepton pair would modify the Drell-Yan process. This possibility will be discussed in Sec. VIII.C.

B. Signals for compositeness in high-$p_\perp$ jet production

The most general helicity-conserving, $SU(3)_c \otimes SU(2)_L \otimes U(1)_Y$-invariant four-fermion contact interaction among up and down quarks is given by

$$\begin{aligned}\mathscr{L}_{qq} = (g^2/2\Lambda^{*2}) \Big[& \eta_0 \bar{q}_L \gamma^\mu q_L \bar{q}_L \gamma_\mu q_L + \eta_1 \bar{q}_L \gamma^\mu \frac{\tau_a}{2} q_L \bar{q}_L \gamma_\mu \frac{\tau_a}{2} q_L + \eta_{0u} \bar{q}_L \gamma^\mu q_L \bar{u}_R \gamma_\mu u_R + \eta_{0d} \bar{q}_L \gamma^\mu q_L \bar{d}_R \gamma_\mu d_R \\ & + \eta_{8u} \bar{q}_L \gamma^\mu \frac{\lambda_A}{2} q_L \bar{u}_R \gamma_\mu \frac{\lambda_A}{2} u_R + \eta_{8d} \bar{q}_L \gamma^\mu \frac{\lambda_A}{2} q_L \bar{d}_R \gamma_\mu \frac{\lambda_A}{2} d_R \\ & + \eta_{uu} \bar{u}_R \gamma^\mu u_R \bar{u}_R \gamma_\mu u_R + \eta_{dd} \bar{d}_R \gamma^\mu d_R \bar{d}_R \gamma_\mu d_R + \eta_{ud} \bar{u}_R \gamma^\mu u_R \bar{d}_R \gamma_\mu d_R + \eta'_{ud} \bar{u}_R \gamma^\mu d_R \bar{d}_R \gamma_\mu u_R \Big] ,\end{aligned} \tag{8.8}$$

[11] This possibility was pointed out to one of us (K. L.) by S. Drell.

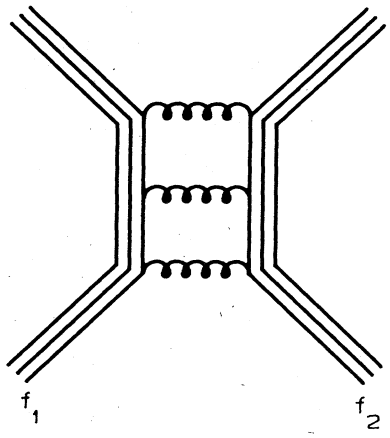

FIG. 231. Interaction between two composite fermion species f_1 and f_2 mediated by metacolor gluon exchange. The induced coupling is flavor conserving, but not flavor diagonal.

where

$$q_L \equiv \begin{bmatrix} u_L \\ d_L \end{bmatrix} , \tag{8.9}$$

the λ_A ($A=1,2,\ldots,8$) are the SU(3) color matrices, and the τ_a ($a=1,2,3$) are the weak-isospin Pauli matrices. As in (8.5), the compositeness scale Λ^* is chosen so that $g^2/4\pi=1$ and the largest $|\eta_{ij}|=1$. At any given compositeness scale and subenergy, we expect each individual term in $\mathscr{L}_{qq}$ to be of comparable importance in its influence on the jet cross section. We shall analyze in detail only the piece of (8.8) which applies if u_L and d_L are composite and interact by color-singlet, isoscalar exchanges in the form

$$\mathscr{L}_{qq}^{(0)} = \eta_0 \frac{g^2}{2\Lambda^{*2}} \bar{q}_L \gamma^\mu q_L \bar{q}_L \gamma_\mu q_L , \tag{8.10}$$

with $\eta_0 = \pm 1$.

The differential cross section for quark-quark scattering now takes the form

$$\frac{d\hat{\sigma}}{d\hat{t}}(ij \to i'j') = \frac{\pi}{\hat{s}^2} |A(ij \to i'j')|^2 , \tag{8.11}$$

where the indices i, j, i', and j' denote up or down quarks or antiquarks, and the amplitude squared includes both the gluon-exchange contributions of QCD and the contact interaction due to metacolor. For the cases of interest, the squared amplitudes are (Abolins *et al.*, 1982; Eichten, Lane, and Peskin, 1983)

$$|A(u\bar{u}\to u\bar{u})|^2 = |A(d\bar{d}\to d\bar{d})|^2 = \frac{4}{9}\alpha_s^2(Q^2)\left[\frac{(\hat{u}^2+\hat{s}^2)}{\hat{t}^2}+\frac{(\hat{u}^2+\hat{t}^2)}{\hat{s}^2}-\frac{2}{3}\frac{\hat{u}^2}{\hat{s}\hat{t}}\right] + \frac{8}{9}\alpha_s(Q^2)\frac{\eta_0}{\Lambda^{*2}}\left[\frac{\hat{u}^2}{\hat{t}}+\frac{\hat{u}^2}{\hat{s}}\right]+\frac{8}{3}\left[\frac{\eta_0\hat{u}}{\Lambda^{*2}}\right]^2 , \tag{8.12}$$

$$|A(uu\to uu)|^2 = |A(dd\to dd)|^2 = |A(\bar{u}\bar{u}\to\bar{u}\bar{u})|^2 = |A(\bar{d}\bar{d}\to\bar{d}\bar{d})|^2 = \frac{4}{9}\alpha_s^2(Q^2)\left[\frac{(\hat{u}^2+\hat{s}^2)}{\hat{t}^2}+\frac{(\hat{s}^2+\hat{t}^2)}{\hat{u}^2}-\frac{2}{3}\frac{\hat{s}^2}{\hat{u}\hat{t}}\right] + \frac{8}{9}\alpha_s(Q^2)\frac{\eta_0}{\Lambda^{*2}}\left[\frac{\hat{s}^2}{\hat{t}}+\frac{\hat{s}^2}{\hat{u}}\right]+\left[\frac{\eta_0}{\Lambda^{*2}}\right]^2(\hat{u}^2+\hat{t}^2+\tfrac{2}{3}\hat{s}^2) , \tag{8.13}$$

$$|A(u\bar{u}\to d\bar{d})|^2 = |A(d\bar{d}\to u\bar{u})|^2 = \frac{4}{9}\alpha_s^2(Q^2)\frac{(\hat{u}^2+\hat{t}^2)}{\hat{s}^2}+\left[\frac{\eta_0\hat{u}}{\Lambda^{*2}}\right]^2 , \tag{8.14}$$

and

$$|A(ud\to ud)|^2 = |A(u\bar{d}\to u\bar{d})|^2 = |A(\bar{u}d\to\bar{u}d)|^2 = |A(\bar{u}\bar{d}\to\bar{u}\bar{d})|^2 = \frac{4}{9}\alpha_s^2(Q^2)\frac{(\hat{u}^2+\hat{s}^2)}{\hat{t}^2}+\left[\frac{\eta_0\hat{u}}{\Lambda^{*2}}\right]^2 . \tag{8.15}$$

In Eqs. (8.12)—(8.15) the strong coupling constant α_s is to be evaluated at a scale Q^2 typical of the process in question. As we remarked in Sec. III, where the sensitivity to this scale was discussed, the choice of Q^2 is somewhat ambiguous. To illustrate this sensitivity further, for this analysis we choose not $Q^2=p_\perp^2/4$, as in Sec. III, but

$$Q^2 = p_\perp^2 , \tag{8.16}$$

where $p_\perp$ is the transverse momentum of the outgoing jet. In writing Eqs. (8.12)—(8.15) we have ignored all contributions of higher order in α_s. These include perturbative corrections to the QCD Born terms as well as the form factor effects associated with quark compositeness. We caution again that the form given for the composite interaction in (8.10) is reliable only for $\hat{s}<\Lambda^{*2}$; above the compositeness scale, inelastic channels become increasingly important.

The differential cross sections $d\sigma/dp_\perp dy|_{y=0}$ for the reaction

$$pp \to \text{jet} + \text{anything} \tag{8.17}$$

that follow from Eqs. (8.11)—(8.15) are shown in Figs. 232—235 for collider energies $\sqrt{s}=10$, 20, 40, and 100

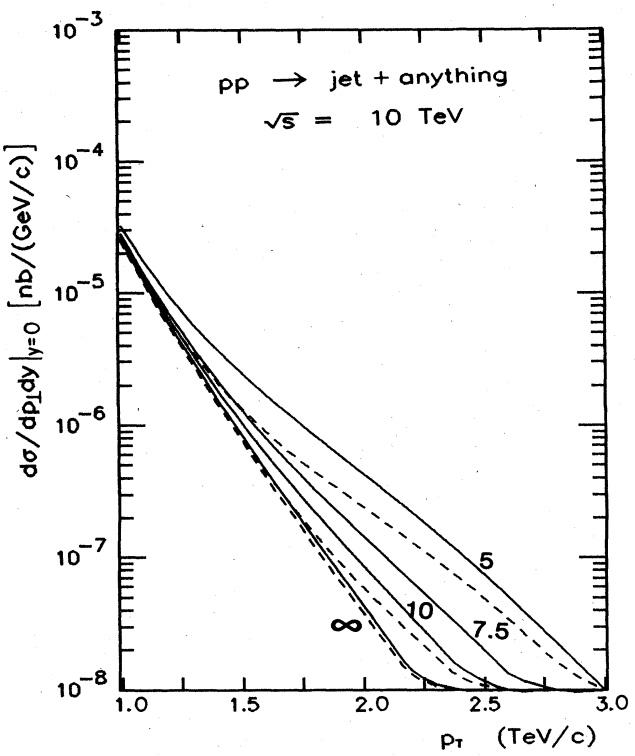

FIG. 232. Cross section $d\sigma/dp_\perp dy\,|_{y=0}$ for jet production in pp collisions at $\sqrt{s}=10$ TeV, according to the parton distributions of Set 2. The curves are labeled by the compositeness scale Λ^* (in TeV). $\eta_0=-1$ (solid lines), $\eta_0=+1$ (dashed lines).

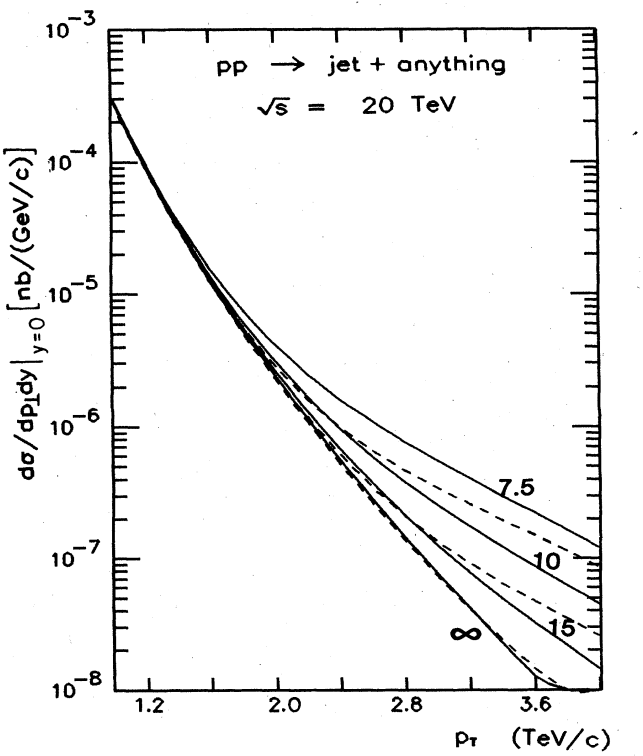

FIG. 233. Cross section $d\sigma/dp_\perp dy\,|_{y=0}$ for jet production in pp collisions at $\sqrt{s}=20$ TeV, according to the parton distributions of Set 2. The curves are labeled as in Fig. 232.

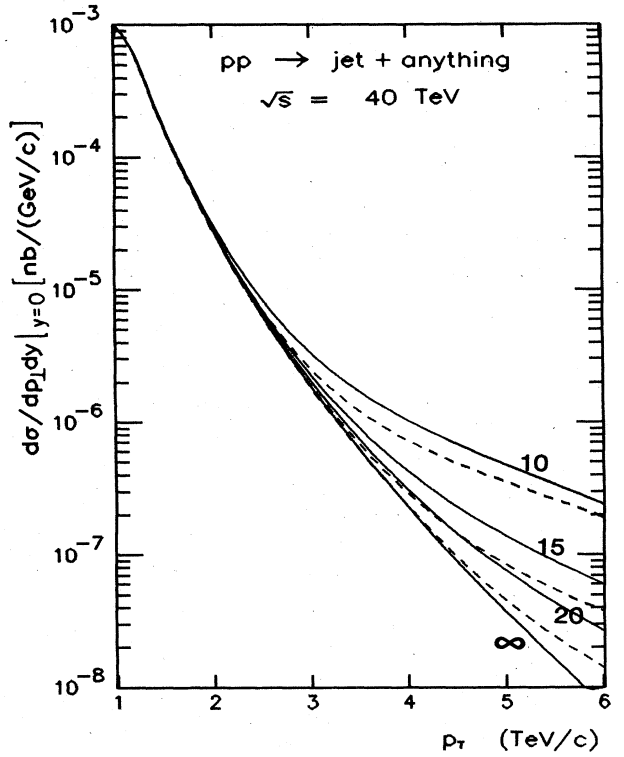

FIG. 234. Cross section $d\sigma/dp_\perp dy\,|_{y=0}$ for jet production in pp collisions at $\sqrt{s}=40$ TeV, according to the parton distributions of Set 2. The curves are labeled as in Fig. 232.

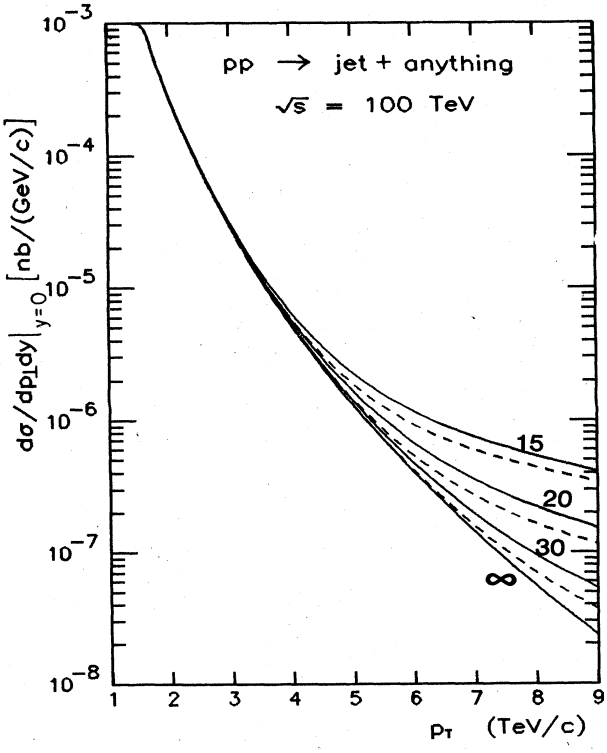

FIG. 235. Cross section $d\sigma/dp_\perp dy\,|_{y=0}$ for jet production in pp collisions at $\sqrt{s}=100$ TeV, according to the parton distributions of Set 2. The curves are labeled as in Fig. 232.

TeV, and for representative values of the substructure scale Λ^*. The latter were chosen to illustrate the reach of colliders for integrated luminosities in the range 10^{39}–10^{40} cm^{-2}.

The gross features of the curves are easily understood. Because the contact term modifies the cross section for (anti)quark-(anti)quark scattering, its effects are most apparent at the large values of $p_\perp$ for which valence quark interactions dominate the jet cross section. In pp collisions, the largest effect comes from the modification to uu scattering given by (8.13). Since $\hat{t}$ and $\hat{u}$ are both negative, the penultimate term corresponds to constructive (destructive) interference for $\eta_0=-1$ $(+1)$. This means that deviations from QCD will be more pronounced for $\eta_0=-1$ than for $\eta_0=+1$, at the same values of s, $p_\perp$, and Λ^*. At the largest values of $p_\perp$ displayed, the interference and direct contact terms are comparable in magnitude for the chosen values of Λ^*.

To estimate what limits can be set on the compositeness scale as a function of pp collider energy and luminosity, it is first necessary to assess how reliably we know the conventional QCD contribution to inclusive jet production. One measure of the uncertainty that resides in the structure functions may be had by comparing the jet cross sections computed using the parton distributions of Set 1 with those obtained from Set 2. As we saw in the comparison of Figs. 78 and 80, the shapes of the QCD-jet cross sections are essentially indistinguishable. The normalizations differ by less than 20% over the range of $p_\perp$ shown in Figs. 232–235. At the values of $p_\perp/\sqrt{s}$ which are important to the search for composite effects, theoretical ambiguities associated with the $x\to 0$ and $x\to 1$ behavior of structure functions are unimportant. We are therefore confident that a departure from the expected behavior which increases or decreases the jet cross section by a factor of 2 signals the onset of new physics.

To be specific, we require that in a bin of width $\Delta p_\perp = 100$ GeV/c, the deviation

$$\Delta(p_\perp)=\frac{\left.\frac{d\sigma}{dp_\perp dy}\right|_{y=0}-\left.\frac{d\sigma^{\rm QCD}}{dp_\perp dy}\right|_{y=0}}{\left.\frac{d\sigma^{\rm QCD}}{dp_\perp dy}\right|_{y=0}} \tag{8.18}$$

correspond to a factor-of-2 change in the cross section ($\Delta>1$ or $\Delta<-0.5$), and that at least 50 events be observed per unit rapidity. This criterion leads to the potential limits of Λ^* displayed in Fig. 236. For example, a 40-TeV pp collider with integrated luminosity of 10^{40} cm^{-2} can reach

$$\Lambda^*=\begin{cases}15 \text{ TeV}\\ 20 \text{ TeV}\end{cases} \tag{8.19}$$

for $\eta_0=\pm 1$.

The analysis of the sensitivity to compositeness in $\bar{p}p$ collisions is somewhat different in detail. For the cross sections $d\sigma/dp_\perp dy\,|_{y=0}$ for the reaction

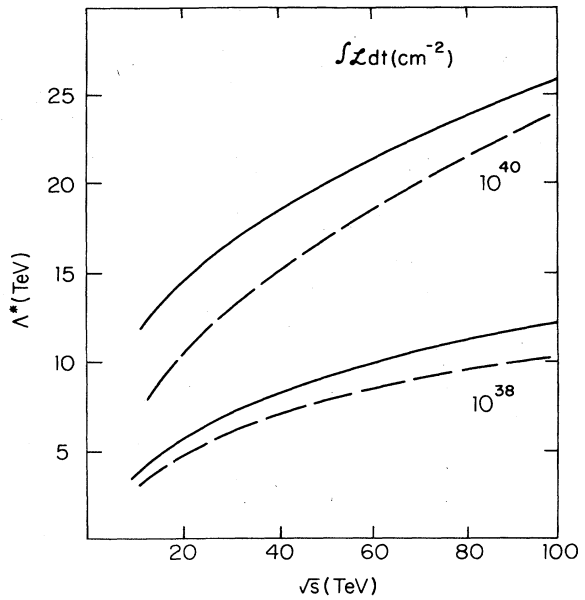

FIG. 236. Maximum compositeness scale Λ^* probed in jet production at $y=0$ in pp collisions as a function of $\sqrt{s}$ for integrated luminosities of 10^{40} and 10^{38} cm^{-2} according to the criterion (8.18). $\eta_0=-1$ (solid lines), $\eta_0=+1$ (dashed lines).

$$\bar{p}p\to \text{jet}+\text{anything} \tag{8.20}$$

plotted in Figs. 237–240, the most important effects of the contact term occur in interactions of valence quarks with valence antiquarks. Of the $q\bar{q}$ interactions given by (8.12)–(8.15), only the flavor-diagonal amplitude of (8.12) contains an interference term. This term tends to be unimportant, because $\hat{s}$ is large and positive, while $\hat{t}$ is large and negative in the regime of interest. As a result, the differences between the predictions for $\eta_0=\pm 1$ are far smaller than the corresponding differences in pp collisions. The potential limits on the compositeness scale that can be set in reaction (8.20) are shown in Fig. 241. Comparing with Fig. 237, we find that for $\eta_0=-1$ there is essentially no difference in reach between pp and $\bar{p}p$ colliders of the same energy and luminosity. For $\eta_0=+1$, the reach of a $\bar{p}p$ collider is somewhat greater than that of a pp collider with the same parameters.

C. Signals for composite quarks and leptons in lepton-pair production

If the leptons and light quarks have common constituents, or if the metacolor gluon exchange mechanism of Fig. 231 is not suppressed, contact interactions will modify lepton-pair production in quark-antiquark annihilations. Under the assumption that only left-handed neutrinos exist, the most general $SU(3)_c\otimes SU(2)_L\otimes U(1)_Y$-invariant interaction among quarks and leptons is

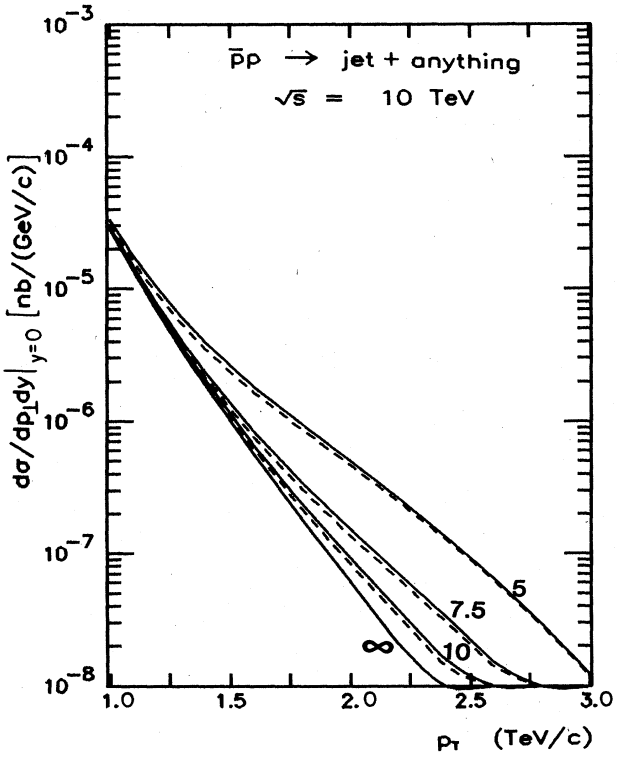

FIG. 237. Cross section $d\sigma/dp_\perp dy\,|_{y=0}$ for jet production in $\bar{p}p$ collisions at $\sqrt{s}=10$ TeV, according to the parton distributions of Set 2. The curves are labeled as in Fig. 232.

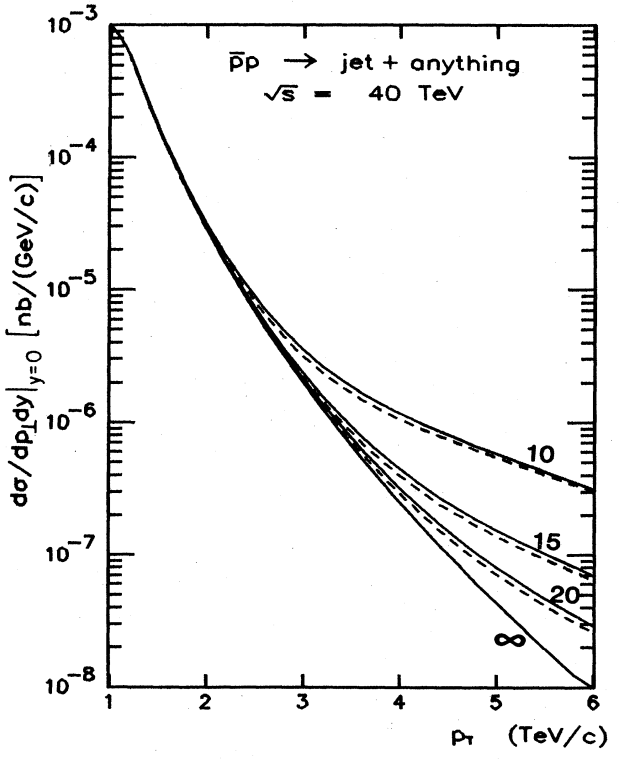

FIG. 239. Cross section $d\sigma/dp_\perp dy\,|_{y=0}$ for jet production in $\bar{p}p$ collisions at $\sqrt{s}=40$ TeV, according to the parton distributions of Set 2. The curves are labeled as in Fig. 232.

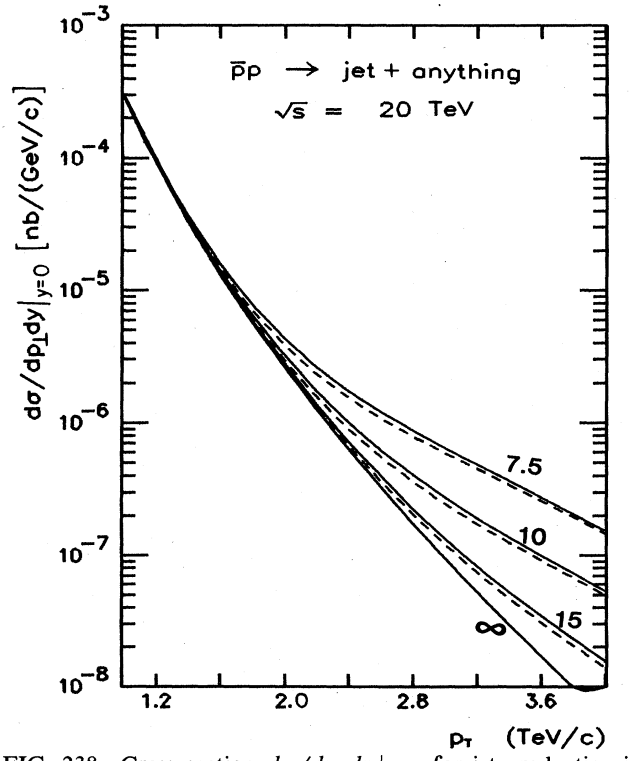

FIG. 238. Cross section $d\sigma/dp_\perp dy\,|_{y=0}$ for jet production in $\bar{p}p$ collisions at $\sqrt{s}=20$ TeV, according to the parton distributions of Set 2. The curves are labeled as in Fig. 232.

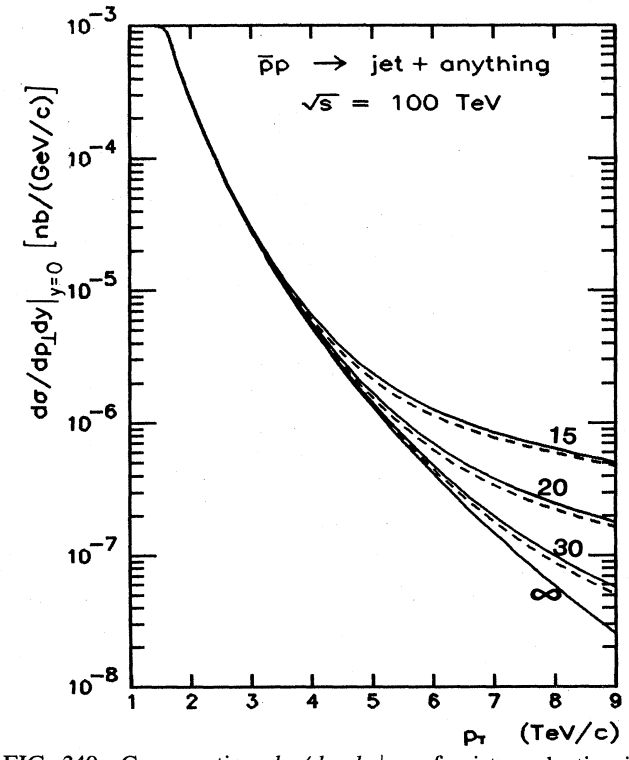

FIG. 240. Cross section $d\sigma/dp_\perp dy\,|_{y=0}$ for jet production in $\bar{p}p$ collisions at $\sqrt{s}=100$ TeV, according to the parton distributions of Set 2. The curves are labeled as in Fig. 232.

$$\mathcal{L}_{ql}=(g^2/\Lambda^{*2})\left[\eta'_0\bar{q}_L\gamma^\mu q_L\bar{L}_L\gamma_\mu L_L+\eta'_1\bar{q}_L\gamma^\mu\frac{\tau_a}{2}q_L\bar{L}_L\gamma_\mu\frac{\tau_a}{2}L_L+\eta'_{0l}\bar{q}_L\gamma^\mu q_L\bar{l}_R\gamma_\mu l_R\right.$$
$$\left.+\eta'_{0u}\bar{L}_L\gamma^\mu L_L\bar{u}_R\gamma_\mu u_R+\eta'_{0d}\bar{L}_L\gamma^\mu L_L\bar{d}_R\gamma_\mu d_R+\eta'_{ul}\bar{u}_R\gamma^\mu u_R\bar{l}_R\gamma_\mu l_R+\eta'_{dl}\bar{d}_R\gamma^\mu d_R\bar{l}_R\gamma_\mu l_R\right], \quad (8.21)$$

where

$$q_{L,R}=\begin{bmatrix}u\\d\end{bmatrix}_{L,R}, \quad (8.22)$$

$$L_L=\begin{bmatrix}\nu_l\\l^-\end{bmatrix}_L, \quad (8.23)$$

and $l=e,\mu,\tau$. As usual, the compositeness scale Λ^* is chosen so that $g^2/4\pi=1$ and the largest $|\eta'|=1$. We consider in detail only the contact term involving the product of the left-handed weak-isoscalar quark and lepton currents,

$$\mathcal{L}^{(0)}_{ql}=\frac{4\pi}{\Lambda^{*2}}\eta'_0\bar{q}_L\gamma^\mu q_L\bar{L}_L\gamma_\mu L_L, \quad (8.24)$$

with

$$\eta'_0=\pm1. \quad (8.25)$$

The differential cross section for the reaction

$$q_i\bar{q}_i\to l^+l^-, \quad (8.26)$$

including the contributions of γ and Z^0 exchanges and the composite contact interaction (8.24), is given by

$$\frac{d\hat{\sigma}}{d\hat{t}}(q_i\bar{q}_i\to l^+l^-)=\frac{\pi\alpha^2}{\hat{s}^2}\left[A_i(\hat{s})\left[\frac{\hat{u}}{\hat{s}}\right]^2+B_i(\hat{s})\left[\frac{\hat{t}}{\hat{s}}\right]^2\right], \quad (8.27)$$

where the quark flavors are $i=$ up, down. The coefficients A_i and B_i may be written as

$$A_i(\hat{s})=\left|Q_i-\frac{L_iL_l}{4x_W(1-x_W)}\frac{\hat{s}}{\hat{s}-M_Z^2+iM_Z\Gamma_Z}-\frac{\eta'_0\hat{s}}{\alpha\Lambda^{*2}}\right|^2+\left|Q_i-\frac{R_iR_l}{4x_W(1-x_W)}\frac{\hat{s}}{\hat{s}-M_Z^2+iM_Z\Gamma_Z}\right|^2, \quad (8.28)$$

$$B_i(\hat{s})=\left|Q_i-\frac{R_iL_l}{4x_W(1-x_W)}\frac{\hat{s}}{\hat{s}-M_Z^2+iM_Z\Gamma_Z}\right|^2+\left|Q_i-\frac{L_iR_l}{4x_W(1-x_W)}\frac{\hat{s}}{\hat{s}-M_Z^2+iM_Z\Gamma_Z}\right|^2, \quad (8.29)$$

where the chiral couplings of the neutral weak current are, as usual,

$$L_i=\tau_3-2Q_ix_W \quad (8.30a)$$

and

$$R_i=-2Q_ix_W. \quad (8.30b)$$

Here the weak mixing parameter is $x_W=\sin^2\theta_W$ and τ_3 is twice the weak-isospin projection of fermion i.

The cross sections $d\sigma/d\mathcal{M}\,dy\,|_{y=0}$ for the reaction

$$pp\to l^+l^-+\text{anything} \quad (8.31)$$

that result from Eqs. (8.27)—(8.30) are plotted as functions of the invariant mass $\mathcal{M}=\sqrt{\hat{s}}$ of the lepton pair for collider energies of 10, 20, 40, and 100 TeV in Figs. 242—245. Similar calculations for $p\bar{p}$ collisions are presented in Figs. 246—249. Whereas the conventional Drell-Yan contribution falls rapidly with $\mathcal{M}$ (because both parton luminosities and the elementary cross section do), the cross sections including the contact interaction have nearly flattened out. The weak dependence upon $\mathcal{M}$ results from the convolution of the rising elementary cross section with the falling parton luminosities. It is evident from (8.28) that $\eta'_0=-1$ corresponds to constructive interference with the dominant up-quark contribution to the cross section. There are no conventional backgrounds to this signal for quark and lepton substructure.

The contributions of contact terms to dilepton production and jet production are comparable. However, in jet

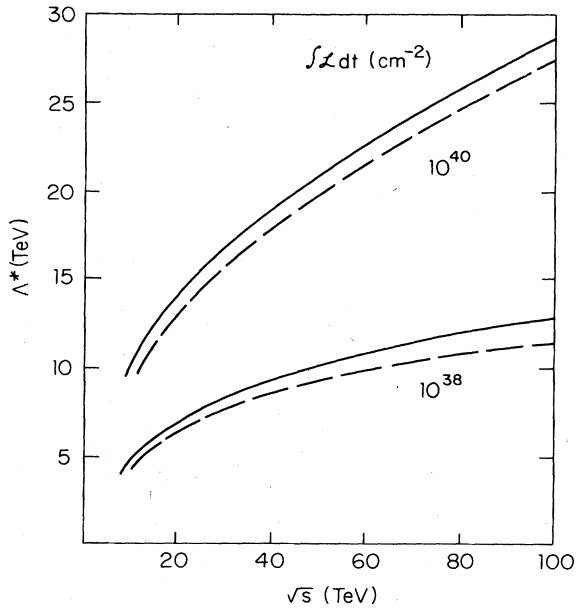

FIG. 241. Maximum compositeness scale Λ^* probed in jet production at $y=0$ for $\bar{p}p$ colliders as a function of $\sqrt{s}$ for integrated luminosities of 10^{38} and 10^{40} cm^{-2} according to the criterion (8.18). $\eta_0=-1$ (solid lines), $\eta_0=+1$ (dashed lines).

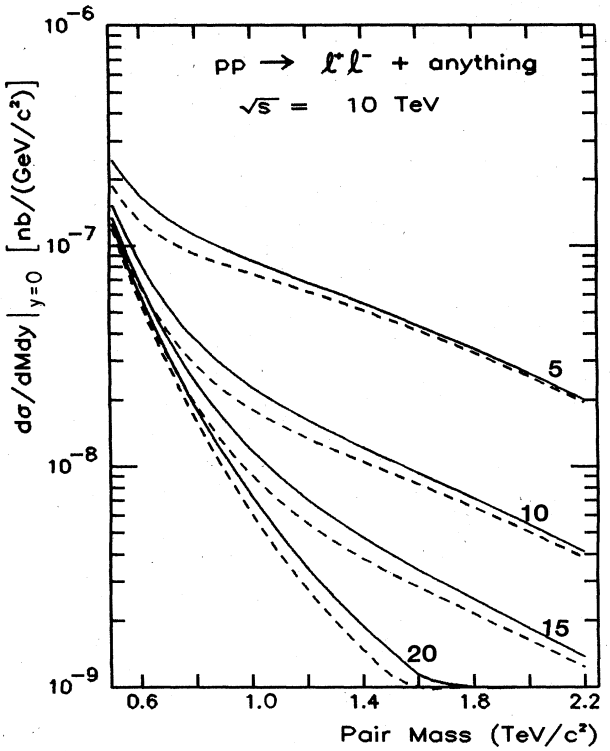

FIG. 242. Cross section $d\sigma/d\mathcal{M}\,dy\,|_{y=0}$ for dilepton production in pp collisions at $\sqrt{s}=10$ TeV, according to the parton distributions of Set 2. The curves are labeled by the compositeness scale Λ^* (in TeV). $\eta_0'=-1$ (solid line), $\eta_0'=+1$ (dashed line).

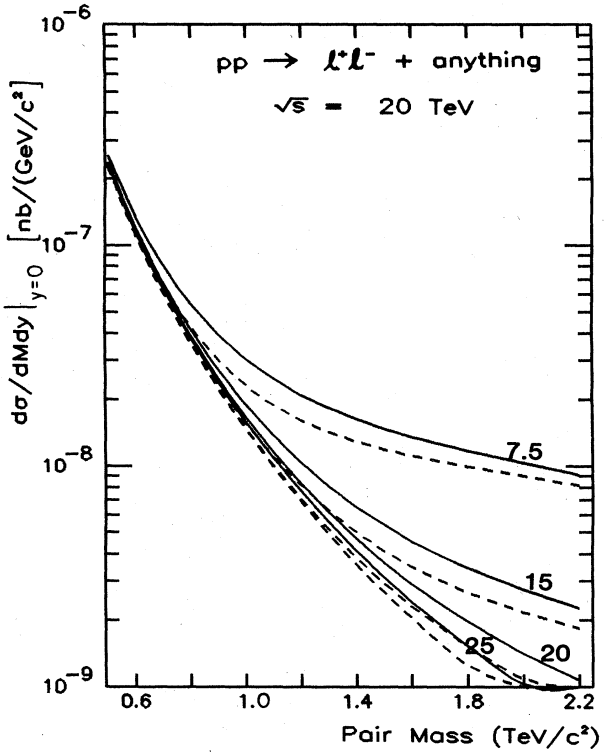

FIG. 243. Cross section $d\sigma/d\mathcal{M}\,dy\,|_{y=0}$ for dilepton production in pp collisions at $\sqrt{s}=20$ TeV, according to the parton distributions of Set 2. The curves are labeled as in Fig. 242.

production there are large and incoherent QCD contributions from gluon-gluon and quark-gluon interactions. In addition, the standard model cross section for $q\bar{q}\to l^+l^-$ is smaller than the quark-quark scattering cross section by a factor of order $(\alpha_{EM}/\alpha_s)^2$. This accounts for the greater prominence of the contact term contribution in dilepton production. To determine the largest compositeness scale that can be probed in lepton pair production, we define $\mathcal{M}_0$ as the mass above which the observed yield is at least a factor of 2 greater than standard model expectations:

$$\left.\frac{d\sigma}{d\mathcal{M}\,dy}\right|_{y=0} \Big/ \left.\frac{d\sigma^{\rm std}}{d\mathcal{M}\,dy}\right|_{y=0} > 2, \quad \mathcal{M} > \mathcal{M}_0 . \tag{8.32}$$

We then require an excess of 75 events in the rapidity interval $-1.5<y<1.5$, which is to say that[12]

$$\int dt\,\mathcal{L} \int_{-1.5}^{1.5} dy \int_{\mathcal{M}_0} d\mathcal{M} \left[\frac{d\sigma}{d\mathcal{M}\,dy} - \frac{d\sigma^{\rm std}}{d\mathcal{M}\,dy}\right] \geq 75 , \tag{8.33}$$

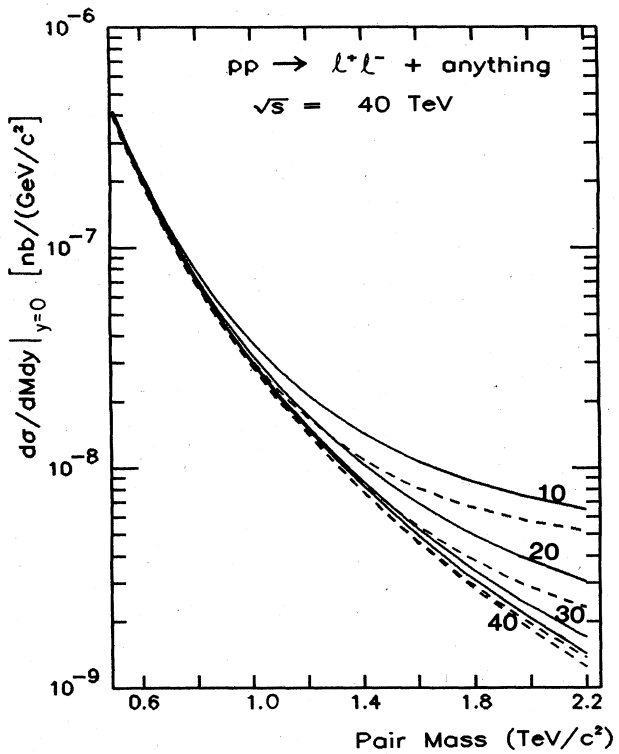

FIG. 244. Cross section $d\sigma/d\mathcal{M}\,dy\,|_{y=0}$ for dilepton production in pp collisions at $\sqrt{s}=40$ TeV, according to the parton distributions of Set 2. The curves are labeled as in Fig. 242.

[12]To an adequate approximation,

$$\int_{-1.5}^{1.5} dy \frac{d\sigma}{d\mathcal{M}\,dy} = 3\left.\frac{d\sigma}{d\mathcal{M}\,dy}\right|_{y=0} .$$

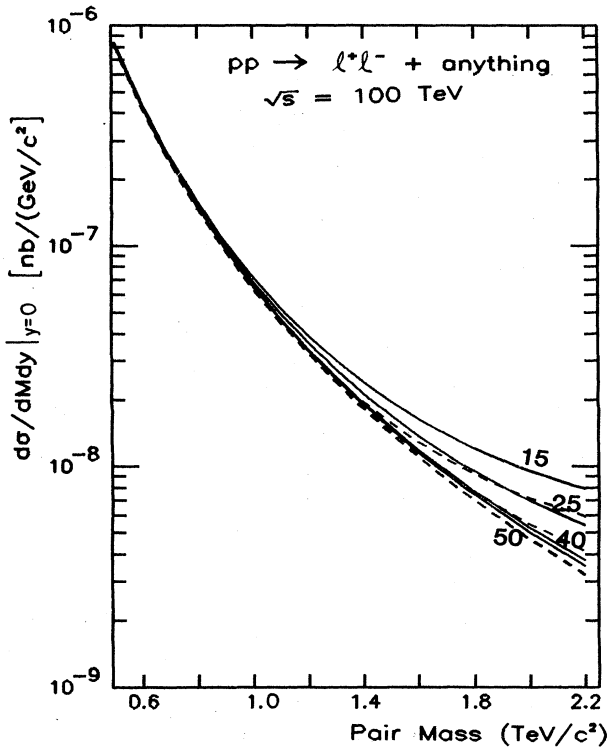

FIG. 245. Cross section $d\sigma/d\mathcal{M}\,dy\,|_{y=0}$ for dilepton production in pp collisions at $\sqrt{s}=100$ TeV, according to the parton distributions of Set 2. The curves are labeled as in Fig. 242.

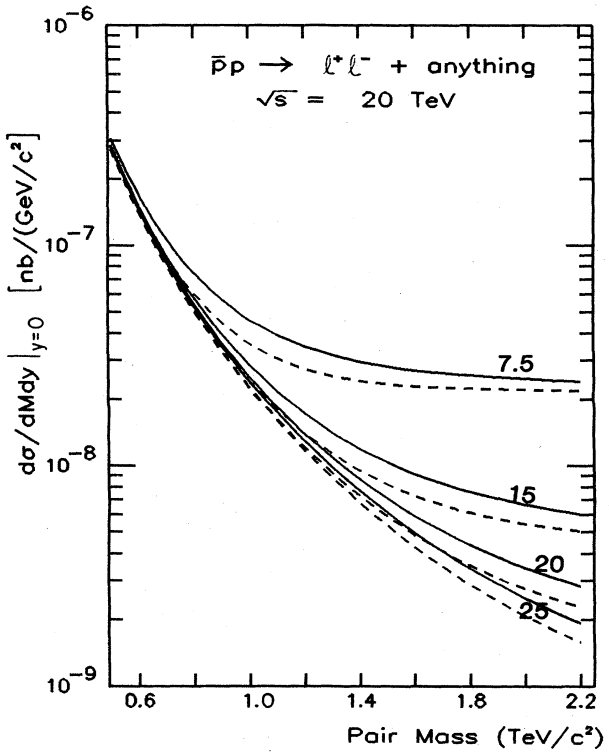

FIG. 247. Cross section $d\sigma/d\mathcal{M}\,dy\,|_{y=0}$ for dilepton production in $\bar{p}p$ collisions at $\sqrt{s}=20$ TeV, according to the parton distributions of Set 2. The curves are labeled as in Fig. 242.

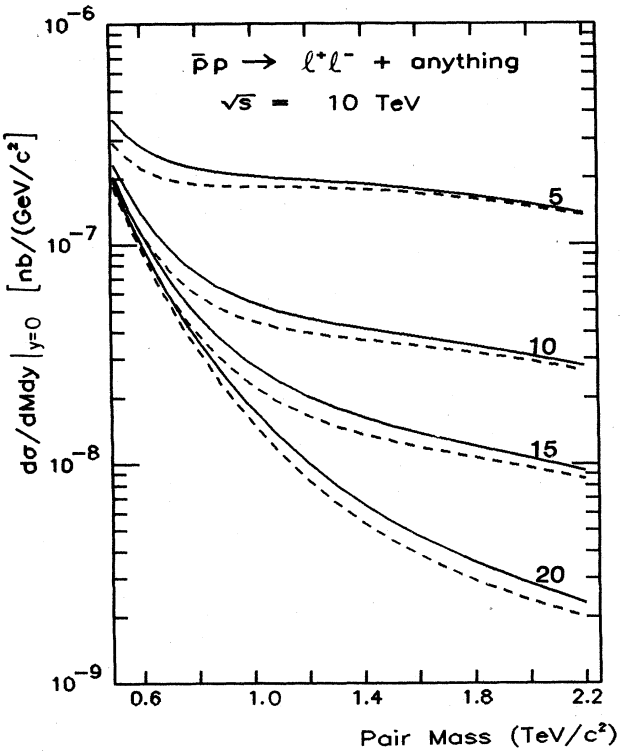

FIG. 246. Cross section $d\sigma/d\mathcal{M}\,dy\,|_{y=0}$ for dilepton production in $\bar{p}p$ collisions at $\sqrt{s}=10$ TeV, according to the parton distributions of Set 2. The curves are labeled as in Fig. 242.

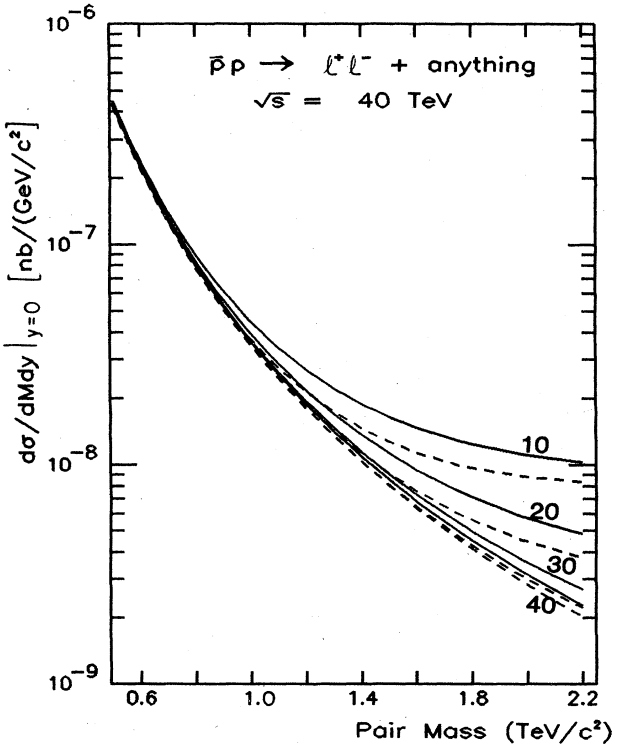

FIG. 248. Cross section $d\sigma/d\mathcal{M}\,dy\,|_{y=0}$ for dilepton production in $\bar{p}p$ collisions at $\sqrt{s}=40$ TeV, according to the parton distributions of Set 2. The curves are labeled as in Fig. 242.

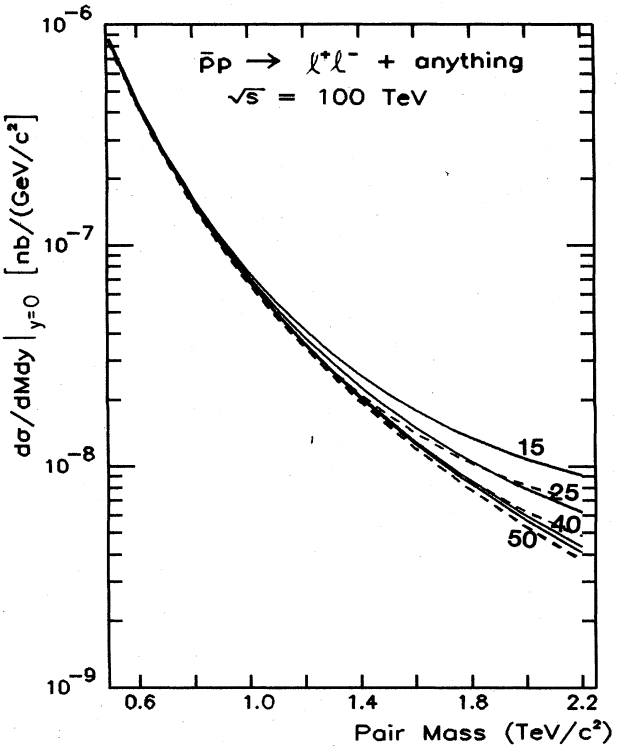

FIG. 249. Cross section $d\sigma/d\mathcal{M}\,dy\,|_{y=0}$ for dilepton production in $\bar{p}p$ collisions at $\sqrt{s}=100$ TeV, according to the parton distributions of Set 2. The curves are labeled as in Fig. 242.

where $\mathcal{L}$ is the luminosity of hadron-hadron collisions.

We show in Fig. 250 the resulting limits on Λ^* for various energies and luminosities in pp collisions. The limits on Λ^* are slightly larger than those accessible in jet production. Corresponding results for $\bar{p}p$ collisions are shown in Fig. 251. The reach of a $\bar{p}p$ collider is considerably greater than that of a pp machine of the same energy and luminosity. This is because the contact term is so large that the greater $u\bar{u}$ luminosity of $\bar{p}p$ collisions at large subenergies can be exploited. For an integrated luminosity of 10^{39} cm^{-2}, a $\bar{p}p$ collider can attain scales 4—5 TeV greater than those accessible to a pp machine; at 10^{40} cm^{-2}, the $\bar{p}p$ collider can reach 7—10 TeV higher than its pp counterpart. For either pp or $\bar{p}p$ collisions, the maximum compositeness scale that can be probed at 10^{40} cm^{-2} is slightly less than twice that attainable at 10^{39} cm^{-2}.

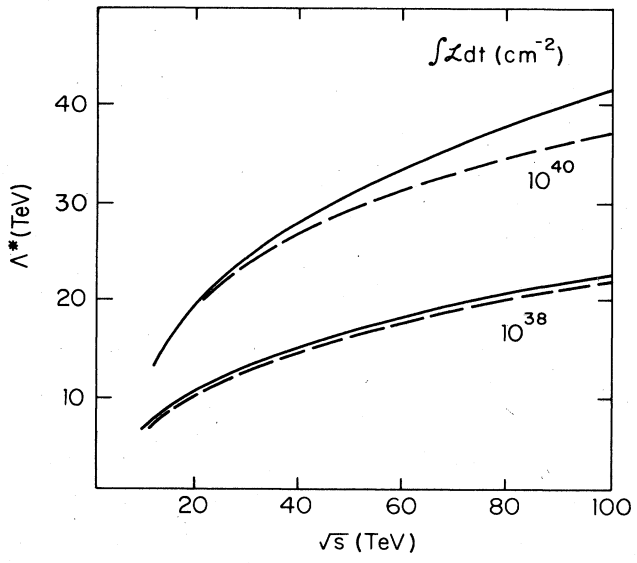

FIG. 250. Maximum compositeness scale Λ^* probed in dilepton production with $|y|<1.5$ for $\bar{p}p$ colliders at integrated luminosities of 10^{38} and 10^{40} cm^{-2} according to the criterion (8.33). $\eta_0'=-1$ (solid lines), $\eta_0'=+1$ (dashed lines).

D. Summary

If quarks and leptons have internal structure with a characteristic size of $1/\Lambda^*$, flavor-diagonal contact interactions will be the low-energy manifestations of constituent interchange processes. Flavor-conserving but nondiagonal contact interactions may exist as well. These effective four-fermion interactions have a dimensionful coupling constant of order $4\pi/\Lambda^{*2}$, and may lead to substantial modifications of the standard-model predictions for hard-scattering processes at subenergies $\sqrt{\hat{s}}$ well below the compositeness scale. These deviations are likely to be the first indications of quark and lepton structure in high-energy colliders. Indeed, if the substructure threshold is not surpassed by the collider, they provide the only accessible signals for compositeness.

We have discussed the modifications to be expected in the production rates for high-$p_\perp$ jets and massive lepton pairs, using in each case an especially simple choice of the contact interaction. In view of the uncertainties that remain in estimates of jet or dilepton production rates, we have required at least a factor-of-2 deviation from conventional expectations as the criterion for establishing the

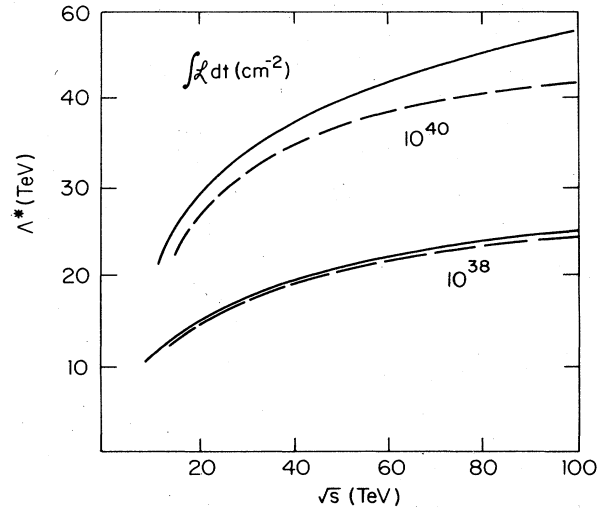

FIG. 251. Maximum compositeness scale Λ^* probed in dilepton production with $|y|<1.5$ for $\bar{p}p$ colliders at integrated luminosities of 10^{38} and 10^{40} cm^{-2} according to the criterion (8.33). $\eta_0'=-1$ (solid lines), $\eta_0'=+1$ (dashed lines).

presence of the contact term. The ensuing limits on Λ^* for the quark-quark composite interaction (8.8) are summarized in Figs. 236 and 241 for pp and $\bar{p}p$ interactions. Our principal conclusions are that for both pp and $\bar{p}p$ colliders at fixed energy, an integrated luminosity of 10^{40} cm^{-2} provides 1.5—2 times the reach of 10^{39} cm^{-2}; and that for collider energies $\sqrt{s} > 20$ TeV, $\bar{p}p$ collisions provide marginally better sensitivity than pp collisions.

The corresponding limits for the quark-lepton contact term of Eq. (8.21) are shown in Figs. 250 and 251 for pp and $\bar{p}p$ collisions. In the case of dilepton production, the advantage of $\bar{p}p$ over pp interactions at the same energy and luminosity is clear.

Finally, some comments are in order regarding the dependence of our results and conclusions upon the particular choice we made for the form of the contact interaction. Since the initial quark-antiquark states are averaged over colors and helicities, other simple choices for contact terms will yield effects of substantially the same magnitude, and with the same dependence on subenergy. We therefore believe our conclusions apply generally to the manifestations of quark and lepton compositeness. Our calculations of the conventional rates all are based on the Born approximation to the elementary cross section, which will surely be modified by perturbative QCD corrections. The resulting changes in absolute normalizations of standard model cross sections can easily be accommodated in the analysis of experimental data. We do not expect these corrections to modify significantly cross section shapes on the transverse momentum and mass scales of interest here. Our inferences about collider reach should be relatively insensitive to such complications.

IX. SUMMARY AND CONCLUSIONS

In this paper we have reviewed the case for exploration of the 1-TeV/c^2 mass scale, and have examined how a multi-TeV hadron collider will meet this task. Here we wish to draw a few lessons from the analysis we have presented.

The description of the strong, weak, and electromagnetic interactions of the fundamental constituents—the quarks and leptons—in terms of gauge theories based on the symmetry group $SU(3)_{color} \otimes SU(2)_L \otimes U(1)_Y$ is aesthetically appealing and has had many experimental successes. The unity and predictive power already achieved, and the promise of more complete unification of the fundamental interactions make it imperative to examine the foundations of the current paradigm and to take seriously its shortcomings as hints for improvements.

The incompleteness of our theoretical description is manifested by our ignorance of the dynamical mechanism that underlies the spontaneous breaking of electroweak gauge symmetry, by the multitude of seemingly arbitrary parameters required to specify the standard model, by the puzzling replication of quark and lepton generations, and by many other questions. For example, we do not know whether additional fundamental forces and elementary constituents remain to be discovered, nor do we understand how (or if) the fundamental interactions can by fully unified.

There are many areas in which we may search for a more complete and satisfying theory. These range from very general questions concerning the origin of gauge symmetries to the specific choice of a unifying gauge group. Any step into a regime of higher energies and shorter distance scales is likely to bring valuable experimental guidance. However, the standard theoretical model helps to define the frontier of our ignorance. The problem of spontaneous symmetry breaking in the electroweak theory is particularly urgent. It is the aspect of the theory which seems the most arbitrary and unpredictive. We have seen that general arguments and specific conjectures set the scale of 1 TeV for sorting out the mechanism for electroweak symmetry breaking. Although we hope and expect to learn much more from experimentation with a new accelerator, we adopt the ability to settle the issue of spontaneous symmetry breaking as a reasonable requirement for the next step.

At the outset of this paper, we stressed that a multi-TeV hadron collider should provide the means to test thoroughly the predictions of the standard model, to illuminate the physics of electroweak symmetry breakdown, and to explore the unknown. In order to translate these sentiments into requirements for accelerator performance, we have considered a broad variety of hard-scattering processes which bear on the capabilities of a hadron-hadron collider. These include conventional processes such as the production of large transverse momentum jets in QCD and the electroweak pair production of gauge bosons. Such processes are of interest as tests of the standard model and as backgrounds to more exotic phenomena. Among the latter, we have analyzed several alternatives for the Higgs sector of the electroweak theory, including the minimal Weinberg-Salam solution, supersymmetry, and technicolor. We have examined modest extensions to the standard model: sequential quarks and leptons, and additional charged and neutral intermediate bosons. We have also looked at manifestations of quark and lepton compositeness. In each case, we have explored the prospects for production and detection, in light of the anticipated conventional backgrounds. We have not considered in detail how to distinguish one new physics signal from another.

The calculations presented in Secs. III—VIII are intended to provide a base of reference information which will provoke informed discussions of the energy and luminosity requirements for a supercollider, and of the relative merits of proton-proton and proton-antiproton collisions. Other elements, including technical feasibility, rate demands on detectors, and cost, must also be weighed in arriving at machine parameters. For each of the principal physics topics, we have given a stylized summary of collider performance as a function of c.m. energy and luminosity. These are based on discovery criteria which we believe reasonable, but which are in the end inevitably

somewhat arbitrary. We encourage each reader to use the calculated cross sections to make an independent assessment of collider capabilities. The parton luminosities presented in Sec. II provide a measure of collider capabilities that is not tied to specific theoretical inventions.

Throughout the text, we have called attention to areas in which further work is required. Many of these have to do with simulations of signals and backgrounds in the context of projected detector performance. A few are of such general importance that we restate them here.

The detection and measurement of intermediate bosons $W^{\pm}$ and Z^0 in their nonleptonic decays should be a priority in detector development. Even if this can be achieved for only specific topologies, the potential rewards in terms of reconstruction efficiency for new phenomena are considerable.

Missing transverse momentum is an important signal (or trigger) for a number of new phenomena. This places a premium on the development of "hermetic" detectors which detect with high efficiency all the hadronic and electromagnetic energy emitted in the central rapidity region characterized by $|y| \lesssim 3$.

The ability to tag and measure heavy quarks and tau leptons would significantly enhance the incisiveness of many searches.

Other topics for study, including the better understanding of conventional backgrounds, must not be neglected.

Although we underline our hope that assiduous readers will arrive at their own conclusions, we cannot avoid stating those that we ourselves have drawn from this study. The most important of these is the conviction that a high-luminosity multi-TeV hadron collider will meet the objective of exploring the TeV energy scale and illuminating the nature of electroweak symmetry breaking. In more detail, we have come to the following conclusions.

- We are confident[13] that a 40-TeV collider which permits experimentation at integrated luminosities of 10^{39} cm^{-2} will make possible a detailed exploration of the 1-TeV scale.
- For a 10-TeV device, the same guarantees cannot so comfortably be made. At this lower energy, the upper reaches of the expected mass ranges for new phenomena are inaccessible, even at an integrated luminosity of 10^{40} cm^{-2}.

We are not so foolish as to say that a 10-TeV collider is without interest, or to assert that our calculations prove that it is inadequate to the task of sorting out the physics of electroweak symmetry breaking. We cannot state the precise location of the dividing line between our confidence at (40 TeV, 10^{39} cm^{-2}) and our trepidation at (10 TeV, 10^{40} cm^{-2}).

- Beyond the 1-TeV electroweak scale, we do not have specific landmarks in sight. However, the $1/\hat{s}$ behavior of hard-scattering cross sections suggests that to exploit collider energies higher than about 40 TeV fully requires an increase in luminosity as well as energy.
- For hard-scattering processes, the advantage of $\bar{p}p$ over pp collisions (at the same energy and luminosity) for the production of massive states is limited to a few special situations in which the presence of valence antiquarks is important and the integrated collider luminosity exceeds 5×10^{38} cm^{-2}. The general point is made clearly in the comparison of $u\bar{u}$ luminosities for pp and $\bar{p}p$ collisions presented in Fig. 57. A significant (factor-of-2) difference appears for $\sqrt{\hat{s}} \gtrsim 0.1\sqrt{s}$, corresponding to $\langle x \rangle \gtrsim 0.1$ and parton-parton luminosities $(\tau/\hat{s})d\mathcal{L}/d\tau \lesssim 10^{-2}$ nb. The choice between pp and $\bar{p}p$ colliders should thus be based on accelerator and detector considerations.
- There is no general relationship that governs energy-luminosity tradeoffs, but a few rules of thumb are useful for orientation.

(i) For a number of processes, and for 10 TeV $\lesssim\sqrt{s}\lesssim$ 40 TeV with $\int dt\,\mathcal{L} \gtrsim 10^{38}$ cm^{-2}, a factor-of-10 increase in luminosity is roughly equivalent to a factor-of-2 increase in the c.m. energy. Processes for which this rule holds are those for which we deemed background unimportant, so that the discovery criterion was some number of events produced. Examples include the production of massive quark pairs or additional intermediate bosons, and signals for compositeness in high-$p_\perp$ jets or high-mass dileptons.

(ii) At fixed c.m. energy, physics reach increases much more rapidly with increasing luminosity below $\int dt\,\mathcal{L} = 10^{38}$ cm^{-2} than it does above this value. This is easily understood from the shape of the parton luminosity curves, which fall more and more steeply as $\tau=\hat{s}/s$ increases.

(iii) Near 40 TeV and above, a tenfold increase in luminosity generally corresponds to more than a factor-of-2 increase in c.m. energy. For central production of both low-mass and high-mass particles, this again can be understood from the shapes of the parton-parton luminosities $(\tau/\hat{s})d\mathcal{L}/d\tau$ as functions of s and τ.

(iv) Finally, of course, no increase in luminosity can compensate for c.m. energy below the threshold for a new phenomenon.

All of our calculations have relied on the renormalization-group-improved parton model and the parton distribution functions we utilized in computations. There may be grounds for doubting that the model is correct in detail, but it has been rather successful in correctly predicting the shape and even the approximate value of several quite diverse reaction distributions such as production of high transverse momentum jets, of high-invariant-mass lepton pairs, and of W's and Z's. The model so far appears to give results accurate to within a factor of 2 or so, and that is sufficient for our

[13]The only exceptions among the processes we have considered are the technirho of the minimal technicolor model and a heavy Higgs boson observable only in $H\to Z^0Z^0\to l^+l^-l^+l^-$.

TABLE XI. Exponents a of $(1-x)$ for parton distributions.

Distribution	Λ (MeV)	Parton u_v	d_v	u_s	G	s_s	c_s	b_s	t_s
Set 1	200	3	4	7	5	7	7	7	7
Set 2	290	3	4	7	6	7	7	7	7

purposes. Our intention was to concentrate, within this framework, on the sensitivity of our calculated cross sections to the Q^2-dependent parton distributions. All cross sections were calculated using two different sets of structure functions. Cross sections obtained from the two sets generally agreed to within 20%. Even very drastic modifications of the small-x region of the gluon distribution at small Q^2 yielded differences of less than a factor of 2 at the smallest values of x we considered for the Q^2 values of interest to the supercollider. Even if there should be a major theoretical problem at small x which upsets our predictions in this region, our conclusions on the physics reach are unlikely to be affected, since they depend for the most part on $x \gtrsim 0.1$. Current indications are that the results are secure down to $x = 10^{-4}$.

The advances of the past decade have brought us tantalizingly close to a profound new understanding of the fundamental constituents of matter and the interactions among them. Progress toward a fuller synthesis surely requires both theoretical and experimental breakthroughs. While many ideas may precede the definitive experiments, it is likely that theoretical insights will require the impetus of experimental discovery. Though we do not know what the future holds, we may be confident that important clues are to be found on the scale of 1 TeV, and that a multi-TeV hadron supercollider will supply the means to reveal them.

ACKNOWLEDGMENTS

It is a pleasure to acknowledge the advice, comments, stimulating questions, and warm encouragement provided by many of our colleagues. We are particularly grateful to R. M. Barnett, J. D. Bjorken, R. N. Cahn, P. Darriulat, S. Dawson, L. di Lella, R. K. Ellis, M. K. Gaillard, H. Georgi, F. Gilman, S. L. Glashow, P. Grannis, F. Paige, R. Peccei, M. E. Peskin, F. Sciulli, M. Shochet, H. H. Williams, and B. Winstein for their contributions to this work. In addition, we have profited greatly from our interactions with participants in the PSSC (Physics at the Superconducting Super Collider) Discussion Group and in the Chicago workshop on $\bar{p}p$ options for the SSC.

We owe a considerable debt of gratitude to the College of Science and Department of Physics of Texas A&M University, who provided facilities and support for three of us (E.E., I.H., and K.L.) during the autumn of 1983 when this project was begun. They also generously placed the Physics Department's VAX-11/782 computer at our disposal for program development and calculations. We especially wish to thank Dean John Fackler and Professor F. Russell Huson, Professor Peter McIntyre, and Professor Robert Tribble for their hospitability and encouragement, and for valuable discussions. Thanks are also due to Professor Thomas Meyer and members of the computation staff for their assistance.

One of us (I.H.) thanks the DAMTP at the University of Cambridge for hospitality, the SERC of the United Kingdom for support, and the Cavendish Laboratory for the use of computing facilities.

This work was supported in part by the Director of Energy Research, Office of High Energy and Nuclear Physics, Division of High Energy Physics of the U.S. Department of Energy under Contract No. DE-AC03-76SF00098. Ohio State University is supported in part by the U.S. Department of Energy under Contract No. EY-76-C-02-1545. Fermi National Accelerator Laboratory is operated by Universities Research Association Inc. under contract with the United States Department of Energy.

APPENDIX. PARAMETRIZATIONS OF THE PARTON DISTRIBUTIONS

The calculations reported in this paper have been carried out using numerical values of the parton distributions obtained by integrating the Altarelli-Parisi (1977) equations. In order that others may use these distribution functions, we present here a parametrization of our numerical results. We have elected to use expansions in terms of orthogonal polynomials in place of the more conventional form (Owens and Reya, 1978; Baier *et al.*, 1979; Glück *et al.*, 1982; Duke and Owens, 1983) inspired by the $x \to 1$ behavior of structure functions. The fitting technique is described in full by Clenshaw and Hayes (1965).

Our parametrizations for $u_v(x,Q^2)$, $d_v(x,Q^2)$, $G(x,Q^2)$, $u_s(x,Q^2)$, and $s_s(x,Q^2)$ reproduce the distributions within 5% for

TABLE XII. Values of $t_{\min}$ for heavy quark distributions.

Distribution	Λ (MeV)	b quark $x>0.1$	b quark $x<0.1$	t quark $x>0.1$	t quark $x<0.1$
Set 1	200	8.1905	8.066 04	11.5528	11.4283
Set 2	290	7.4474	7.447 4	10.8097	10.8097

TABLE XIII. Coefficients c_{ij} for expansion (A2) for the parton distributions of Set 1 with $\Lambda=200$ MeV.

	$j \backslash i$	0	1	2	3	4	5
u_v	0	+0.772 11	−0.208 89	−0.331 13	−0.026 38	−0.016 52	−0.000 24
	1	−0.528 94	−0.264 50	+0.322 59	+0.121 39	+0.025 79	+0.008 93
	2	+0.213 04	+0.184 12	−0.086 28	−0.067 17	−0.018 59	−0.005 97
	3	−0.089 61	−0.095 73	+0.015 89	+0.026 44	+0.009 51	+0.003 08
	4	+0.035 31	+0.041 88	−0.000 29	−0.008 69	−0.003 80	−0.001 29
	5	−0.015 02	−0.019 43	−0.002 45	+0.002 64	+0.001 46	+0.000 54
d_v	0	+0.383 89	−0.080 68	−0.163 69	−0.022 45	−0.008 86	−0.000 67
	1	−0.292 90	−0.142 68	+0.167 83	+0.067 58	+0.015 53	+0.004 80
	2	+0.123 36	+0.101 93	−0.048 66	−0.037 97	−0.011 04	−0.003 39
	3	−0.053 24	−0.054 47	+0.010 19	+0.015 65	+0.005 78	+0.001 83
	4	+0.021 31	+0.024 28	−0.000 81	−0.005 41	−0.002 39	−0.000 80
	5	−0.009 21	−0.011 48	−0.001 11	+0.001 77	+0.000 96	+0.000 35
u_s	0	+0.073 43	−0.065 26	+0.035 09	−0.002 91	+0.005 84	+0.000 11
	1	−0.017 44	−0.001 87	+0.007 16	−0.009 13	+0.001 38	−0.001 78
	2	−0.006 36	−0.000 21	−0.007 88	−0.000 57	−0.001 82	−0.000 55
	3	+0.007 61	+0.004 32	+0.004 32	+0.002 21	+0.001 34	+0.000 71
	4	−0.004 46	−0.003 45	−0.001 90	−0.001 31	−0.000 68	−0.000 38
	5	+0.002 62	+0.002 39	+0.000 86	+0.000 61	+0.000 29	+0.000 16
G	0	+0.970 96	−0.956 21	+0.122 99	−0.098 46	+0.042 06	−0.025 82
	1	−0.960 43	+0.527 90	+0.339 20	−0.100 00	+0.016 06	−0.021 08
	2	+0.423 70	−0.079 78	−0.342 83	+0.048 01	−0.010 70	+0.009 05
	3	−0.186 03	−0.015 29	+0.220 21	+0.009 07	+0.005 16	−0.000 61
	4	+0.077 73	+0.015 95	−0.107 60	−0.020 36	−0.003 32	−0.001 25
	5	−0.036 82	−0.009 53	+0.055 84	+0.020 12	+0.003 97	+0.001 58
s_s	0	+0.054 14	−0.038 19	+0.026 15	−0.000 82	+0.005 25	+0.000 35
	1	−0.005 71	−0.014 84	+0.007 25	−0.007 49	+0.001 03	−0.001 57
	2	−0.010 22	+0.003 30	−0.006 80	−0.001 32	−0.001 73	−0.000 60
	3	+0.008 97	+0.003 28	+0.003 70	+0.002 45	+0.001 33	+0.000 72
	4	−0.004 93	−0.003 14	−0.001 63	−0.001 39	−0.000 68	−0.000 38
	5	+0.002 79	+0.002 29	+0.000 74	+0.000 63	+0.000 30	+0.000 16
c_s	0	+0.011 21	−0.013 45	+0.006 89	−0.002 24	+0.001 06	−0.000 52
	1	+0.008 01	−0.009 54	+0.005 52	−0.002 00	+0.001 00	−0.000 48
	2	−0.005 07	+0.005 45	−0.002 22	+0.000 31	−0.000 21	+0.000 07
	3	+0.000 42	−0.001 52	+0.000 13	−0.000 14	−0.000 11	−0.000 02
	4	+0.001 09	−0.000 07	+0.000 27	+0.000 15	+0.000 13	+0.000 01
	5	−0.001 07	+0.001 19	−0.000 15	+0.000 02	−0.000 01	+0.000 02
b_s	0	+0.006 69	−0.008 49	+0.004 77	−0.001 94	+0.000 87	−0.000 46
	1	+0.005 36	−0.006 31	+0.003 90	−0.001 50	+0.000 78	−0.000 38
	2	−0.002 19	+0.002 73	−0.001 24	+0.000 40	−0.000 15	+0.000 07
	3	+0.000 01	−0.000 71	+0.000 08	−0.000 17	−0.000 04	−0.000 02
	4	+0.000 44	−0.000 08	+0.000 11	+0.000 06	+0.000 04	+0.000 01
	5	−0.000 32	+0.000 51	−0.000 05	+0.000 05	+0.000 01	+0.000 01
t_s	0	+0.003 34	−0.004 57	+0.002 64	−0.001 30	+0.000 54	−0.000 34
	1	+0.003 30	−0.004 06	+0.002 53	−0.001 10	+0.000 54	−0.000 29
	2	−0.000 55	+0.001 07	−0.000 41	+0.000 29	−0.000 05	+0.000 07
	3	−0.000 26	+0.000 02	−0.000 08	−0.000 06	−0.000 02	−0.000 01
	4	+0.000 21	−0.000 31	+0.000 07	−0.000 04	−0.000 00	−0.000 00
	5	−0.000 07	+0.000 25	−0.000 05	+0.000 05	−0.000 00	+0.000 01

TABLE XIV. Coefficients d_{ij} for expansion (A6) for the parton distributions of Set 1 with $\Lambda=200$ MeV.

	j \ i	0	1	2	3	4	5
u_v	0	+0.240 48	+0.291 94	+0.098 41	+0.021 74	+0.003 53	+0.000 54
	1	+0.018 48	−0.004 72	−0.026 24	−0.018 83	−0.007 83	−0.002 63
	2	−0.005 87	−0.005 25	+0.000 94	+0.002 38	+0.001 47	+0.000 70
	3	+0.001 75	+0.001 99	+0.000 33	−0.000 31	−0.000 28	−0.000 16
	4	−0.000 53	−0.000 65	−0.000 17	+0.000 04	+0.000 06	+0.000 04
	5	+0.000 17	+0.000 23	+0.000 08	+0.000 01	−0.000 01	−0.000 01
d_v	0	+0.126 72	+0.136 15	+0.039 88	+0.008 35	+0.001 70	+0.000 46
	1	+0.004 44	−0.010 88	−0.015 94	−0.009 45	−0.003 64	−0.001 20
	2	−0.001 99	−0.000 69	+0.001 52	+0.001 53	+0.000 80	+0.000 36
	3	+0.000 65	+0.000 51	−0.000 13	−0.000 28	−0.000 17	−0.000 09
	4	−0.000 20	−0.000 19	−0.000 00	+0.000 06	+0.000 04	+0.000 02
	5	+0.000 07	+0.000 08	+0.000 02	−0.000 01	−0.000 01	−0.000 01
u_s	0	+1.037 42	−1.129 35	+0.343 13	−0.074 90	+0.008 84	−0.000 89
	1	+0.949 25	−1.313 66	+0.454 41	−0.098 49	+0.014 13	−0.001 14
	2	+0.049 85	−0.129 88	+0.086 80	−0.026 14	+0.004 74	−0.000 60
	3	−0.027 98	+0.050 52	−0.018 19	+0.001 74	+0.000 24	−0.000 05
	4	+0.007 29	−0.011 45	+0.001 65	+0.000 69	−0.000 21	−0.000 00
	5	−0.001 74	+0.002 30	+0.000 42	−0.000 36	+0.000 04	+0.000 01
G	0	+29.398 5	−38.776 5	+14.449 6	−3.266 25	+0.491 24	−0.057 72
	1	+25.404 5	−39.147 6	+16.339 4	−4.198 27	+0.668 28	−0.080 47
	2	−1.778 39	+1.341 95	+1.025 88	−0.675 37	+0.186 06	−0.023 05
	3	−0.213 53	+0.815 07	−0.715 12	+0.186 69	−0.019 99	−0.002 92
	4	+0.220 41	−0.452 24	+0.230 98	−0.027 20	−0.003 19	+0.001 80
	5	−0.094 45	+0.164 72	−0.058 24	−0.002 22	+0.002 63	−0.000 45
s_s	0	+0.946 51	−1.108 36	+0.352 14	−0.072 57	+0.009 13	−0.000 92
	1	+0.956 94	−1.301 98	+0.458 09	−0.098 37	+0.013 75	−0.001 33
	2	+0.048 45	−0.132 37	+0.085 58	−0.026 47	+0.004 71	−0.000 57
	3	−0.027 63	+0.051 18	−0.017 83	+0.001 87	+0.000 27	−0.000 05
	4	+0.007 19	−0.011 63	+0.001 54	+0.000 64	−0.000 22	−0.000 00
	5	−0.001 71	+0.002 35	+0.000 45	−0.000 35	+0.000 05	+0.000 01
c_s	0	+0.420 71	−0.528 00	+0.174 18	−0.034 64	+0.004 14	−0.000 52
	1	+0.470 47	−0.622 78	+0.221 02	−0.047 18	+0.006 23	−0.000 71
	2	+0.012 63	−0.053 01	+0.036 97	−0.012 14	+0.002 31	−0.000 22
	3	−0.016 00	+0.025 57	−0.008 38	+0.000 83	+0.000 08	−0.000 04
	4	+0.009 82	−0.010 39	+0.001 86	+0.000 23	−0.000 07	−0.000 00
	5	−0.007 97	+0.006 60	−0.001 05	−0.000 08	+0.000 01	+0.000 01
b_s	0	+0.416 04	−0.548 47	+0.190 96	−0.039 29	+0.004 91	−0.000 56
	1	+0.428 54	−0.583 26	+0.215 14	−0.047 41	+0.006 50	−0.000 73
	2	−0.012 26	−0.003 46	+0.014 17	−0.006 69	+0.001 54	−0.000 17
	3	−0.004 62	+0.008 69	−0.003 95	+0.000 71	−0.000 04	−0.000 02
	4	+0.006 74	−0.008 17	+0.002 46	−0.000 29	+0.000 01	−0.000 00
	5	−0.006 97	+0.007 92	−0.002 27	+0.000 30	−0.000 02	+0.000 01
t_s	0	+0.343 13	−0.472 32	+0.176 58	−0.039 30	+0.005 41	−0.000 59
	1	+0.357 80	−0.498 74	+0.191 74	−0.044 32	+0.006 42	−0.000 71
	2	−0.011 89	+0.008 36	+0.003 17	−0.002 72	+0.000 78	−0.000 11
	3	−0.008 27	+0.011 35	−0.004 32	+0.000 89	−0.000 10	+0.000 01
	4	+0.009 26	−0.011 88	+0.004 04	−0.000 76	+0.000 08	−0.000 01
	5	−0.005 95	+0.007 54	−0.002 47	+0.000 45	−0.000 04	+0.000 01

TABLE XV. Coefficients c_{ij} for expansion (A2) for the parton distributions of Set 2 with $\Lambda=290$ MeV.

	$j \backslash i$	0	1	2	3	4	5
u_v	0	+0.728 07	−0.219 48	−0.300 31	−0.020 20	−0.015 50	+0.000 18
	1	−0.528 66	−0.242 29	+0.330 45	+0.113 97	+0.023 61	+0.008 29
	2	+0.225 65	+0.185 14	−0.100 90	−0.070 86	−0.018 55	−0.005 98
	3	−0.101 81	−0.104 88	+0.023 18	+0.031 18	+0.010 61	+0.003 40
	4	+0.042 52	+0.048 93	−0.002 70	−0.011 33	−0.004 65	−0.001 55
	5	−0.019 13	−0.024 12	−0.002 01	+0.003 89	+0.001 96	+0.000 70
d_v	0	+0.360 29	−0.086 27	−0.148 29	−0.018 95	−0.008 20	−0.000 46
	1	−0.291 22	−0.130 42	+0.170 71	+0.063 55	+0.014 30	+0.004 43
	2	+0.129 95	+0.101 89	−0.056 15	−0.039 76	−0.010 98	−0.003 37
	3	−0.060 18	−0.059 33	+0.014 26	+0.018 24	+0.006 40	+0.002 00
	4	+0.025 53	+0.028 18	−0.002 27	−0.006 92	−0.002 88	−0.000 94
	5	−0.011 67	−0.014 15	−0.000 77	+0.002 53	+0.001 27	+0.000 45
u_s	0	+0.105 99	−0.068 04	+0.025 01	−0.003 42	+0.004 91	+0.000 07
	1	−0.052 39	−0.020 87	+0.018 35	−0.007 38	+0.001 82	−0.001 63
	2	+0.010 54	+0.016 28	−0.010 46	−0.001 89	−0.001 87	−0.000 65
	3	+0.000 23	−0.005 19	+0.003 98	+0.003 02	+0.001 44	+0.000 82
	4	−0.001 67	+0.000 81	−0.001 23	−0.001 70	−0.000 78	−0.000 46
	5	+0.001 58	+0.000 48	+0.000 27	+0.000 75	+0.000 36	+0.000 21
G	0	+2.491 64	+0.627 56	+0.533 96	+0.209 59	+0.205 34	+0.057 73
	1	−3.265 98	−1.987 73	−0.106 13	−0.400 57	−0.161 39	−0.109 21
	2	+1.827 08	+1.488 16	−0.225 87	+0.057 88	+0.017 56	+0.024 48
	3	−0.991 71	−0.919 24	+0.261 85	+0.151 82	+0.070 22	+0.029 20
	4	+0.471 58	+0.456 21	−0.166 64	−0.150 03	−0.070 94	−0.032 95
	5	−0.250 44	−0.248 04	+0.105 21	+0.127 20	+0.066 50	+0.031 92
s_s	0	+0.069 46	−0.042 27	+0.021 39	−0.001 25	+0.004 63	+0.000 31
	1	−0.021 98	−0.023 68	+0.012 75	−0.007 10	+0.001 15	−0.001 56
	2	−0.002 85	+0.012 29	−0.007 80	−0.001 76	−0.001 58	−0.000 60
	3	+0.006 38	−0.001 71	+0.003 24	+0.002 92	+0.001 34	+0.000 79
	4	−0.004 27	−0.001 09	−0.001 13	−0.001 67	−0.000 75	−0.000 45
	5	+0.002 77	+0.001 53	+0.000 34	+0.000 76	+0.000 35	+0.000 21
c_s	0	+0.011 40	−0.014 61	+0.007 38	−0.002 44	+0.001 01	−0.000 50
	1	+0.007 71	−0.009 86	+0.005 68	−0.002 17	+0.000 99	−0.000 48
	2	−0.005 49	+0.006 38	−0.002 54	+0.000 35	−0.000 15	+0.000 05
	3	+0.000 73	−0.001 76	+0.000 30	−0.000 10	−0.000 12	−0.000 00
	4	+0.000 99	−0.000 14	+0.000 22	+0.000 14	+0.000 12	−0.000 00
	5	−0.001 14	+0.001 27	−0.000 20	−0.000 02	−0.000 00	+0.000 02
b_s	0	+0.006 57	−0.008 86	+0.004 97	−0.002 09	+0.000 88	−0.000 47
	1	+0.005 10	−0.006 45	+0.003 93	−0.001 60	+0.000 78	−0.000 38
	2	−0.002 28	+0.003 01	−0.001 38	+0.000 45	−0.000 14	+0.000 07
	3	+0.000 11	−0.000 71	+0.000 15	−0.000 16	−0.000 03	−0.000 02
	4	+0.000 40	−0.000 10	+0.000 10	+0.000 06	+0.000 03	+0.000 01
	5	−0.000 33	+0.000 48	−0.000 08	+0.000 03	+0.000 01	−0.000 00
t_s	0	+0.003 25	−0.004 65	+0.002 74	−0.001 38	+0.000 58	−0.000 36
	1	+0.003 15	−0.004 11	+0.002 58	−0.001 16	+0.000 57	−0.000 30
	2	−0.000 59	+0.001 13	−0.000 49	+0.000 32	−0.000 07	+0.000 07
	3	−0.000 23	+0.000 04	−0.000 08	−0.000 06	−0.000 02	−0.000 02
	4	+0.000 22	−0.000 30	+0.000 11	−0.000 04	+0.000 01	−0.000 00
	5	−0.000 08	+0.000 25	−0.000 07	+0.000 06	−0.000 00	+0.000 01

TABLE XVI. Coefficients d_{ij} for expansion (A6) for the parton distributions of Set 2 with $\Lambda=290$ MeV.

	$j \backslash i$	0	1	2	3	4	5
u_v	0	+0.242 14	+0.289 94	+0.094 39	+0.019 28	+0.002 63	+0.000 28
	1	+0.018 72	−0.007 73	−0.029 72	−0.020 53	−0.008 31	−0.002 70
	2	−0.006 58	−0.005 51	+0.001 56	+0.002 98	+0.001 77	+0.000 81
	3	+0.002 14	+0.002 36	+0.000 29	−0.000 45	−0.000 37	−0.000 21
	4	−0.000 69	−0.000 83	−0.000 20	+0.000 07	+0.000 08	+0.000 05
	5	+0.000 23	+0.000 31	+0.000 11	+0.000 01	−0.000 02	−0.000 01
d_v	0	+0.126 99	+0.134 22	+0.037 66	+0.007 19	+0.001 30	+0.000 35
	1	+0.004 26	−0.012 81	−0.017 64	−0.010 16	−0.003 81	−0.001 22
	2	−0.002 19	−0.000 52	+0.001 96	+0.001 85	+0.000 95	+0.000 41
	3	+0.000 78	+0.000 57	−0.000 22	−0.000 37	−0.000 23	−0.000 12
	4	−0.000 26	−0.000 24	+0.000 01	+0.000 08	+0.000 06	+0.000 03
	5	+0.000 09	+0.000 10	+0.000 02	−0.000 01	−0.000 01	−0.000 01
u_s	0	+1.107 09	−1.215 03	+0.393 59	−0.086 76	+0.011 15	−0.001 20
	1	+1.019 89	−1.427 67	+0.507 74	−0.116 66	+0.016 67	−0.001 74
	2	+0.051 85	−0.136 67	+0.092 46	−0.028 94	+0.005 83	−0.000 65
	3	−0.033 05	+0.058 98	−0.021 24	+0.002 59	+0.000 10	−0.000 09
	4	+0.009 29	−0.014 32	+0.002 12	+0.000 63	−0.000 23	+0.000 02
	5	−0.002 37	+0.003 01	+0.000 53	−0.000 40	+0.000 06	+0.000 01
G	0	+30.263 9	−40.346 8	+15.575 2	−3.621 33	+0.585 17	−0.068 56
	1	+26.788 3	−41.227 8	+17.395 4	−4.691 53	+0.760 16	−0.103 36
	2	−2.037 21	+1.540 90	+1.023 06	−0.680 24	+0.213 00	−0.023 79
	3	−0.245 27	+0.976 60	−0.810 19	+0.210 90	−0.030 49	−0.004 21
	4	+0.261 43	−0.558 77	+0.274 07	−0.033 97	−0.001 39	+0.002 67
	5	−0.116 40	+0.213 23	−0.071 37	−0.001 90	+0.002 67	−0.000 79
s_s	0	+1.012 03	−1.197 34	+0.400 70	−0.085 19	+0.011 23	−0.001 27
	1	+1.028 31	−1.414 57	+0.512 36	−0.116 02	+0.016 52	−0.001 85
	2	+0.050 25	−0.139 58	+0.090 97	−0.029 43	+0.005 73	−0.000 66
	3	−0.032 62	+0.059 79	−0.020 78	+0.002 78	+0.000 15	−0.000 08
	4	+0.009 17	−0.014 56	+0.001 98	+0.000 57	−0.000 25	+0.000 01
	5	−0.002 33	+0.003 08	+0.000 58	−0.000 37	+0.000 07	+0.000 01
c_s	0	+0.451 68	−0.574 25	+0.196 93	−0.040 91	+0.005 07	−0.000 75
	1	+0.504 13	−0.675 85	+0.247 58	−0.055 22	+0.007 64	−0.000 96
	2	+0.011 59	−0.054 32	+0.038 62	−0.013 53	+0.002 76	−0.000 24
	3	−0.018 10	+0.029 38	−0.009 80	+0.001 27	+0.000 02	−0.000 06
	4	+0.011 02	−0.012 08	+0.002 32	+0.000 18	−0.000 08	+0.000 01
	5	−0.008 48	+0.007 20	−0.001 27	−0.000 09	+0.000 01	+0.000 01
b_s	0	+0.452 34	−0.603 32	+0.216 64	−0.046 65	+0.006 13	−0.000 77
	1	+0.457 33	−0.630 02	+0.239 29	−0.055 13	+0.007 98	−0.000 96
	2	−0.017 72	+0.003 12	+0.012 37	−0.006 83	+0.001 74	−0.000 19
	3	−0.003 13	+0.007 40	−0.003 82	+0.000 82	−0.000 08	−0.000 02
	4	+0.005 93	−0.007 52	+0.002 41	−0.000 32	+0.000 02	−0.000 00
	5	−0.006 40	+0.007 50	−0.002 29	+0.000 33	−0.000 03	−0.000 00
t_s	0	+0.376 36	−0.523 35	+0.200 81	−0.046 60	+0.006 76	−0.000 78
	1	+0.383 46	−0.540 05	+0.213 01	−0.051 29	+0.007 84	−0.000 93
	2	−0.018 04	+0.016 65	+0.000 23	−0.002 25	+0.000 80	−0.000 11
	3	−0.006 73	+0.009 56	−0.003 90	+0.000 87	−0.000 12	+0.000 01
	4	+0.009 13	−0.011 93	+0.004 24	−0.000 85	+0.000 11	−0.000 01
	5	−0.005 93	+0.007 64	−0.002 63	+0.000 51	−0.000 06	+0.000 01

$$Q^2_{\min} \equiv 5 \text{ GeV}^2 < Q^2 < 10^8 \text{ GeV}^2 \equiv Q^2_{\max} , \tag{A1}$$

except at $x > 0.9$, where the distributions are negligibly small. The heavy quark distributions are reproduced less accurately, particularly near threshold and at $x > 0.6$. The rapid Q^2 variation of the distributions near threshold causes difficulty for the fitting routine. However, the distributions (and the parametrizations) are small ($\sim 10^{-5}$) in the region where the fits are reliable only within a factor of 2 or so. The parametrizations yield tiny negative values ($\sim -10^{-7}$) for the heavy flavors near threshold at large values of x.

The small-x region is very important for our applications, so a reliable parametrization there is vital. For this reason we have divided the x range at $x = 0.1$. For $x > 0.1$ we parametrize the distributions as

$$f(x,Q^2) = x^{-1}(1-x)^a \sum_{i,j=0}^{5} c_{ij} T_i(x') T_j(t') , \tag{A2}$$

where

$$x' = \frac{2x - 1.1}{0.9} , \tag{A3}$$

$$t' = \frac{2t - (t_{\max} + t_{\min})}{t_{\max} - t_{\min}} , \tag{A4}$$

and

$$t \equiv \ln(Q^2/\Lambda^2) . \tag{A5}$$

The Chebyshev polynomials $T_n(x)$ are defined, for example, in Table 22.3 of Abramowitz and Stegun (1965). For smaller values of x in the interval $10^{-4} < x < 0.1$ we employ polynomials in $\ln x$:

$$f(x,Q^2) = x^{-1}(1-x)^a \sum_{i,j=0}^{5} d_{ij} T_i(y) T_j(t') , \tag{A6}$$

where

$$y = \frac{2 \ln x + 11.512\,93}{6.907\,76} . \tag{A7}$$

Notice that the arguments of the Chebyshev polynomials vary from -1 to 1. The exponents a are given in Table XI.

For all the distributions considered,

$$t_{\max} = \ln(Q^2_{\max}/\Lambda^2) = \ln(10^8 \text{ GeV}^2/\Lambda^2) . \tag{A8}$$

Except for the b and t quarks, the lower limit of the Q^2 variable is

$$t_{\min} = \ln(Q^2_{\min}/\Lambda^2) = \ln(5 \text{ GeV}^2/\Lambda^2) . \tag{A9}$$

For the heavy quarks [compare (2.39)] the distributions must vanish if

$$\beta^2 = 1 - 4M_q^2/Q^2(1-x) \tag{A10}$$

is negative, where the heavy quark mass M_q is

$$M_b = 5.5 \text{ GeV}/c^2 , \quad M_t = 30 \text{ GeV}/c^2 . \tag{A11}$$

Consequently the lower limit of Q^2 is raised; this leads to the values of $t_{\min}$ given in Table XII.

The coefficients c_{ij} and d_{ij} are given in Tables XIII and XIV for the distributions of Set 1 and in Tables XV and XVI for the distributions of Set 2.

REFERENCES

Abbott, L. F., E. Farhi, and S.-H. H. Tye, 1982, in *Proceedings of the 1982 DPF Summer Study on Elementary Particle Physics and Future Facilities,* edited by R. Donaldson, R. Gustafson, and F. Paige (Fermilab, Batavia, Illinois), p. 288.

Abolins, M., *et al.*, 1982, in *Proceedings of the 1982 DPF Summer Study on Elementary Particle Physics and Future Facilities,* edited by R. Donaldson, R. Gustafson, and F. Paige (Fermilab, Batavia, Illinois), p. 274.

Abramowicz, H., *et al.*, 1982, Z. Phys. C **13**, 199.

Abramowicz, H., *et al.*, 1983, Z. Phys. C **17**, 283.

Abramowitz, M., and I. Stegun, 1965, *Handbook of Mathematical Functions* (Dover, New York).

Aitchison, I. J. R., and A. J. G. Hey, 1982, *Gauge Theories in Particle Physics* (Hilger, Bristol).

Albrow, M. G., 1983, in *Proceedings of the 1983 International Europhysics Conference on High Energy Physics,* edited by J. Guy and C. Costain (Rutherford Laboratory, Chilton, England), p. 134.

Ali, A., J. G. Körner, Z. Kunst, J. Willrodt, G. Kramer, G. Schierholz, and E. Pietarinen, 1979a, Phys. Lett. **82B**, 285.

Ali, A., J. G. Körner, G. Kramer, and J. Willrodt, 1979b, Z. Phys. C **1**, 25, 203.

Ali, A., E. Pietarinen, G. Kramer, and J. Willrodt, 1980, Phys. Lett. **93B**, 155.

Altarelli, G., R. K. Ellis, M. Greco, and G. Martinelli, 1984, CERN Report TH3851.

Altarelli, G., R. K. Ellis, and G. Martinelli, 1978, Nucl. Phys. B **143**, 521; **146**, 544(E).

Altarelli, G., and G. Parisi, 1977, Nucl. Phys. B **126**, 298.

Althoff, M., *et al.* (TASSO collaboration), 1983, Phys. Lett. **122B**, 95.

Amaldi, U., 1980, Ed., *Proceedings of the Second Workshop on Possibilities and Limitations of Accelerators and Detectors, Les Diablerets, Switzerland, 1979* (CERN, Geneva).

Andersson, B., G. Gustafson, G. Ingelman, and T. Sjöstrand, 1983, Phys. Rep. **97**, 31.

Antonelli, F., M. Consoli, and G. Corbo, 1980, Phys. Lett. **91B**, 90.

Arnison, G., *et al.*, 1983a, Phys. Lett. **122B**, 103.

Arnison, G., *et al.*, 1983b, Phys. Lett. **123B**, 115.

Arnison, G., *et al.*, 1983c, Phys. Lett. **126B**, 398.

Arnison, G., *et al.*, 1983d, "Hadronic Jet Production at the CERN Proton-Antiproton Collider," CERN-EP/83-118.

Arnold, R. G., *et al.*, 1984, Phys. Rev. Lett. **52**, 727.

Asratyan, A. E., *et al.*, 1983, Moscow preprint ITEP-110.

Aubert, J. J., *et al.*, 1983a, Phys. Lett. **121B**, 87.

Aubert, J. J., *et al.*, 1983b, Phys. Lett. **123B**, 123.

Aubert, J. J., *et al.*, 1983c, Phys. Lett. **123B**, 275.

Aubert, J. J., *et al.*, 1983d, Nucl. Phys. B **213**, 1.

Aubert, J. J., *et al.*, 1983e, Nucl. Phys. B **213**, 31.

Axelrod, A., 1982, Nucl. Phys. B **209**, 349.

Bagnaia, P., *et al.*, 1983a, Z. Phys. C **20**, 117.
Bagnaia, P., *et al.*, 1983b, Phys. Lett. **129B**, 130.
Bagnaia, P., *et al.*, 1984, CERN-EP/84-12.
Baier, R., J. Engels, and B. Petersson, 1979, Z. Phys. C **2**, 265.
Baltay, C., L. Littenberg, and F. Paige, in *Proceedings of the 1982 DPF Summer Study on Elementary Particle Physics and Future Facilities,* edited by R. Donaldson, R. Gustafson, and F. Paige (Fermilab, Batavia, Illinois), p. 521.
Banner, M., *et al.*, 1982, Phys. Lett. **118B**, 203.
Banner, M., *et al.*, 1983, Phys. Lett. **122B**, 476.
Barbiellini, G., *et al.*, 1981, "Technicolor Particles at LEP," DESY Report 81-064.
Barbieri, R., 1983, in *Proceedings of the 1983 International Symposium on Lepton and Photon Interactions at High Energies,* edited by D. G. Cassel and D. L. Kreinick (Newman Laboratory of Nuclear Studies, Cornell University, Ithaca, New York), p. 479.
Barbieri, R., L. Maiani, and R. Petronzio, 1980, Phys. Lett. **96B**, 63.
Bardeen, J., L. N. Cooper, and J. R. Schrieffer, 1962, Phys. Rev. **106**, 162.
Bardeen, W. A., H. Fritzsch, and M. Gell-Mann, 1973, in *Scale and Conformal Symmetry in Hadron Physics,* edited by R. Gatto (Wiley, New York), p. 139.
Barger, V., H. Baer, K. Hagiwara, and R. J. N. Phillips, 1984, University of Wisconsin preprint MAD/PH/150.
Bars, I., 1982, in *Quarks, Leptons, and Supersymmetry,* edited by J. Tran Thanh Van (Editions Frontieres, Gif-sur-Yvette, France), p. 541.
Baulieu, L., J. Kaplan, and P. Fayet, 1984, Phys. Lett. **141B**, 198.
Benvenuti, A., *et al.*, 1974, Phys. Rev. Lett. **32**, 800.
Berends, F. A., R. Kleiss, P. de Causmaecker, R. Gastmans, and T. T. Wu, 1981, Phys. Lett. **103B**, 124.
Berger, E. L., P. K. Malhotra, R. Orava, and H. B. Thacker, Eds., 1983, *Proceedings of the Drell-Yan Workshop* (Fermilab, Batavia, Illinois).
Bergsma, F., *et al.* (CHARM collaboration), 1983, Phys. Lett. **123B**, 269.
Berman, S. M., J. D. Bjorken, and J. B. Kogut, 1971, Phys. Rev. D **4**, 3388.
Bjorken, J. D., 1976, in *Weak Interactions at High Energy and the Production of New Particles,* edited by Martha C. Zipf, SLAC Report No. 198, p. 1.
Bodek, A., M. Breidenbach, D. L. Dubin, J. E. Elias, J. I. Friedman, H. W. Kendall, J. S. Poucher, E. M. Riordan, M. Sogard, D. H. Coward, and D. J. Sherden, 1979, Phys. Rev. D **20**, 1471.
Bodek, A., and J. Ritchie, 1981, Phys. Rev. D **23**, 1070.
Bodek, A., N. Giokaris, W. B. Atwood, D. H. Coward, D. J. Sherden, D. L. Dubin, J. Elias, J. I. Friedman, H. W. Kendall, J. S. Poucher, and E. M. Riordan, 1983a, Phys. Rev. Lett. **50**, 1431.
Bodek, A., N. Giokaris, W. B. Atwood, D. H. Coward, D. L. Dubin, M. Breidenbach, J. E. Elias, J. I. Friedman, H. W. Kendall, J. S. Poucher, and E. M. Riordan, 1983b, Phys. Rev. Lett. **51**, 534.
Bosetti, P. C., *et al.*, 1982, Nucl. Phys. B **203**, 362.
Brandelik, R., *et al.* (TASSO collaboration), 1982, Phys. Lett. **117B**, 365.
Branson, J. G., 1981, in *Proceedings of the 1981 International Symposium on Lepton and Photon Interactions at High Energies,* edited by W. Pfeil (Physikalisches Institut, Universität Bonn), p. 279.
Brodsky, S. J., and R. W. Brown, 1982, Phys. Rev. Lett. **49**, 966.
Brodsky, S. J., and S. D. Drell, 1980, Phys. Rev. D **22**, 2236.
Brodsky, S. J., P. Hoyer, C. Peterson, and N. Sakai, 1980, Phys. Lett. **93B**, 451.
Brodsky, S. J., C. Peterson, and N. Sakai, 1981, Phys. Rev. D **23**, 2745.
Brown, R. W., K. L. Kowalski, and S. J. Brodsky, 1983, Phys. Rev. D **28**, 624.
Brown, R. W., and K. O. Mikaelian, 1979, Phys. Rev. D **19**, 922.
Brown, R. W., D. Sahdev, and K. O. Mikaelian, 1979, Phys. Rev. D **20**, 1164.
Buras, A. J., 1980, Rev. Mod. Phys. **52**, 199.
Cabibbo, N., 1963, Phys. Rev. Lett. **10**, 531.
Cabibbo, N., L. Maiani, G. Parisi, and R. Petronzio, 1979, Nucl. Phys. B **158**, 295.
Cahn, R. N., 1982, in *Proceedings of the 10th SLAC Summer Institute,* edited by Anne Mosher, SLAC Report No. 259, p. 1.
Cahn, R. N., and S. Dawson, 1984, Phys. Lett. **136B**, 196.
Calmet, J., S. Narison, M. Perrotet, and E. de Rafael, 1977, Rev. Mod. Phys. **49**, 21.
Cazzoli, E. G., A. M. Cnops, P. L. Connolly, R. I. Louttit, M. J. Murtagh, R. B. Palmer, N. P. Samios, T. T. Tso, and H. H. Williams, 1975, Phys. Rev. Lett. **34**, 1124.
Chadha, S., and M. Peskin, 1981a, Nucl. Phys. B **185**, 61.
Chadha, S., and M. Peskin, 1981b, Nucl. Phys. B **187**, 541.
Chanowitz, M. S., and S. D. Drell, 1973, Phys. Rev. Lett. **30**, 807.
Chanowitz, M. S., M. A. Furman, and I. Hinchliffe, 1979, Nucl. Phys. B **153**, 402.
Chanowitz, M. S., and M. K. Gaillard, 1984, Berkeley preprint LBL-17496; UCB-PTH-84/5.
Chanowitz, M. S., and S. Sharpe, 1983, Phys. Lett. **126B**, 225.
Claudson, M., L. Hall, and I. Hinchliffe, 1983, Nucl. Phys. B **228**, 501.
Clenshaw, C. W., and J. G. Hayes, 1965, J. Inst. Math. Appl. **1**, 164.
Collins, J., 1984, "Report of the Subgroup on Theoretical Problems at Small x," in *Proceedings of the 1984 Summer Study on the Design and Utilization of the Superconducting Super Collider,* edited by R. Donaldson and J. Morfin (Fermilab, Batavia, Illinois) (in press).
Combley, F., F. J. M. Farley, and E. Picasso, 1981, Phys. Rep. **68**, 93.
Combridge, B. L., 1979, Nucl. Phys. B **151**, 429.
Cooper, A. M., *et al.*, 1984, Phys. Lett. **141B**, 133.
Dawson, S., E. Eichten, and C. Quigg, 1984, Fermilab-Pub-83/82-T.
Deser, S., and B. Zumino, 1976, Phys. Lett. **62B**, 335.
Diebold, R., 1983, Science **222**, 13.
Dimopoulos, S., 1980, Nucl. Phys. B **168**, 69.
Dimopoulos, S., S. Raby, and G. L. Kane, 1981, Nucl. Phys. B **182**, 77.
Dimopoulos, S., and L. Susskind, 1979, Nucl. Phys. B **155**, 237.
Dine, M., and W. Fischler, 1982, Phys. Lett. **110B**, 227.
Donaldson, R., R. Gustafson, and F. Paige, 1982, Eds., *Proceedings of the 1982 DPF Summer Study on Elementary Particle Physics and Future Facilities* (Fermilab, Batavia, Illinois).
Drell, S. D., and T. M. Yan, 1970, Phys. Rev. Lett. **25**, 316.
Drell, S. D., and T. M. Yan, 1971, Ann. Phys. (N.Y.) **66**, 578.
Duke, D. W., and J. F. Owens, 1984, Phys. Rev. D **27**, 508.
Eichten, E., I. Hinchliffe, K. Lane, and C. Quigg, 1984,

Fermilab-Conf -84/76-T.
Eichten, E., and K. Lane, 1980, Phys. Lett. **90B**, 125.
Eichten, E., and K. Lane, 1984 (unpublished).
Eichten, E., K. Lane, and M. E. Peskin, 1983, Phys. Rev. Lett. **50**, 811.
Eichten, E., K. Lane, and J. Preskill, 1980, Phys. Rev. Lett. **45**, 255.
Einhorn, M. B., and B. G. Weeks, 1978, Nucl. Phys. B **146**, 445.
Eisele, F., 1982, in *Proceedings of the 21st International Conference on High Energy Physics,* edited by P. Petiau and M. Porneuf, J. Phys. (Paris) **43**, Suppl. 12, C3-337.
Ellis, J., M. K. Gaillard, G. Girardi, and P. Sorba, 1982, Ann. Rev. Nucl. Part. Sci. **32**, 443.
Ellis, J., M. K. Gaillard, and D. V. Nanopoulos, 1976, Nucl. Phys. B **106**, 292.
Ellis, J., M. K. Gaillard, D. V. Nanopoulos, and P. Sikivie, 1981, Nucl. Phys. B **182**, 529.
Ellis, J., J. Hagelin, D. V. Nanopoulos, and M. Srednicki, 1983, Phys. Lett. **127B**, 233.
Ellis, R. K., M. A. Furman, H. E. Haber, and I. Hinchliffe, 1980, Nucl. Phys. B **173**, 397.
Farhi, E., and R. Jackiw, 1982, Eds., *Dynamical Gauge Symmetry Breaking* (World Scientific, Singapore).
Farhi, E., and L. Susskind, 1979, Phys. Rev. D **20**, 3404.
Farhi, E., and L. Susskind, 1981, Phys. Rep. **74**, 277.
Farrar, G., and S. Weinberg, 1983, Phys. Rev. D **27**, 2732.
Fayet, P., 1975, Nucl. Phys. B **90**, 104.
Fayet, P., 1981, in *QCD and Lepton Physics,* edited by J. Tran Thanh Van (Editions Frontieres, Dreux, France), p. 347.
Fayet, P., 1982, in *Proceedings of the 21st International Conference on High Energy Physics,* edited by P. Petiau and M. Porneuf, J. Phys. (Paris) **43**, Suppl. 12, C3-673.
Fayet, P., and S. Ferrara, 1977, Phys. Rep. **32C**, 249.
Fernandez, E., *et al.*, 1983, Phys. Rev. Lett. **51**, 1022.
Feynman, R. P., 1972, *Photon-Hadron Interactions* (Benjamin, Reading, Massachusetts).
Field, R. D., 1983, in *Proceedings of the 1983 International Symposium on Lepton and Photon Interactions at High Energies,* edited by D. G. Cassel and D. L. Kreinick (Newman Laboratory of Nuclear Studies, Cornell University, Ithaca, New York), p. 593.
Field, R. D., and S. Wolfram, 1983, Nucl. Phys. B **213**, 65.
Frere, J.-M., and G. L. Kane, 1983, Nucl. Phys. B **223**, 331.
Furmanski, W., R. Petronzio, and S. Pokorski, 1979, Nucl. Phys. B **155**, 253.
Gaillard, M. K., and R. Stora, 1983, Eds., *Gauge Theories in High Energy Physics,* 1981 Les Houches Summer School (North-Holland, Amsterdam).
Georgi, H., and S. L. Glashow, 1974, Phys. Rev. Lett. **32**, 438.
Georgi, H., S. L. Glashow, M. E. Machacek, and D. V. Nanopoulos, 1978, Phys. Rev. Lett. **40**, 692.
Georgi, H., and H. D. Politzer, 1974, Phys. Rev. D **9**, 416.
Georgi, H., and S. Weinberg, 1978, Phys. Rev. D **17**, 275.
Gildener, E., 1976, Phys. Rev. D **14**, 1667.
Ginzburg, V. L., and L. D. Landau, 1950, Zh. Eksp. Teor. Fiz. **20**, 1064.
Glashow, S. L., 1961, Nucl. Phys. **22**, 579.
Glashow, S. L., J. Iliopoulos, and L. Maiani, 1970, Phys. Rev. D **2**, 1285.
Glashow, S. L., D. V. Nanopoulos, and A. Yildiz, 1978, Phys. Rev. D **18**, 1724.
Glück, M., E. Hoffmann, and E. Reya, 1982, Z. Phys. C **13**, 119.
Goldhaber, G., *et al.*, 1976, Phys. Rev. Lett. **37**, 255.
Goldstone, J., 1961, Nuovo Cimento **19**, 154.
Gol'fand, Yu. A., and E. P. Likhtman, 1971, Zh. Eksp. Teor. Fiz. Pis'ma Red. **13**, 452 [JETP Lett. **13**, 323 (1971)].
Gordon, B. A., *et al.*, 1979, Phys. Rev. D **20**, 2645.
Gordon, H. A., W. Marciano, F. E. Paige, P. Grannis, S. Naculich, and H. H. Williams, 1982, in *Proceedings of the 1982 DPF Summer Study on Elementary Particle Physics and Future Facilities,* edited by R. Donaldson, R. Gustafson, and F. Paige (Fermilab, Batavia, Illinois), p. 161.
Gottschalk, T. D., 1984, Nucl. Phys. B **239**, 349.
Gribov, L. V., E. M. Levin, and M. G. Ryskin, 1983, Phys. Rep. **100**, 1.
Gribov, V. N., and L. N. Lipatov, 1972a, Yad. Fiz. **15**, 781 [Sov. J. Nucl. Phys. **15**, 438 (1972)].
Gribov, V. N., and L. N. Lipatov, 1972b, Yad. Fiz. **15**, 1218 [Sov. J. Nucl. Phys. **15**, 675 (1972)].
Gross, D. J., and F. Wilczek, 1973a, Phys. Rev. Lett. **30**, 1343.
Gross, D. J., and F. Wilczek, 1973b, Phys. Rev. D **8**, 3633.
Gross, D. J., and F. Wilczek, 1974, Phys. Rev. D **9**, 980.
Haber, H. E., and G. L. Kane, 1984, University of Michigan preprint UM-HE TH 83-17.
Halzen, F., and A. D. Martin, 1984, *Quarks and Leptons* (Wiley, New York).
Halzen, F., and D. M. Scott, 1978, Phys. Rev. D **18**, 3378.
Hanson, G., *et al.*, 1975, Phys. Rev. Lett. **35**, 1609.
Harari, H., 1982, in *Proceedings of the 10th SLAC Summer Institute,* edited by Anne Mosher, SLAC Report No. 259, p. 211.
Hasert, F. J., *et al.*, 1973a, Phys. Lett. **46B**, 121.
Hasert, F. J., *et al.*, 1973b, Phys. Lett. **46B**, 138.
Hasert, F. J., *et al.*, 1974, Nucl. Phys. B **73**, 1.
Higgs, P. W., 1964, Phys. Rev. Lett. **12**, 132.
Hinchliffe, I., 1982, in *Particles and Fields—1981: Testing the Standard Model,* edited by C. A. Heusch and W. T. Kirk (American Institute of Physics, New York), p. 173.
Hinchliffe, I., and L. Littenberg, 1982, in *Proceedings of the 1982 DPF Summer Study on Elementary Particle Physics and Future Facilities,* edited by R. Donaldson, R. Gustafson, and F. Paige (Fermilab, Batavia, Illinois), p. 242.
Hoyer, P., P. Osland, H. G. Sander, T. F. Walsh, and P. M. Zerwas, 1979, Nucl. Phys. B **161**, 349.
Ibañez, L., and G. G. Ross, 1981, Phys. Lett. **110B**, 215.
Jacob, M., 1983, CERN report TH-3693, to appear in the Proceedings of the 1983 SLAC Topical Conference.
Kagan, H., 1982, in *Proceedings of the 1982 DPF Summer Study on Elementary Particle Physics and Future Facilities,* edited by R. Donaldson, R. Gustafson, and F. Paige (Fermilab, Batavia, Illinois), p. 432.
Kane, G. L., and R. Shrock, 1983, in *Intense Medium Energy Sources of Strangeness,* edited by T. Goldman, H. E. Haber, and H. F.-W. Sadrozinski (American Institute of Physics, New York), p. 123.
Kaul, R., 1983, Rev. Mod. Phys. **55**, 449.
Kobayashi, M., and T. Maskawa, 1973, Prog. Theor. Phys. (Kyoto) **49**, 652.
Lane, K., 1982, in *Proceedings of the 1982 DPF Summer Study on Elementary Particles Physics and Future Facilities,* edited by R. Donaldson, R. Gustafson, and F. Paige (Fermilab, Batavia, Illinois), p. 222.
Lane, K., 1984, "The State of Electroweak Interactions," to appear in the Proceedings of the 1983 DPF Meeting, Blacksburg, edited by A. Abashian.
Leader, E., and E. Predazzi, 1982, *An Introduction to Gauge Theories and the New Physics* (Cambridge University Press, Cambridge).

Lee, B. W., C. Quigg, and H. B. Thacker, 1977, Phys. Rev. D **16**, 1519.
Lepage, G. P., 1983, in *Proceedings of the 1983 International Symposium on Lepton and Photon Interactions at High Energies,* edited by D. G. Cassel and D. L. Kreinick (Newman Laboratory for Nuclear Studies, Cornell University, Ithaca, New York), p. 565.
Leung, C. N., and J. L. Rosner, Phys. Rev. D **28**, 2205.
Leurer, M., H. Harari, and R. Barbieri, 1984, Phys. Lett. **141B**, 455.
Linde, A. D., 1976, Zh. Eksp. Teor. Fiz. Pis'ma Red. **23**, 73 [JETP Lett. **23**, 64 (1976)].
Littenberg, L., 1984, cited in R. M. Barnett, in $\bar{p}p$ *Options for the Supercollider,* edited by J. E. Pilcher and A. R. White (University of Chicago), p. 273.
Llewellyn Smith, C. H., 1983, in *Proceedings of the 1983 International Symposium on Lepton and Photon Interactions at High Energies,* edited by D. G. Cassel and D. L. Kreinick (Newman Laboratory of Nuclear Studies, Cornell University, Ithaca, New York), p. 835.
Lockyer, N. S., *et al.*, 1983, Phys. Rev. Lett. **51**, 1316.
Loken, S. C., and P. Nemethy, 1983, Eds., *Proceedings of the 1983 DPF Workshop on Collider Detectors: Present Capabilities and Future Possibilities,* Berkeley report LBL-15973.
Lyons, L., 1983a, Prog. Part. Nucl. Phys. **10**, 227.
Lyons, L., 1983b, "Recent Developments Concerning the Possible Substructure of Quarks and Leptons," Oxford University report.
MacFarlane, D. B., *et al.*, 1983, "Nucleon Structure Functions from High Energy Neutrino Interactions with Iron and QCD Results," Fermilab-PUB-83/108-EXP.
McIntyre, P., *et al.*, 1984, Proceedings of the SSC Fixed Target Workshop (Texas A&M Report).
McLerran, L., 1983, "Heavy Ions and the CBA," Brookhaven report.
Marciano, W. J., 1979, Phys. Rev. D **20**, 274.
Marciano, W. J., and Z. Parsa, 1982, in *Proceedings of the 1982 DPF Summer Study on Elementary Particle Physics and Future Facilities,* edited by R. Donaldson, R. Gustafson, and F. Paige (Fermilab, Batavia, Illinois), p. 155.
Marciano, W. J., and G. Senjanovic, 1982, Phys. Rev. D **25**, 3092.
Marciano, W. J., and A. Sirlin, 1981, Phys. Rev. Lett. **46**, 163.
Marciano, W. J., and A. Sirlin, 1984, Phys. Rev. D **29**, 75.
Marx, J. (coordinator), 1984, Report of the Reference Designs Study Group on the Superconducting Super Collider (Department of Energy Report).
Mazzanti, P., and R. Odorico, 1980, Phys. Lett. **95B**, 133.
Mess, K. H., and B. H. Wiik, 1983, in *Gauge Theories and High Energy Physics,* 1981 Les Houches lectures, edited by M. K. Gaillard and R. Stora (North-Holland, Amsterdam), p. 865.
Mikaelian, K. O., M. A. Samuel, and D. Sahdev, 1979, Phys. Rev. Lett. **43**, 746.
Mohapatra, R. N., 1983, "Left-Right Symmetric Models of Weak Interactions: A Review," University of Maryland preprint.
Mohapatra, R. N., and J. C. Pati, 1975, Phys. Rev. D **11**, 566.
Mohapatra, R. N., and G. Senjanovic, 1981, Phys. Rev. D **23**, 165.
Mueller, A. H., 1983a, Nucl. Phys. B **213**, 85.
Mueller, A. H., 1983b, Nucl. Phys. B **228**, 351.
Nappi, C., and B. Ovrut, 1982, Phys. Lett. **113B**, 175.
Odorico, R., 1980a, Nucl. Phys. B **172**, 157.
Odorico, R., 1980b, Z. Phys. C **7**, 61.
Odorico, R., 1983, CERN preprint TH.3760.
Okun, L. B., 1981, *Leptons and Quarks* (North-Holland, Amsterdam).
Okun, L. B., and M. B. Voloshin, 1977, Nucl. Phys. B **120**, 459.
Owens, J. F., and E. Reya, 1978, Phys. Rev. D **17**, 3003.
Owens, J. F., E. Reya, and M. Glück, 1978, Phys. Rev. D **18**, 1501.
Paige, F., 1984, in $\bar{p}p$ *Options for the Supercollider,* edited by J. E. Pilcher and A. R. White (University of Chicago), p. 1.
Paige, F., and S. Protopopescu, 1980, Brookhaven report BNL-29777.
Pati, J. C., and A. Salam, 1973a, Phys. Rev. D **8**, 1240.
Pati, J. C., and A. Salam, 1973b, Phys. Rev. Lett. **31**, 661.
Pati, J. C., and A. Salam, 1974, Phys. Rev. D **10**, 275.
Paver, N., and D. Treleani, 1983, ISAS, Trieste preprint 60/83/E.P.
Perkins, D. H., 1982, *Introduction to High Energy Physics,* 2nd ed. (Addison-Wesley, Reading, Massachusetts).
Peruzzi, I., *et al.*, 1976, Phys. Rev. Lett. **37**, 569.
Peskin, M., 1980, Nucl. Phys. B **175**, 197.
Peskin, M., 1981, in *Proceedings of the 1981 International Symposium on Lepton and Photon Interactions at High Energies,* edited by W. Pfeil (Physikalisches Institut, Universität Bonn), p. 880.
Petcov, S., and D. R. T. Jones, 1979, Phys. Lett. **84B**, 440.
Politzer, H. D., 1973, Phys. Rev. Lett. **30**, 1346.
Pondrom, L., 1982, in *Proceedings of the 1982 DPF Summer Study on Elementary Particle Physics and Future Facilities,* edited by R. Donaldson, R. Gustafson, and F. Paige (Fermilab, Batavia, Illinois), p. 98.
Preskill, J., 1981, Nucl. Phys. B **177**, 21.
Rubbia, C., 1984, Seminar at the 1984 Summer Study on the Design and Utilization of the Superconducting Super Collider (Snowmass, Colorado).
Quigg, C., 1977, Rev. Mod. Phys. **49**, 297.
Quigg, C., 1983, *Gauge Theories of the Strong, Weak, and Electromagnetic Interactions* (Benjamin/Cummings, Reading, Massachusetts).
Renard, F., 1982, Nucl. Phys. B **196**, 93.
Resnick, L., M. K. Sundaresan, and P. J. S. Watson, 1973, Phys. Rev. D **8**, 172.
Ritchie, J. L., *et al.*, 1983, Phys. Lett. **126B**, 499.
Robinett, R. W., 1983a, Phys. Rev. D **28**, 1185.
Robinett, R. W., 1983b, Phys. Rev. D **28**, 1192.
Rosner, J. L., P. Langacker, and R. Robinett, 1984, University of Chicago preprint EFI-84/8.
Salam, A., 1968, in *Elementary Particle Theory: Relativistic Groups and Analyticity (Nobel Symposium No. 8),* edited by N. Svartholm (Almqvist and Wiksell, Stockholm), p. 367.
Salam, A., and J. Strathdee, 1974a, Nucl. Phys. B **76**, 477.
Salam, A., and J. Strathdee, 1974b, Nucl. Phys. B **80**, 499.
Salam, A., and J. Strathdee, 1975, Nucl. Phys. B **87**, 85.
Samuel, M. A., 1983, Phys. Rev. D **27**, 2724.
Savoy-Navarro, A., 1984, Phys. Rep. **105**, 91.
Shizuya, K.-I., and S.-H. H. Tye, 1978, Phys. Rev. Lett. **41**, 787.
Sirlin, A., and W. J. Marciano, 1981, Nucl. Phys. B **189**, 442.
Sivers, D., and T. Gottschalk, 1980, Phys. Rev. D **21**, 102.
Slominski, W., 1981, Ph.D. thesis (Jagellonian University, Krakow).
Sterman, G., and S. Weinberg, 1977, Phys. Rev. Lett. **39**, 1436.
Susskind, L., 1979, Phys. Rev. D **20**, 2619.
Suzuki, M., 1982, Phys. Lett. **115B**, 40.
't Hooft, G., 1980, in *Recent Developments in Gauge Theories,*

Proceedings of the 1979 NATO Advanced Study Institute, Cargese, edited by G. 't Hooft *et al.* (Plenum, New York), p. 135.
Tigner, M., 1983, Ed., *Report of the 20 TeV Hadron Collider Technical Workshop* (Cornell University, Ithaca, New York).
Vainshtein, A. I., V. I. Zakharov, and M. A. Shifman, 1980, Usp. Fiz. Nauk **131**, 537 [Sov. Phys.—Usp. **23**, 429 (1980)].
Veltman, M., 1977a, Acta Phys. Polon. B **8**, 475.
Veltman, M., 1977b, Nucl. Phys. B **123**, 89.
Veltman, M., 1980, Phys. Lett. **91B**, 95.
Veltman, M., 1983, "Bound States of Vector Bosons," University of Michigan preprint UM HE 83-22.
Volkov, D. V., and V. P. Akulov, 1973, Phys. Lett. **46B**, 109.
Weinberg, S., 1967, Phys. Rev. Lett. **19**, 1264.
Weinberg, S., 1973, Phys. Rev. Lett. **31**, 494.
Weinberg, S., 1976a, Phys. Rev. Lett. **36**, 294.
Weinberg, S., 1976b, Phys. Rev. D **13**, 974.
Weinberg, S., 1979a, Phys. Rev. D **19**, 1277.
Weinberg, S., 1979b, Phys. Lett. **82B**, 387.
Weinstein, M., 1973, Phys. Rev. D **8**, 2511.
Wess, J., and J. Bagger, 1983, *Supersymmetry and Supergravity* (Princeton University Press, Princeton, New Jersey).
Wess, J., and B. Zumino, 1974a, Nucl. Phys. B **70**, 39.
Wess, J., and B. Zumino, 1974b, Phys. Lett. **49B**, 52.
Wess, J., and B. Zumino, 1974c, Nucl. Phys. B **78**, 1.
Wheater, J. F., and C. H. Llewellyn Smith, 1982, Nucl. Phys. B **208**, 27.
Wilson, K. G., 1971, Phys. Rev. D **3**, 1818.
Wojcicki, S., J. Adams, T. Appelquist, C. Baltay, M. K. Gaillard, J. D. Jackson, D. Keefe, A. Kerman, L. Pondrom, J. Rees, C. Rubbia, F. Sciulli, M. Tigner, S. Treiman, J. Vander Velde, H. Williams, and B. Winstein, 1983, *Report of the 1983 Subpanel on New Facilities for the U.S. High Energy Physics Program of the High Energy Physics Advisory Panel* (U.S. Department of Energy, Washington, D.C.).
Yamada, S., 1983, in *Proceedings of the 1983 International Symposium on Lepton and Photon Interactions at High Energies,* edited by D. G. Cassel and D. L. Kreinick (Newman Laboratory of Nuclear Studies, Cornell University, Ithaca, New York), p. 525.